Swansea University
Prifysgol Abertawe

Optimisation of Sinter Quality using the Sinter Pot Pilot Facility

Dissertation Submitted to Swansea University

in fulfilment of the requirements for the Degree of Doctor of Engineering

Sullayman Butt [redacted]

Swansea University

2024

1 Abstract

This investigation studies the complex area of sinter production, conducting an analysis of factors influencing thermodynamics, metallurgical testing, bed permeability, mineralogy formation, and blast furnace efficiency. Employing extensive experimentation and advanced data analysis, including leveraging computational tools such as thermodynamic prediction software FactSage and deploying a computer vision application named Intellesis, a novel aspect of this research emerges in iron ore sintering. The quality indicators for the sinter were examined through assessments of cold strength, degradation properties, chemical composition, microscopy, and mineralogy. Additionally, meticulous monitoring of process parameters, encompassing sintering time, temperature, flow rates, and flame front characteristics, ensured precision and accuracy in drawing conclusions.

This investigation delves into the influential domain of particle size of flux, unravelling their intricate roles in shaping sintering thermal profiles and enhancing quality. Operating within the 1mm to 3.15mm particle size fraction demonstrates improved stability and homogeneity in iron ore sinter. The influence of particle size on oxygen accessibility to coke particles unfolds profound effects on combustion rates and temperature profiles.

Exploring basicity levels provides a pivotal perspective on sinter quality. Operating within the optimal range of basicity 1.4 to 2.0, indicated by lower reduction degradation index (RDI) values and superior mineralogical features, emerges as a significant finding. Analysis of Intellesis data reveals a uniform distribution of renown favoured Silico Ferrite of Calcium and Aluminium (SFCA) among iron oxide phases and a correlation corroborated by X-ray fluorescence (XRF) analysis indicating that higher basicity values correlate with stronger sinter and optimal FeO content. The findings here suggest that they agree with the current industry practice which is at a basicity of 1.7.

The study dissects sinter properties related to silica and magnesium oxide (MgO) levels, shedding light on their intricate roles in sinter yield, SFCA formation, and productivity. A 7.0% silica level yields substantial sinter, coupled with remarkable SFCA formation. Furthermore, an optimal 2.5% MgO level was found, supported by

optimal RDI values and superior SFCA production, which emphasises the critical role of compositional changes.

Incorporating these insights, this thesis explains the pivotal role of key factors influencing sinter production, aiding the advancement of knowledge for iron and steel manufacturing. By optimising basicity value, particle size of flux, and other compositional changes, this study propels knowledge enhancement for an efficient and productive sintering process. This research marks substantial progress toward an efficient and productive sintering process through the optimisation of basicity levels, particle size of flux, and chemistry. The innovative use of Intellesis to analyse basicity, flux, and various chemistry levels further validates the findings, aligning with other quality indicators.

Declaration

This work has not previously been accepted in substance for any degree and is not being concurrently submitted in candidature for any degree.

Signed: …  . Date: 22/03/2024

Statement 1

This dissertation is the result of my own independent work/investigation, except where otherwise stated. Other sources are acknowledged by giving explicit references. A bibliography is appended.

Signed:  . Date: 22/03/2024

Statement 2

I hereby give consent for my dissertation, if accepted, to be available for photocopying and for interlibrary loan and for the title and summary to be made available to outside organizations.

Signed: …  .. Date 22/03/2024

Acknowledgements

اللهم لك الحمد حتى ترضى ولك الحمد يالله إذا رضيت ولك الحمد يالله بعد الرضا

Translation:

"O Allah I thank you for every blessing you have bestowed upon me and for every praise and gratitude I offer to you."

I would like to express my deepest gratitude to Professor Cameron-Pleydell Pearce, Dr Kevyn Bevan and Dr. Christopher Melvin for their invaluable guidance, unwavering support, and insightful feedback throughout the duration of this research project. Their expertise and mentorship have been instrumental in shaping the trajectory of this thesis.

I extend my sincere appreciation to the entire sinter pot team for their generous assistance, valuable discussions, and collaborative efforts, which have significantly contributed to the optimisation of iron ore sinter quality explored in this thesis.

I extend my sincere appreciation to Tata Steel, EPSRC and M2A the sponsoring companies whose generous support has made this research possible. Your investment in this project has enabled the exploration of vital aspects within the realm of iron ore sinter quality optimisation.

To my dear parents, Mum and Dad, your love, encouragement, and unwavering belief in me have been my greatest source of strength throughout this journey. I am eternally grateful for your sacrifices and unwavering support.

To my beloved wife Hind and son, your patience, understanding, and steady support have been the cornerstone of my perseverance. Your love and encouragement have sustained me through the challenges and triumphs of this endeavour.

Special appreciation goes to my family and close friends, whose encouragement and support have been a constant source of motivation and inspiration.

Lastly, I extend my heartfelt gratitude to all those who have contributed in ways seen and unseen to the completion of this thesis. Your support and encouragement have been invaluable and deeply appreciated.

Table Of Contents

List Of Figures

List Of Tables

List of Abbreviations

Full name	Abbreviation
Silico ferrite of calcium and aluminium	SFCA
Reduction degradation index	RDI
Reducibility index	RI
Multi-phase equilibrium	MPE
Calcium aluminium ferrite	CFA
Xray diffraction	XRD
Xray fluorescence	XRF
Tumbler index	TI
Thermocouple	TC
Basicity	B2
Particle size of flux	PSF
Particle size distribution	PSD
Scanning electron microscopy	SEM
Energy dispersive spectroscopy	EDS
Extended depth of field	EDF
Alumina	A
Hematite	H
Magnetite	M
Wustite	W
Calcium carbonate	CC
System performance measurement	SPM
Confidence interval	CI

2 Introduction

Iron ore sinter is a crucial product that is created by heating and fusing fine iron ore particles through the sintering process. This process is an essential step in the production of iron. To produce sinter, raw materials such as iron ore fines, fluxes (e.g., limestone), and coke breeze are mixed granulated and heated. As a result, they create a solid mass that binds the fine iron ore particles into larger agglomerates. This agglomeration facilitates their handling in subsequent steps. The sintered product is used as a feed material for the blast furnace, which is crucial in pig iron production. The efficient combustion of the feed material is necessary for molten iron generation in the blast furnace. Additionally, sintering increases porosity, enhancing the material's suitability for the blast furnace by maintaining structural integrity and optimising gas flow during the reduction process. The improved permeability of the sintered material further enhances gas flow efficiency in the blast furnace.

There are currently 34 iron ore sinter plants with 63 iron ore sinter strands operating in 14 countries throughout Europe. In the early 2000s, these plants produced an annual total of 130 million tons of sinter[1]. The graphical representation provided in Figure 2.1 illustrates the average percentage of sinter utilised in this particular blast furnace[2] over the course of a year. The data reflects a range between 65% and 72%, which is typically observed within the industry[2].

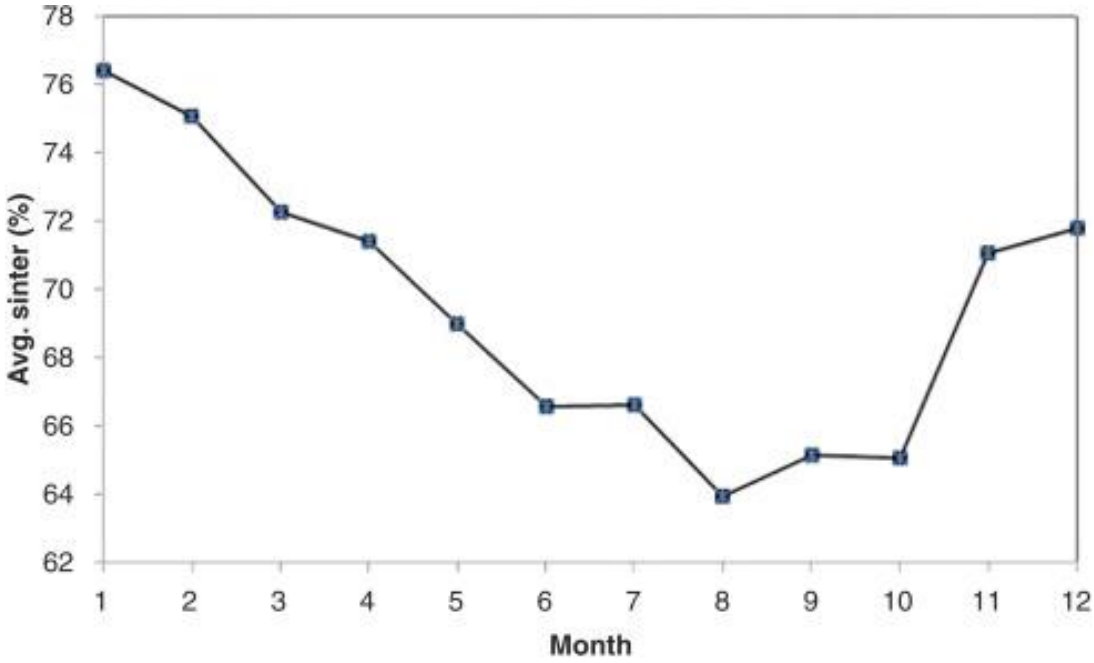

Figure 2.1 Typical sinter percentage over a year in the burden of the blast furnace[2]

The pre-production stage of steel production is heavily reliant on the process of iron ore sintering due to its cheap production. Without this critical step, the acquisition of steel would become increasingly challenging financially. The quality of the sinter, as determined by its final properties, serves as a crucial factor in enabling the blast furnace to function at a low fuel rate, thereby reducing costs for the steel manufacturing process. The steel industry serves as the foundation for global economic development, catering to various sectors such as machinery, automotive, shipbuilding, appliances, and construction[3].

The research conducted in this thesis examined the key factors that affect the quality of iron ore sinter. The focus was on controlling basicity within the range of 1.0 to 3.0, as this parameter significantly influences sinter temperature profiles, reducibility, and fines content[4 5]. The study investigated the formation of the Silico ferrite of calcium and aluminium (SFCA) phase and its impact on sinter mechanical strength and reactivity to identify the ideal basicity range that enhances blast furnace performance. Additionally, the research explored the significance of flux particle size, targeting particles between 0.25 to 5mm, and its effect on sinter homogeneity, fines content, and reduction degradation properties. The influence of SiO_2 and MgO content on RDI, SFCA formation, and post-discharge sintered material characteristics was examined. The investigation was conducted through laboratory experiments and advanced

analytical techniques to interpret correlations between process conditions, sinter mineralogy, and theoretical predictions. It is important to note, this study used a novel computer vision application called Intellesis to observe mineralogical changes in iron ore sinter.

This thesis aims to comprehensively analyse the optimisation of iron ore sinter quality to improve steel production. Chapter 3 covers various aspects of steel production, the iron ore sintering process, blast furnace operation, and critical factors affecting sinter quality, such as sinter conditions, mineralogy, and particle size distribution of raw materials. This section forms the basis for the subsequent parts of the thesis. Chapter 4 details the research design and analytical techniques used, followed by three experimental chapters in Chapter 5, 6 and 7. Each experimental chapter investigates different factors affecting sinter quality, including thermodynamics, sinter bed permeability, formation of different phases, and metallurgical testing. Chapter 5 addressed the correlation between altering basicity levels and its resultant impact on the quality of sinter. Chapter 6 investigates the effects of modifying the size of flux particles on sinter quality. Lastly, Chapter 7 is focused on analysing the impact of varying levels of MgO, silica, and basicity on the quality of sinter.

3 Literature Review

3.1 Overall Steel Production

The production of steel is essential for various industries, including automotive, construction, and consumer products.[6] As a result, maintaining the highest quality of materials is crucial for the industry since many stakeholders rely on the integrity of the final product. Steel production involves various steps as depicted by Figure 3.1.

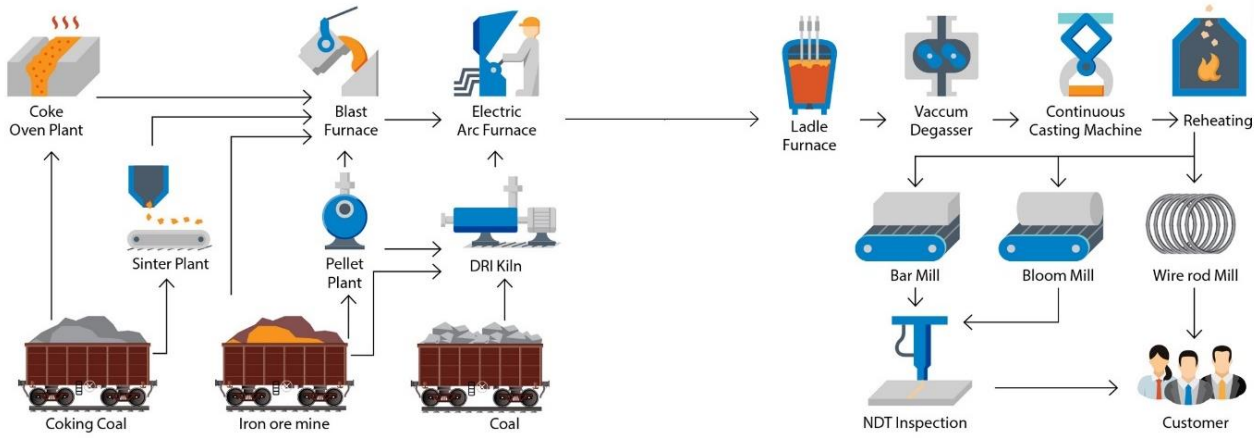

Figure 3.1 Process flow diagram of entire steel production route[7]

The steel production process begins with the ironmaking process located in the blast furnace where molten iron is produced. After which, molten iron passes through the Basic Oxygen Steelmaking (BOS) plant, followed by refining and secondary processes, which refine the steel further to enhance its quality and properties. These processes may include ladle refining, vacuum degassing, and continuous casting. Ladle refining removes additional impurities and adjusts the chemical composition, while vacuum degassing eliminates gases from the molten steel. Continuous casting solidifies the molten steel into semi-finished products like slabs, billets, or blooms.[8] The semi-finished steel products are then subjected to rolling mills to shape and convert them into final products. Depending on the desired properties and product specifications, rolling can involve hot or cold rolling. The rolled steel may undergo additional treatments such as heat treatment, surface coating, or further processing steps specific to the intended application.[9] The finished product is then ready to sell to the customer after being inspected for any defects.

The process of iron ore sintering plays a crucial role in the production of steel as it serves as one of the primary ingredients for the blast furnace. Sinter production is particularly important because it is more cost-effective than pellets and more easily reducible compared to lump ore which are its alternatives. Additionally, iron ore sinter allows for the calcination reaction of limestone (Equation 3.4) to occur outside of the blast furnace, thereby reducing heat consumption.

The quality of sinter holds significant importance for blast furnace operators as they require sinter that exhibits high cold strength, low Reduction Degradation Index (RDI), and high Reducibility Index (RI), as outlined in Table 3.1. Furthermore, it is imperative to maintain consistent chemical composition, minimise the content of fines, and achieve an ideal average size, as indicated in Table 3.1, to ensure stable and predictable operation of the blast furnace.[10] [11]

Table 3.1 Sinter quality requirements[11]

	Minimum value	Maximum value	Typical
Coke consumption ($kg \cdot t^{-1}$ sinter)	39	54	–
Productivity ($t \cdot m^{-2}$ per 24h)	26	43	–
Fe total (%)	51	61	>56
Basicity Index			1.70
FeO (%)	4.0	11	
Al_2O_3 (%)	0.6	1.8	1.35
MgO (%)	0.7	2.2	1.65
SiO_2 (%)	5.3	5.4	
Alkalis (%)		0.11	
Phosphorus (%)		0.04	
RDI (% < 3mm)	27	33	<33
Tumbler (% > 6.3mm)	63	79	>74
Reducibility (R_{60}, %)	49	78	
% < 0.125 mm		15	
0.2 mm < % < 0.7 mm		18	

3.2 Iron Ore Sintering Procedure

Upon producing iron ore sinter, several stages must be completed. The initial stage involves preparing the raw materials, which consist of iron ore fines, fluxes, and fuel. Typically, limestone and magstone are used as fluxes, while coke breeze serves as the fuel. These raw materials are carefully chosen based on their quality and chemistry to meet the specific needs of the customer[12]. Following this step is the process of mixing and blending, which ensures that the raw materials are thoroughly combined to achieve a consistent composition. After mixing, the materials are granulated to create a feedstock for the sintering process. Granulation requires adding water to the mixture, resulting in granules of the appropriate size usually between 5-20mm.[12] This technique aids in achieving the ideal permeability of the sinter mixture throughout the sintering process.

In Port Talbot, two sinter beds, each of 60-metre length, are laid out with the raw mix of sinter as displayed in Figure 3.2. One bed is laid with 130 layers, while the material from the second bed is applied to the sinter strand. The bed may undergo preheating to eliminate any excess moisture and enhance the efficiency of the sintering process. The chemical composition of the bed is closely monitored by operators on computers to ensure that it meets the chemical specifications as demanded by the blast furnace department. A variety of iron ores are being added to the sinter bed to meet the target iron ore composition, considering the high cost of low phosphorus ores which are ideal. Hence, an optimum mix of ores with low and high levels of phosphorus must be used. The basicity index required by the blast furnace department is achieved by mixing a combination of basic and acidic materials.

To ignite the sintering bed, the ignition hood is used as depicted in Figure 3.2. This triggers the combustion process of the coke breeze which generates heat essential for the sintering reactions. The combustion process releases energy and by-products, including carbon dioxide (CO_2), as the solid fuel burns in the presence of oxygen. The heat produced from the combustion of solid fuels increases the temperature of the sintering bed, creating an environment that allows for various chemical reactions to occur. These reactions include the reduction of iron oxides, the formation of liquid

phases, and the bonding of iron ore particles, which are dependent on the specific composition and characteristics of the sinter feedstock. The elevated temperature from combustion also leads to the melting and fusion of certain components present in the sinter, such as fluxes like limestone, which helps in the formation of cohesive iron ore sinter.[8]

The sintering bed undergoes a controlled temperature profile as it moves through the sintering machine. Due to the heat from combustion and the surrounding environment, the granules experience a range of physical and chemical transformations. The iron ore particles bond together, resulting in a solid yet porous sinter.[13]

At this stage the iron ore sinter is cooled, crushed, and screened. The sizes are split into <5mm, and >5mm. The >5mm fraction size is submitted to the blast furnace whilst the <5mm fraction size which is also known as 'return fines' is recycled back into the sintering process. During the sintering process, it is crucial to ensure that the outgas suction holes are protected from the melt generated. This is to prevent any sticking of materials inside the holes and to ensure that no fine particles leak into them[14]. The strand measures approximately 100 meters in length, 4 meters in width, and 1 meter in depth. While most sinter plants can manufacture up to 500 tonnes of sinter per hour, the production quantity is usually determined by the requirements of blast furnace operations.

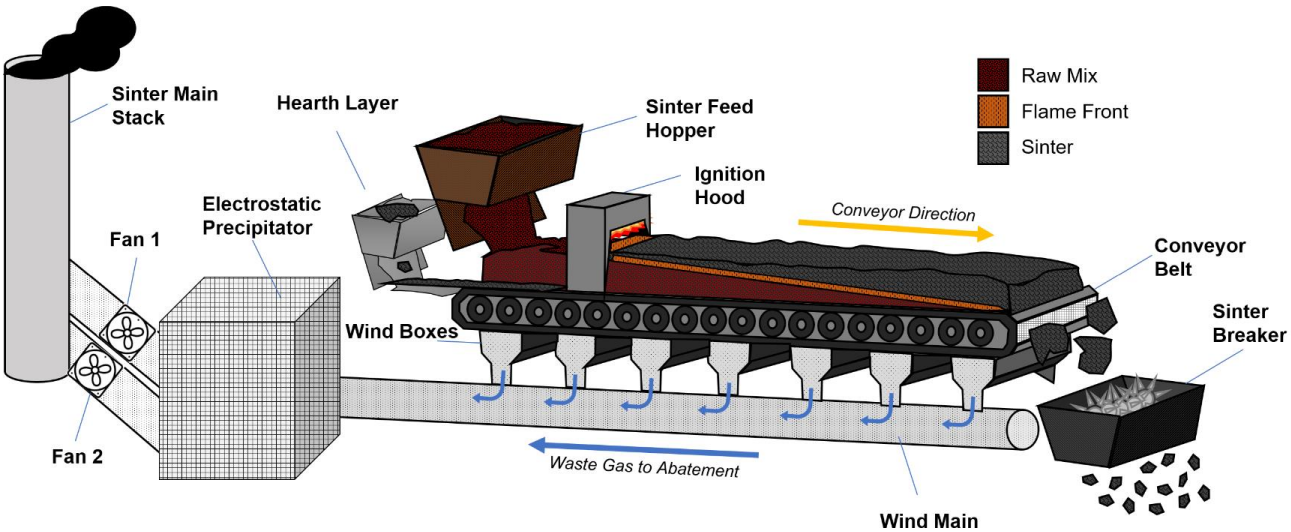

Figure 3.2 Schematic of sinter process on strand (industrial scale)[15]

The production of iron ore sinter is crucial for several reasons. Iron ore fines are tiny particles of iron ore that can be challenging to handle and use effectively in the blast furnace. The sintering process enables these fine particles to agglomerate or bind together into larger, porous lumps known as sinter. This agglomeration enhances the handling, transportation, and permeability properties of the iron ore, making it more suitable for the blast furnace[16].

Iron ore sinter, combined with coke and fluxes, serves as a feed material in blast furnaces. The sinter's porous composition enables efficient gas-solid interactions, aiding in the reduction of iron oxides and the creation of liquid iron (see Chapter 3.3). Sintering also improves the burden's permeability in the blast furnace, thereby enhancing the overall efficiency of the ironmaking process.

The overall sinter quality is subject to a range of input parameters that require careful consideration. These parameters include the chemical composition of the raw material, with specific attention given to the levels of Al_2O_3, SiO_2 and MgO present. Additionally, the amount of flux, such as limestone and magstone must be carefully measured. Other critical factors include the moisture and carbon content of the green mix, as well as the firing conditions, including firing temperature and burn through temperature. Finally, machine parameters such as machine speed, bed height, and feed rate must be optimised to ensure the highest possible quality of the final sinter product[17].

3.3 Blast Furnace Operation

To produce molten iron in the blast furnace, the production of iron ore sinter is key, thus it is essential to understand the necessary requirements for the blast furnace. The high temperatures generated in the furnace cause the iron ore to melt, which produces molten iron and slag. This molten iron, also known as hot metal, is the main ingredient in steelmaking.[8]

To maintain the efficient operation of the blast furnace, a precise combination of materials is required. This combination should include a ferrous component, carbon input, and fluxed material in the burden. Iron ore can be found in the form of lump, pellet, or sinter, with sinter typically being the main component used in the production of iron in blast furnaces[18]. Carbon input is provided by metallurgical coke and granulated coal. Additionally, the fluxed material is fused into the sinter. Refer to Figure 3.3 for more information.

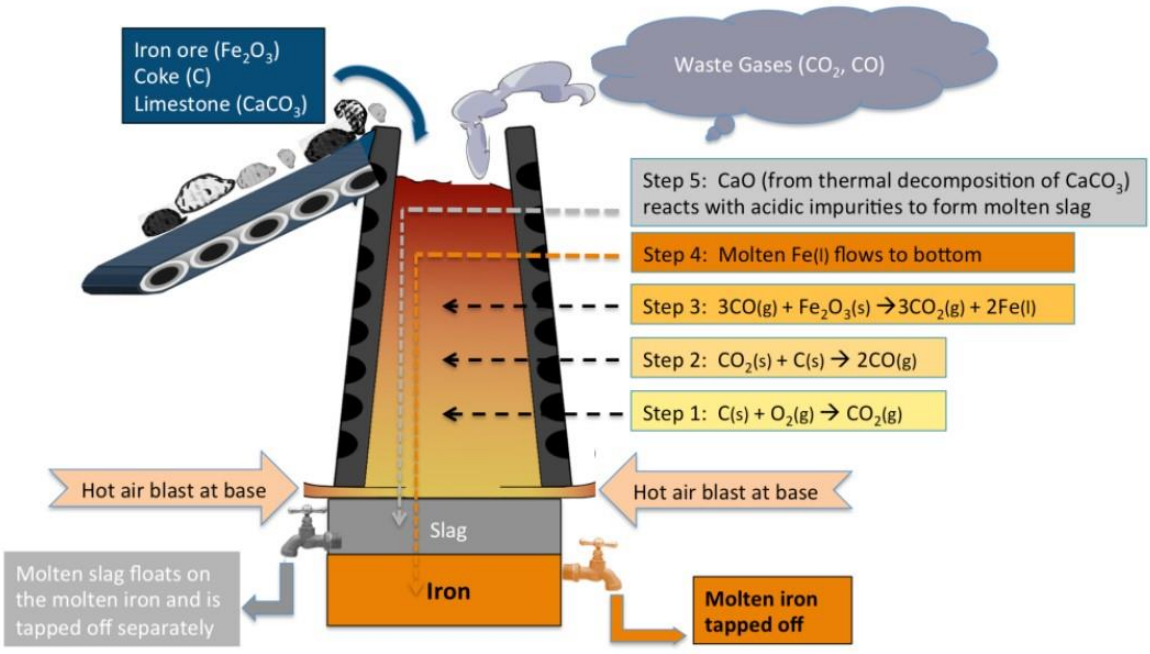

Figure 3.3 Blast Furnace production schematic[19]

Additionally, vital reactions, like those illustrated in Equation 3.1-Equation 3.5[20], need to occur to produce the molten iron, and sinter contains the necessary compounds for these reactions to take place.

As seen by Equation 3.1 the carbon which is in the form of coke reacts with oxygen in the air in the lower blast furnace.

Equation 3.1

$$C(s) + O_2(g) \rightarrow CO_2(g) + heat$$

The carbon dioxide produced is then reduced to form the necessary carbon monoxide for the following step, as demonstrated in Equation 3.2.

Equation 3.2

$$CO_2(g) + C(s) \rightarrow 2CO(g) - heat$$

To produce metallic iron in its molten state and ready to be discharged from the blast furnace, the next crucial step is to reduce the hematite (Fe_2O_3) by using carbon monoxide as a reducing agent as shown in Equation 3.3.

Equation 3.3

$$Fe_2O_3(s) + 3CO(g) \rightarrow 2Fe(l) + 3CO_2(g)$$

Equation 3.4 is the thermal decomposition of calcium carbonate. This is important as it facilitates the removal of impurities and the formation of slag. Also, the production of carbon dioxide (CO_2) enables additional reactions with carbon monoxide (CO) to form an additional reducing agent, such as carbon within the blast furnace. This reducing agent then participates in the reduction reactions[21].

Equation 3.4

$$CaCO_3(s) \rightarrow CaO(s) + CO_2(g)$$

In Equation 3.5, it is shown that there is an extra chemical reaction taking place in the background to create slag, such as silicates. The slag is produced and then floats on top of the iron, providing a protective layer that stops the iron from oxidising. Additionally, it helps to remove impurities through separation[22].

Equation 3.5

$$2CaO(s) + SiO_2(s) \rightarrow Ca_2SiO_4(l)$$

In the steel manufacturing process, the sinter that enters the blast furnace often includes different by-products and waste materials like mill scale, sludge, LD slag, and powders. These elements can affect the quality of the sinter and cause inconsistent and unstable operation of the blast furnace[11]. To ensure smooth operation, it is recommended to control the physical, chemical and mineralogical properties of the iron ore sinter whilst possessing homogeneous and consistent properties in terms of thermal and mechanical factors.[10]

3.4 Sinter Conditions

This section explores how the production conditions of sinter affect its quality. The necessary temperature for producing crucial phases and compounds will be examined, such as SFCA's, as well as the pressure conditions studied in existing literature. Additionally, the impact of granulation, moisture, and permeability on the quality of iron ore sinter, as discussed in various studies will be analysed. Lastly, an assessment of the vital role of basicity will be studied and the precise amount that is beneficial was determined.

3.4.1 Sinter Thermodynamics

In the sintering process, the coke breeze serves as the primary fuel source. This fuel possesses the necessary metallurgical properties, such as high carbon content, clean combustion, and sufficient heat content, to support the process. Figure 3.4 illustrates the impact of temperature variation of chemical reactions that can take place during the production of sinter. The logarithm of the equilibrium constant (log K) measures the thermodynamic favourability of a reaction. Positive values of log K (log $K > 0$) suggest that the equilibrium favours the products, indicating that the reaction is more likely to proceed in the forward direction. In contrast, negative values of log K (log $K < 0$) indicate a reactant-favoured equilibrium, which means there is a reduced likelihood of the forward reaction occurring.

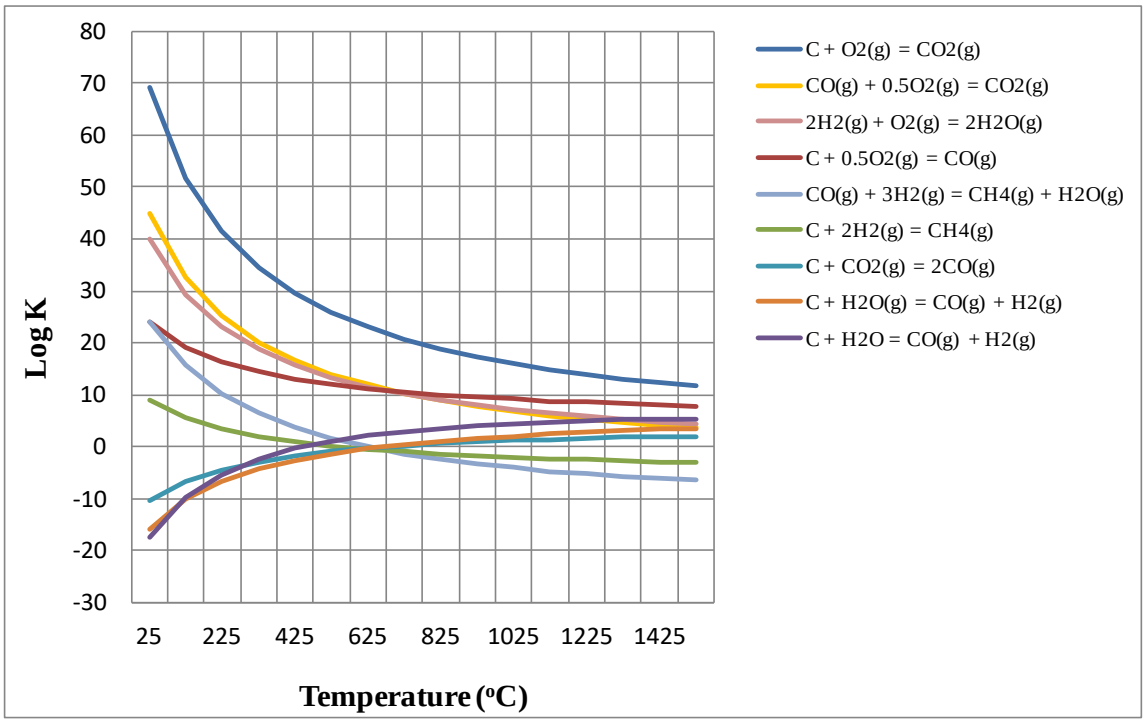

Figure 3.4 The impact of temperature variation on the course of chemical reactions[23]

Figure 3.5 displays the ideal flame front profile for the sintering process. Fernández-González et al. found that it is crucial to limit the heating time in the high temperature zone (above 1100°C) to just 1.5 minutes due to the low partial oxygen pressure resulting from coke combustion and FeO formation. Conversely, the cooling time (from 1250°C to 1100°C) should be extended to 3-5 minutes to aid the formation of a strong sinter structure and prevent a gangue matrix. Consistency in maximum temperature and heat distribution is vital to achieve a uniformity that results in homogeneous sinter, process efficiency, and sinter quality[24].

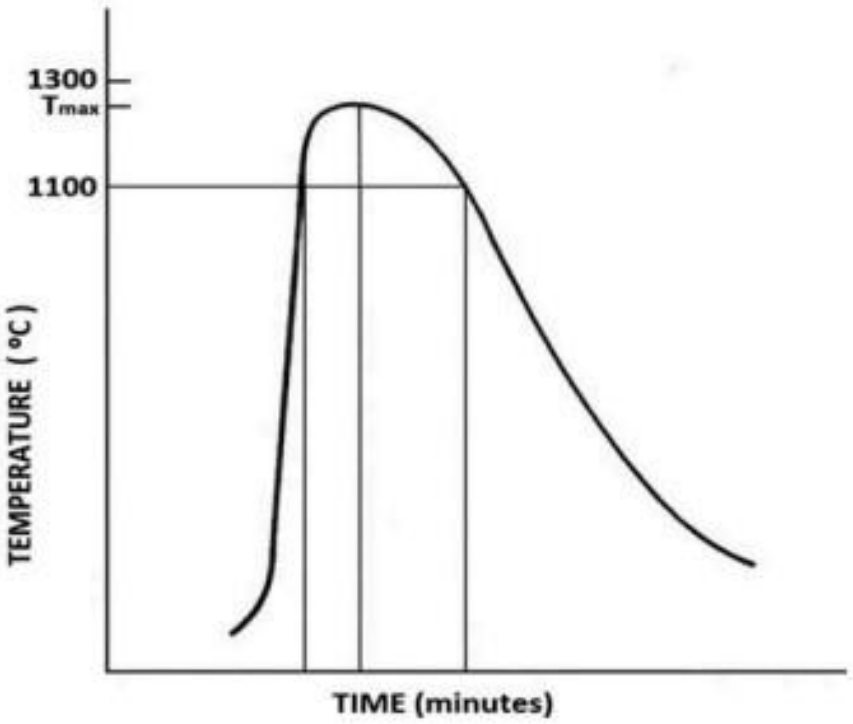

Figure 3.5 Ideal temperature profile for iron ore sinter[24] [25]

By referring to Figure 3.6, the conceptual diagram of the flame front structure in relation to temperature can be observed. When analysing the temperature of the sinter bed, it is noticed that the peak displayed represents a standard stable peak curve during the process. The sintering bed is a complex system that consists of distinct zones with unique functions. The sintered zone facilitates the exchange of heat between hot sinter and cold air. The combustion and melting zones, on the other hand, are areas where temperatures can exceed 1000K and 1373K, respectively. In the combustion zone, coke particles undergo ignition, while in the melting zone, the materials produce sinter with high porosity and strength. The flue gas preheats the materials located just below the combustion zone, giving rise to the drying and preheating zone, where carbonate decomposition mainly occurs. Lastly, the downstream flue gas encounters the cold raw mix, leading to water condensation and the formation of the water condensation zone.[26]

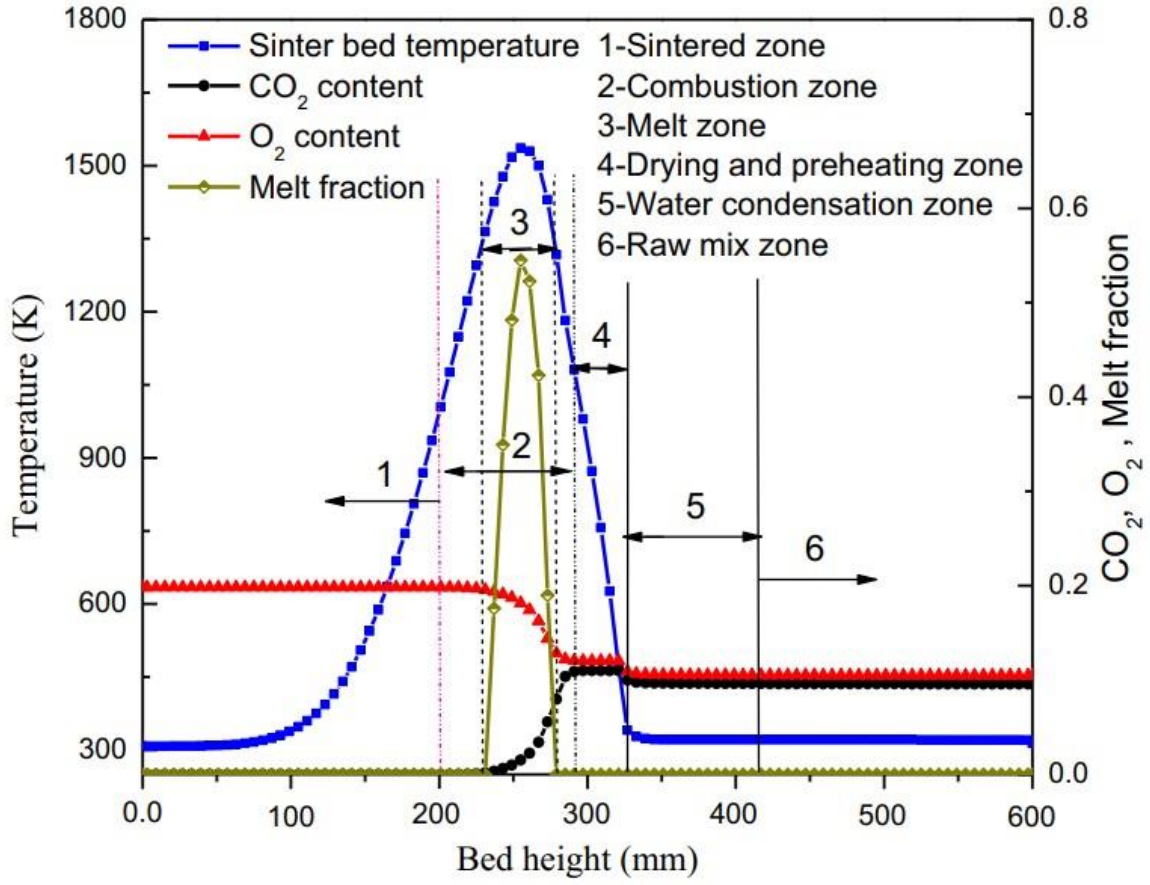

Figure 3.6 Thermodynamics of the flame front structure[26]

The global steel industry is witnessing a rise in the number of firms supplying steel, leading to an increase in demand for coke - a crucial material in steel production. Consequently, obtaining coke has become challenging for many companies. In search of alternatives, Legemza et al.[23] conducted a study on substituting coke breeze with charcoal. The investigation aimed to determine if charcoal could match the thermodynamic properties of coke breeze and serve as a viable substitute. Additionally, Legemza et al. wanted to prove that the compound formed would be stable with respect to temperature. Results of the experiment showed that partial utilisation of charcoal was beneficial from a thermodynamic point of view, as the use of charcoal reduced the $CO_{2(g)}/CO_{(g)}$ ratio in the exhaust gases. As well as this there was a higher content of $H_{2(g)}$ noted. With this increase of $H_{2(g)}$ and $CO_{(g)}$, this meant that there was now a potential for more reduction to take place and thus more Fe_3O_4 and FeO in the agglomerate respectively. This means that the RDI lowered, hence improving the quality of the sinter as a result. Legezma et al.[23] carried out a laboratory

experiment which confirmed that when 20% of coke breeze was replaced by charcoal the presence of higher content of FeO was evident in the agglomerate, up to about 5%.

In iron ore sintering the main phase which has the most significant effect on sinter quality is the silico-ferrite of calcium and aluminum (SFCA) phase. The study conducted by Chen et al focused on the thermodynamic perspective of the creation of the SFCA phase during sintering. SFCA is a crucial element in iron ore sinter as it acts as a bonding agent, alongside iron oxides, calcium ferrites, dicalcium silicate, and glasses. SFCA greatly influences various sinter quality parameters, including mechanical strength, reducibility, and reduction degradation. Previous studies had explored the melting behaviour through thermodynamic modelling, but there was a lack of research on SFCA formation during sintering. This article found that at constant oxygen partial pressure, wustite was the most stable, followed by magnetite and hematite with increasing temperature. This led to the conclusion that a lower sintering temperature would likely lead to a transition from wustite to magnetite and hematite, resulting in a higher formation of SFCA based on thermodynamics. Figure 3.7 illustrates the impact of the presented conditions on the number of constituents formed at a given temperature.

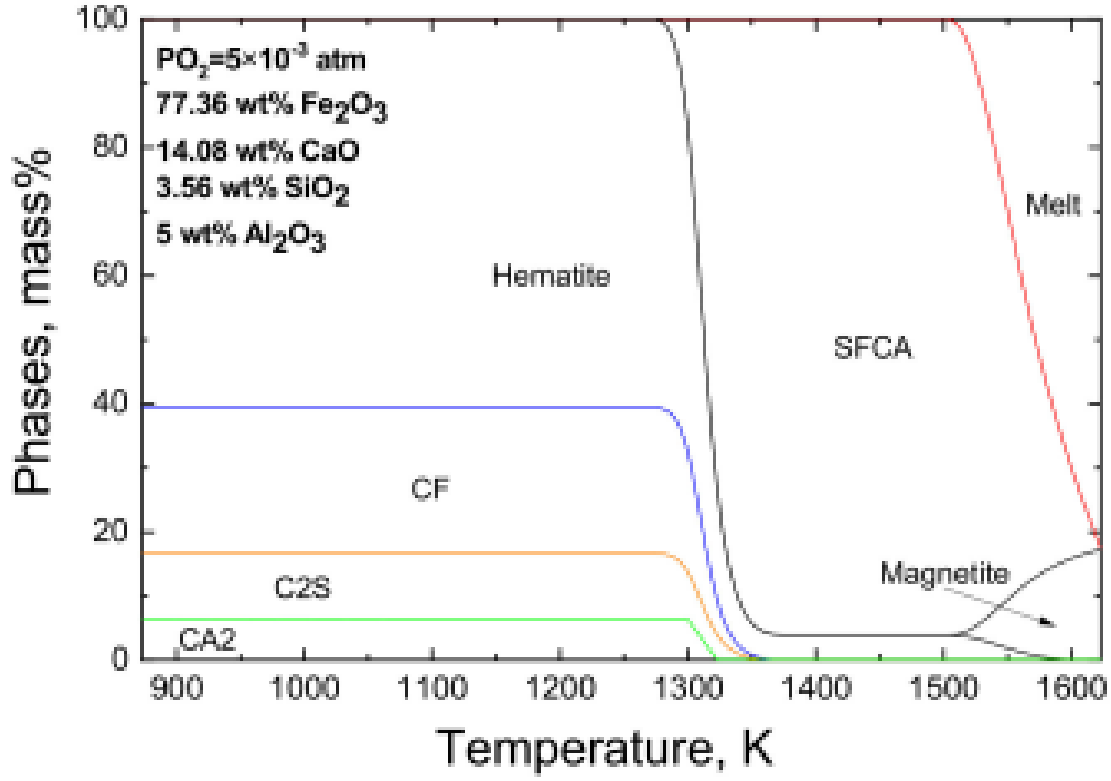

Figure 3.7 Mineralogy composition as a function of temperature[27]

Researchers[27] have created a thermodynamic software called multi-phase equilibrium (MPE) to examine the SFCA phase. To analyse its formation, X-ray powder diffraction (XRD) was conducted, and a solid solution model was included in the MPE. Comparing the MPE model and XRD findings, it was determined that higher basicity in raw materials can increase the SFCA phase presence. Additionally, increasing raw material basicity can reduce melt viscosity and improve fluidity.[27]

A recent study conducted by Majumder et al.[28] has revealed that temperatures ranging from 1250-1300°C are conducive to the formation of SFCA. This discovery has been corroborated by other studies conducted by researchers[29 30 31 32]. As well as this another finding established 1300-1400°C is the best sintering maximum temperature for iron ore sinter with high quality[33].

Iron ore sintering involves the transformation of various iron oxide phases, such as hematite (Fe_2O_3) and magnetite (Fe_3O_4), during heating and cooling. Thermodynamics helps determine the conditions under which these phase transformations occur and

provides insights into the stability and equilibrium of different iron oxide phases. Understanding the phase transformations is essential for controlling the sintering process and achieving the desired sinter quality.

The Gibbs free energy measures the maximum work that can be extracted from a system at constant temperature and pressure. It considers both enthalpy and entropy to determine the feasibility of a process. Enthalpy (H) represents a system's heat content, while entropy (S) measures the system's disorder. The Gibbs free energy (G) change as defined by Equation 3.6, where T is temperature. A negative ΔG indicates a spontaneous and energetically favourable process, while a positive ΔG means the process requires energy input. Equilibrium conditions determine a system's stability and phase composition.[34]

Equation 3.6 Calculation for Gibbs free energy change

$$\Delta G = \Delta H - T\Delta S$$

During iron ore sintering, enthalpy and entropy changes occur during phase transformations like the conversion of iron oxide phases and the formation of iron oxide compounds. Gibbs free energy values can determine the stability of different iron oxide phases during sintering, which helps identify the favoured phases and their transformations under specific conditions[35]. By understanding the stability and transformation of iron oxide phases during sintering, the microstructure, composition, and mechanical properties of the final sintered material can be controlled.

During the process of sintering, the combustion of coke provides approximately 80% of the necessary heat to produce enough melt to generate strong sinter[36]. Lovel et al.[37] suggested that if the temperature for firing is too low, the granules may not bind together due to inadequate heating. On the other hand, if the temperature is too high, the permeability of the bed may decrease, resulting in longer sintering times and loss of productivity. Moreover, when the temperature is too high excessive magnetite formation may occur.

The particles in a sinter mix can be categorised as nuclei and adhering, with nuclei being larger than adhering. The coke particles position within a granulated sinter mix

affects their access to oxygen, when they are the nuclear particles of granules, combustion rate tends to be controlled by mass transfer because the oxygen for combustion and the products of combustion must diffuse though the gas boundary layer and the adhering fines layer. However, when the coke particles are in the adhering fines layer the easy access to oxygen means that the combustion process tends to be kinetically controlled[36], the latter requires less activation energy for the combustion to occur.

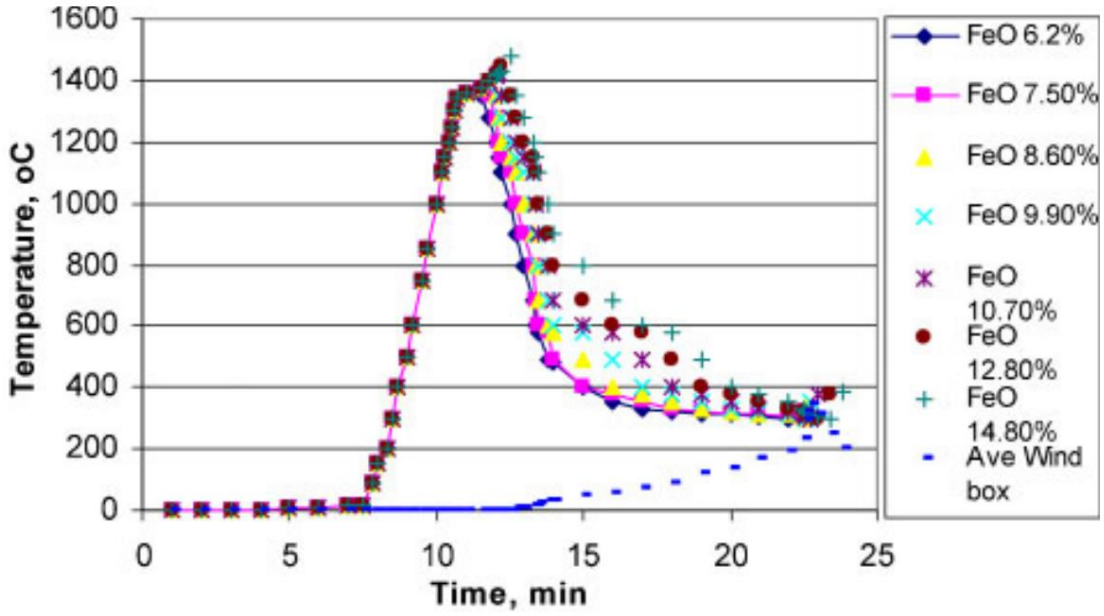

Figure 3.8 Temperature as a function of time for varying levels of FeO[38]

The graph in Figure 3.8 displays the relationship between time and temperature for iron ore sinter, at varying levels of FeO. It is evident from the graph that an increase in FeO content leads to a longer cooling time for the peak. Sinter with FeO levels ranging from 8.60% to 9.88% exhibit greater productivity, due to improved sinter bed permeability, optimal time and temperature for sintering, desired flame front speed, and proper assimilation of mineral phases. The sinter bed's permeability is crucial in regulating its properties and productivity, as it controls the temperature profile by determining the gas flow rate. The movement of the flame front throughout the bed height is a crucial process parameter that influences the formation and stabilization of phases in the sinter. The flame front's travel rate affects both productivity and quality.[38]
[39]

According to a study conducted by Hosotani et al[40], reducing the holding time during sintering at temperatures of 1173K and above resulted in the formation of more ideal heat patterns in the middle and lower layers. The heat patterns in this region were more ideal, leading to a decrease in sintering time and improvement in RDI[40]. These findings highlight the importance of carefully monitoring and adjusting the holding time during high temperature sintering processes to optimise the final product quality.

As the temperature in the sinter bed decreases, there is a corresponding reduction in the size of calcium ferrite grains, fine pores are further dispersed. These pores play a crucial role in mitigating the negative effects of pore closure that can occur during the reduction process, particularly at high temperatures of 1273K and above. The presence of these small pores enhances the sinter's ability to undergo reduction at high temperatures. However, it is advisable to limit the use of limestone and coke breeze to prevent the micro-pores from merging into larger ones. This will restrict the expansion of the temperature pattern in the sinter bed, thereby maintaining the integrity of the smaller pores and ensuring optimal sinter reduction[40].

It was reported in the literature[41] that many researchers have found, that enhancing the quantity of micro pores and limiting the amalgamation of micro pores during the sintering procedure can result in a significant enhancement in reducibility via an increase in surface area of the iron ore sinter.

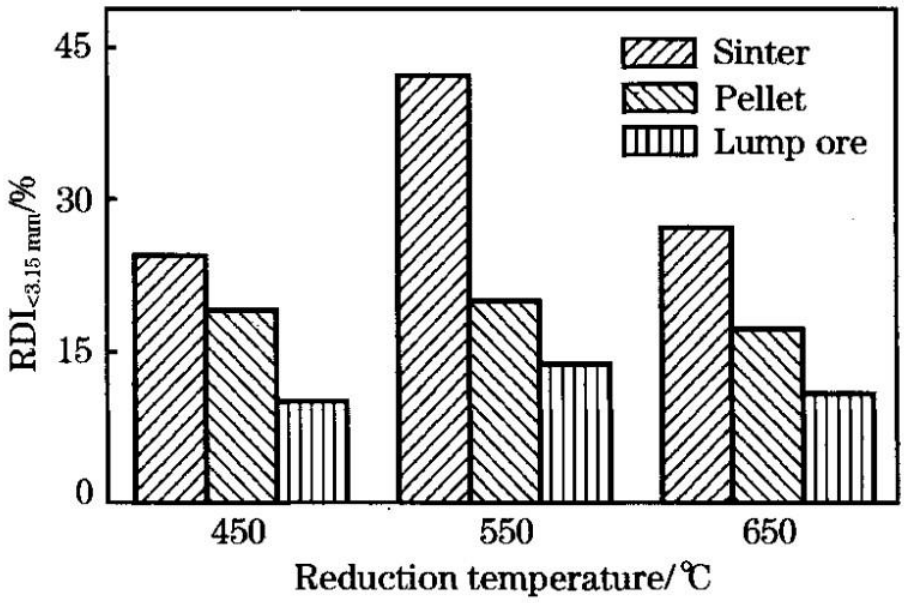

Figure 3.9 Comparison of RDI for different iron ores as a function of reduction temperature[42]

The temperature fluctuations that occur during the reduction of iron ore sinter can have a significant impact on its structural integrity and overall quality as it can be seen by focusing exclusively on the 'Sinter' bars as depicted by Figure 3.9. Wu et al.[42] has found that the effect of these fluctuations is the acceleration of the reduction rate as the temperature rises. It has been reported that this can cause the sinter to expand and crack, which can compromise its integrity. It was also found that, at higher temperatures the sinter becomes more plastic and able to withstand some degree of expansion stress, which can limit cracking. There is a critical point in the reduction degradation process, when the hematite turns into magnetite completely, the inner stress of the iron ore sinter continues to increase, the plasticity of the iron ore sinter increases with the rising temperature, and the reduction degradation index goes on to increase. By closely monitoring the temperature and taking measures to control expansion stress and cracking, it is possible to produce iron ore sinter that yields the desired outcomes.

The combustion in the sinter process can result in inhomogeneity within the sinter bed. This can lead to a multitude of issues, including inconsistencies in gas flow and temperature history within the sinter bed[43 44]. The chemical reactions and shrinkage

that occur during the process can exacerbate these issues, which can ultimately impact the sinter yield and reducibility[45].

One of the primary concerns is the edge effect near the wall, which can result in a lower temperature and decreased sinter yield and quality. Additionally, the top layer of the sinter bed is also susceptible to lower temperatures, while the bottom part can become excessively hot[4446].

The quality of the sinter produced is of paramount importance in determining the productivity of the blast furnace[46], as well as the associated CO_2 emissions. Thus, it is imperative to make improvements in the sintering process to reduce the steel industry's carbon footprint and ensure that high-quality sinter is consistently produced.

3.4.2 Sinter Pressure

The quality of the sinter is greatly influenced by the temperature profile and the partial pressure of oxygen. The latter is crucial for igniting the Coke breeze, which then allows for the combustion of other reactions that produce CO and CO_2 in the bed. This paper[47] investigates what the effects were of the coke breeze rate and sinter gas flow on the temperature profiles. An example of the different zones and their respective reactions that take place whilst sintering is depicted in Figure 3.10.

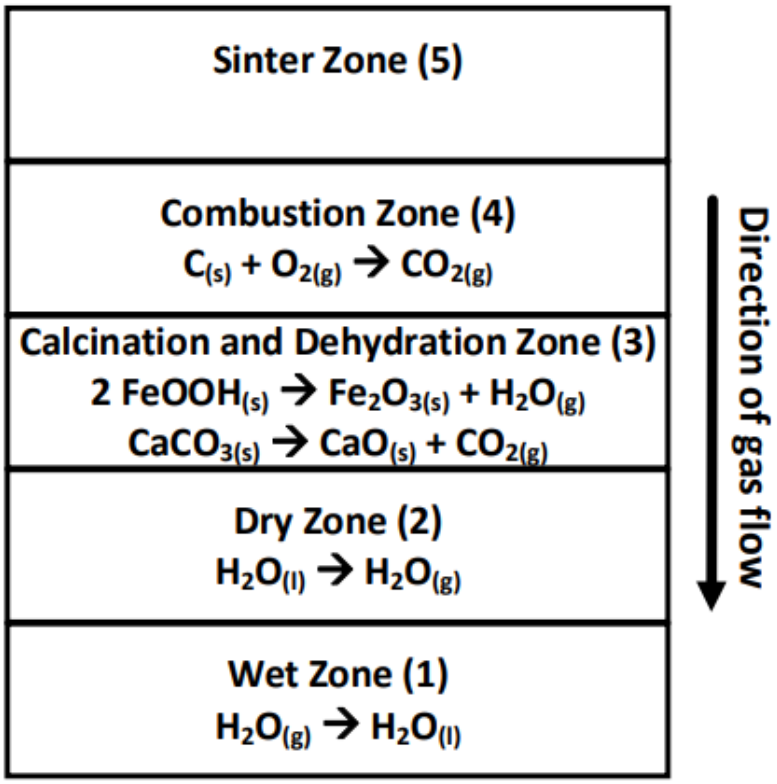

Figure 3.10 Different zones whilst sintering[47]

Previous studies[48] on this topic have shown that raising the coke rate results in an increase in the temperature of the sinter peak bed. Similarly, it has been reported by German et al.[49] that an increase in draft pressure leads to a decrease in the corresponding sinter peak bed temperature. German et al. found that increasing the coke rate resulted in a faster heating rate, along with a higher peak bed temperature that lasted for a longer duration. This is beneficial as it suggests that the sintering process was occurring for a longer period.

German et al. also found that the sinter was not exposed to the peak bed temperature for an optimal duration, which they reported was not ideal. Further exploration uncovered that the oxygen partial pressure and temperature profiles had a significant influence on the sinter's different phases. In this study, it was discovered that the transformation of pure hematite to pure magnetite is hindered when the partial pressure of oxygen decreases at a certain temperature. It's worth noting that using thermodynamic data for the respective phases can help predict the required amount of hematite and magnetite for the reduction reaction's spontaneity. Nicol et al's sinter pot

experiments found that hematite can be reduced to magnetite naturally in the air at a partial pressure of 0.21 atm at around 1330°C, which is also the peak sinter temperature in most sinter pot tests.[47]

Researchers are dedicated to improving the efficiency of the sintering process by studying its mechanisms. A study undertaken by Webster et al investigates the impact of partial pressure on the formation of Calcium Aluminium Ferrite (CFA), Silico ferrite of calcium and alumina (SFCA) and SFCA-I, to predict the optimal sintering conditions for producing high-quality sinter. Phase equilibria and XRD experiments were conducted from 298-1623K at partial pressure values of 1 x 10^{-4}, 5 x 10^{-3}, and 0.21 atm to characterise the phase evolution. Figure 3.11 illustrates the effect of phase concentration on temperature for different phases in iron ore sinter at 1 x 10^{-4} atm.

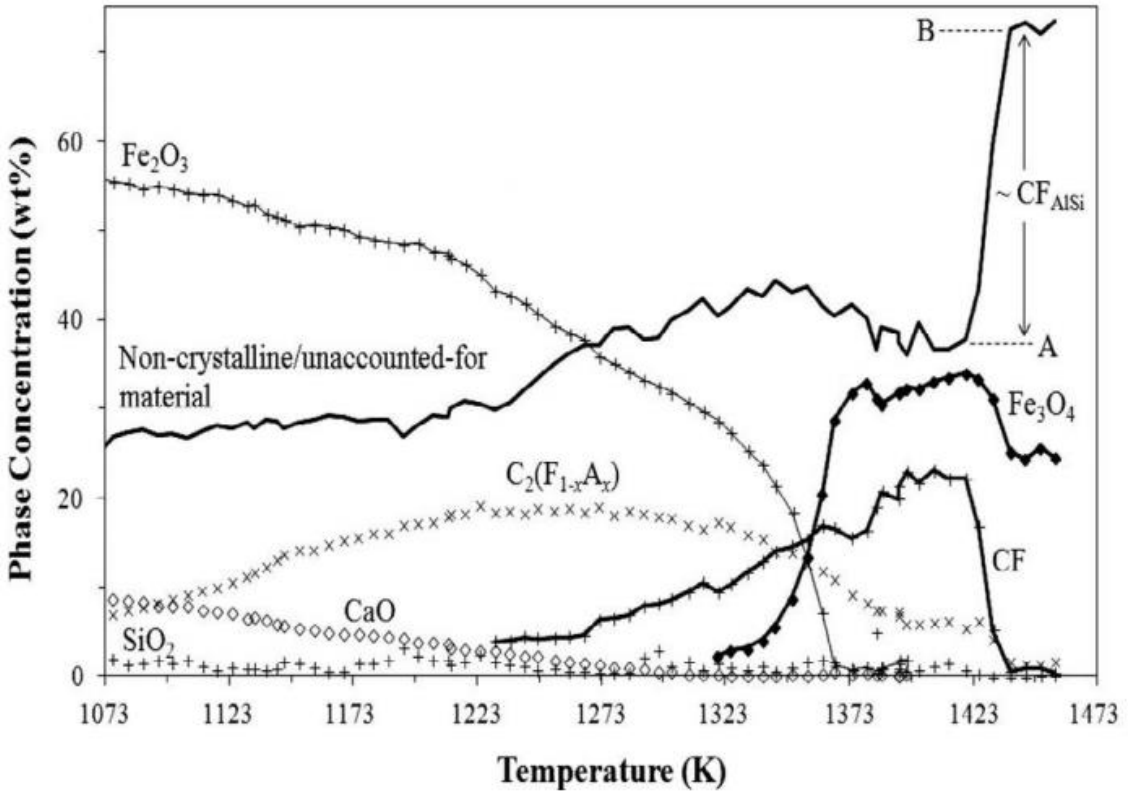

Figure 3.11 Rietveld refinement-based quantitative phase analysis at 1 x 10^{-4} atm[50]

Previous work has been carried out by Hsieh and Whiteman[50] where they found using the partial pressure of 5 x 10^{-3} atm ensured maximum production of Ca-rich ferrite phases, which are one of the most desirable bonding phases in iron ore sinter[51]. This

is due to its nature of being high in reducibility and mechanical strength, which also helps to produce a low reduction degradation index, which all aid in influencing the efficiency and productivity of the blast furnace. The results of the experiment indicate that the oxygen partial pressure significantly affects the formation of calcium aluminium ferrite (CFA), SFCA-I, and SFCA. Webster et al. discovered that high partial pressure leads to a decrease in the temperature required to form SFCA-I while maintaining stability. Furthermore, excessive partial pressure reduces the production of the critical precursor phase, CFA. On the other hand, low partial pressure prevents the formation of the most desirable SFCA-I phase.[50]

An article written by Chen et al[27] showed when the oxygen partial pressure is constant, the stability of iron oxides increases as the temperature rises, with hematite being the least stable, followed by magnetite and then wüstite. This means that lower sintering temperatures are more conducive to the solid transition of wüstite to magnetite and hematite, resulting in the thermodynamically favourable formation of SFCA.

3.4.3 Sinter Granulation Moisture & Permeability

Litster et al[52] investigated the kinetics of the sinter feed granulation as a function of granule size distribution which is a step which takes place before the sintering process. The experiments were carried out in a 0.5m diameter drum (pilot scale) to replicate the successful results on a large scale in the sinter plant. It was observed that there were two stages present to explain the growth of granules. The first was the fine particles tended to quickly adhere to the intermediate and bigger particles. The second is as the tumbling of the drum persists, the intermediate particles continue to be merged into the layers around the larger particles. This can be schematically represented in Figure 3.12.

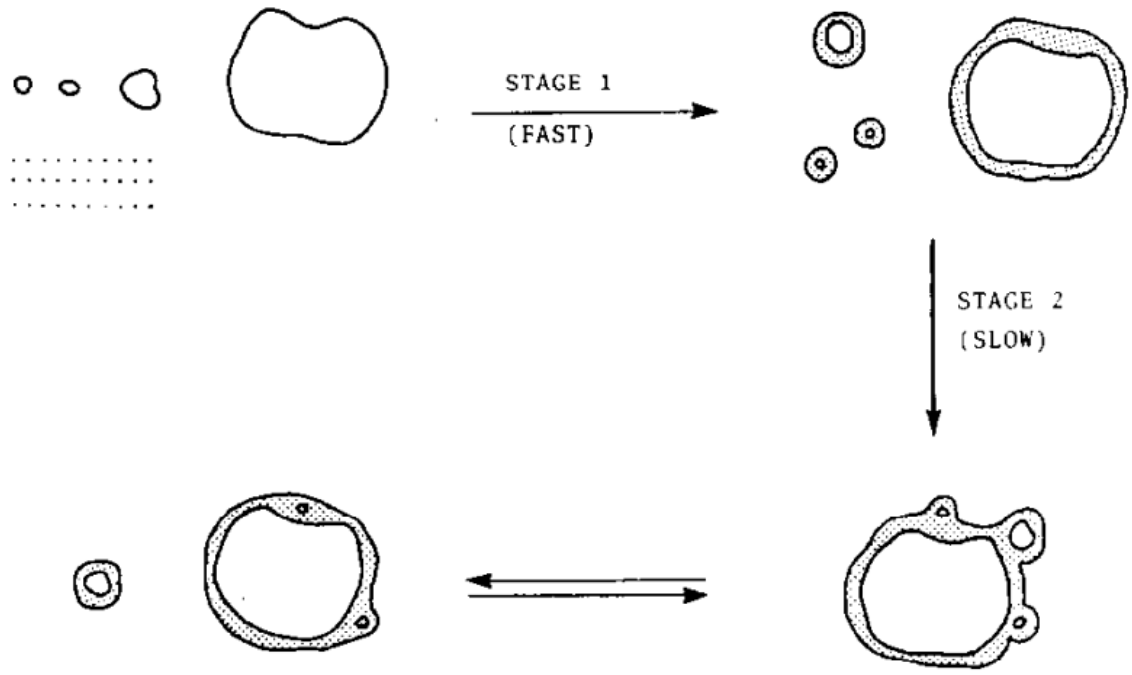

Figure 3.12 Granulation mechanism proposed by Litster[52]

The ability to calculate the granule size distribution at any given time was also mentioned in this paper from some previous work carried out by Litster et al and Roller[52] and was termed the population balance model. Although, it is important to note that these equations were based on the fact the partition coefficients must be known and on the assumption that an optimum granule size was present. Moreover, how the granulation kinetics was modelled in this calculation for scale-up purposes was a simple first-order global kinetic equation which demonstrated the change in the Sauter mean granule size with time. Experimental data and the data gathered from these models were plotted on a graph.

The population balance model was also tested against the experimental data. It was also found that plotting the partition coefficient against the time to find the rate constant for different particle sizes showed that the rate constant did not change very significantly with particle size. Thus, this is the reason why a constant value of 0.11 min^{-1} was chosen for 'k' from the global kinetic data. Results show that the Sauter mean granule size increased by 45% from 5 mins of the drum rotating to 30 mins of the drum rotating. Also, after these 30 minutes, the granules were said to be at their "maximum stable size". The granulation experiments carried out on the pilot scale

confirmed to the researchers that granulation time had a substantial effect on the productivity of the sinter pot. As the granulation time decreased and the granulation distribution improved the on-strand permeability and thus the strand productivity and ultimately the sinter quality could be improved. Litster et al found that from the experiments carried out the required residence time for a certain blend for granulation (t) is inversely proportional to the square root of the drum diameter (d) as shown in Equation 3.7.[52]

Equation 3.7 Required residence time for a certain blend for granulation.

$$t = \frac{1}{\sqrt{d}}$$

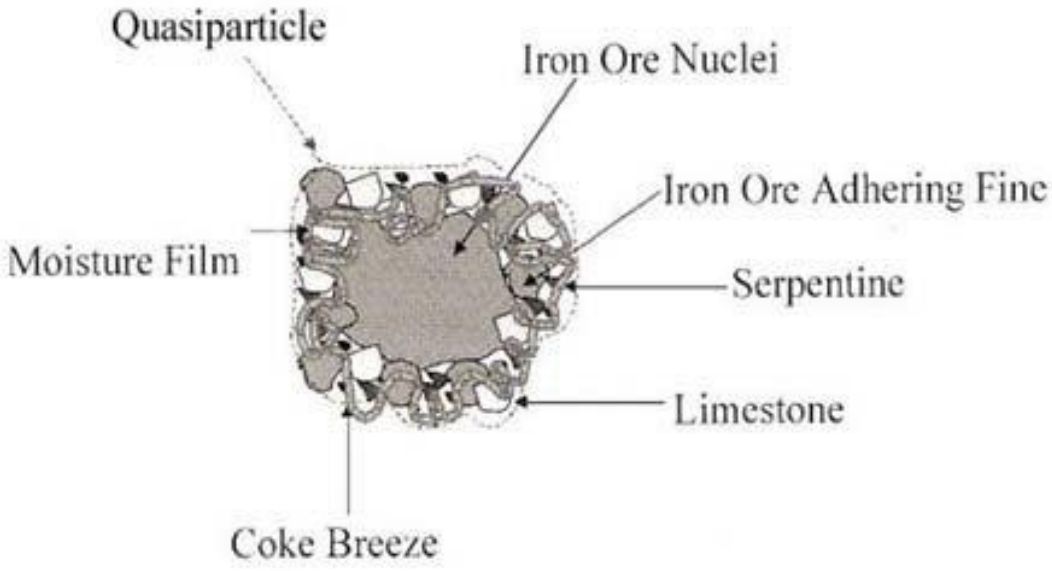

Figure 3.13 Typical 'quasi-particle' containing all the different constituents[25]

Nippon Steel Corporation (NSC) conducted the initial research on granulated raw mix structures and introduced the term "quasi-particle"[53]. In the field of materials science, the term "quasiparticle" refers to a distinct particle composed of an iron ore nucleus that remains partially unmelted during sintering. This nucleus is surrounded by finer ore grains containing silica gangue and is present in high basicity. As illustrated in Figure 3.13, a quasiparticle is comprised of larger nuclei particles exceeding 0.7 mm and smaller adherent fines below 0.2 mm. Minimising the number of particles between 0.2 and 0.7 mm is critical as they negatively impact mix permeability in two ways.

Firstly, as nuclei, they result in a smaller quasiparticle size, ultimately reducing bed permeability. Secondly, as adherent fines, they are poorly bonded and easily separate from the dry particles, further hindering bed permeability[54]. To counteract this issue, increasing the water content added to the raw mix during granulation can help intermediate particles adhere to the coarse nuclei. It is vital to note, however, that these particles may detach during drying, leading to a decline in the overall quality of the quasiparticle.

A study by Mathur et al. [55] has found that the iron ore sintering process can be affected by the amount of return fines. The study reveals that an increase in return fines leads to a decrease in sintering time due to the higher porosity of the sinter. However, it is important to note that too much sinter fines can negatively impact the strength of the sinter. Therefore, it is crucial to monitor the production of sinter fines to prevent overproduction and maintain control over the desired sintering time and optimal strength.

The effectiveness of a sinter plant is largely determined by the airflow rate and flame front speed during the sintering process, which are heavily influenced by the permeability of the sinter bed. Factors such as water addition, particle size distribution, ore porosity, surface properties of the iron ore, and the wettability of the iron ore by water all play a significant role in determining the granulation efficiency and permeability of the green sinter bed. Ultimately, the permeability of the sinter bed governs the productivity of the sinter plant, as well as the microstructure and other properties of the final sinter product[18].

It is crucial to understand that the sintering process favours diffusion bonding for larger particles and slag bonding for smaller particles. However, an excessive amount of smaller particles can lead to the formation of an excessive melt, which can have a negative impact on sinter bed permeability. Conversely, too many larger particles may not fully enter the melt, resulting in poor sinter characteristics and higher return fines. It is imperative to ensure the right balance of particle size for optimal sintering results.[18]

Optimising green granule bed permeability heavily relies on maintaining the appropriate moisture level. Inadequate moisture can hinder green granule growth, whereas excessive water can oversaturate and collapse the lower bed, ultimately leading to reduced permeability[37].

Mathur et al.[55] has determined that the optimal moisture level for the green bed is precisely 7%. This carefully controlled moisture level has proven to be highly effective in enhancing the bed's permeability and significantly boosting the flow rate of cold air. As a direct result of this precise moisture management, the sinter produced is of superior quality, delivering exceptional performance and reliability.

Previous findings from Umadevi et al.[17] showed when making iron ore sinter, having more moisture in the green bed makes it stronger. Insufficient moisture prevents the ideal agglomeration of fines, consequently filling the voids in the dry and wet areas. Water helps regulate temperature and makes sinter stronger by making the flame front sharper, but too much water can make the sinter bed structure collapse. Therefore, an optimum moisture level is important. Umadevi et al concluded, when increasing the moisture from 6 to 8% the sinter produced was stronger overall.

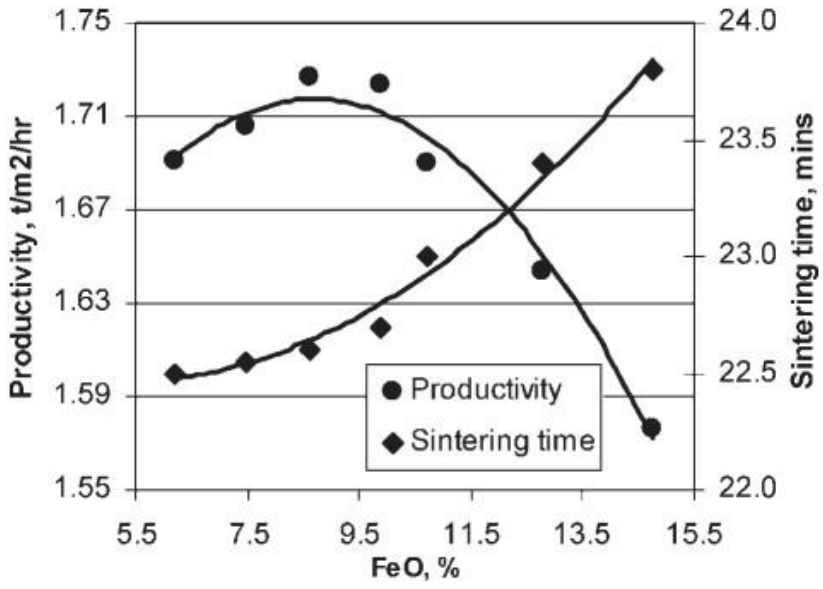

Figure 3.14 FeO content as a function of productivity and sintering time in iron ore sintering[38]

The effectiveness of granulation has a direct impact on the bed permeability and air flow in the sintering bed[56]. When permeability is improved, the velocity of flow

increases, sintering velocity speeds up, and the combustion of fuels and heat transfer between gas and solid are also improved[57] [58]. This leads to higher productivity and lower energy consumption.

The graph in Figure 3.14 illustrates the impact of FeO content on sinter productivity and sintering time. It was reported[38] as FeO levels rise, the sintering rate declines, and the time required for sintering increases. This decrease in rate is due to reduced sinter bed permeability, resulting in less air passing through the bed. The study[38] shows that sinter productivity rises initially and reaches its peak at a sinter FeO level of 8.60-9.88%. After that, productivity starts to decline as FeO content increases further.

A recent investigation[59] was conducted to explore the correlation between FeO and RDI. The study revealed that iron ore sinter with increased levels of FeO displayed remarkable RDI properties[59]. Furthermore, other researchers[38] explained that this phenomenon was due to the magnetite phase and an increased coke breeze rate during sintering. With the addition of higher levels of coke breeze, a stable wustite phase was formed. The weakening and degradation of sinter occur when there is an expansion in volume due to the phase transformation of hematite to magnetite. Additionally, it was discovered that further reductions of magnetite and wustite did not contribute to the intensity of degradation.

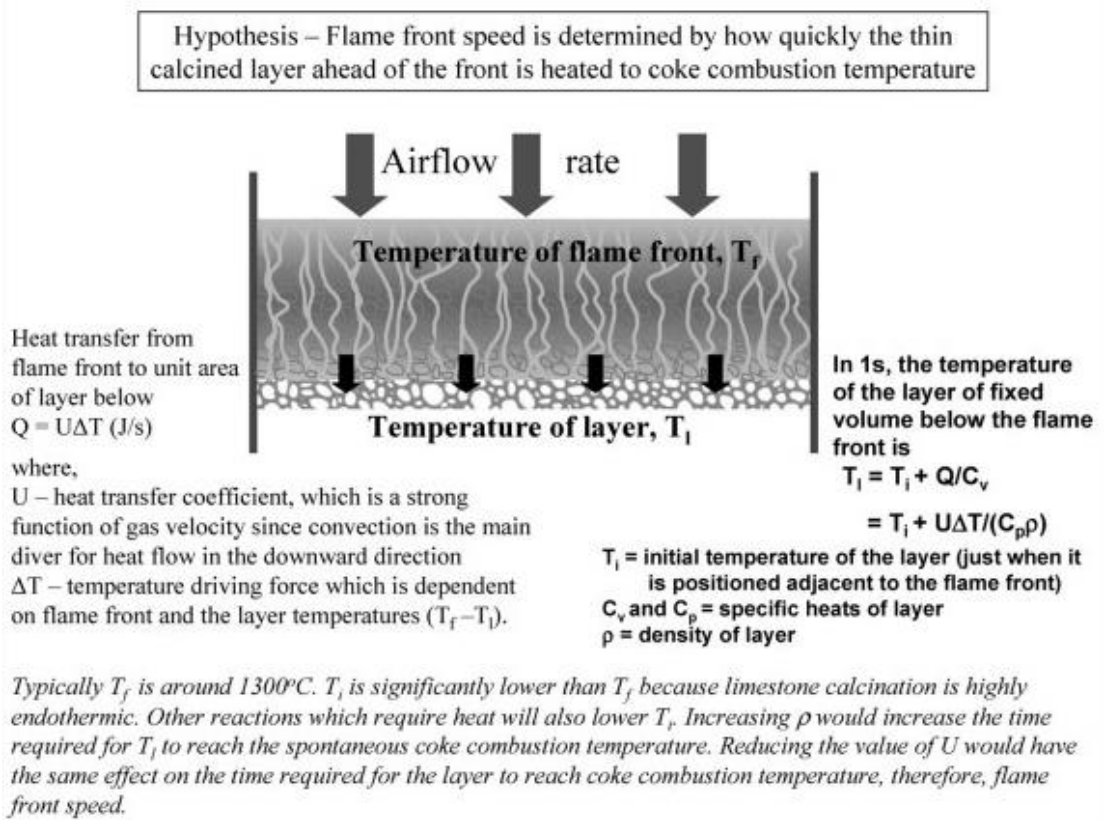

Figure 3.15 Factors impacting the sintering time and flame front speed[43]

The transfer of heat from the flame front to the thin layer through convection is crucial. Even though heat can be transferred through conduction and radiation, only convection causes the net downward flow of heat, which has a significant impact on the descent of the flame front. By increasing the rate of airflow, the downward transfer of heat through convection (represented by the convective heat transfer coefficient, U, in Figure 3.15) will also increase, thus increasing the speed of the flame front. Therefore, there is such a close relationship between granulation efficiency and productivity[43].

Bhagat et al.[59] has identified a notable association between the length of time spent on sintering and the RDI within the iron ore sinter. The findings demonstrate that an increase in the duration of sintering directly corresponds to an increase in the RDI, leading to a weaker sinter[59]. This phenomenon is attributed to the permeability of the bed, which has a significant impact on the RDI of the sinter. It is important to note that the RDI is a critical indicator of the quality and durability of the sinter, highlighting the importance of maintaining an optimal sintering duration for quality assurance purposes.

The reducibility of sinter is a critical property that is determined by its porosity and mineral composition. Porosity plays a significant role in gas-solid reactions, especially in the reduction of hematite. According to a study conducted by Restrepo et al.[60], it is recommended that the pore diameter of sinter should exceed 0.01 μm to facilitate the effective penetration of reducing gas into the pores, thereby enhancing the reduction of iron ore sinter.

In addition, the FeO content of sinter is another crucial factor that affects its reducibility. This is because FeO reacts with SiO_2 to form fayalite, which is difficult to reduce[11]. Consequently, higher FeO content in sinter translates to a lower reducibility. Conversely, increasing calcium ferrite and decreasing silicates can improve the reducibility of sinter[11].

3.4.4 Sinter Basicity

Sinter basicity is constantly globally recognised in the literature as the mass ratio between the amount of CaO and SiO_2 in the sinter. Basicity amongst a few other parameters can impact the SFCA formation within the sinter and thus the quality of the sinter. As well as this, an increase in basicity can lead to a fall in melt viscosity which allows the fluidity of the melt to develop which consequently betters the adjustment of the sinter. [27] The basicity of sinter is said to play an instrumental role in deciding the formation of the different mineralogy that is present in iron ore sinter. The different morphologies that are present also vary and this leads to large changes in quality indicators such as reduction degradation index (RDI) and reducibility index (RI). [28]

Similarly in an article by Hapugoda et al., it is said that varying the basicity impacts the different mineralogy that is present and consequently affects the metallurgical properties the sinter adheres to[61]. It was found that calcium ferrite is one of the primary bonding phases in sinter. With an increase in basicity, this phase becomes more abundant. In another article by Bolukbasi et al.[4] researchers found that when decreasing the silica content in iron ore sinter to increase the basicity it improves the

sintering productivity, RDI and properties. This improvement may be a direct result of the increase in basicity which decreased the porosity in the sinter.

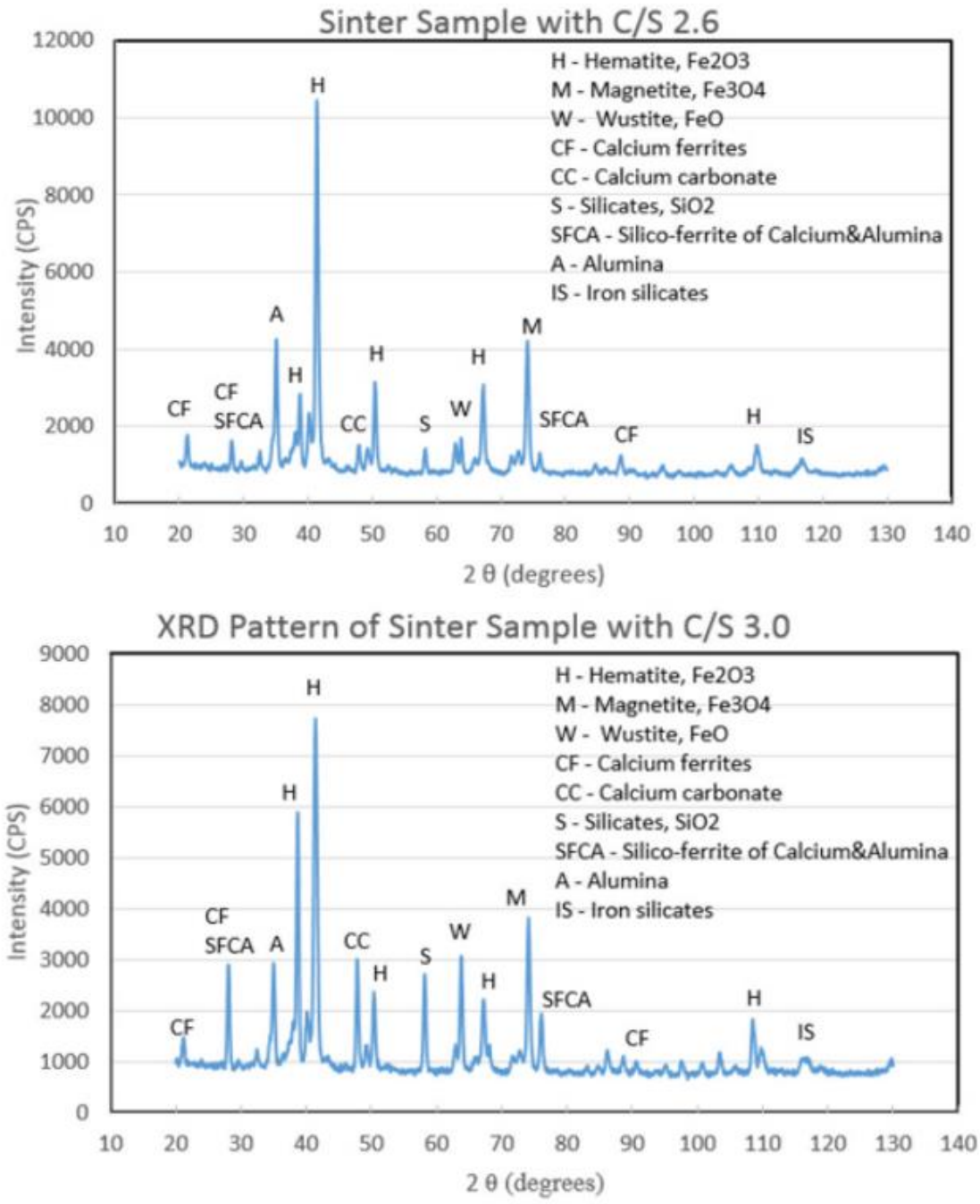

Figure 3.16 XRD patterns of sinter with different basicities[5]

Zhang et al mention how the basicity of the sinter is very important for the sinter quality. In this experiment, whereby the impact of sinter basicity was explored based on the outcome of the sinter quality and productivity in sinter plants which were

operating with a high rate of recycled materials. Zhang et al found that by increasing the sinter basicity the sinter productivity and reducibility increased. The reason for this increase may be attributed to the fact that as the sinter basicity was increased, XRD data showed that the peaks for silico ferrite of calcium and aluminium (SFCA) and calcium ferrites intensified which meant more of these mineralogical phases was present in the higher basicity sinter as can be seen from Figure 3.16.[5]. Webster et al found that using basicity higher than 1.5-1.8 tends to favour the formation of Ca-rich ferrites. On the other hand, lower basicity is said to favour the formation of calcium silicates and glass.[30]

Basicity is an extremely important parameter in a good-quality sinter. CaO is important in sinter as the products formed from the reactions that take place with the CaO help to reduce the decomposition temperature of $CaCO_3$. SiO_2 is also important as it takes part in key reactions with CaO and FeO during the sintering process. Figure 3.17 is a representation of how the basicity (value) affects the reducibility and strength of the sinter.

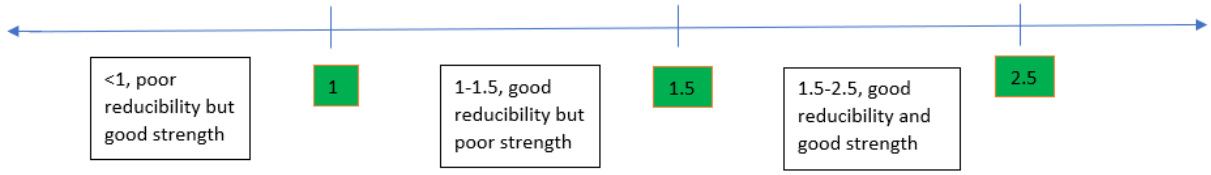

Figure 3.17 Schematic representing the effect of basicity on reducibility and strength of iron ore sinter[62]

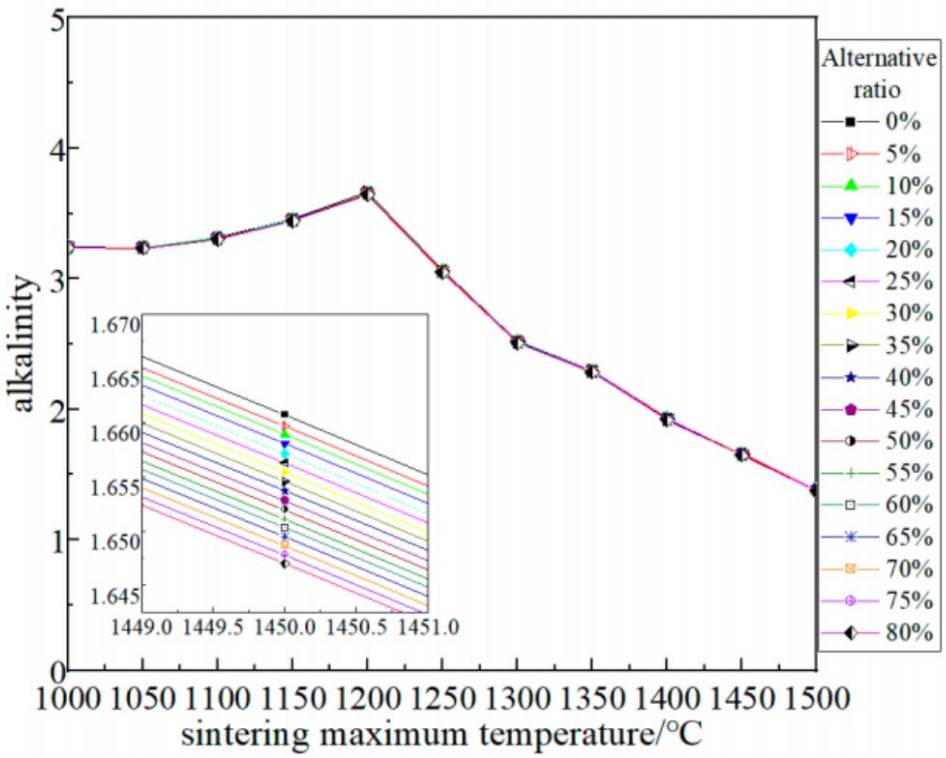

Figure 3.18 Variation in sintering maximum temperature and the corresponding effect on alkalinity[33]

Alkalinity refers to the alkaline compounds in the mix such as CaO and MgO. In this article, the author uses alkalinity to describe the basicity. As can be seen in Figure 3.18 in this experiment the level of basicity (alkalinity) is being measured as a function of the maximum temperature of the sinter. Initially, the basicity is seen to have increased from a sintering maximum temperature of 1000-1200°C. The basicity at this point was approximately 3.7 (peak). After this, as the maximum sintering temperature increases to 1440°C, the basicity fell to 1.7, which is generally the least the basicity can be for the sinter to still be of high-quality standard according to this article[33]. Zhou et al. believed that when the CaO level and thus the basicity is high the sintering maximum temperature is low, the amount of CaO rises because of increased temperature and as a result, the basicity increases too, but as the sintering maximum temperature keeps rising basicity will start to fall as can be seen from Figure 3.18.

FeO is formed via the ion Fe^{2+} and is a major compound which is commonly known to control the quality of the sinter. In this paper, it states that when the FeO content in the sinter is low there are negative consequences, one of which is lower strength of the

sinter produced. Moreover, when the content of the FeO is high it still does have some negative consequences such as vertical sintering speed, reduction degradation index and reducibility. Therefore, it is important to find a balance in the FeO content. In this article, it can be identified that the limit of the standard is 9%.

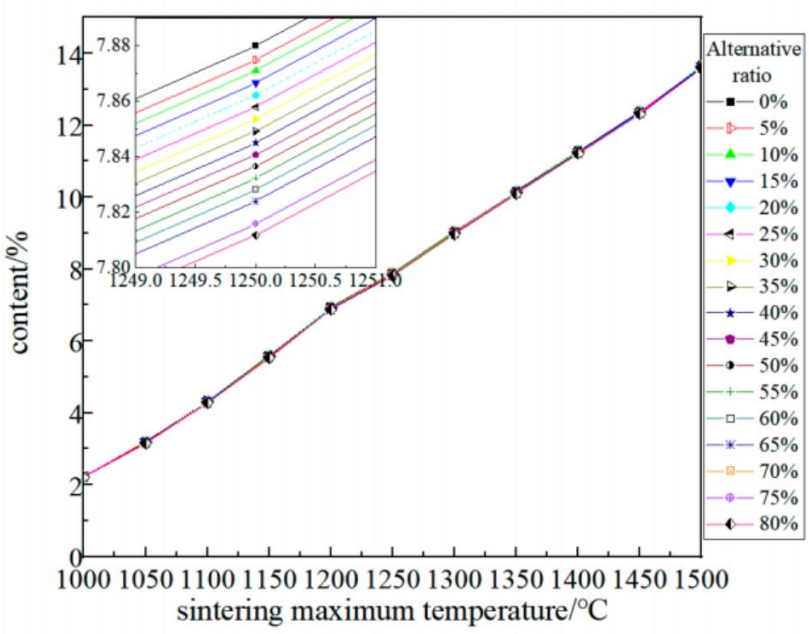

Figure 3.19 Variation in sintering maximum temperature and the corresponding effect on FeO content[33]

Figure 3.18 shows that when the sintering maximum temperature was at 1000°C the corresponding amount of FeO was at a low 2.2%. However, as the sintering maximum temperature increases the FeO content increases in the case of biomass charcoal substitution. Eventually, at 1300°C the amount of FeO reaches 9%.

In conclusion, from the figures above (Figure 3.18 and Figure 3.19) it can be said that when the maximum temperature for sintering reaches between 1200-1400°C the amount of FeO and the basicity can be at a standard where high-quality iron ore sinter can be produced. Also, the paper found that the chemical composition and metallurgical properties remained the same when producing sinter with coke breeze or biomass charcoal. However, as expected the biomass replacement had a significant impact on the pollutant gas emissions, all SO_2, NO_x, CO_2 and CO were lower in terms of the amount of emissions when using biomass charcoal as opposed to when using coke breeze.[33]

An interesting article by Jian-Ming Zhi et al[63] discusses the different structures that can be found in iron ore sinter as the basicity changes. Their study observed the structures present when the basicity ranged from 0.6 to 2.4. When the basicity was between 0.6-1.0, a granular and porphyritic mineral structure was evident (Figure 3.20). The mineral structure was relatively uniform, with magnetite distributed evenly and often cemented by a glassy phase. The distribution of hematite was not uniform, as it was primarily located around the pores. Within this range of basicity, the glassy phase material was the main bonding phase and was distributed uniformly. Data from this structure and basicity level indicated that the magnetite content in the iron oxide phases was significantly greater than the hematite content.

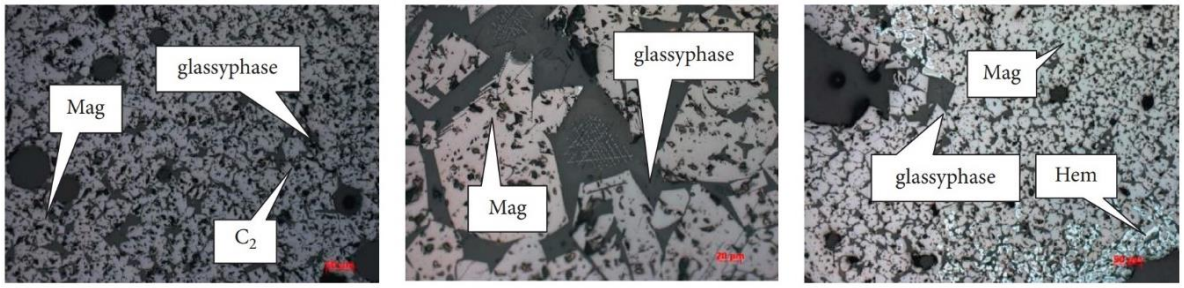

Figure 3.20 Granular and porphyritic structures between 0.6-1.0 basicity[63]

Looking at Figure 3.21 it can be seen that when the basicity increased to 1.5-1.6, the mineral structure became less uniform. The vitreous, dicalcium silicate (C_2S), and calcium ferrite sticking together, created what is called a local corrosion structure. Many corrosion structures could be clearly seen locally. In addition, magnetite, calcium ferrite, and dicalcium silicate were found together in the glassy phase.

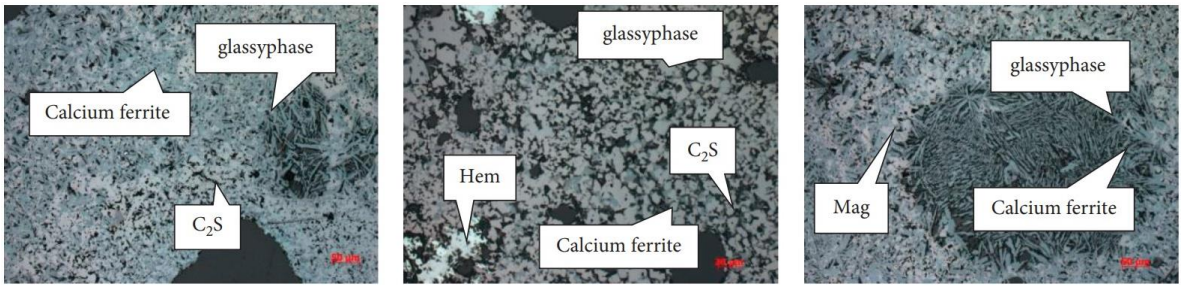

Figure 3.21 Corrosion structures between 1.5-1.6 basicity[63]

Based on Figure 3.22, it can be observed that the sinter with a basicity of 2.0 exhibited a more stable mineral structure, characterised by an interweaving corrosion structure. Such a structure is formed by the cementation of calcium ferrite and dicalcium silicate, while the content of hematite was low. Notably, the content of calcium ferrite reached the highest value in the entire basicity range, and the microstructure showed a significant presence of calcium ferrite, confirming the accuracy of the data.

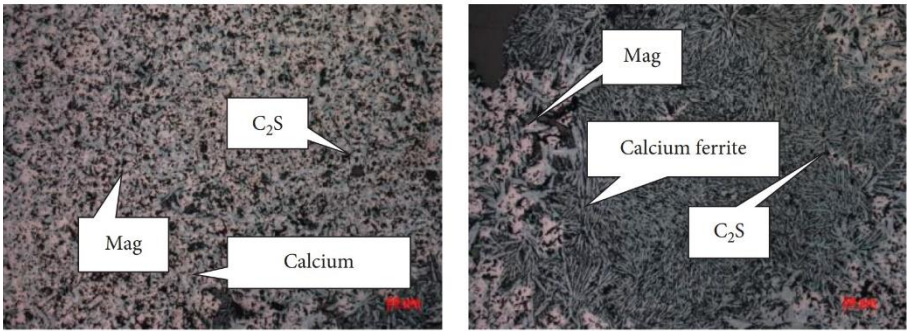

Figure 3.22 Interweaving corrosion structures at basicity of 2.0[63]

As the basicity increased beyond 2.2, Figure 3.23 shows the emergence of local corrosion and a porphyritic-granular structures. Additionally, a few cracks were visible. Magnetite started binding with the glassy phase and dicalcium silicate in the iron oxide phases, resulting in the formation of a porphyritic granular structure. Despite this, the distribution of hematite remained uneven, mostly concentrated around the pores, leading to reduced content.

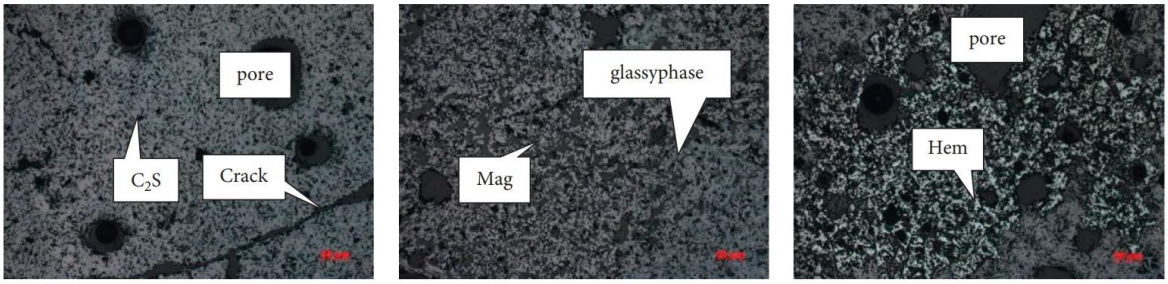

Figure 3.23 Corrosion & porphyritic structures between 2.2-2.4 basicity[63]

Umadevi et al.[64] analysed two types of alumina ores, one with high alumina content and the other with low alumina content. The main objective was to determine how sinter basicity affects sinter mineralogy, properties, and productivity. Figure 3.24 illustrates that an increase in sinter basicity led to a decrease in RDI for both types of

ores. It is important to note maintaining the blast furnace bed permeability requires monitoring the RDI parameter.

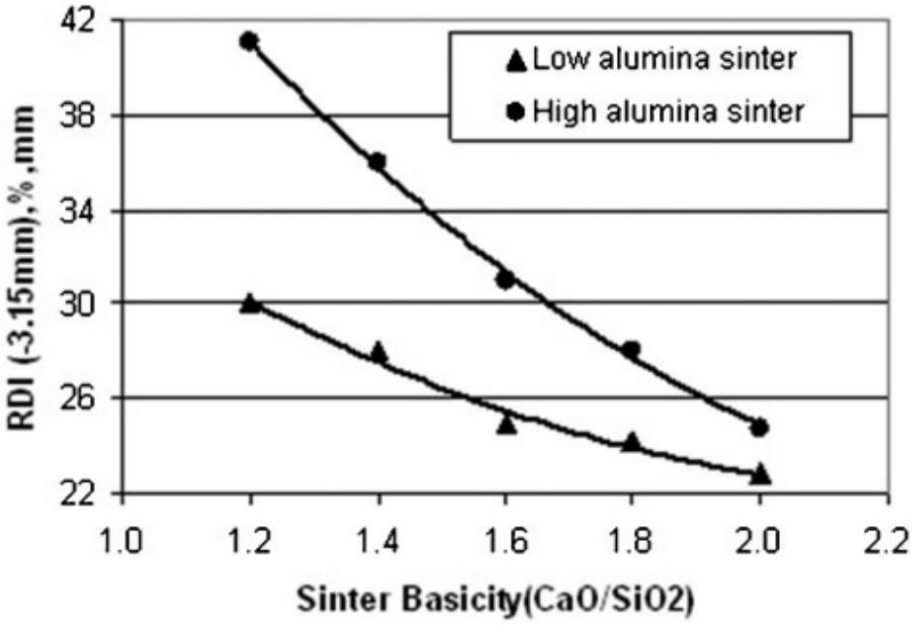

Figure 3.24 RDI results for high and low alumina sinters with basicity ranging from 1.2-2.0 [64]

Recent research indicates that if the basicity level is at 2.0, mineralogical analysis reveals that the sinter's structure may become heterogeneous, consisting of both acidic and basic phases[65]. This can lead to the formation of small cracks in the sinter, which may have a detrimental impact on its RDI[66].

Raising the basicity level of sinter production yields a promising reduction in sintering time. The increased air utilisation efficiency attributed to higher basicity levels results in a decrease in specific air requirement, thereby contributing to a shorter sintering time[67]. Furthermore, preignition permeability and average permeability show significant improvement[68]. The reduced resistance in the drying zone, a critical factor in water migration, leads to an increase in average permeability. Additionally, the combustion zone's resistance decreases, further enhancing the average permeability.

Nyquist et al discussed the reason of rapid sintering with lime additions, (and thus increase in basicity) particularly in relation to the combustion zone. High surface

tension and low viscosity of the melt, combined with short solidification time, and a high temperature coefficient of viscosity have been found to lead to fast sintering.

The research conducted by Nyquist et al.[69] investigated the underlying factors behind the rapid sintering process that occurs when lime is increased in the iron sintering process. The phenomenon is typically observed when the basicity level is increased, particularly in the combustion zone. It was discovered that the low viscosity and high surface tension of the melt are the root cause of this occurrence. Additionally, the solidification time is notably brief while the temperature coefficient of viscosity is relatively high, which collectively contribute to the rapid sintering process.

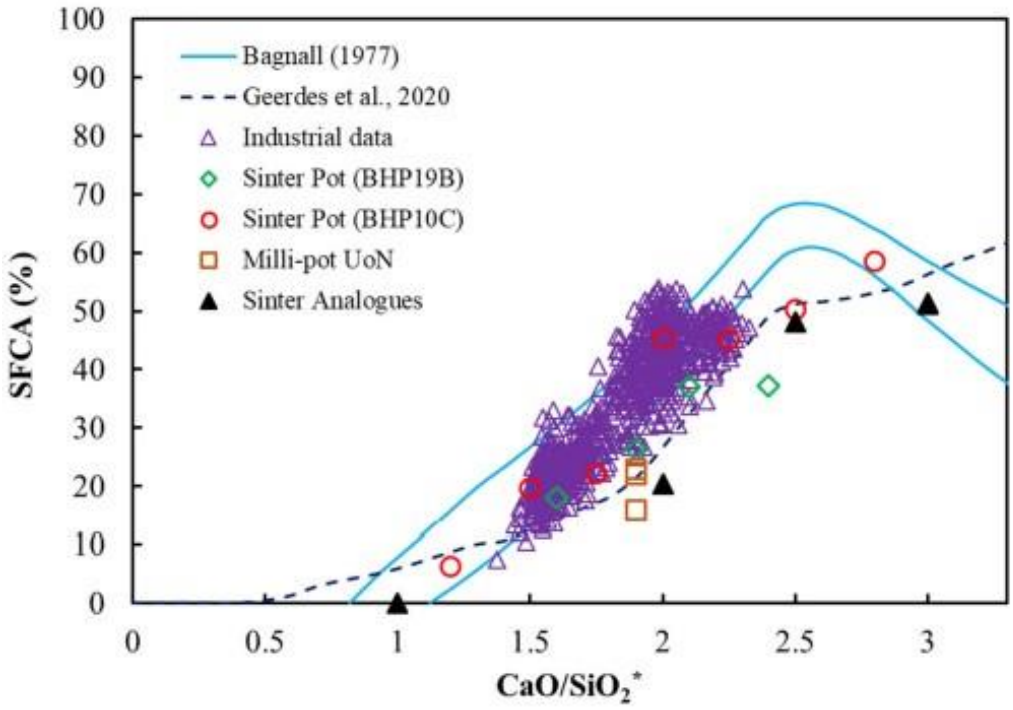

Figure 3.25 SFCA production (%) as a function of CaO/SiO_2 for different studies[70]

Based on the data in Figure 3.25, it is evident that the basicity level (CaO/SiO_2) has a significant impact on the formation of SFCA phase, as observed in various research studies. These studies have examined basicity levels ranging from 0.5 to 3.0. According to Bagnall et al.[71], the amount of SFCA production increased as the basicity level increased up to 2.5. However, at a basicity level of 3.0, the amount of SFCA began to decrease.

A comprehensive study on the influence of basicity levels on SFCA formation was conducted by Geerdes et al.[72], which yielded significant findings. The results indicated that an increase in basicity levels led to a proportional increase in SFCA formation. The research utilised data obtained from sinter pots BHP19B and BHP10C, as well as industrial data. The industrial data, as presented in Figure 3.25, revealed a vast sample of 805 data points, with the most frequent data points grouped around a basicity level of approximately 1.6 and 2.0[70 73 30].

3.5 Sinter Mineralogy

This section covers the essential mineralogy needed for high-quality iron ore sinter. It examined different amounts and reasons for using them, drawing comparisons from relevant literature. Key minerals, including SiO_2, Al_2O_3, and MgO, will be studied to determine the best ratios for iron sinter and their benefits. Additionally, this section will investigate hematite and magnetite, their effects, and how to treat them for ideal conditions. Finally, the SFCA and calcium ferrite structure will be introduced and analysed to determine optimum conditions for these phases.

3.5.1 Presence of SiO_2, Al_2O_3 & MgO

The level of silica is crucial in iron ore sintering. It serves as a fluxing agent, promotes liquid phase formation, and influences bed permeability, melting behaviour, and sinter microstructure. All these factors play a role in the quality and outcome of the sintering process. However, excessive levels of silica can lead to brittleness, as the formation of silicate phases can result in a sinter that is more fragile with lower mechanical strength.[74]

The presence of MgO in the sinter mix enhances the sinter strength and mechanical properties of the final product. It promotes improved bonding between particles, resulting in a stronger and more durable sinter. However, the excessive fluidity can be a problem whereby the high MgO content can increase the fluidity of the liquid phase, leading to poor granulation, reduced permeability, and irregular sinter structure formation.[75]

Chemical analysis of a research study taken place by Zhiyun Ji et al[76] showed that the presence of SiO_2 and Al_2O_3 is very important in the microstructure of a sinter. They are strongly believed to affect the metallurgical and mechanical properties of the sinter. A study was carried out where the presence of Al_2O_3 was tested against productivity and the Tumbler index. Productivity in this case was the amount of sinter being produced concerning time. Tumbler index in this case refers to the resistance of the sinter to degradation by impact. The factors that were kept the same throughout the experiment were the amount of SiO_2 which was approximately 4.8%, the basicity (CaO/SiO_2, mass ratio) which was 2, and the amount of MgO which was 2%. Permeability was also a factor which was considered to stay at a similar amount for each sintering bed, thus not allowing permeability to impact the sinter quality. Figure 3.26 below, is a representation taken from the study to portray the outcome of the experiment.

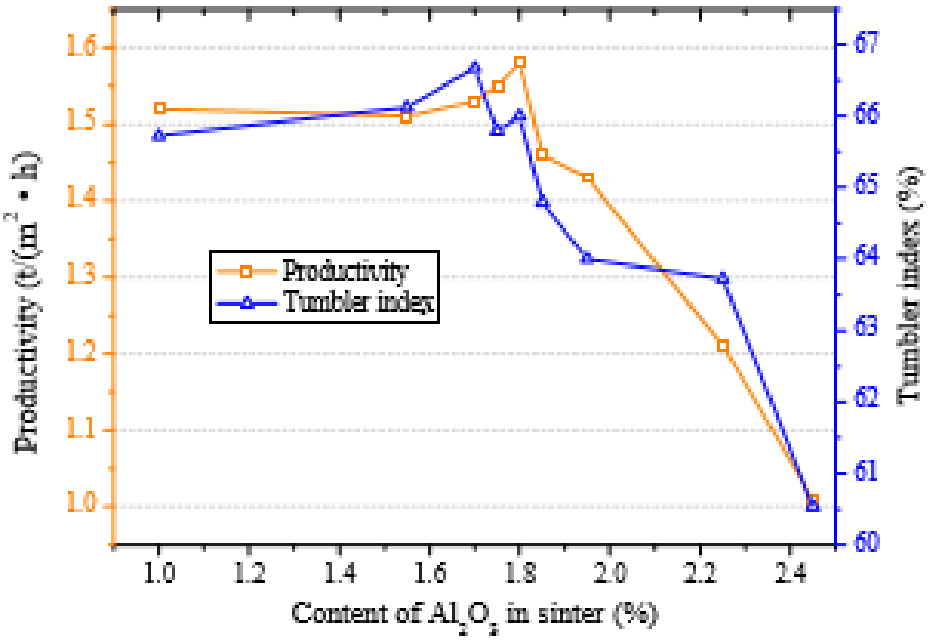

Figure 3.26 Effect of Al_2O_3 presence on tumbler index and productivity[76]

Figure 3.26 shows that up to approximately 1.8% from 1% of the presence of Al_2O_3, the Tumbler index and productivity did not change very significantly. Although when the content of Al_2O_3 was increased beyond 1.8% the Tumbler index and productivity both, plummeted significantly, indicating that at this amount a weakened sinter is

experienced. From this experiment, it can be deduced that the optimum amount of Al_2O_3 content that should be present in the sinter should be up to 1.8%.

Similarly, for the presence of SiO_2, Zhiyun Ji et al experimented to show the effect of SiO_2 on the Tumbler index and productivity. The factors that were kept the same throughout this experiment were the amount of CaO which was around 9.6%, the content of MgO which was 2%, and the content of Al_2O_3 which was around 1.6%. Figure 3.27 below, is a representation taken from the study to portray the outcome of this experiment.

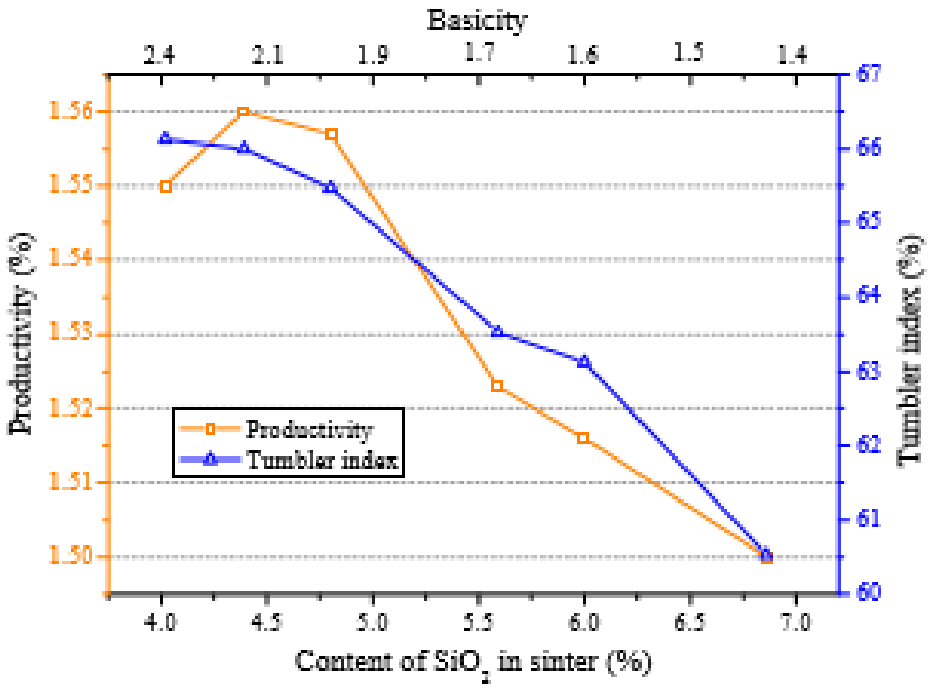

Figure 3.27 Effect of SiO_2 presence on tumbler index and productivity[76]

Figure 3.27 shows that up to approximately 5.5% from 4% of the presence of Al_2O_3, the Tumbler index and productivity dropped significantly, especially when the content of SiO_2 was at around 4.8% the Tumbler index was plummeting at an increased rate. The productivity is seen to have remained almost constant through the region of 4-4.8% of SiO_2 content, and after this amount, the productivity starts to plummet at a faster rate. Therefore, for this reason, it can be deduced that the optimum amount of SiO_2 content that should be present in the sinter should be up to 4.8%. [76]

An informative study by Bolukbasi et al.[4] investigates the chemical and physical properties of iron ores' influence on the sintering performance. This piece of literature states to lower the amount of SiO_2 (which is used to increase the basicity) and reduce the amount of MgO, this may improve the sinter. However, it can be observed that a decrease in the amount of SiO_2, could decrease the porosity in sintering, hence a balance or compromise must be found. It was found in this article that the content of MgO in sinter should be between the ranges of 1.2-1.7%. The reason the MgO improves the RDI is because magnetite is easily stabilised by MgO and as a result, the hematite produced is less. Therefore, later when the sinter is charged into the blast furnace there is a lower amount of stress on the sinter when the hematite-to-magnetite reduction reaction is taking place.

Furthermore, during this reduction, the porosity (which is negatively affected by too little MgO) needs to be high to promote the transformation from hematite to magnetite. Also concluded in this paper was, during the cooling stage of sintering, magnesia formed tends to slow the formation of reoxidised hematite. The secondary hematite is a product which can be detrimental to the degradability of the sinter and therefore is the most disadvantaged phase of the RDI. Most of the secondary hematite is reoxidised hematite. So, therefore, all the hematite that gets reoxidised is problematic for the RDI. The final reduction that takes place is the iron oxide to the metallic iron. Thus, the importance of the presence of FeO in sinter is crucial for this reason, as well as being informative about the coke rate[4].

Moreover, it gives information as to the thermal state of the overall process. The more the presence of FeO in the sinter, the less the reduction degradation index (RDI) is, which is what the blast furnaces demand. However, the more the FeO content, the less the reducibility, which the blast furnace does not demand[4]. Therefore, a balance must be met to fulfil both criteria that the blast furnace demands (high reducibility and low RDI).

Bolukbasi et al[4] claims a content of FeO of less than 8% will favour the reducibility. Another way in which RDI can be worsened is with an increase of alumina observed. This paper states that with experience in the industry, it has been observed that with a sinter of content, 10-10.5% CaO a rise of 0.1% alumina results in the RDI increasing

by 2 points. Therefore, it is beneficial if the amount of Al_2O_3 is low, approximately 1-1.6%. In addition to this, in an environment where the basicity is high more calcium ferrites are produced and thus is beneficial as calcium ferrite is known to be the main bonding phase in the sinter. When the hematite and the Fe_2O_3.CaO melt react in a solid liquid reaction they form the Silico ferrites of calcium and aluminium (SFCA). In this paper, the chemical formula was found of this 'SFCA' component, which is $5CaO.2SiO_2.9(Fe, Al)_2O_3$[4].

As per literature, an excess of MgO can prove to be detrimental to the productivity of a sinter plant. Figure 3.28 depicts that an increase in the percentage of MgO results in a significant decrease in plant productivity. Magnesium minerals are known to be challenging to assimilate, and in highly fluxed compositions, MgO acts as a refractory phase[77], causing magnesium to remain either in relicts or in reaction zones. The addition of MgO can create a melt with SiO_2 at temperatures above 1350°C and with Fe_2O_3 at temperatures above 1600°C, which increases the liquidus temperature of the melt, resulting in a reduction of the sintering rate[78]. Furthermore, the poor sintering behaviour of MgO and inadequate bond strength among sintered particles lead to increased return fines, which ultimately reduces productivity[79].

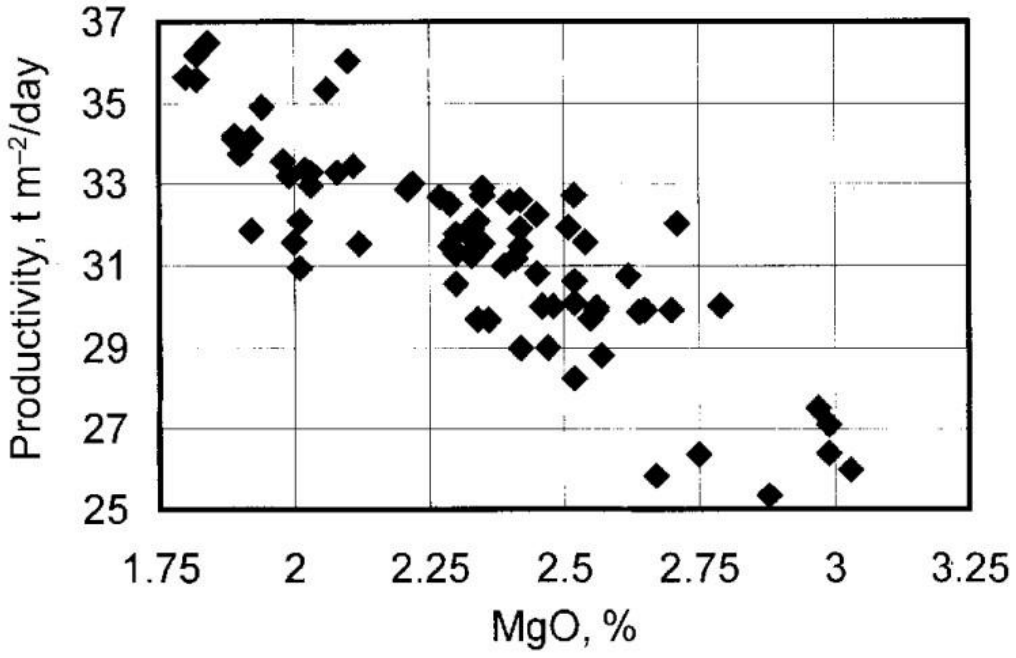

Figure 3.28 Productivity of a sinter plant as a function of the MgO content[79]

The microstructure of sinter products has a significant impact on their properties. Figure 3.29 demonstrates that sinter containing 3.9% SiO_2 had fewer SFCA's and more non-melted hematite and magnetite particles. Conversely, an increase in SiO_2 content to 4.2% resulted in the formation of platy SFCA's that held the solid particles of hematite and magnetite together. Further increases in SiO_2 content to 4.5% and 4.8%

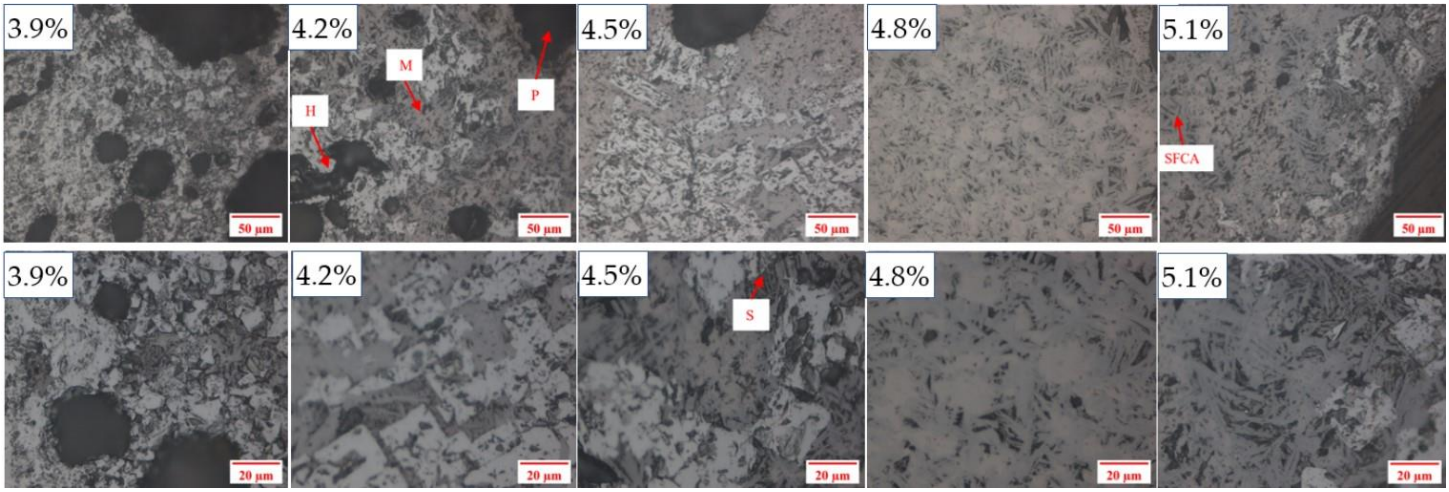

led to the generation of even more SFCA's, resulting in a dense and homogeneous structure that contributed to high mechanical strength and exceptional quality for the sinter product. However, when the SiO_2 content reached 5.1%, some siliceous mineral particles existed independently, leading to a relatively loose and inhomogeneous structure. Therefore, it is crucial to produce enough SFCA as the primary binding phase, which necessitates ensuring a sufficient level of SiO_2 to guarantee the mechanical strength and performance of the sinter.[80]

Figure 3.29 Microstructures of iron ore sinter with different SiO_2 content. (H- hematite, M- magnetite, S-silicate, P-pore) [80]

According to a study conducted by Zhang et al, laboratory pot-grate sintering tests were carried out to observe the impact of MgO and basicity on sinter microstructure. The results showed that higher concentrations of MgO improved lower temperature degradation but hindered the reducibility index. Additionally, it was found that sinter samples with higher MgO content produced more magnesioferrite phase and SFCA and SFCA-I phases, as observed through XRD analysis[81].

Compared to high alumina iron ore sinter, low alumina ore sinter demonstrated greater productivity and strength, as well as lower RDI. This is due to the higher presence of SFCA and magnetite phase, and lower pore phase[64].

The sinter properties are influenced by the presence of SiO_2 and basicity, and their effects are further impacted by the addition of MgO. A higher basicity level is beneficial for sinter properties, while an increased amount of SiO_2 has negative effects. However, the effects of both basicity and silica are weakened by the addition of MgO.[74]

During the sintering process, MgO level is controlled by the magstone added to the mixture, the MgO acts as a fluxing agent which promotes the formation of liquid phases. This, in turn, improves the sintering kinetics and strengthens the bonding between particles. Ponghis et al[78] found that when the basicity was low, adding MgO reduces the amount of hematite and increases magnetite formation. This comes at the cost of hematite, but ultimately improves the RDI. As well as this, Umadevi et al[74] also found that the addition of MgO resulted in an improvement in sinter RDI. This was because with the addition of MgO they also reported that hematite to magnetite formation was more, and this meant there was less availability of hematite.

On the other hand, it has been reported that the addition of MgO has been reported to speed up the thermal decomposition of hematite and promote the creation of the Fe_3O_4 ($FeO.Fe_2O_3$)–Mg phase, which is less reducible. Furthermore, the addition of MgO limits the formation of the melt, causing an increase in the sinter's porosity. This increase in porosity exposes more surface area to the reducing gases, leading to better reducibility, however a poorer RDI[79].

According to recent reports, it is recommended that the addition of MgO to iron ore sinter does not surpass 2.80% to attain the required sinter properties essential for the efficient functioning of the blast furnace[74].

SiO_2 plays a crucial role in the formation of the liquid phase, specifically calcium ferrite. This process is highly dependent on sintering temperature and atmosphere, ultimately impacting the overall sinter quality. A higher SiO_2 content contributes to the formation of additional silicate phases, which can then melt into calcium ferrite,

resulting in the formation of compounds like silico ferrite of calcium and aluminium (SFCA)[82]. According to research conducted by Liu et al, the presence of silica in iron ore sintering led to an improvement in the RDI results. Specifically, the RDI results increased from 58.03% and 66.50% to 63.93% and 68.28% with an increase in SiO_2 content[80].

Recent research[17] [83] [82] has demonstrated that an increase in alumina content in the sinter leads to a corresponding decrease in its strength. Figure 3.30 clearly depicts this trend by showing a noticeable decline in sinter strength as the alumina content increases.

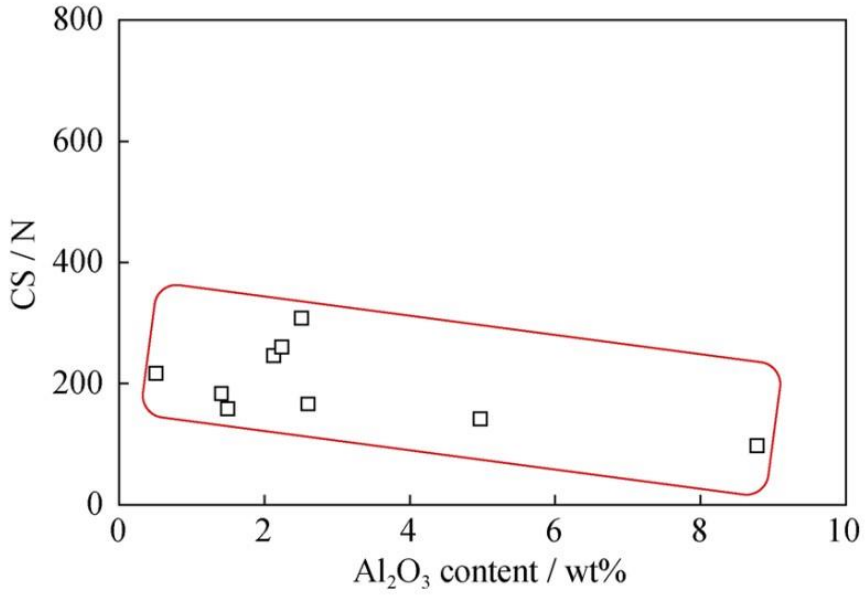

Figure 3.30 Alumina as a function of compressive strength (CS) of iron ore sinter[83]

Moreover, a different study by Guo et al.[84] has reported that the presence of high levels of SiO_2 in iron ores can result in an upsurge of silicate or glass phase in the bonding phase, while simultaneously decreasing the strength of the iron ore sinter. Moreover, an escalation in the SiO_2 content in iron ores may lead to a reduction in the amount of calcium ferrite formed, as more CaO reacts with SiO_2, ultimately leading to decreased sinter strength. Further research[83] has revealed that an increase in alumina content, as illustrated in Figure 3.30, corresponds with an increase in both pore area and size. This phenomenon results in a decrease in sinter strength.

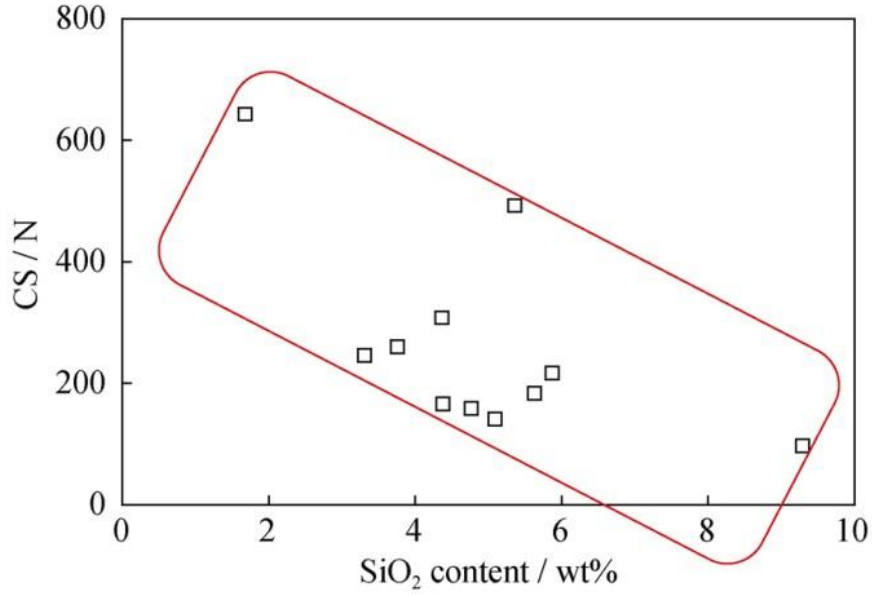

Figure 3.31 Silica as a function of compressive strength (CS) of iron ore sinter[83]

When the basicity is held constant, the addition of additional vitreous silica increases the CaO content of the material[13]. Researchers suggests that the sinter structure is more influenced by the CaO content than by the basicity. According to the Fe_2O_3-CaO-SiO_2 phase diagram, an increase in the CaO level beyond a certain point (approximately 30%) will result in a rise in the liquidus temperature. Therefore, it is critical to identify the optimal CaO level to ensure a solid sinter, as further increases may lead to reduced coalescence and reshaping[13].

According to a research conducted by Umadevi et al.[74], it has been identified that raw materials with high levels of magnesium oxide can trigger the replacement of Fe^{2+} by Mg^{2+} in the magnetite crystal lattice. This phenomenon leads to the formation of magnesium-containing magnetite and magnesium ferrite during sintering experiments. Consequently, the oxidation of magnetite to hematite is inhibited, which limits the production of calcium ferrite and encourages the formation of silicate[85]. As a result, there is a decrease in the mass fraction of calcium ferrite, while the magnetite content experiences an increase.

As per the research conducted by Hino et al.[86], it has been found that the inclusion of Al_2O_3 in iron ore sinter leads to a reduction in the temperature required for the primary melt formation. This, in turn, results in an increase in the hold-up of slag melt in the

pores of sinter. As a result, this adversely affects the sinter permeability resistance and indirectly affects the reduction process in the blast furnace. Hence, it can be concluded that the presence of Al_2O_3 in iron ore sinter has a significant impact on the overall efficiency of the blast furnace process.

Furthermore, in an in-depth investigation conducted by Pimenta et al.[87], a greater understanding of the impact of alumina on the breakdown characteristics of sinter at low temperatures has been obtained. The study reveals that the presence of Al_2O_3, whether as an inclusion or solid solution, is a key factor in the disintegration of secondary hematite. Specifically, the difference in the extent of expansion between hematite and Al_2O_3 results in internal tension, which eventually leads to the creation of cracks and brittleness in the sinter. These valuable insights into the fundamental mechanisms of sinter degradation hold significant implications to produce iron ore sinter.

3.5.2 Presence of Hematite & Magnetite

Hematite is very abundant as well as being present in many parts of the world's deposits, for this reason, it is extensively used in sintering processes. The presence of hematite can either be in the form of primary, secondary, or recrystallised. The primary form is what remains from the original material put into the blend. The secondary or recrystallised form is that which is obtained through the crystallisation of the molten phase which can be formed via three processes, by oxidation in the liquid phase of the magnetite crystals, directly being crystallised or synthesised by magnetite oxidation in the solid phase. An example of the difference between primary and secondary hematite from literature is demonstrated in Figure 3.32[88].

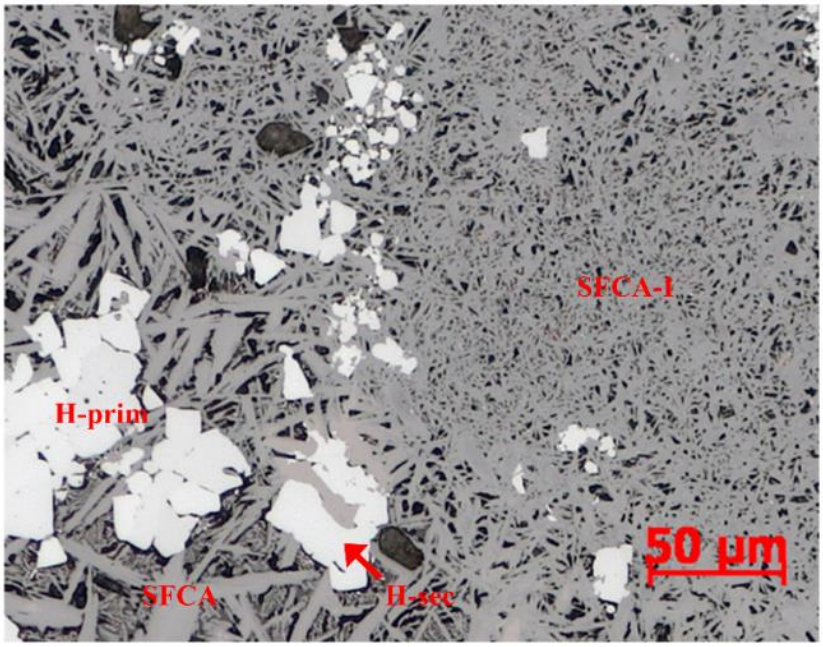

Figure 3.32 Reflected light photomicrograph at 50 microns showing the difference between primary hematite (H-prim) and secondary hematite (H-sec)[88]

Sinter quality and sinter reducibility usually are improved with the presence of higher hematite as opposed to magnetite. According to Bolukbasi et al[4], the structure of the sinter is improved with the increased presence of either primary or residual hematite and ferrites instead of secondary and precipitated hematite. Moreover, Bolukbasi et al found that the optimal structure found in the sintering process would be a hematite nucleus with an acicular ferrite lattice surrounding it.[4]

Alternatively, it has been understood from a study in Umadevi et al.[64] that the RDI of iron ore sinter is primarily affected by the levels of hematite and pore phase within it. As the levels of hematite and pore phase increase, the RDI of the sinter declines. Conversely, the presence of magnetite and acicular SFCA phase in the sinter can have a positive impact on its RDI.

The exact reasons behind the worsening of the RDI with an increase in alumina are still not fully known. Despite numerous studies, no agreement has been reached on the mechanisms that lead to RDI deterioration. In Japan, it is commonly believed that secondary hematite, also called skeletal rhombohedral hematite, is the primary reason for sinter's poor RDI[89]. This is mainly due to the frequent observation of cracks around the narrow neck regions of such hematite[90]. Some researchers[91] think that cracks

caused by a volume change during the transformation of hematite to magnetite are the main reason for a weak sinter reduction degradation.

Pimenta et al.[92] have come to a different conclusion, stating that hematite with alumina creates a magnetite phase that has a distorted structure during low temperature reduction. This, along with the structural deformation caused by the hematite crystal's volumetric change, can lead to the initiation and spread of cracks in the sinter. This ultimately results in a higher RDI.

It has been observed that Al_2O_3 tends to be concentrated in the secondary hematite when the transformation of Fe_2O_3 (primary) into Fe_2O_3 (secondary) occurs. Increasing Al_2O_3 and TiO_2 concentration in sinter is harmful for the RDI.

During the cooling process, magnetite can transform into hematite and react with the silicate melt to create a large quantity of columnar calcium ferrite, as seen in Figure 3.33(a). In Figure 3.33(b), magnetite is visible as an off-white colour with a granular structure. The inclusion of magnetite can improve sinter strength and productivity, due to its high melting point. The presence of predominantly magnetite in the inner sinter indicates a robust core.[93]

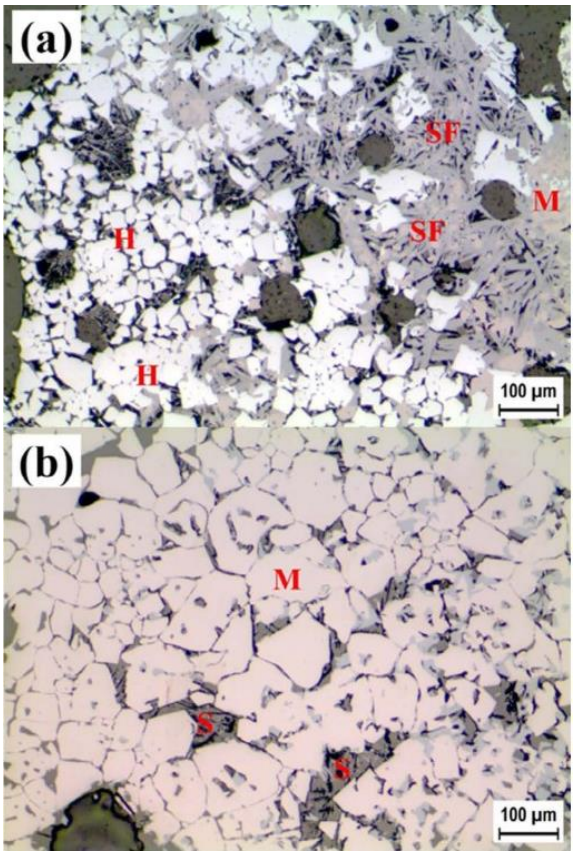

Figure 3.33 Typical microstructure of a sinter. (a) Outer and (b) inner of iron ore sinter[93]

The FeO content of sinter is directly related to the magnetite phase of the sinter. The effect of the magnetite phase on sinter FeO is illustrated in Figure 3.34. With an increase in the magnetite phase in the sinter, there is a corresponding increase in the sinter FeO[38]. Equation 3.8 shows that FeO (wustite) plays the role of a reactant in the formation of magnetite (Fe_3O4) during sintering. As the FeO content in the sinter rises, there is a greater amount of FeO available for reaction with hematite (Fe_2O_3), leading to the formation of more magnetite.

Equation 3.8 Formation of magnetite[94]

$$FeO + Fe_2O_3 \rightarrow Fe_3O_4$$

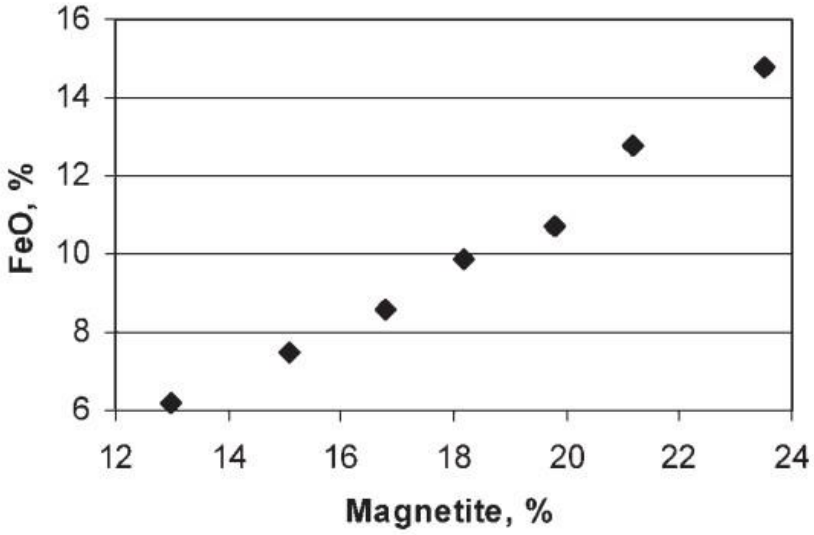

Figure 3.34 Magnetite as a function of FeO content[38]

During the process of converting primary hematite to secondary hematite, it has been observed that the compound Al_2O_3 tends to accumulate in the secondary hematite[11]. It is important to take into consideration, however, that increasing the concentration of Al_2O_3 in sinter may have negative effects on the RDI. Therefore, it is imperative to maintain a balanced concentration of Al_2O_3 during the transformation process to achieve optimal outcomes.

Throughout the reduction process, the creation of fines can be impacted by several different factors. These factors may include the mineralogical and chemical compositions of the sinter, as well as the specific process conditions being employed. Depending on the specific circumstances, these factors can activate one or more mechanisms, such as increased hematite reduction, higher residual stresses, or the presence of weakened areas within the overall structure[41].

Furthermore, the reducibility of sinter varies depending on the type of hematite present. Primary hematite, for instance, is more reducible than secondary hematite due to its intrinsic porosity[11]. Additionally, the formation of acicular ferrite at low temperatures (<1300°C) results in higher reducibility compared to columnar ferrite (>10 μm) formed at high temperatures (>1300°C), which is less reducible[11].

3.5.3 Presence of SFCA & Calcium Ferrites

The majority of sinter is generally composed of iron oxides, glasses, dicalcium silicate and silica ferrites of calcium and aluminium (SFCA). The SFCA phase is incredibly instrumental in aiding the bonding in iron ore sinter. As well as this it helps to improve the reducibility, mechanical strength, and reduction degradation[27].

There are two different types of SFCA's commonly found in literature. One takes the name SFCA and the other SFCA-I. SFCA is a low-Fe variation which is often found in a unique prismatic arrangement (morphology) and is usually observed as being blocky or columnar. Whereas the latter is a high Fe and low Si variation normally in a platy arrangement (morphology) and is observed as being acicular in cross-section and needle-like.

The processing conditions as well as the chemistry of the sinter blend is what determines which of the two forms is found in the produced sinter. Scarlett et al.[31] came to the following conclusion after an investigation into the formation of SFCA and SFCA-I. Where it was discovered routes to the synthesis of SFCA, and SFCA-I which is depicted in Figure 3.35. The most important part of the routes is where the ferrites are formed, and this happens as hematite first reacts with the CaO at a temperature of 750°C to form the ferrite $2CaO.Fe_2O_3$ (C_2F). The C_2F then reacts with some of the remaining hematite to form the next ferrite at 1000°C which is $CaO.Fe_2O_3$ (CF). Eventually, the mechanism in which the final SFCA and SFCA-I are produced is from a solid-state reaction. [31]

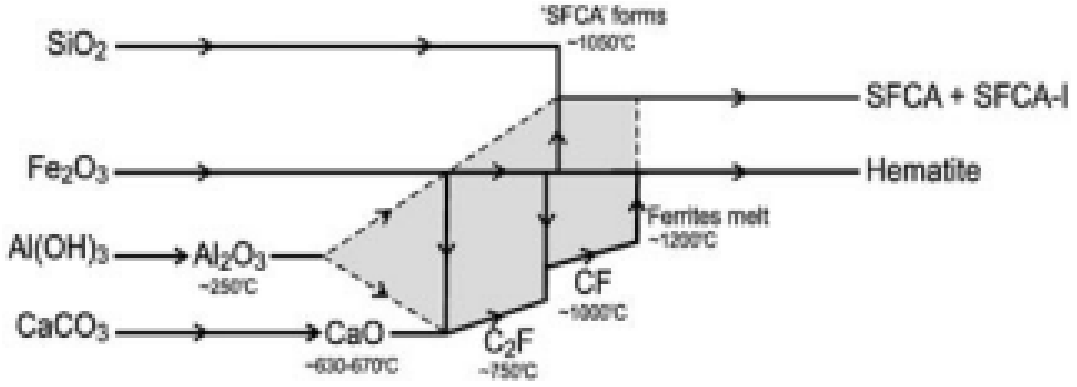

Figure 3.35 Reaction sequences for the formation of SFCA and SFCA-I (C2F and CF are abbreviations for dicalcium ferrite and calcium ferrite respectively)[31]

When evaluating new sinter mixes mineralogically, the concentrations and morphologies of the silicoferrites of calcium and aluminium (SFCA) are essential. These bonding phases, with stoichiometry M14O20 for SFCA and M20O28 for SFCA-I (where M represents Ca, Fe, Al, and Si), significantly impact sinter quality and blast furnace performance.[95]

The SFCA phase is incredibly important to iron ore sinter. The integration of CaO and Al_2O_3 into the liquid phase enables the resulting phase to interact with iron oxide, resulting in the formation of acicular calcium ferrites[96]. The SiO_2 and Al_2O_3 are produced as dissolutions (solid). The phase produced is commonly referred to as silico ferrites of calcium and aluminum (SFCA)[96], and is advantageous for the iron ore sinter structure in terms of enabling good reducibility[24]. The relationship between SFCA formation and the sinter quality is of great importance as the presence of SFCA can influence the mechanical strength, reduction degradation as well as reducibility, which are all parameters required by the blast furnace[27]. As stated by Umadevi et al.[18] sinter with better strength, lower fines and lower RDI were subject to effective distribution of acicular SFCA phases. This was one of the key findings made when observing the influence of iron ore fines feed size on microstructure.

According to Pownceby et al.[32], low-temperature iron ore sinter should ideally consist of unreacted hematite nuclei making up approximately 30% of the composition. The remaining 70% should be a porous matrix comprised mainly of SFCA. Figure 3.36

illustrates the difference between a poor and good matrix in iron ore sinter containing the two SFCA's. In the undesirable (poor) microstructure, there are noticeable areas of silicate glass that have mixed with magnetite and the columnar SFCA texture. This type of microstructure is considered inadequate. Conversely, the desirable (good) microstructure consists of a significant amount of the acicular SFCA-I phase. A study conducted by Harvey et al. explored the reducibility of sinter and sinter phases. Based on their findings, SFCA-I, identified through XRD analysis, demonstrated greater reducibility when compared to SFCA[97].

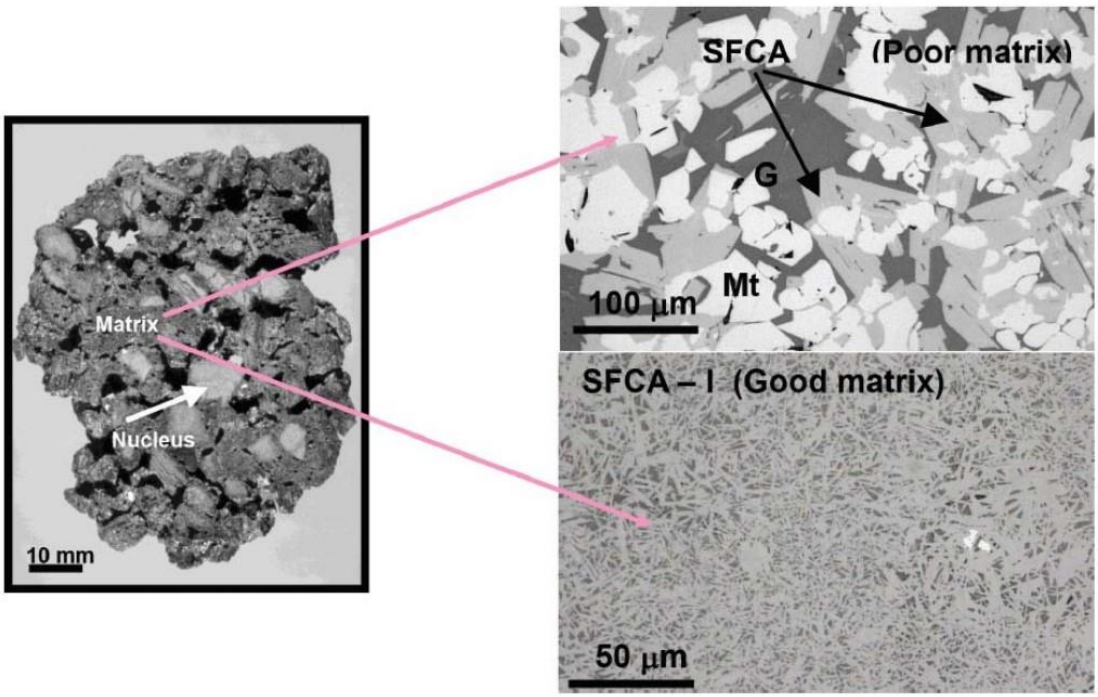

Figure 3.36 (Left) Macrostructure of iron ore sinter. (Right) optical micrograph microstructure of SFCA-I and SFCA matrix textures[32]

In earlier research conducted by Hapugoda et al[98], the SFCA phases were distinguished through optical micrographs. The prismatic/columnar SFCA phase, referred to as "S2", is illustrated in Figure 3.37 (a) and Figure 3.37 (b), while Figure 3.37 (c) depicts the platy/blocky SFCA-I phase, labelled as "S1".

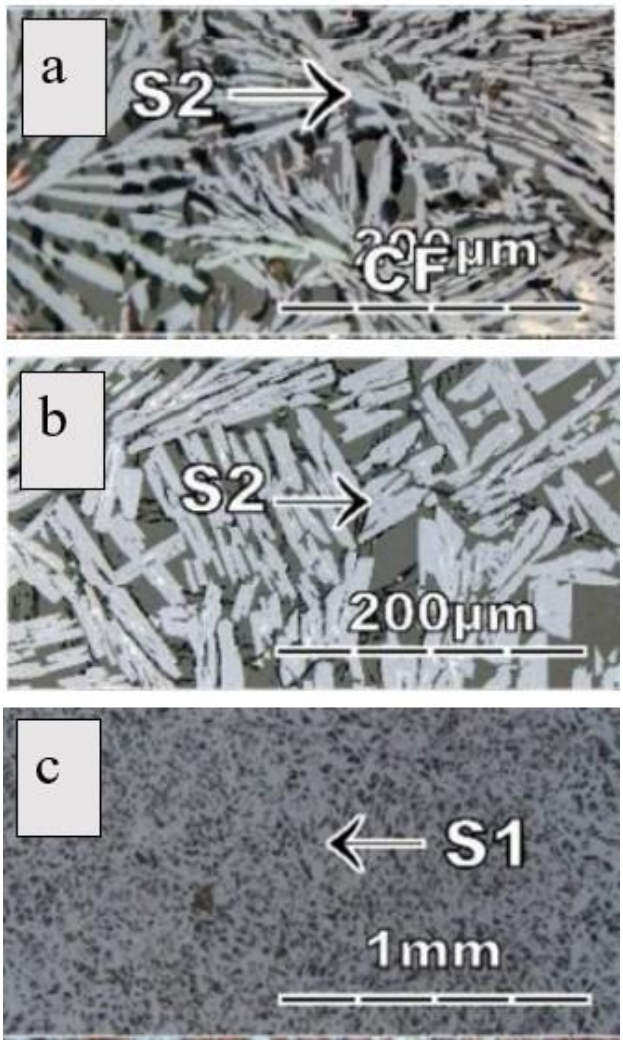

Figure 3.37 a) First variation of SFCA from literature. b) Second variation of SFCA from literature. c) SFCA-I from literature [98]

Liang et al. conducted a recent study on the impact of differing levels of basicity on the formation of SFCA in sinter. The study found that there was a gradual increase in the formation of SFCA as basicity levels increased from 1.8 to 2.0. Figure 3.38 illustrates SFCA as grey particles (red). At a basicity level of 1.8, SFCA formation was minimal, and the crystals were small. However, as basicity increased to 1.9, SFCA content increased, resulting in thicker, stripe-shaped, and columnar crystalline grains. At a basicity level of 2.0, the SFCA content reached its highest value (25.1%), and the crystalline grains became even thicker. The study also found that some of the solid iron oxide phases (which are the lighter phases in colour) are surrounded by the SFCA, thereby enhancing the binding force of the liquid-solid phase and increasing the strength of the sinter. As SFCA is a critical mineral in the binding phase of aluminum-

containing sinter, a higher content of SFCA leads to a stronger sinter. Consequently, a mixture with a basicity level of 2.0 is likely to exhibit the highest sintering index.[99]

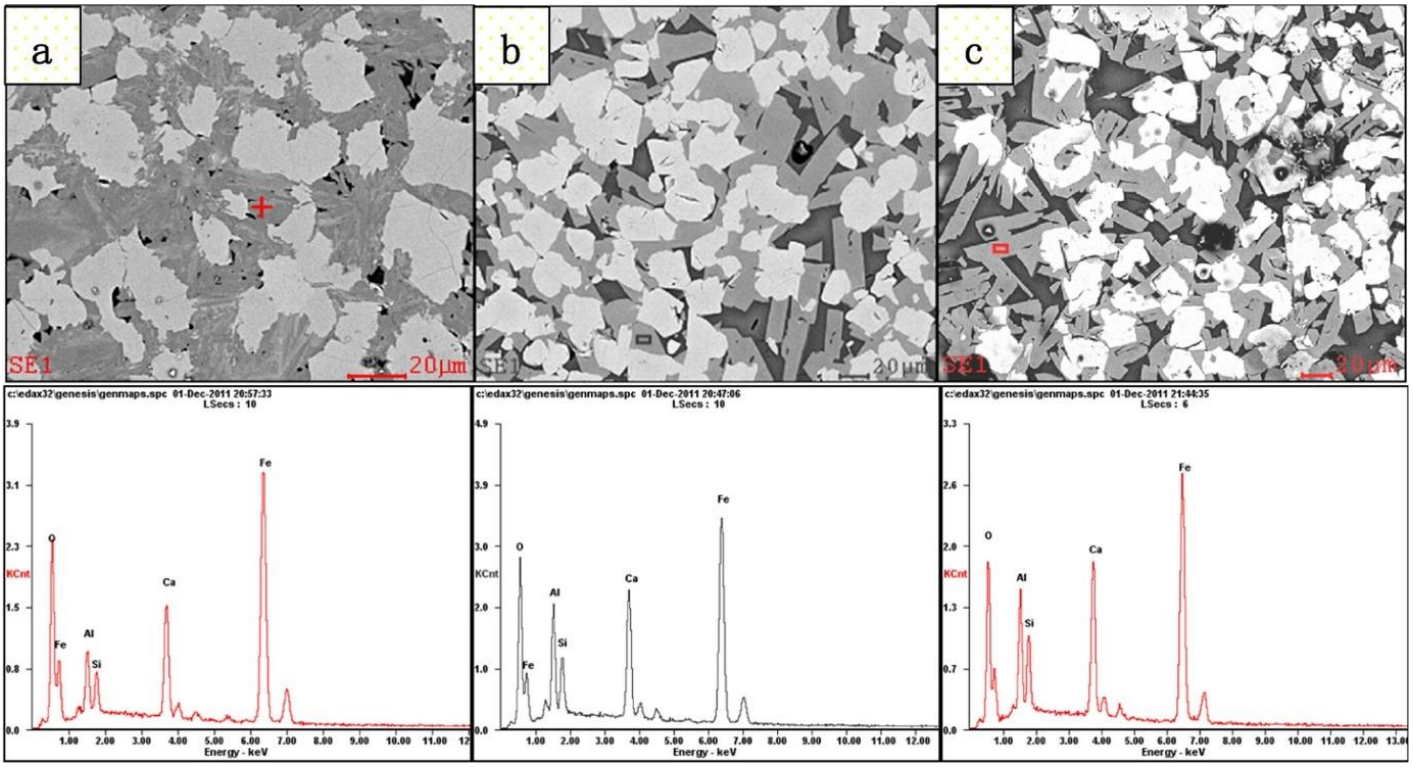

Figure 3.38 SEM images and corresponding EDS spectrum for SFCA formation with varying basicities a)1.8 b)1.9 c)2.0[99]

The tumbler index is a crucial parameter used to measure the ability of a particular material to withstand various stresses and strains that it may encounter during transportation, handling, and storage. In the context of industrial processes, particularly in the steelmaking industry, a higher tumbler index value is considered desirable as it suggests that the material possesses excellent handling properties and produces minimal dust. In contrast, a lower tumbler index value implies that the material may disintegrate into fine particles, which can lead to operational difficulties and increased dust levels. Therefore, the tumbler index serves as an essential tool for assessing the quality and suitability of different materials for various industrial applications[100]. Recent research[18] has uncovered a significant correlation between an increase in the SFCA phase and a corresponding increase in the tumbler index. The findings have been clearly illustrated in Figure 3.39. Essentially, the data suggests that the presence of SFCAs plays a crucial role in enhancing the strength of the produced iron ore sinter.

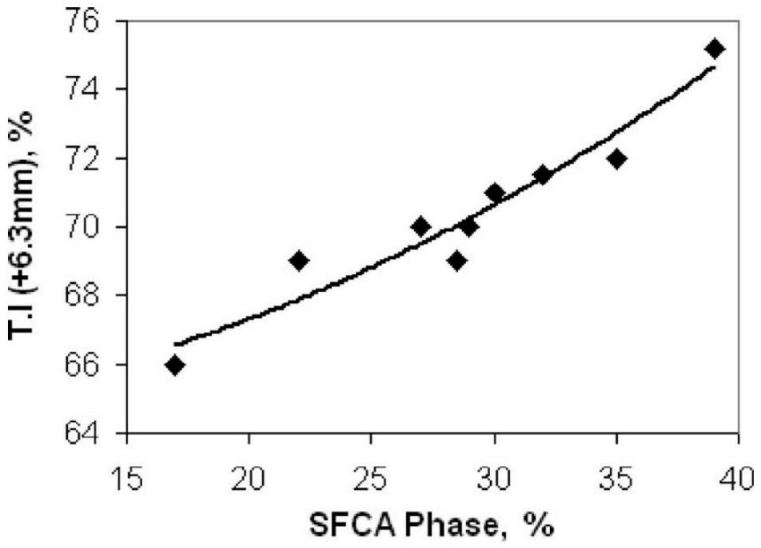

Figure 3.39 Effect of tumbler index as a function of the SFCA phase in iron ore sinter[18]

Recent research has uncovered a noteworthy correlation between temperature and the concentration of SFCA. Lower temperatures appear to result in higher concentrations, which can be attributed to the decomposition of carbonates and subsequent reduction in sintering temperature[101]. This finding holds implications for both understanding the factors that determine SFCA concentrations and optimising temperature control in production processes.

Based on recent findings, it has been determined that the inclusion of calcium ferrites within sinter is of utmost importance due to their ability to effectively absorb and mitigate the mechanical impact resulting from disintegration during low temperature reduction processes[41]. Such a feature is deemed necessary for ensuring optimal sinter quality and overall operational efficiency.

McAndrew and Clout's[102] research reveals that the presence of intersecting microplates within the SFCA-I texture significantly bolsters the strength and reducibility of iron ore sinter. Sinters that contain a significant amount of this specific phase are widely regarded as being of superior quality when compared to those primarily consisting of SFCA. These findings have significant implications for the iron ore industry, as they highlight the importance of understanding the role that different microstructures play in the quality and performance of iron ore sinter.

3.5.4 Identification of Different Phases

In this section, the focus will be centred on the various techniques that have been utilised in the past to identify mineralogy. The aim is to provide a comprehensive literature review that will help in making informed judgements about the microstructures that are present in the Intellesis images produced in this project.

Honeyands et al.[88] used optical image analysis, point counting, quantitative X-ray diffraction, and two scanning electron microscopy systems, namely QEMSCAN and TIMA, to identify minerals. They found each method had its own advantages and disadvantages depending on the desired result. Together, they provided a comprehensive understanding of the amounts, textures, and chemical compositions of the mineral phases. However, there were differences between QXRD and microscopy techniques. QXRD identified more amorphous concentration, while microscopy detected higher amounts of magnetite, total SFCA concentration, and more glass content. Although microscopy provided chemical analysis, it did not always match the textural types. Further research is needed to differentiate SFCA and SFCA-I phases.

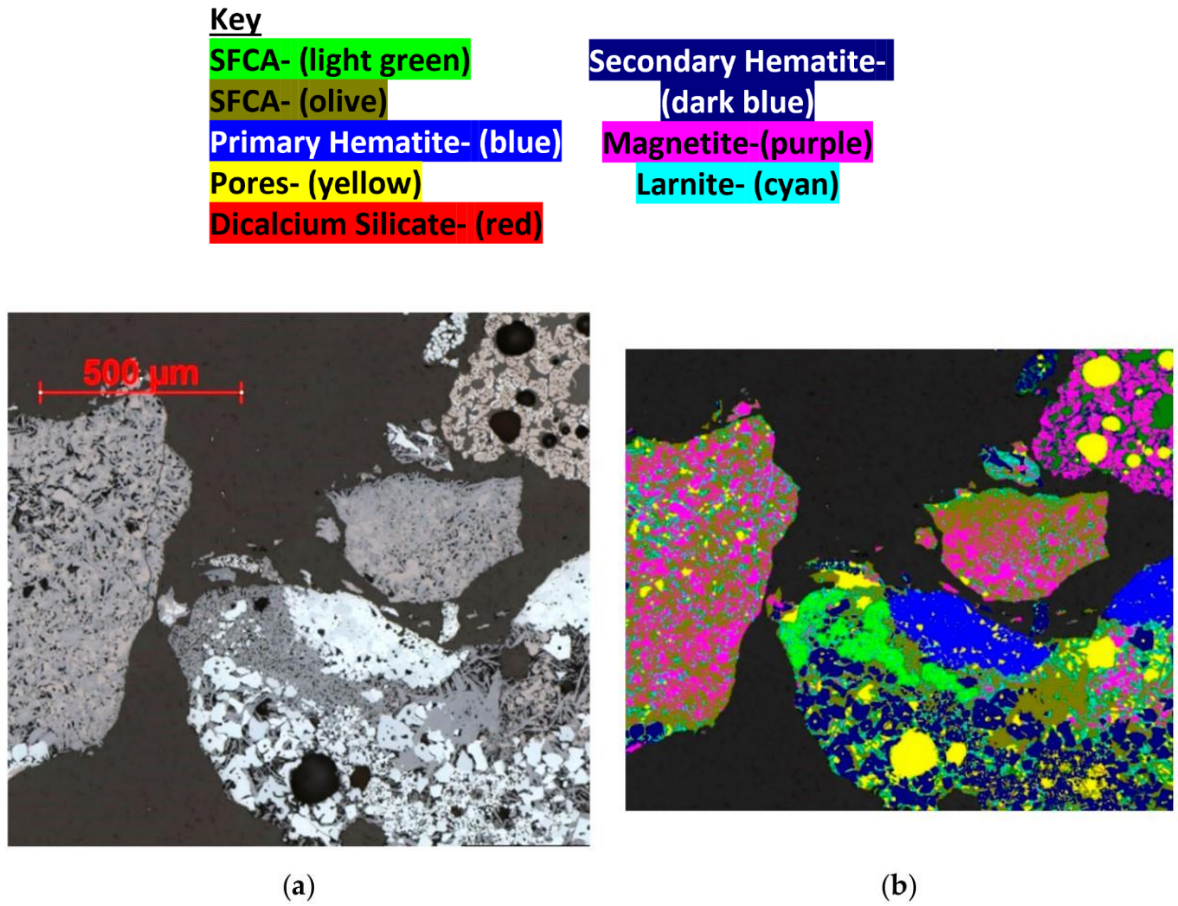

Figure 3.40 Two images of sample UN154 compared: a) MosaiX image showing the sample under reflected light microscopy, and b) mineral map created with CSIRO's AIA system. [88]

In the MosaiX image shown in Figure 3.40 (a), a reflected light photomicrograph is observed. Figure 3.40 (b) shows the mineral map, which is created using CSIRO's Automated Image Analysis (AIA) system. This image was selected to display all the identified phases, including SFCA-I. In both images in Figure 3.40, it is observed that SFCA is primarily linked to magnetite, whereas SFCA-I is found in limited occurrences and mostly associated with primary and secondary hematite[88].

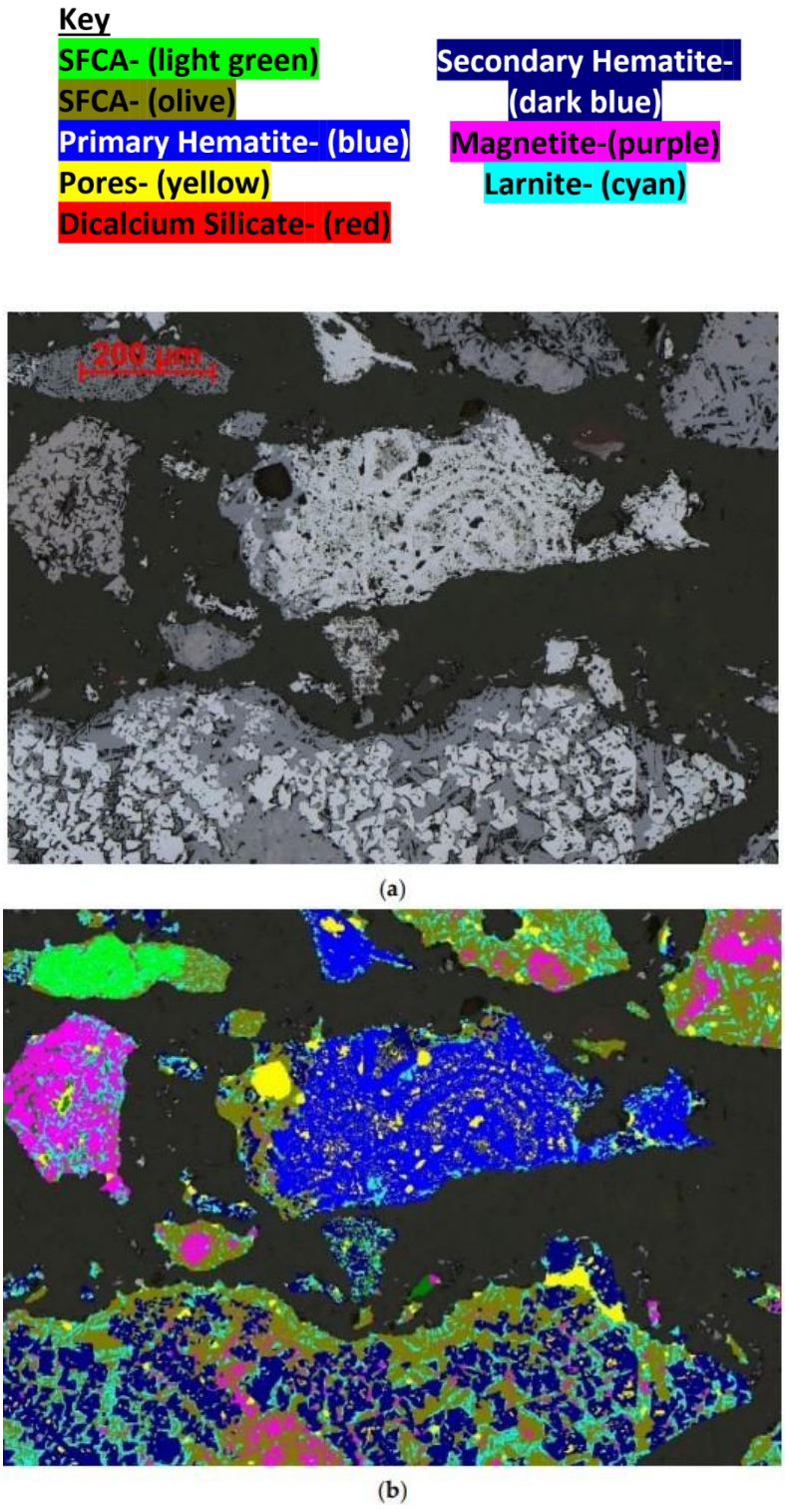

Figure 3.41 (a) Reflected light photomicrograph of crushed sinter, magnification 200X and, (b) Mineral4 software (automated image analysis tool)[103]

The visual representation in Figure 3.41 displays sinter particles that contain various mineral components such as hematite, SFCA, magnetite, larnite, and glass. Donskoi et al.[103] found that distinguishing between primary and secondary hematite was a

challenging task based solely on colour, however, they found that the morphology of these particles can be used for identification purposes. Secondary hematite particles are typically coarse-grained and are commonly associated with SFCA and glass, whereas primary hematite particles do not exhibit such characteristics.

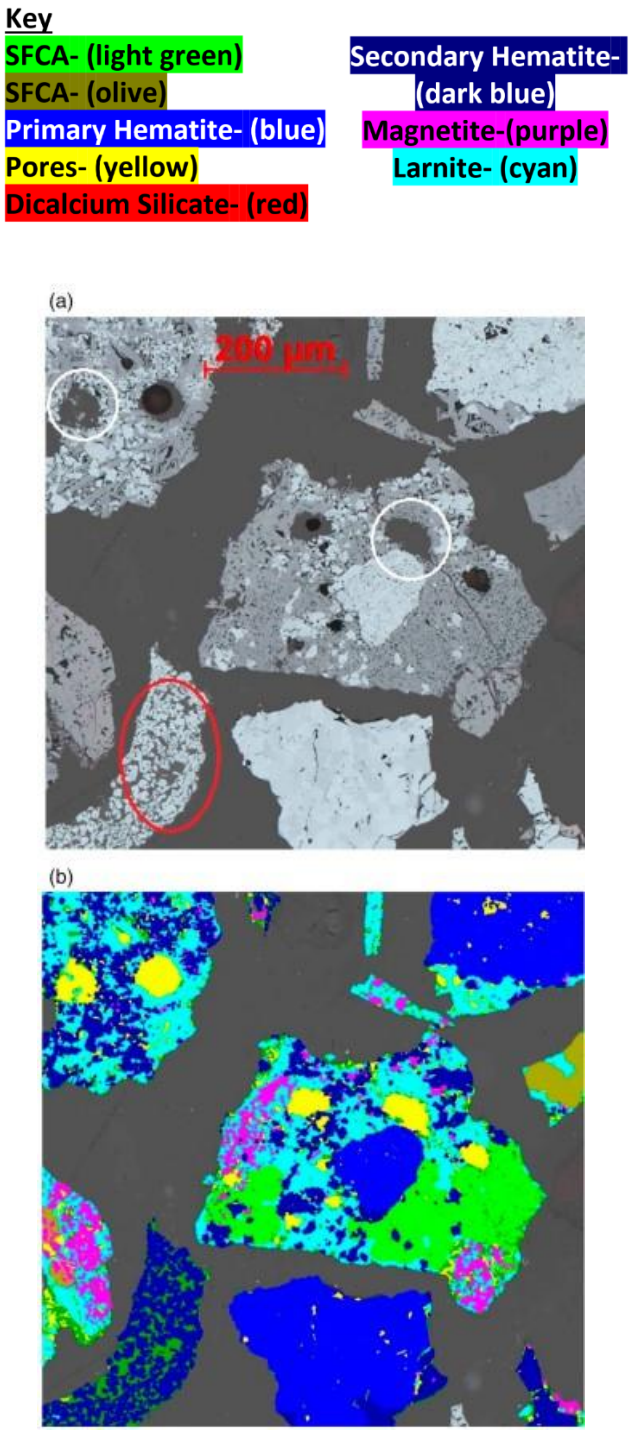

Figure 3.42 (a) Optical photomicrograph of sinter (b) mineral map obtained from AIA[61]

Researchers Hapugoda et al. [61] used AIA to study the microstructures of iron ore sinter. Their findings showed that the mineralogy and microstructure of sinter have a significant impact on the physical and metallurgical properties of iron ore sinter. Therefore, they suggest that characterising sinter phases is a useful and cost-effective tool for evaluating and predicting sinter quality, complementing traditional physical and metallurgical testing methods.

In this project the application Intellesis was used extensively. The areas of literature where it has been used in the past as close to the iron and steel industry have been in the context of an experiment where there was an investigation into the creation and propagation of incipient melting in a chosen aluminium alloy[104]. Time dependent results were confirmed by changes seen in the Intellesis results as a function of the hold time and area percentage of certain phases seen in the software. The computer vision was used successfully as it produced valuable data and showed promise for future microstructural analysis. The results showed that both the temperature-dependent and time-dependent data showed interesting trends with the microstructural constituents. Also, the data was consistent with observations from optical microscopy.

3.6 Particle size distribution (PSD) of raw materials

In this section, the meaning of flux, ore, and fuel in relation to the process of iron ore sintering will be outlined. Additionally, how the particle size of these raw materials can impact the quality of the resulting iron ore sinter will be explored. Relevant literature will be reviewed to determine which particle sizes have been tested and why they may be advantageous. Table 3.2 shows the different authors and what particle sizes they varied. This has been explored further through Chapter 3.6.

Table 3.2 Literature review of different authors that investigated particle size related experiments that effected productivity, quality, and mineralogy.

Author	Ore size	Fuel size	Flux size	Basicity	Limestone	Hematite	Dolomite
A.G. Neysov et al. [105]	✓	✓	✓	-	✓	-	-
Ichiro et al.[106]	-	-	✓	-	✓	-	-
Merkin et al.	-	-	✓	-	✓	-	-
R P. Bhagat[107]	-	-	✓	✓	✓	-	-
J F Hannah[108]	-	-	✓	-	✓	-	-
N. Standish[109]	-	-	✓	-	✓	✓	-
I. Shigaki[89]	-	-	✓	-	✓	-	-
Y. Hosotoni [40]	-	✓	✓	-	✓	-	-
Kenichi et al.	-	-	✓	-	✓	-	✓
T. Umadevi et al [110]	-	-	✓	-	✓	-	✓

3.6.1 PSD of Flux

For the successful utilisation of iron ore sinter in blast furnaces, the addition of fluxing agents such as limestone ($CaCO_3$) and dolomite ($CaMg(CO_3)_2$) is imperative. These agents serve as a means of introducing CaO and MgO which are essential for balancing the acidic components present in the iron ore and coke, such as silicon and aluminum oxides. The combination of CaO and MgO generates a slag that effectively eliminates impurities, such as sulphur, from the final product.[111]

Umadevi et al[110] look at how the particle size of limestone affects the productivity and quality of the iron ore sinter produced. Different mean particle sizes ranging from 0.14-1.85 mm were studied on a small-scale pot, where the tests were carried out. Limestone is a fluxing agent which is added to iron ore sinter to develop a suitable slag composition in the blast furnace further in the process of iron making. Also, flux tends to improve the sinter properties. The investigation of flux size is crucial as it plays a pivotal role in enhancing the overall quality and productivity of sinter. The particle size distribution of the flux has a major impact on the green permeability of the bed, which is a crucial factor that needs to be considered. As it can be seen by Figure 3.43

the results show the effect of limestone particle size on the flame front speed and productivity of the sinter. From the test results productivity increases with increase in the limestone mean particle size. The productivity of the sinter mainly depends on the bed permeability of the sinter bed. This article claims that when the particle size distribution of limestone is more uniform it tends to produce sinter of higher strength and better bed permeability.

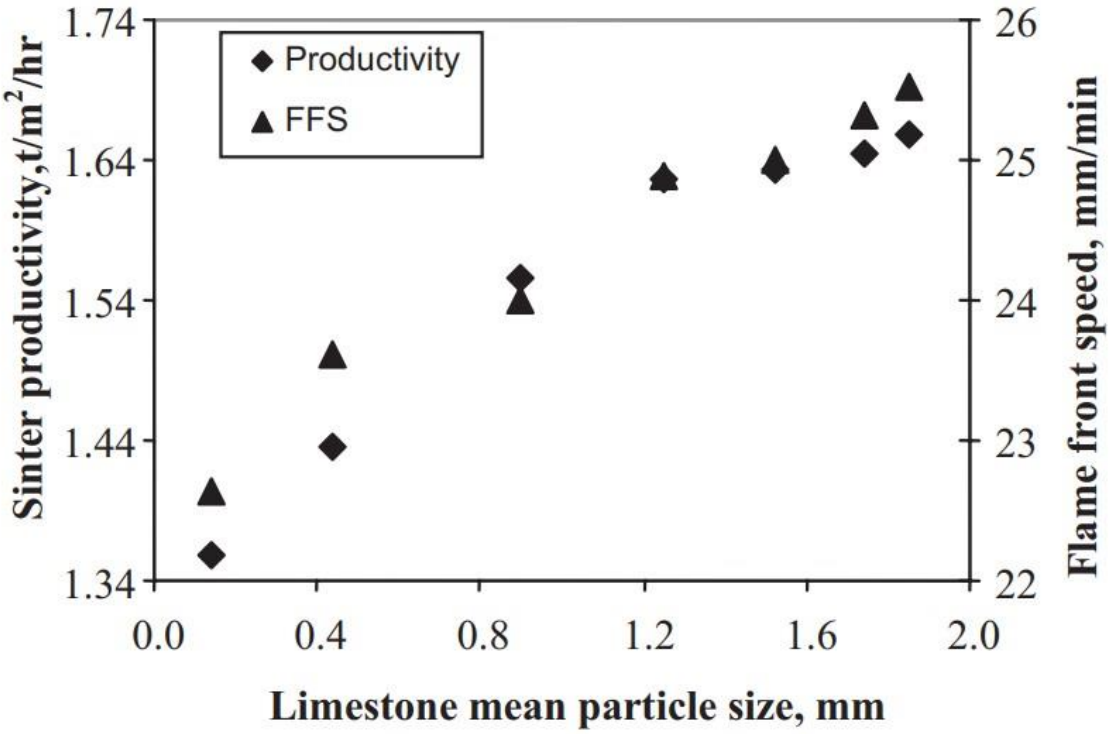

Figure 3.43 Productivity and flame front speed (FFS) as a function of limestone mean particle size[110]

Additionally, previous literature by Neysov et al[105] carried out a series of tests, one of which included varying the flux size. The researchers concluded that a flux size between the range of 0-3mm were the most beneficial for the base mix of the sinter. Limestone mean particle sizes between 1.25 and 1.52 mm produced the best sinter strength and lowest RDI's compared to other sizes.

Moreover, Hosotani et al. [40] conducted research on the size of flux particles and found that removing the -1.0 mm fraction of limestone from the sinter mix led to better granulation and green bed permeability. As a result, the pores became more dispersed and finer, ultimately improving the sinter reducibility.

There is potential for improvement when varying the particle size of the flux of all raw material in anticipation of finding optimum sizes. Literature suggests the flux size has huge ramifications on the sinter process. One study[112] found that more than 3 mm PSD of flux should be restricted because this coarser particle size is more difficult to calcine in a shorter time of sintering.

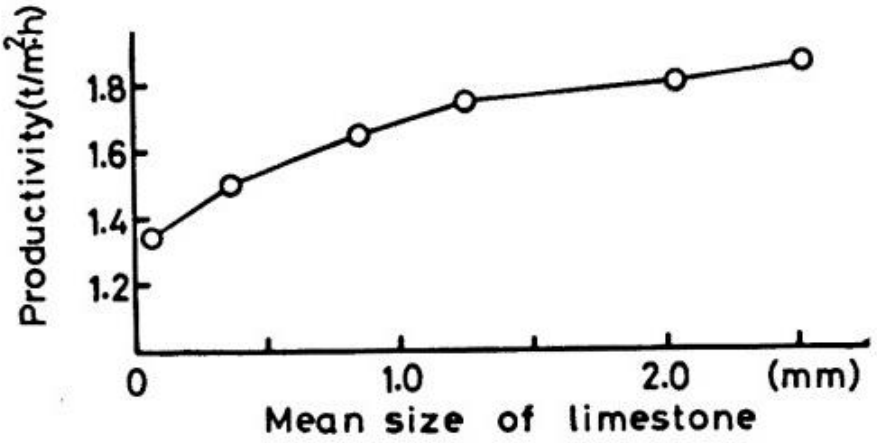

Figure 3.44 Productivity or iron ore sinter production as a function of mean size of limestone[106]

Similar to Umadevi et al[110], according to Ichiro et al.[106], there was a noticeable delay observed in the decomposition of limestone and melt formation when the average size of limestone particles was increased to 2.51mm. This delay had a positive impact on the heat pattern, which led to the production of high-quality iron ore sinter. This increase in quality, in turn, contributed towards the improvement of permeability and productivity. Figure 3.44 has been included to provide a visual representation of this phenomenon.

R P. Bhagat et al.[107] learned that flux sizes of less than 3 mm and more than 0.5 mm resulted in 7% higher productivity compared to less than 5 mm and more than 3 mm, showing the coarser particle size distribution hinders productivity. In terms of mineralogy the researchers understood that the thermal efficiency is worsened whilst the basicity is high and the presence of many limestone fines (<0.5mm) effects the calcination of limestone and the dissolution of hematite and other mineral phases in it. This is because of the cementing behaviour the limestone fines in the sinter mix demonstrate[113]. Moreover, Bhagat et al.[114] found that the appropriate integration of

fluxes with hematite during the sintering process yields fewer return fines and good mechanical strength[114]. To determine the generation of fines, it is important to conduct appropriate tests such as tumbler index, particle size distribution, and shatter index to evaluate the strength of the material[17].

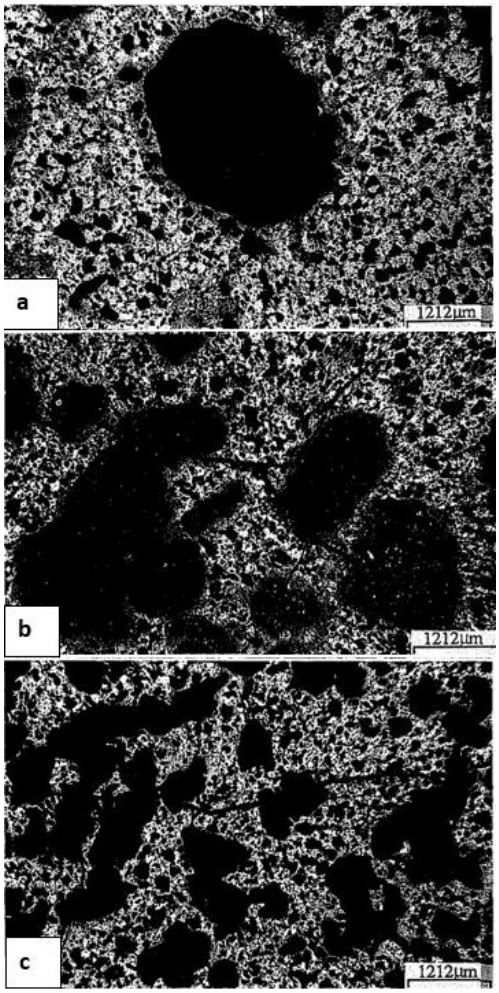

Figure 3.45 Microscopy images of post iron ore sinter with limestone particle size between a.) 1.4-1.68mm. b.) 0.71-1.0mm. c.)355-500µm [109]

Shigaki et al.[115] discusses the coarser limestone particle sizes allowed an increase in the amount of calcium ferrites observed as well as a fall in the skeletal hematite noted which improved the RDI[115]. Moreover, Yang et al.[109] found at larger limestone particle sizes larger pores were formed in iron ore sinter as depicted by Figure 3.45, suggesting the pores were formed at the sites of the limestone particles. They also found that when the porosity of the iron ore sinter was low, the iron ore particles between pores were not able to react. However, if the porosity was increased, the voids between particles

were less filled, which increased the total surface area available for reaction. This resulted in a decrease in diffusion resistance through the mineral walls and an increase in reduction degree.

Bhagat et al.[116] conducted a comprehensive study to compare the effectiveness of dolomite and pyroxenite fluxes in sintering. Through their experiments, they found that substituting pyroxenite with dolomite resulted in a slight improvement in the reducibility of the sinter. Specifically, the process of Mg^{2+} diffusion into the magnetite lattice during sintering played a crucial role in determining the reducibility and mineralogy of the sinter[85]. These findings have significant implications for the optimisation of the sintering process and may lead to more efficient methods in the future.

The process of pore formation in iron ore sinter involves the reaction between flux particles and the iron ore particles. This reaction creates low-melting-point compounds. As a result, the melted liquid which is produced flows a lot faster due to surface tension or capillary force, leaving pores in its place once the flux particles have been fully consumed[117]. It is important to note that as the liquid flows, it fills adjacent interparticle voids and some inner pores within the iron ore particles. Additionally, pores also become visible at the sites of coke particles once they have burned away[118].

Research has also saw that the porosity of the sinter will rise with a decrease in the limestone particle size or increase in the limestone content[117]. The increase in limestone content will lead to an increase in sinter basicity, and thus, the pores of the basic sinter are larger than those of the acid sinter because of the different phases formation in the basic and acid sinters.

3.6.2 PSD of Ores

Ores play a crucial role as a raw material in the production of iron ore sinter. This is primarily because of their high iron content, which is essential for manufacturing iron and steel. The appropriate PSD is especially critical as it determines whether the particles can fuse together correctly and form a sturdy sinter cake.

Steel manufacturers heavily depend on iron ore as its main raw material. This type of ore usually comprises hematite (Fe_2O_3) and magnetite (Fe_3O_4), or goethite (FeOOH)[111]. The ores contain these compounds as a means of fluxing and reducing agents. Some hematite and magnetite ores contain impurities like silica, alumina, and lime. These impurities act as fluxing agents during the sintering process. Fluxes help in the formation of liquid slag, which improves the sintering efficiency by promoting the agglomeration of fine particles and facilitating the removal of impurities[119]. Magnetite ores tend to have inherent reducing properties. During the sintering process, these ores can contribute to the reduction of iron oxide (Fe_2O_3) to metallic iron (Fe). The reduction reaction generates heat, which aids in the sintering process and improves the sinter bed strength[120].

The observed decrease in sinter RDI by Ichiro et al.[106], particularly at an average iron ore size of 2.59 mm, can be attributed to changes in the mineralogy of the sinter. The rise in magnetite phase and decrease in skeletal hematite are factors that contribute to the improvement in the sinter's RDI value. These changes result in enhanced bed permeability prior to ignition and during the sintering process. This improvement may be because of the control of the coarser (+10 mm) and finer (–0.15 mm) fractions in the iron ore fines.

Moreover, in an article by Hsieh[121], it was observed that productivity, TI, RDI, RI, moisture, and coke rate were affected by an increase in ore mean size from 1.0-2.6mm. Three types of ores were utilized - Ore A, Ore C, and a blend of both known as "two-ore." The outcomes for each sinter characteristic are displayed in Figure 3.46. Productivity increases for all three ores when the mean ore particle size is increased. Additionally, in all three cases, the TI generally decreased as the mean ore particle size increased. The RDI for Ore C and the two-ore increased with an increase in mean ore particle size, but for Ore A, there was a slight decrease in RDI. The suitable moisture content decreased as the mean ore particle size increased. There was a slight decrease in the coke rate with an increase in mean ore particle size.

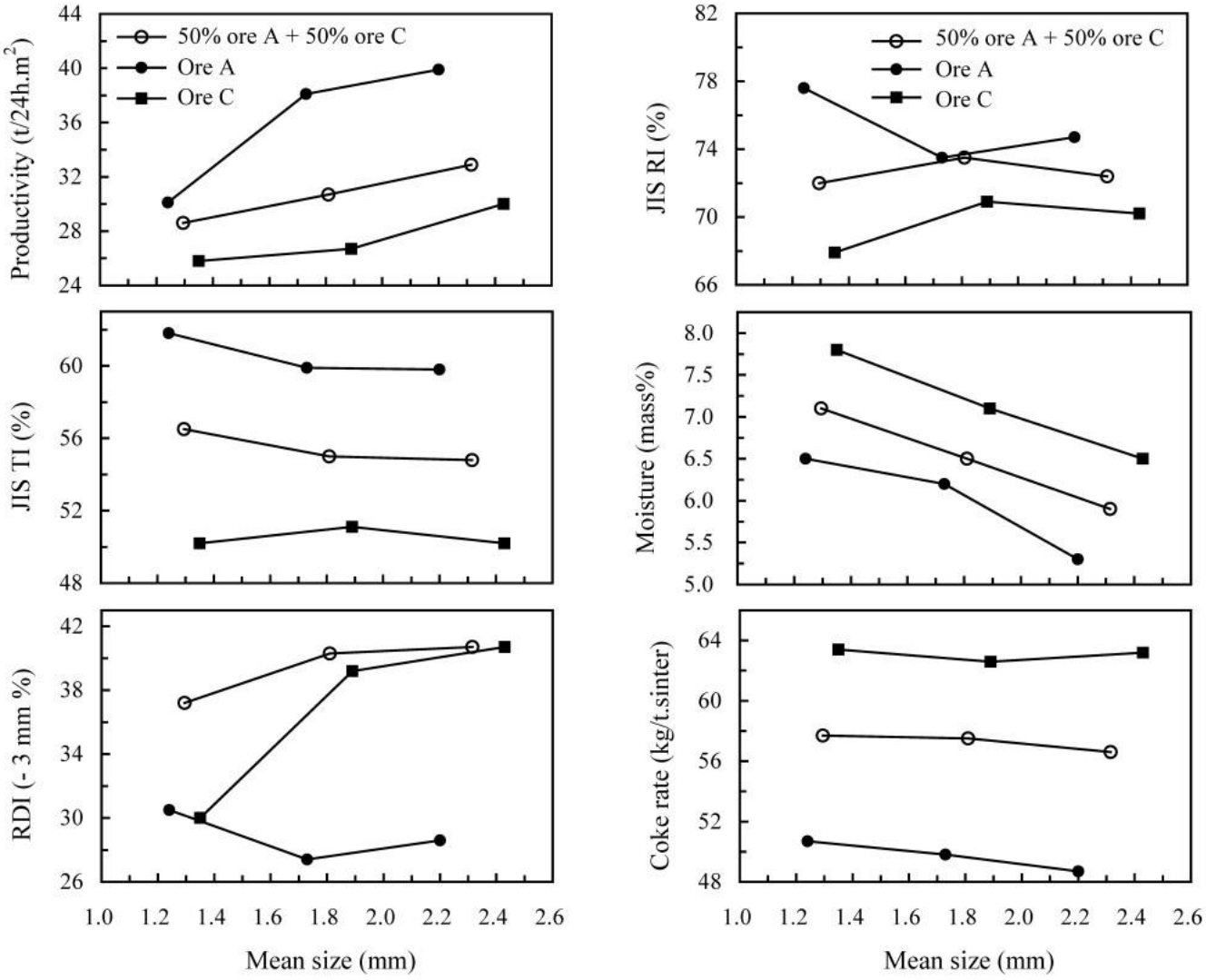

Figure 3.46 Impact of iron ore size on sintering characteristics[121]

When producing sinter, there are three primary factors to consider: the quantity of pores in the ore, the compactness of the resulting sinter, and the transformation of pores during the melting process. As the ore melts, the sinter's pore count decreases due to the expansion and eventual collapse of larger pores in the ore. However, the original pores originating from the ore remain intact, albeit reduced in size. Through their research, Hosotani and a team of other researchers[40] discovered an intriguing insight: by reducing the amount of limestone and coke breeze in the raw mix, the resulting sinter contains more small pores. This discovery has significant implications for the manufacturing process of sinter and its overall quality.

The reduction process of sinter materials containing small pores undergoes a significant change as the size of wustite particles decreases. This decrease in particle size results in an increase in the number of particles and fragmentation of the wustite network into smaller fragments. Such fragmentation is primarily attributed to the effect of fine pore dispersion. The creation of more fine pores during the reduction process is due to their inability to close during high-temperature reduction[40].

Further studies conducted by Nagasaka et al.[122] have shown that the reduction rate of wustite through carbon monoxide (CO) experiences a discontinuous shift at the melting point of wustite. Moreover, they discovered that the reduction rate constant increases by approximately six times on the melt side. It is believed that the increased number and dispersion of fine pores are responsible for allowing more gas to enter the pores, which in turn, accelerates the reduction of molten wustite by CO. Therefore, the reduction process of sinter materials with small pores is a complex phenomenon that involves various factors such as particle size, network fragmentation, fine pore dispersion, and gas permeability.

Research by Bhagat et al[116] has found that using smaller ore fines in the mix increases the micro-porosity of the iron ore sinter. This means that the average pore radius and density of the sinter sample also increase. Micro-porosity refers to pores with a radius 2 nanometres (nm). Sato et al[123] reported similar findings, showing that reducing the particle size of iron ore results in smaller pores in sinter and a more uniform pore distribution. This ultimately improves sinter reducibility. Meanwhile, Jeulin et al[124] found that iron ore sinter reducibility increases with their pore specific area and decreases with the range of pore co-variance.

3.6.3 PSD of Fuel

The ideal characteristics for fuel used in iron ore sintering are high calorific value, low volatile matter, and uniform combustion properties. The most suitable fuel for this process is coke breeze, which is obtained from the coke plant that produces coke for the blast furnace. Coke breeze is highly valued for its exceptional combustion properties, as well as its mechanical and structural properties. The SEM image in Figure 3.47 reveals several internal pores in the coke, which contribute to its

favourable structural properties. Additionally, impurities are minimal in coke breeze because they are driven off during the process at the coke ovens. These qualities make coke breeze an ideal choice for the sinter plant.[125 126].

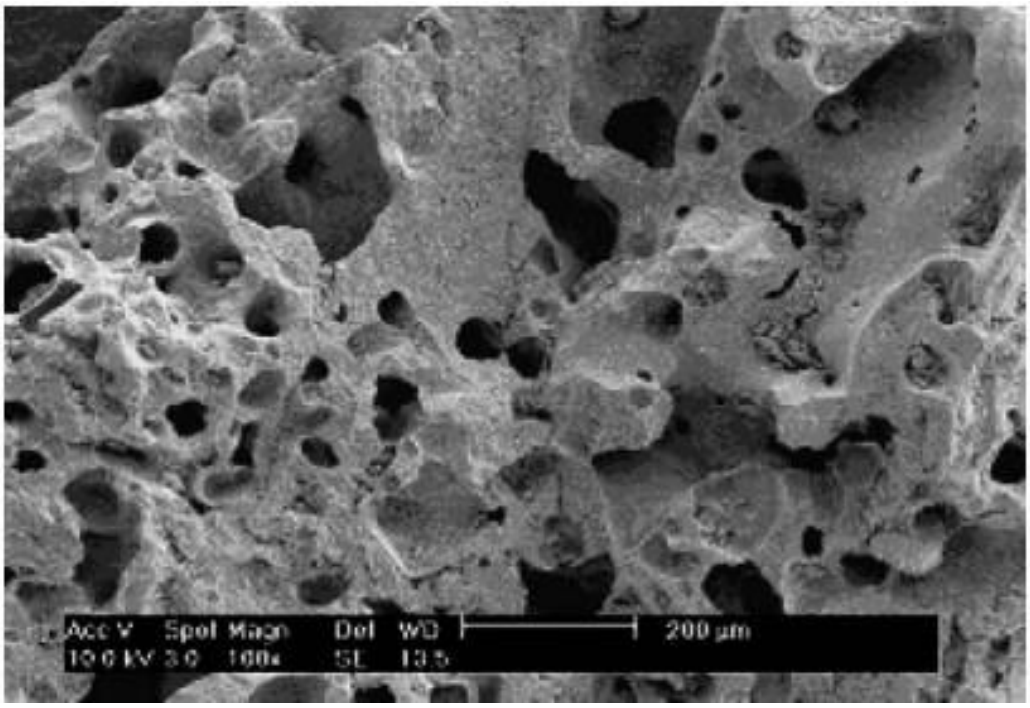

Figure 3.47 Coke breeze SEM image[125]

The location of coke particles within a granule can have a significant impact on their ability to access oxygen, which, in turn, affects the combustion rate. When the particles are situated at the centre of the granule, the rate of combustion is typically governed by mass transfer, as oxygen and combustion by-products must diffuse through multiple layers, including the gas boundary layer, the adhering fines layer, and the forming ash layer. Conversely, when the coke particles are in the adhering fines layer, they have better access to oxygen, resulting in a combustion process that is typically controlled by kinetics[36], which has a lower activation energy thus making it more favourable.

Several physical properties of fuel can impact its reactivity, including porosity, active surface area, gas diffusion rates, concentration of active sites, and hydrogen and oxygen content. Out of all these factors, porosity has a significant impact on the bulk density of the bed, bed porosity, permeability, and heat transfer during the sintering process[37]. Hosotani et al.[40] removed the -0.5 mm fraction of coke breeze from the sinter

mix. Which lowered the high temperature holding time during sintering and increased the maximum sintering temperature.

Biomass is an example of a fuel which is being studied extensively as a substitute for the coke breeze generically used. Implementing the use of renewable biomass as a substitute for fossil fuels presents a viable solution for mitigating CO_2 emissions in the steel industry. This approach aligns with the industry's sustainability goals and can contribute to a reduced carbon footprint. By adopting this alternative energy source, companies can demonstrate their commitment to environmental responsibility while fostering a more sustainable future[127]. While it has been established that biomass can be used partially, it has not been widely adopted in industry due to the large amounts required to match the calorific value of coke breeze[128]. The weak sinter production is caused by the lack of heat release in the melting zone of the biomass and the excessively high combustion rate[45].

According to the research conducted by Karabasov et al.[129] and Kornilava et al.[130], the addition of coke breeze of various sizes was studied. It was found that the ideal coke particle size for efficient combustion and productivity is between 0.25 mm and 3 mm, neither too fine nor too coarse[41]. Additionally, it was discovered that the quality of sinter also improved with the appropriate sizing of the mix ingredients[41].

A study conducted by Murty et al[131] has determined that an enhancement of 6 percentage points in sinter RDI can result in a substantial reduction of 14 kilograms of fuel per ton of hot metal for the blast furnace coke rate. Additionally, this improvement in sinter RDI can lead to a 3% increase in blast furnace productivity. Therefore, it is crucial to accurately model RDI as the initial step towards achieving optimal energy consumption in the iron-making process[132]. These findings underscore the importance of implementing measures to enhance sinter RDI to optimise efficiency and productivity in iron production.

3.7 Sinter Pilot Pot Facility Operating Principle

The sinter pot is a cylindrical apparatus with dimensions 100x500mm, that operates by drawing air from its base. The pot is filled with a raw granulated mix comprising of iron ore, flux, and fuel, which is then ignited at the top. The heat accumulated begins to travel down the pot with the help of the air being drawn from its base, creating a flame front as shown in Figure 3.50.

Although it may be tempting to model the flame front as a straight line, it may deviate from this in certain circumstances. The speed at which the flame front progresses is influenced by several factors, including fuel type, air supply, sinter bed temperature, and permeability of the bed.[18] Of these, the literature review has suggested that permeability plays the most critical role, as the flame front is more likely to follow the more porous routes within the mix to reach the bottom of the bed. As the flame front travels down the sinter pot, part of the granulated mix begins to liquefy due to the heat generated in areas where there is flux. At this point, the heterogeneity of the system may result in multiple outcomes.

A potential outcome may be that the flame front rapidly progresses down the pot in a linear trajectory, facilitated by the effective assimilation of the melt and optimal particle orientation, as depicted in Figure 3.48. This also results in an increase in the hot flow rate, which as a result allows the flame front to propagate and consequently a more uniform temperature profile is produced within the pot. This will also mean when the mix liquifies the voids between the particles will fill thus will be bonded tighter together. This as a result will mean if the sinter is subjected to reduction the gases will seep through the pores successfully. If the sinter is subjected to a force the sinter will not disintegrate very easily.

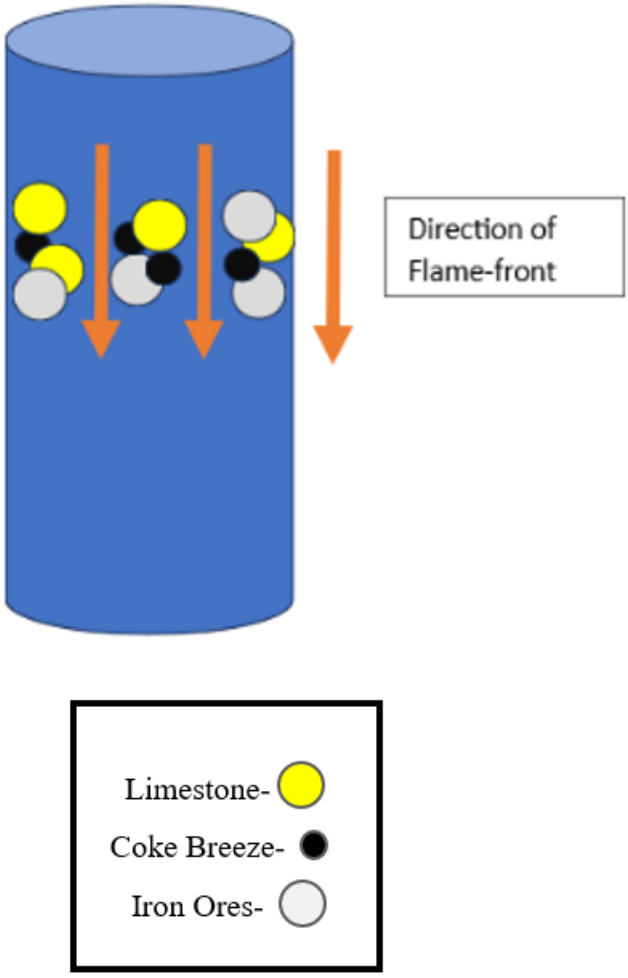

Figure 3.48 Schematic of first possible scenario when the flame front travels down the sinter pot.

Another possible scenario is where on one side the flame front is propagating through the voids and on the other it is being hindered by particles in the way, as demonstrated by A and B respectively in Figure 3.49. This will mean half of the sinter cake will be liquifying whilst the other half is still just raw mix. Pathway A will go on to cool down and become solid whereas pathway B will be too much of a raw mix for it to assimilate with pathway A, in this scenario the porosity is poor and will create a sinter cake which is weak. This is due to the lack of strength created by the two pathways. This also will make the flame front bent and thus reduce the hot air flow rate. The reduction gases will find it harder to seep through the sinter cake and therefore the reducibility of this sinter cake will be poor. Additionally, this will create an unstable temperature throughout the pot which will mean the phases which are required at those higher

temperature will not have the chance to form such as SFCA's and calcium ferrites which have been reported to give strength to the sinter[27].

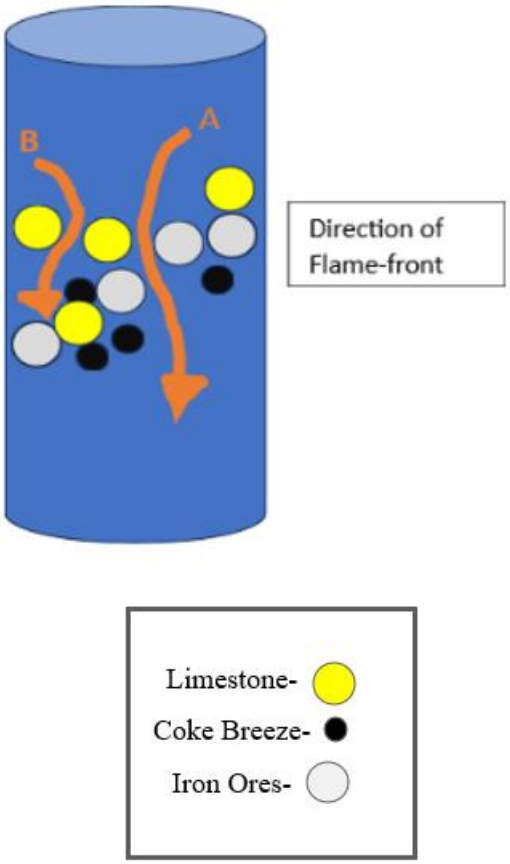

Figure 3.49 Schematic of second possible scenario when the flame front travels down the sinter pot

During the process of sintering, coke combustion provides around 80% of the necessary heat required to produce enough melt and create strong sinter[36]. If the temperature for firing is too low, the granules may not bind together properly because of inadequate heating. Conversely, if the temperature is too high, the permeability of the bed may decrease, leading to longer sintering times and loss of productivity. Additionally, excessive magnetite formation may occur when the temperature is too high[37]. The particles in a sinter mix can be classified as nuclei and adhering, with nuclei being larger than adhering. The position of coke particles within a granulated sinter mix affects their access to oxygen. When they are the nuclear particles of granules, the combustion rate tends to be controlled by mass transfer because the oxygen for combustion and the products of combustion must diffuse through the gas boundary

layer and the adhering fines layer. However, when the coke particles are in the adhering fines layer, easy access to oxygen means that the combustion process tends to be kinetically controlled, which requires less activation energy for the combustion to occur[36].

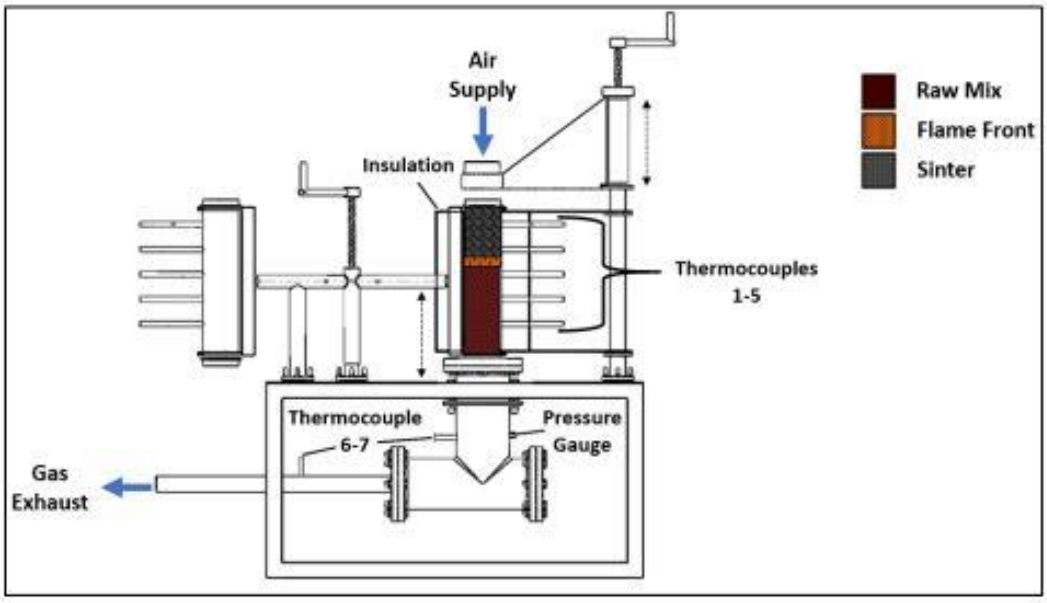

Figure 3.50 Schematic of the sinter pilot pot facility[133]

3.8 Summary

3.8.1 Literature Review

After a thorough review of the literature, certain sources are more pertinent to the goals of this project than others. Nevertheless, the remaining sources could serve as a basis for future project objectives.

i. The production of sinter is a crucial aspect of steel production as it is a primary ingredient for the blast furnace[7]. This means that the optimisation of the sinter quality would enable the blast furnace to operate more efficiently, therefore produce better grade molten iron, which will go on to produce better grade steel.

ii. Sinter is preferred over pellets due to its cost-effectiveness and ease of reduction compared to lump ore. This means when the reduction reaction occurs in the blast furnace for the removal of oxygen from iron ore to produce iron, the sinter is easier compared to lump ore and pellets. Sintered iron ore has a porous structure, which facilitates better gas-solid reactions during the reduction process, making it more efficient.

iii. Producing the sinter and then inserting it into the blast furnace reduces heat consumption in the blast furnace. This is because inside the blast furnace the calcination reaction of limestone does not need to occur. This saves on a lot of energy costs as that process can be quite energy intensive due to the reaction being highly endothermic.

iv. This literature review focuses primarily on the critical factors that affect sinter quality. These factors include the conditions set, mineralogy, and particle distribution of the raw materials.

v. One crucial aspect that has a significant impact on sinter quality is the formation of the SFCA phase, which is greatly influenced by the conditions. Research has proven that the ideal temperature range for SFCA formation is between 1250-1300°C[28 29 30 31 32].

vi. Moreover, maintaining a 7% moisture level can significantly enhance the permeability of the green bed, leading to an increase in cold air flow rate. Proper moisture management can result in top-tier reliability and performance[55].

vii. Various studies have well documented the impact of basicity on iron ore sinter parameters, investigating productivity, reducibility, mechanical strength, chemical composition, and reactivity.

viii. This literature review also offers valuable insights into the desired phases, as well as those that may hinder the quality of the iron ore sinter.

ix. Particle size of the raw materials plays a vital role in the quality of the produced iron ore sinter, as it affects the distribution within the sintering process.

x. The Intellesis work which has already been carried out by Brehm et al.[104] in conjunction with some of the mineralogical analysis by Hapugoda et al.[61], Honeyands et al.[70] and Donskoi et al.[103] has paved the way for more microstructural analysis.

3.8.2 Gaps in Literature

i. Improving the quality of sinter is an essential aspect of steel production, and it is evident that this improvement will automatically enhance the overall steel-making process. It is the researchers responsibility to develop innovative ways to enhance the quality of iron ore sinter constantly. Utilising cutting-edge computer vision technology, such as Intellesis, to capture visualisations of different images and quantify mineralogy is a novel approach that can provide reliable and accurate statistical data for the iron and steelmaking industries.

ii. Microstructural analysis of iron ore sinter has not been observed via intellesis anywhere in literature, using this computer vision will also give more data for future generations to have to compare to.

iii. Qualitatively speaking there is little to no literature on close magnification of phases within iron ore sinter. Observing the phases at these close magnification levels will add knowledge to the iron making industry.

3.9 Thesis Aims & Objectives

i. Sinter basicity effect on sinter quality- There is minimal literature available regarding the quantification of phases in close microscopic images and their link to sinter quality. Overall aims were to maximise the ratio for better sinter quality and to further the understanding of mineralogical changes. This study is novel in using Intellesis for analysing sinter microstructure. The ultimate research question for this experiment is "What is the effect of an increase in Basicity on the quality of sinter produced?". The prediction for this experiment is as the basicity increases the sinter quality will improve.

ii. Particle size of flux impact on the sinter quality mainly focussing on limestone and magstone- Similar investigations of flux particle size (particularly magstone) have received little to no attention in the scientific literature. Also, flux tends to improve the sinter properties. Particle size is worthy of attention because it dictates the hot and cold permeability of the bed, which in turn is strongly related to sinter quality and productivity. Magstone is a fluxing agent used in some plants including Tata Steel UK. The reason for this inclusion is due to historical knowledge of benefits from the chemistry of the magstone. Fluxing the sinter mix with magstone also has benefits for the blast furnace as it positively impacts the blast furnaces slag properties, which have direct impact on the process stability. The ultimate research question for this experiment is "What is the effect of an increase in the particle size of flux on the quality of sinter produced?". The prediction for this experiment is as the particle size of the flux decreases the sinter quality will improve.

iii. Varying the levels of SiO_2, MgO and basicity to see the effect of sinter quality- According to literature, there is a gap in determining the optimal levels of Basicity, MgO, and SiO_2 for iron ore sinter. These factors are crucial in achieving the desired quality of sinter that is suitable for blast furnace use. The aim is to identify the most optimal mixture of these factors in terms of sinter production rate, strength, and permeability, which are all important parameters for the blast furnace. Intellesis will conduct an analysis with the objective of providing comprehensive details on the mineralogy acquired in each sinter.

This data is instrumental in determining the quality of each blend, as well as identifying the existing microstructures and their respective quantities. The ultimate research question for this experiment is “What is the ideal level of SiO_2, MgO and Basicity required to produce sinter of high quality?”. The prediction for this experiment is as the basicity in in the range of 1.5-2.0% the sinter quality will be better. Additionally, an increase in SiO_2 percentage is expected to improve the quality of the resulting sinter. Lastly, it is believed that lower percentages of MgO, around 1.5%, will produce the best sinter quality.

4 Materials and methods

This section examines the materials used, including how they were sourced and their chemical composition. Additionally, the process of post-sinter analysis was investigated. The use of the novel AI software (Intellesis) was explored. Moreover, an explanation of the employment of the Taguchi method for an experiment discussed later in Chapter 7 was explained.

4.1 Raw Materials

Table 4.1 shows all the raw materials used in this project including the iron ores that were used throughout all the experiments. It is important to note the iron content is sufficient at over 60% for these ores, making it an ideal raw material for producing iron of high quality[134]. This high iron content ensures that the resulting sinter has a significant iron content as well. In addition, the sinter mix also contained limestone, magstone, coke breeze (as fuel), and sinter fines which were all sourced from the TATA Steel stockyard and the description as to how they were processed can be seen in chapter 4.1.1.

Table 4.1 Chemical composition of all raw material used in this project.

Material	TFe	CaO	SiO_2	MgO	Al_2O_3	FeO	Carbon	LOI
Iron Ore A	65.58	0.44	4.34	0.42	0.03	12.76	0.00	0.38
Iron Ore B	61.28	0.01	6.76	0.02	1.99	3.20	0.00	3.18
Iron Ore C	63.22	0.13	6.51	0.06	1.51	1.72	0.00	2.86
Iron Ore D	66.56	1.08	3.21	0.02	0.89	37.58	1.50	0.71
Iron Ore E	65.31	0.04	2.05	0.03	1.31	0.45	0.00	2.51
Iron Ore F	66.56	1.08	3.21	0.02	0.89	37.58	1.50	0.71
Iron Ore G	63.53	0.06	5.62	0.17	0.56	0.30	0.00	4.22
Iron Ore H	61.23	0.07	6.08	0.13	0.83	0.48	0.00	4.87
Limestone	0.00	54.13	1.15	1.65	0.12	0.00	14.06	43.55
Magstone	0.00	30.35	2.07	18.52	0.62	0.00	13.99	45.11
Coke Breeze	0.00	0.92	5.66	0.25	2.94	0.00	85.85	85.85
Sinter Fines	55.56	10.14	5.86	2.36	1.26	9.16	0.38	0.00

TFe: Total iron content, LOI: loss on ignition at 950°C in air

4.1.1 Raw material processing

Port Talbot stockpiles underwent raw material processing using the "BS EN 932-1: 1997 tests for general properties of aggregates" code. The scoop technique was employed to extract from the top, middle, and bottom thirds of the stockpile. This was so that a varied range of materials was utilised.

4.1.2 Pre-Test Material Preparation

To ensure the correct preparation of raw materials, they must be dried for a minimum of 24 hours at a temperature of 105°C. The recommended procedure involves sieving the ore and fluxes to a size smaller than 5 mm and the fuel to a size smaller than 3.15 mm.

During the pre-test material preparation stage of this experiment, a slightly different procedure for the flux material compared to the rest of the materials was followed. A

quantity of flux material on top of a sieve was placed and separated one at a time into the five different categories based on size: 0.25-1mm, 1-2mm, 2-3.15mm, 3.15-3.35mm, and 3.35-5mm. Round sieves were used that were available at the facility at the time, which were supplied by Endecotts[135]. The process of manually screening out the material was carried out for 5 minutes.

4.2 Pilot scale sinter rig

This information pertains to a sinter pilot pot experiment being conducted at Port Talbot Tata Steel.

Please note that the following details only apply to the experiment's running process. To ensure safety, the necessary personal protective equipment (PPE) included:

i. Flame-proof overalls
ii. Steel toe-cap boots
iii. Appropriate gloves
iv. Face mask
v. Eye Protection

4.2.1 Mixing of Blends

To meet the sinter blend model requirements, each material was weighed using a Minebea Intec Signum 1 scale. Next, the Altrad Belle Maxi 140 cement mixer (depicted in Figure 4.1) was utilised to ensure a well-mixed blend. The mixer is loaded when in an upright position and the lid is securely fastened to prevent any loss of material. Once in place, the vessel is tilted horizontally, and the blend is mixed for a duration of 2 minutes. Finally, the lid is carefully removed, and the material is discharged.

Figure 4.1 Altrad Belle Maxi 140 cement mixer (used to mix raw materials to ideal consistency)

4.2.2 Moisture Content Testing

To measure the moisture content in the sinter, the Mettler Toledo HB43 Halogen Moisture Analyser (as seen in Figure 4.2) was used. First, the lid was raised, and around 10 g of the mixed blend is added to the moisture analyser tray. Next, the "Start" button on the keypad was pressed and the moisture is calculated after a few minutes, depending on the dryness of the mixture. This process is repeated twice more to obtain an average moisture content. To determine the amount of water needed to achieve the target moisture, refer to Equation 4.1. Once the appropriate volume of water was measured, add 75 ml to account for any errors and add to the sprayer. An illustration can be seen from Equation 4.1 where V_t is the required water volume (ml), M is the

moisture content and M_{avg} is the average moisture content of the mix.

Equation 4.1 Moisture calculation equation

$$V_t = 16000\ (g) \times \frac{M - M_{avg}}{100}$$

Figure 4.2 Mettler Toledo HB43 Halogen Moisture Analyser

4.2.3 Granulation

Before adding the mixed blend, the drum's guard and lid were removed, and it was tilted to a 45° angle to the left. The granulation drum used in this process was the Gladstone Engineering G94 Special Granulator as shown in Figure 4.3. Once the blend was added, the lid was reattached, and the drum was returned to a horizontal position. It is important to ensure that the sprayer is pressurized with 70 pumps before turning on the granulation drum and water can be added to the drum using the sprayer by

moving the nozzle in and out of the drum in a consistent motion until all water has been discharged. After all the water has been discharged, the blend should be granulated for an additional 5 minutes to achieve a consistent wet blend. Once complete, the lid can be removed as shown in Figure 4.4, and the drum can be carefully moved to the riffle box using proper heavy lifting techniques. The Gilson SP-1 Universal Splitter was used as the riffle box to transfer and gently spread out the granulated material, taking care not to disturb the granulation effect. Finally, the lever on the riffle box was pulled to split the granulated blend (green blend) into two equal portions.

Figure 4.3 Granulation drum with the guard on (granulating)

Figure 4.4 Granulation drum with the guard off (ready to be transferred into riffle box)

4.2.4 Charging the Sinter Pot

A refractory lined pilot facility for sinter pot with dimensions 100x500mm was operated under a 100mbar pressure drop. For accurate measurements of the sinter pot via computational software, refer to Figure 4.6. Figure 4.5 shows a visual image of the sinter pot, which can produce up to 6.5 kg of iron ore sinter at temperatures of up to 1400°C. A hearth layer of sinter 10-16 mm was spread equally at the bottom of the pot, weighing 400g, to prevent any green blend from falling through and avoid the granulated blend from fusing to the pot's base during sintering. The green blend was then carefully poured into the top of the sinter pot at a 90° angle, ensuring equal distribution of the material in the pot. The top of the pot should have a flush finish, and the blend's height must not be compromised in the pot. To confirm that the airflow inside the pot is running smoothly, a cold permeability test was run using the VP FlowScope flowmeter at 100 mbar pressure. The thermocouples were inserted (supplied by TC Ltd), the heat jacket was put on, and the top of the green bed was lit for 60 seconds using the burner head to run a sinter test.

Figure 4.5 Sinter pilot pot lab

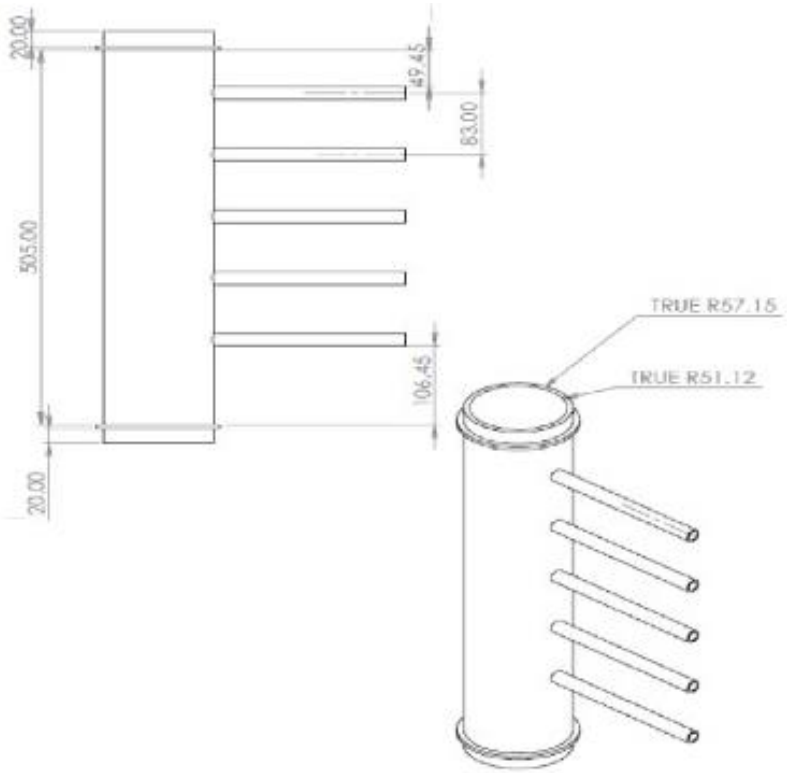

Figure 4.6 Sinter pot dimensions[126]

4.2.5 Discharging the Sinter Pot

The finished sinter was then discharged from the rig once all the recorded temperatures fell below 100°C. The process was monitored via a computer panel, and data was recorded in five-second intervals. After discharge of the pilot-scale sinter rig, the sinter cake was subjected to the desired post-analysis testing. Tariq Al-Haji et al.[126] provide a detailed view of the laboratory configuration and equipment.

4.3 Sinter pot parameters

When operating the pilot-scale sinter rig, a formula sheet has been provided for reference:

• Sintering time: The duration between the 1st thermocouple reaching 40 ℃ and the maximum off-gas thermocouple being reached.

• Cold flow - The measurements were taken five minutes prior to ignition once the necessary pressure drop was achieved.

• Hot flow - The process involved recording measurements starting from the moment thermocouple 2 reached its maximum value until thermocouple 4 reached its maximum value.

• Sintered airflow - The measurements were recorded and averaged during a 5-minute burn.

• Flame front speed – The calculation was based on the time it took for each thermocouple to reach its peak temperature, considering the distance between them over time.

• Flame front thickness – This was calculated using a known flame at 1100 ℃ and determined the midpoint of the flame front based on time and distance.

• Cooling rate - This measurement begins at the highest sintering temperature and goes down to 600 ℃.

All experiments underwent two sinter rig tests. The standard error was determined based on the methodology outlined in Section 4.4 and calculated accordingly for each sinter pot parameter.

4.4 Error Calculation

This thesis utilised the standard deviation function available in Microsoft Excel to calculate the standard deviation of repeated operations (between 2-4). This function enables the calculation of the deviation result based on a dataset centred around the mean value of the results. The resultant figures have been presented where appropriate.

4.5 Moisture optimisation

In this section, the optimisation of permeability was investigated. To achieve this, the base blend used in the experiment when varying the basicity level was utilised. Moisture percentages of 5.5, 6, 6.5, 7, and 7.5% were tested, and as can be seen in Figure 4.7, the highest flow rate was observed at 7% moisture, indicating optimum permeability. This finding, combined with previous literature indicating 7% moisture as optimal[55], led to this moisture level for all future experiments to avoid wasting time on further optimisation tests.

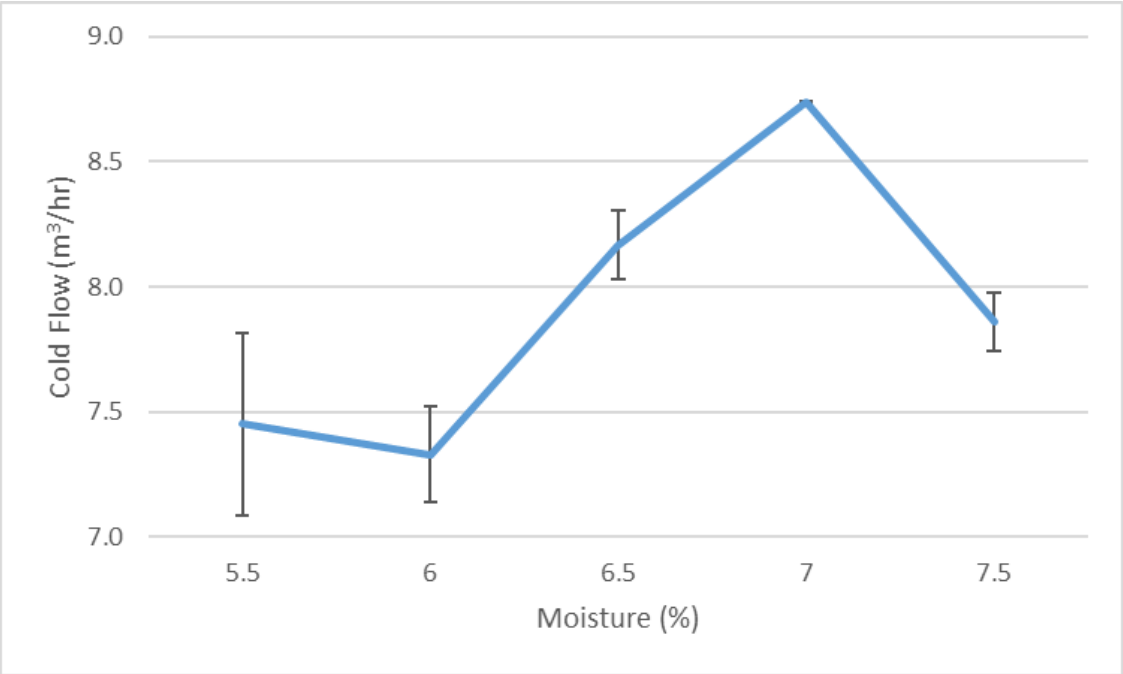

Figure 4.7 Moisture optimisation test for the base blend in the experiment where the basicity was varied

4.6 Experimental Matrix

In this chapter, a detailed analysis of the different raw materials used in each blend for every experiment is shown. Additionally, essential process parameters that were utilised during these experiments are included.

4.6.1 Varying the levels of Basicity (B2) to see changes in Sinter Quality

Table 4.2 Raw materials content of each blend (%) as the B2 is varied.

Component (%)	Basicity (B2)				
	B2=1.0	B2=1.4	B2=1.7	B2=2.0	B2=3.0
Ores					
Iron Ore A	19	18	18	17	15
Iron Ore B	7	7	7	7	6
Iron Ore C	15	14	14	13	12
Iron Ore D	7	7	7	7	6
Iron Ore G	26	25	25	24	21
Flux, Fuel & Fines					
Limestone	2	5	8	10	17
Magstone	5	5	5	5	5
Coke Breeze	5	5	5	5	5
Sinter Fines	13	13	13	13	13

Process parameters:

• Moisture content – 7%

• Granulation time – 5 minutes

• Ignition period – 1 minute

• Pressure drops set point - 100mbar

4.6.2 Impact of Particle Size of Flux (PSF) on Sinter Quality

Table 4.3 Raw materials content of each blend (%) as the PSF is varied.

Component (%)	Particle Size of Flux (PSF) (mm)				
	0.25-1	1-2	2-3.15	3.15-3.35	3.35-5
Ores					
Iron Ore A	19	19	19	19	19
Iron Ore B	11	11	11	11	11
Iron Ore D	11	11	11	11	11
Iron Ore G	26	26	26	26	26
Flux, Fuel & Fines					
Limestone	8	8	8	8	8
Magstone	5	5	5	5	5
Coke Breeze	7	7	7	7	7
Sinter Fines	13	13	13	13	13

Process parameters:

• Moisture content – 7%

• Basicity- 1.70

• Granulation time – 5 minutes

• Ignition period – 1 minute

• Pressure drops set point - 100mbar

4.6.3 Varying SiO_2, MgO and Basicity to see changes in the sinter quality

Table 4.4 shows the different factor levels that were used in this experiment. Factor level refers to the blend composition, i.e. the base blend in this experiment had a factor level of 5.5 SiO_2, 2.0 MgO and B2=1.6.

Table 4.4 Raw materials content of each blend (%) as the factor level is varied.

Component (%)		Ores			Flux, Fuel & Fines			
		Iron Ore A	Iron Ore E	Iron Ore H	Limestone	Magstone	Coke Breeze	Sinter fines
Factor Levels	5.5 SiO2, 2.0 MgO, B2=1.6	25	4	43	6	5	5	13
	4.5 SiO2, 1.5 MgO, B2=1.5	19	57	0	2	4	5	13
	4.5 SiO2, 2.0 MgO, B2=2.0	18	54	0	4	6	5	13
	4.5 SiO2, 2.5 MgO, B2=2.5	17	52	0	5	8	5	13
	5.0 SiO2, 1.5 MgO, B2=1.5	19	45	11	4	4	5	13
	5.0 SiO2, 2.0 MgO, B2=2.0	18	41	12	5	5	5	13
	5.0 SiO2, 2.5 MgO, B2=2.5	17	39	12	7	7	5	13
	5.5 SiO2, 1.5 MgO, B2=2.0	18	30	24	8	3	5	13
	5.5 SiO2, 2.0 MgO, B2=2.5	17	27	24	9	5	5	13
	5.5 SiO2, 2.5 MgO, B2=2.5	18	32	22	2	8	5	13
	6.0 SiO2, 1.5 MgO, B2=2.5	17	14	36	12	3	5	13
	6.0 SiO2, 2.0 MgO, B2=1.5	18	19	35	5	5	5	13
	6.0 SiO2, 2.5 MgO, B2=2.0	17	17	34	7	7	5	13
	6.5 SiO2, 1.5 MgO, B2=2.0	18	4	49	11	3	5	13
	6.5 SiO2, 2.0 MgO, B2=2.5	16	1	47	13	5	5	13
	6.5 SiO2, 2.5 MgO, B2=1.5	18	6	46	5	7	5	13
	7.0 SiO2, 1.5 MgO, B2=2.5	0	0	65	15	2	5	13
	7.0 SiO2, 2.0 MgO, B2=1.5	0	4	67	7	5	5	13
	7.0 SiO2, 2.5 MgO, B2=2.0	0	0	66	9	7	5	13

Process parameters:

• Moisture content – 7%

• Granulation time – 5 minutes

• Ignition period – 1 minute

• Pressure drops set point - 100mbar

4.7 Post sinter analysis

Upon completion of the pilot-scale sinter experiments, the sintered product was screened via particle size distribution (PSD) to establish the sinter yield and various size fractions for the sinter cake product and the cold strength. The sintered product from 16-20mm was subjected to reduction degradation index (RDI) testing which is a globally recognised technique which is used to understand how it would react and reduce in a blast furnace environment[136]. Chemical analysis via x-ray fluorescence (XRF) was conducted to determine the chemical composition. X-ray diffraction (XRD) and Optical microscopy images were produced to identify the mineralogy and phases present. Scanning Electron Microscopy with Energy Dispersive Spectroscopy (SEM-EDS) was also observed for specific blends. It has been determined that conducting post-analysis is crucial in determining the impact of each experiment and gaining a better understanding of the quality of the raw materials and sintered products produced. The post-analysis process remained consistent across all experiments and samples. All techniques were utilised in every experiment, but only the key findings have been presented. All post sinter analysis' error was determined based on the methodology outlined in Chapter 4.4.

4.7.1 Particle Size Distribution (PSD)

Post-analysis on each sinter cake (subjected to crushing and vibrating) was carried out to observe the distribution of the sinter in terms of PSD. The square sieves were orientated vertically with a receiver at the bottom. Once the sieves were properly stacked, they were placed on a Siebtechnik sieve shaker for 1 minute. After the time was up, the contents were weighed of each test sieve separately using a calibrated Minebea Intec Signum 1 scale. The tested ranges are then divided into six groups, which are categorised based on size. These groups include greater than 40 mm, 25-40 mm, 16-25 mm, 10-16 mm, 5-10 mm, and less than 5 mm (which is collected in the receiver).

4.7.2 X-ray fluorescence (XRF)

XRF results were obtained using a Axios X-ray analyser (Malvern Pan analytical, Malvern UK)[137]. The process of emission of fluorescent X-rays, known as secondary X-rays, was utilised to analyse the chemical and elemental composition of materials. To prepare the samples a 0.6 g to 6 g of flux ratio was used for analysis, they were crushed, dried, and then converted into glass beads. This method is employed because the emission of fluorescent X-rays, as utilised in techniques such as XRF, offers a precise and non-destructive means of determining the elemental composition of materials. Preparing glass beads ensures uniformity, which enhances the accuracy of the analysis[138]. This analysis was conducted on all the sintered products to gain a better understanding of their element composition.

4.7.3 Reduction Degradation Index (RDI)

An RDI (ISO: 4696:2015 - Iron ores for blast furnace feedstocks[136]) value was confirmed via the procedure where a sample size of approximately 500g of iron ore sinter was subjected to reduction. The mass is isothermally reduced in a fixed bed, at 900° C, using a reducing gas consisting of CO and N2 for 180 mins. The degree of reduction is calculated from the oxygen mass loss after the 180 min. For the RDI calculated in this experiment only 1 reduction degradation indices was calculated as the mass percentage of material less than 6.3mm. The reduction reaction which resembles that found in the upper part of the blast furnace is carried out in the RB Automazione Control Panel, Reactivity Furnace, and RB Tumbler (TB 3000). Equation 4.2 was used to calculate the RDI where m_2 = the mass (g) of the sinter after reduction and before tumbling and m_1 = the mass (g) of the fraction left over on the 6.3 mm sieve. From literature it has been seen a 6 point change in RDI resulted in a 3% rise in blast furnace productivity[132]. Judging by this finding, it is possible that for every 1 point change in RDI this could result in a 0.5% rise in blast furnace productivity. This means that every point counts when analysing the RDI results, even a 1 point change in RDI is a real change.

Equation 4.2- RDI calculation

$$RDI_{<6.3mm} = 100 - \frac{m_2}{m_1} \times 100$$

4.7.4 X-ray diffraction (XRD)

In preparation for the XRD the iron ore sinter was grinded down using a ball mill and then screened to 50 μm. The grinded sample was then spread perfectly flat over a sample holder and was inserted into the XRD machine for analysis. To assess the crystalline structure of the sinter, Bruker D8 (Bruker Corporation, Billerica (MA), United States)[139] was utilised. The scans were carried out using a copper source between 20 and 80° 2 theta, step size of 0.04° and a time per step of 1s. To improve the background, the discriminators were set between 0.190 and 0.250V. Diffrac.Eva was used for data interpretation analysis. The software automatically compared each phase's peaks with pure spectra to calculate the percentage of each phase present. (quantification)[140]. Diffrac.Eva[139] helps to interpret the data obtained from the XRD. Pre-defined peaks of each phase are already established within the software. The XRD patterns are matched with the pre-defined ones to find the best match. Once the best match is found and all the peaks are defined the software carries out a percentage calculation for each phase present (semi-quantification)[140].

This method was used as opposed to Rietveld analysis as semi-quantification is a simpler approach that involves comparing the intensities of diffraction peaks to estimate the relative abundance of different phases in the sample. This method is less accurate compared to Rietveld analysis, as it does not consider factors like peak overlap, preferred orientation, and crystallite size[141]. However, it can be useful for quickly identifying major phases and providing a general overview of the sample composition. There was limited access to specialised software, hardware, and expertise required for Rietveld analysis, therefore semi-quantitative analysis was a more feasible option for obtaining phase information from the XRD data.

4.7.5 Metallographic Preparation

For optical and SEM analysis iron ore sinter samples of 16-25mm sinter were mounted grinded and polished. To mount the specimen, it was placed it in a 40mm mounting cup and combined epoxy resin, conductive filler, and epoxy hardener (Buehler) in a 7:1:1 ratio. After stirring with a wooden stirrer, the mixture was degassed for two minutes inside a vacuum chamber to prevent frothing. The mixture was then poured over the specimen in the mounting cup and left to cure overnight. The grinding stage consisted of using silicon carbide 120 grit (coarse) and 800 grit (fine) grinding pads for 5 minutes each. To polish the samples Diatwin Max Poly solutions for 1, 3, and 6 microns with corresponding polishing pads was used. To avoid scratching or other unwanted sample preparation errors that could affect the final image quality, the specimen was washed with water and industrial methylated spirits and dried with compressed air between phases.

4.7.6 Optical Microscopy

Photographs were captured using the Primotech MAT[142] and adjusted using aperture and extended depth of field (EDF) to enhance the image quality and clearly display the microstructures of interest. A magnification level of 10 and 20X was utilised to enhance the visibility of microstructures in all images captured, maintaining consistency throughout. To ensure accurate observations of each blend between 3-57 pictures were taken throughout each experiment.

4.7.7 Scanning Electron Microscopy (SEM) / Energy Dispersive Spectroscopy (EDS)

SEM was carried out for the previously polished sinter cross section resins to obtain validation for the chemistry present. The resin was inserted into a sample holder and was attached by carbon stickies and was carefully pressed. Backscattered images and EDS maps were captured by the Zeiss EVO LS25 scanning electron microscope to identify and quantify the chemistry present. As well as this, the EDS mapping enabled the discovery of the chemistry present in precise locations on the resin. To obtain the

best results, a kV ranging from 15-20, I Probe of 250 pA, and a working distance of 10-13mm was used for the images obtained.

4.8 Computational Procedures

4.8.1 FactSage

4.8.1.1 Varying the levels of Basicity (B2) to see changes in Sinter Quality

This test was simulated into a thermodynamic modelling application called FactSage[143], which predominantly focused on the thermodynamic database which produces Gibbs free energy, enthalpy, entropy, and other thermodynamic properties of thousands of substances. This was so that the stability of the phases formed in this experiment at different temperatures could be established. The data gathered utilised the equilib module of FACTSAGE 8.2.

Table 4.5 shows the material and each of their respective compositions that was used in the programme. The weight percentages of each material for the different BASICITY's was deemed to be that which was anticipated to go into the actual experiment as shown in Table 4.6. It is essential to recognize that not all compounds involved in the formation of the material were included in the input for FactSage. According to literature[144] on computational thermodynamics, any amounts less than 0.5 wt. % can be ignored if they do not affect the system's sensitivity, experimental accuracy, or research objective. The compounds in question had extremely small quantities, all less than 0.3 wt. %. Additionally, these compounds were considered less important compared to the ones mentioned. All values were taken from the chemistry which was verified by the XRF from material attained from TATA Steel. Limestone was entered into FactSage as $CaCO_3$ and Magstone was entered as MgO, whilst the coke breeze was entered as C (carbon). All pure solid species from the input reaction was considered from the FTOxid and FactPS databases. Some liquid phase two alloy solutions were formed which were taken from the FSstel database. The method used to determine the thermodynamics of this complex heterogeneous system was based upon the Gibbs free energy minimisation method.

The Gibbs free energy minimisation method was used to determine the equilibrium state of the system by minimising the Gibbs free energy, represented by Equation 3.6. Under conditions of constant temperature and pressure, the system adjusts itself to minimise G, allowing for the prediction of equilibrium compositions, phases, and reactions.

Table 4.5 Chemistry of each material inserted into FactSage.

Material	**Blend Composition (wt.%)**							
	Fe	**CaO**	**SiO_2**	**MgO**	**Al_2O_3**	**FeO**	**C**	**$CaCO_3$**
Iron Ore A	65.58	0.44	4.34	0.42	0.03	12.76	0	0
Iron Ore B	61.28	0.01	6.76	0.02	1.99	3.20	0	0
Iron Ore C	63.22	0.13	6.51	0.06	1.51	1.72	0	0
Iron Ore D	66.56	1.08	3.21	0.02	0.89	37.58	0	0
Iron Ore G	63.53	0.06	5.62	0.17	0.56	0.30	0	0
Limestone	0	0	0	0	0	0	0	100
Magstone	0	0	0	100	0	0	0	0
Own breeze	0	0	0	0	0	0	100	0

Table 4.6 Amounts of each material inserted into FactSage for different levels of B2

Material/Amount (g)	**B2=1.0**	**B2=1.4**	**B2=1.7**	**B2=2.0**	**B2=3.0**
Iron Ore A	4000	4000	4000	4000	4000
Iron Ore B	1600	1600	1600	1600	1600
Iron Ore C	3200	3200	3200	3200	3200
Iron Ore D	1600	1600	1600	1600	1600
Iron Ore G	5600	5600	5600	5600	5600
Limestone	448	1200	1768	2384	4576
Magstone	1128	1096	1080	1056	984
Own breeze	800	800	800	800	800

4.8.2 **Machine learning (Intellesis)**

The Zeiss Intellesis image analysis programme (Carl Zeiss AG, Oberkochen, Baden-Württemberg, Germany)[145] was employed to create an image analysis procedure that analysed the microstructural characteristics of iron ore sinter. When an image was uploaded onto the application, mineralogy can be manually shaded to give the software the training it needs to be able to identify this automatically in the future. Upon carrying out multiple iterations of training by the user, a template can be produced which can be applied to other images that contain similar mineralogy. It is important to note that there is error in this procedure which cannot easily be calculated for measurements which may be generated from the user's shading accuracy and the applications ability to apply the shading to a whole micrograph. This template was designed in conjunction with other characterisation methods, such as XRF, XRD, RDI, SEM/EDS and Optical microscopy which provided further validation for the process.

This application utilised artificial intelligence computer vision and was taught to recognise microstructural characteristics based on colour, morphology, and literature. In this experiment, the software assisted in quantifying the percentage of the microstructure throughout the sinter which included the SFCA, SFCA-I, primary hematite, pores, dicalcium silicate, secondary hematite, magnetite and larnite areas. In literature there is no Zeiss Intellesis data for iron ore sinter, thus unfortunately no comparison could be made and therefore is missing in the literature review in this thesis.

However, one application which has been cited in literature and carries out similar tasks to Intellesis is Mineral4. This software, initially for iron ore, now covers various ores and materials. It automates image collection using a ZEISS optical microscope, allowing identification of particles, minerals, and porosity. The tool supports manual and automated measurements, providing comprehensive characterisation of particles, including textural classification, liberation analysis, mineral association analysis, and calculation of composition, assay, density, and characteristics. Customisable reporting is available based on user-defined criteria. The software uses advanced identification techniques for improved phase identification, crucial in sinter OIA characterisation. Users can create specific textural classification schemes for different ores and

sinters[103]. Operation of the Intellesis application was a more feasible option for this project with the resources available.

Therefore, this is a huge novel aspect to this thesis and is a study that was put into place to be able to provide the foundational data required for future comparisons to be made where the quality of sinter requires explanation in terms of mineralogy. Between 3-57 iterations were taken to demonstrate more robust findings of the different microstructures present.

This application utilised artificial intelligence and was taught to recognise microstructural characteristics based on colour, morphology, and literature. In this experiment, the software assisted in quantifying the percentage of the microstructure throughout the sinter which included the SFCA, SFCA-I, primary hematite, pores, dicalcium silicate, secondary hematite, magnetite and larnite areas.

4.8.3 Taguchi method

Genichi Taguchi developed Taguchi methods, which are statistical techniques used to enhance the quality of manufactured goods, which in this case is the iron ore sinter. These techniques have also been applied to engineering in recent times[146]. This makes it applicable for this project too. Process optimisation involves adjusting a process to achieve optimal results within specific parameters while adhering to constraints. The objective is to minimise costs, maximise efficiency or quality and throughput, making it an essential tool in industrial decision-making. In this case it was used to maximise three specifications while ensuring all other constraints are met[147].

This approach was used in Chapter 7, Page 190 in this document. The problem that was set out to be solved was reaching an optimum performance for 3 different independent variables (control factors) which were Basicity, MgO, and SiO_2. The level for each control factor was set as follows; Basicity- 1.5-2.5%, MgO- 1.5-2.5% and SiO_2- 4.5-7.0%. The system performance parameters for this experiment was RDI, Average Sintering Time, Average Sinter Yield, Average Sinter Rate, Average Hot Permeability, Average Maximum Sintering Temperature and Total SFCA Production. Table 4.7 shows the orthogonal array constructed for this experiment using Minitab[148] an application which provided support for the design of experiments.

Table 4.7 Orthogonal array using Taguchi's method.

Blend	SiO_2	MgO	Basicity
1 (Base Blend)	5.5	2.0	1.6
2	4.5	1.5	1.5
3	4.5	2.0	2.0
4	4.5	2.5	2.5
5	5.0	1.5	1.5
6	5.0	2.0	2.0
7	5.0	2.5	2.5
8	5.5	1.5	2.0
9	5.5	2.0	2.5
10	5.5	2.5	2.5
11	6.0	1.5	2.5
12	6.0	2.0	1.5
13	6.0	2.5	2.0
14	6.5	1.5	2.0
15	6.5	2.0	2.5
16	6.5	2.5	1.5
17	7.0	1.5	2.5
18	7.0	2.0	1.5
19	7.0	2.5	2.0

5 Effect of Change in Basicity (B2) on the Sinter quality

5.1 Introduction

The current research on basicity mainly focusses on only high and low levels[5]. To gain a more comprehensive understanding, this study examines a wider range of basicities, ranging from 1-3 (1, 1.4, 1.7, 2, and 3). This approach allows for more data points and stronger trends to be identified. Chapter 4.6.1 shows the raw material contents and the process parameters used in this experiment. The ultimate research question for this experiment is "What is the effect of an increase in Basicity on the quality of sinter produced?".

This investigation was carried out at a pilot sinter pot facility in Port Talbot, with the help of Tata Steel UK ltd. The motivation for this experiment was two-fold: Firstly, there was an industrial imperative to optimise this ratio as it influences key sinter quality parameters such as cold strength and reduction degradation index (RDI). Secondly, there was an academic objective of greater understanding the mineralogical changes as a function of basicity. Basicity is the mass ratio between CaO and SiO_2.

In this experiment the MgO level was kept the same and the CaO and SiO_2 levels were manipulated to obtain the required basicity. The basicity has previously been investigated with its effect on RDI and sinter productivity, researchers found that when increasing the basicity it improved the sintering productivity, RDI and properties[4 5].

Limited research exists on the identification and quantification of various phases within micrographs of iron ore sinter, and their correlation to the overall quality of the material. When referring to 'quality', the physical, chemical, and metallurgical properties of the iron ore sinter are discussed. By using computer vision in combination with conventional analysis methods such as x-ray diffraction (XRD), x-ray fluorescence (XRF), and reduction degradation index (RDI), this article aims to investigate:

1.) How the microstructure of sinter is observed visually when the basicity was changed, aided by optical microscopy images and consequential Intellesis images.

2.) Confirmation of the existence of SFCA's in terms of quantitative data gathered by novel method of Intellesis.

3.) Understanding more about the influence of basicity changes on, thermodynamics, sinter bed permeability, formation of different phases and metallurgical testing.

5.2 Results

5.3 FactSage

During the experiment, various phases were generated and utilised until a point of stability was achieved, which was dependent on the temperature it reached. Figure 5.1 depicts the formation of each of the phases as a function of temperature under equilibrium conditions in the experiment where basicity was 1.0. As it can be seen in Figure 5.1 between the mass ranges of 0-2000g, the relevant phase present denoted by SFCA, as it can be seen it peaks at approximately 1200°C in terms of mass which means this is the temperature where the phase can be seen to be most stable, which is in the range between 1200-1300°C reported in literature[24]. This process was repeated for each of the different basicities following the methodology outlined in Chapter 4.8.1.

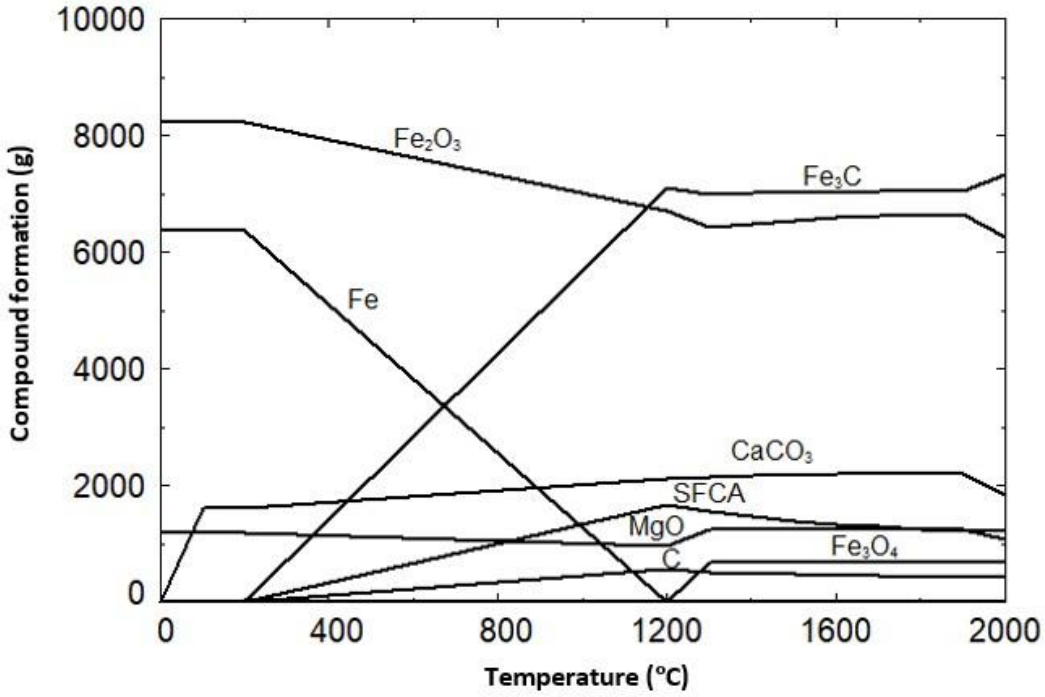

Figure 5.1 Formation of each phase as a function of temperature under equilibrium conditions for the B2=1.0 experiment according to FactSage

As per the data provided in Figure 5.2, there has been a noticeable increase in the amount (%) of SFCAs with higher basicity levels according to FactSage simulation. The results indicate that the highest number of SFCAs were observed at a basicity level of 3.0 at 23%. The lowest number of SFCAs were observed at a basicity level of 1.4 at 11%. At a maximum production level, it has been observed that the most stable SFCA phase occurred at 1200°C.

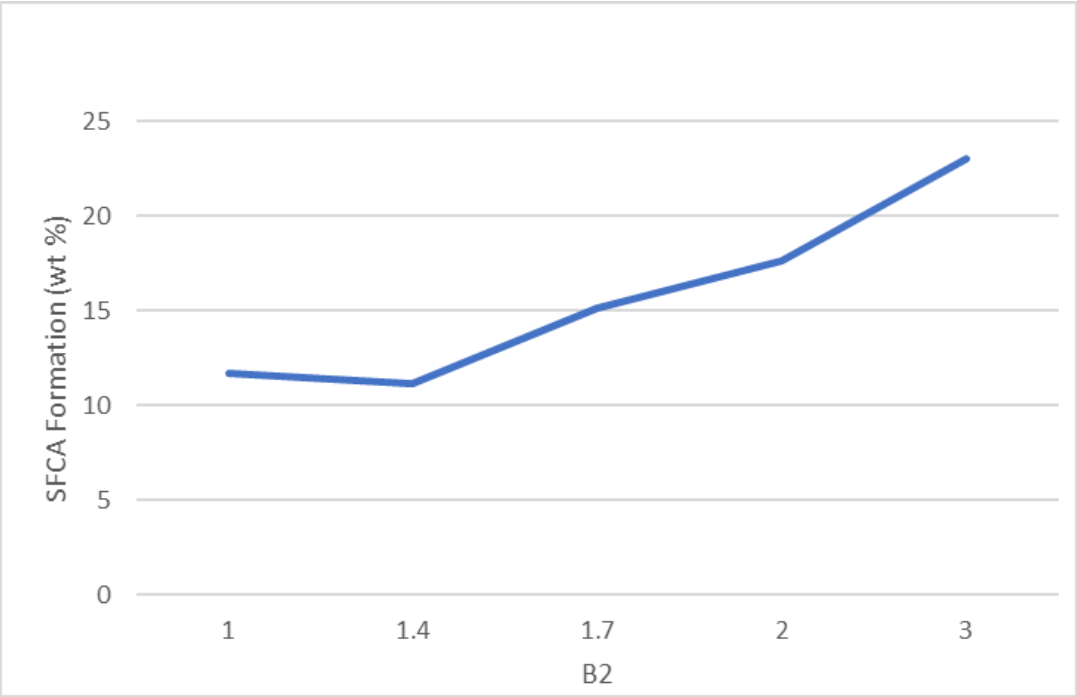

Figure 5.2 Maximum amount of SFCA formation as a function of basicity at 1200℃ according to FactSage simulation.

5.1 Sinter pot parameters

Upon analysing the impact of basicity on temperature profiles, certain observations can be made from Figure 5.3. Firstly, it's evident that Figure 5.3 (b), (c), and (d) exhibit stable temperature patterns. From Figure 5.3 (a) and (e) which show the temperature profiles for when the basicity was 1.0 and 3.0 respectively show unstable temperature profiles. The TC's do not peak sequentially as seen for the other levels of basicity illustrated in Figure 5.3 (b), (c), and (d) Also, only TC2, 3 and 4 for B2=1.0 exceeded 1200°C, while other TCs did not reach the desired temperature. For B2=3.0, excessive levels of basicity could be the cause, and for B2=1.0, an insufficient basicity level could be responsible. From Figure 5.3 (a) the TC3 (which measures the middle layer) at a B2 level of 1.0 had a holding time of 230 seconds at and above 900°C. This holding time was longer than that observed for when the B2 level was at 1.4 as depicted by Figure 5.3 (b).

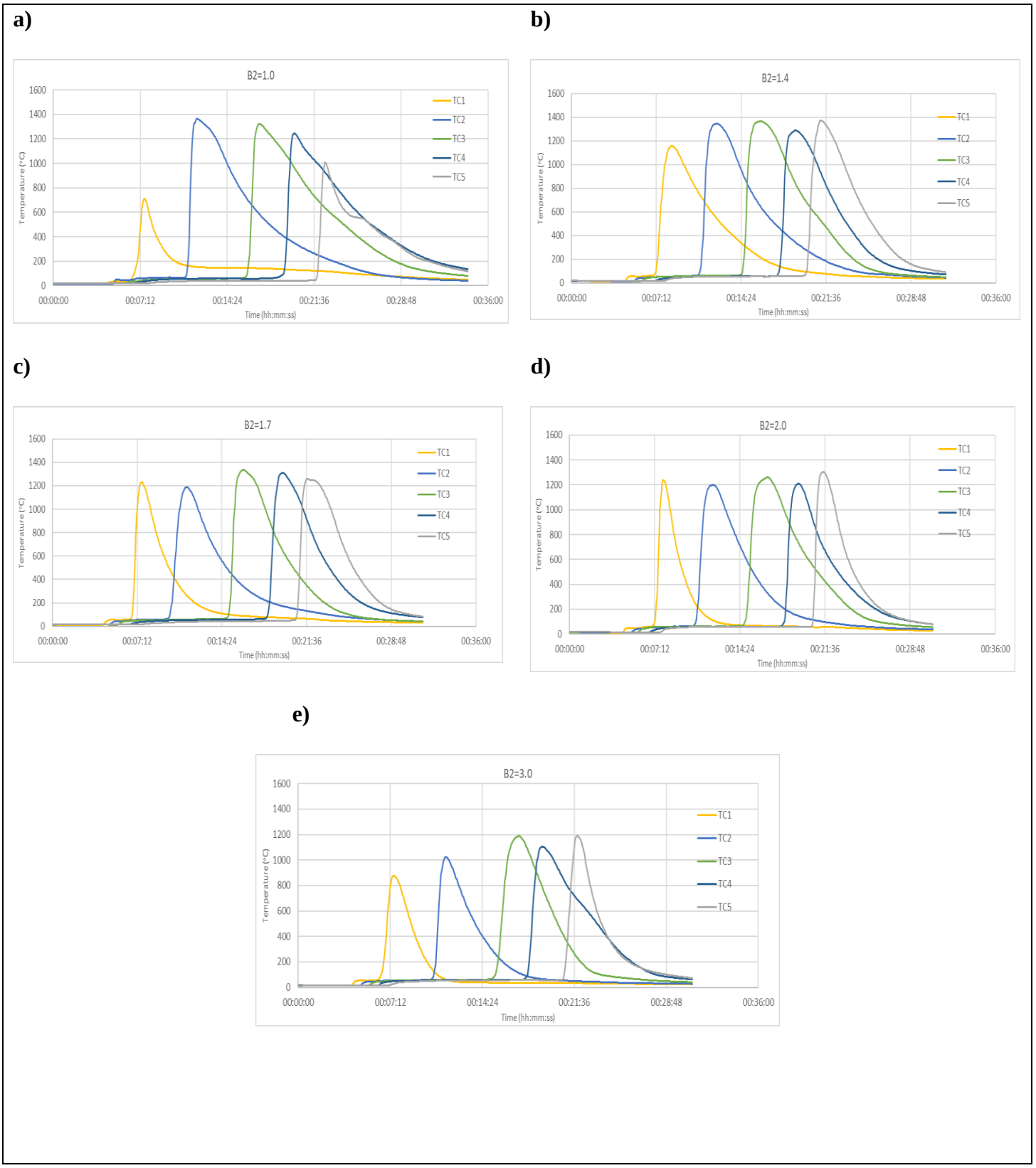

Figure 5.3 Temperature profiles for each blend. a) B2=1.0 b) B2=1.4 c) B2=1.7 d) B2=2.0 and e) B2=3.0

Table 5.1 shows the average (2 runs) sintering time for when the basicity was 1.4 which was the shortest at 19 minutes 30 seconds. The average time to sinter was the longest when the basicity was 1.0 at 21 minutes and 27 seconds. The data shows a variation from the slowest to the fastest time of this experiment of approximately 3 minutes. As well as this there was a reduction in sintering time going from basicity levels 1.7 to 2.0 from 21 minutes and 10 seconds to 20 minutes.

Average maximum temperature data for this experiment suggests that when the basicity was 1.4 the temperature reached a high of 1373°C. Subsequently, increased basicity led to a 13% reduction in the maximum temperature for the remaining blends resulting in B2=3.0 experiencing the lowest average maximum temperature of 1163° C.

Table 5.1 Contrast of parameters at different basicities (B2)

Parameters/B2	**1.0**	**1.4**	**1.7**	**2.0**	**3.0**
Average Max Temperature (°C)	1336	1373	1320	1272	1163
Average Sintering Time (hh:mm:ss)	00:21:27	00:19:30	00:21:10	00:20:00	00:19:32
Average cold flow rate (m3/hr)	9	10	11	10	11
Average hot flow rate (m3/hr)	7	8	7	7	8

Figure 5.4 has been included to aid in observing the trend of maximum temperature as basicity increases. The graph displays the average maximum sintering temperature starting at 1000°C. It is evident from the graph that a basicity value of 3.0 does not reach the same maximum temperature as the other blends, while the blends with other basicity values do not reach the same maximum temperature as when the basicity was 1.4. The trend shows the average maximum temperature generally decreased as a function of an increase in the basicity.

Data from the average cold air flow rates showed the most permeable and thus the blend with the highest average cold air flow rate was recorded when the basicity was 1.7 at 11 m^3/hr and the lowest cold air flow rate noted was when the basicity was 1.4 and 2.0. Similarly, data for the average hot air flow rate showed when the basicity was 1.4 and 3.0 the hot air flow rate was recorded at its highest at 8 m^3/hr and when the basicity was 1.0, 1.7 and 2.0 the rate was recorded at a low of 7 m^3/hr.

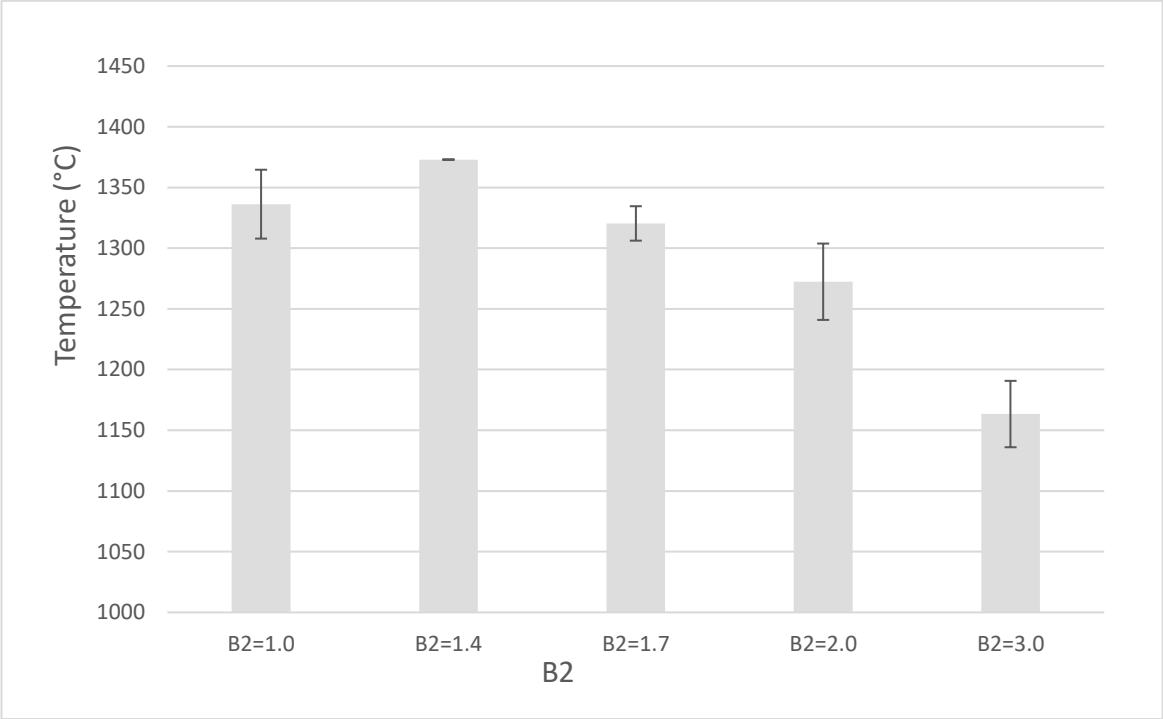

Figure 5.4 Average sintering maximum temperature from 1000°C for the different basicity (B2)

After observing minimal difference in the average hot air flow rate as shown by Table 5.1, it was determined that a more thorough investigation was necessary to fully understand the hot air flow during the sintering tests and thus the permeability of the sinter bed. To achieve this, a minute-by-minute analysis of the flow rates for the three blends, B2=1.4, 1.7, and 3.0, was conducted. These blends were chosen as they had the highest recorded average hot air flow rate. The analysis focused each blend's air flow measured from between 5-6 minutes to its end sintering time. All blends followed the same curve type, where the flow increased to around 10m^3/hr at approximately 7 minutes. After this, all the curves fluctuated within the 5-11m^3/hr air flow rate range until around 20 minutes. Figure 5.5 depicts the cold flow average of each basicity level and whether the hot air flow rate surpassed it. Figure 5.5 a) displays a gradual increase

in hot air flow, with a minimum value of 6.5 m3/hr and a maximum of 11.0 m3/hr, ensuring that the average cold air flow rate was met. In contrast, Figure 5.5 b) and Figure 5.5 c), which represent the hot flow permeability for B2=1.7 and 3.0, respectively, remained less inclined and did not exceed the average (2 runs) cold flow rate of their respective basicity levels.

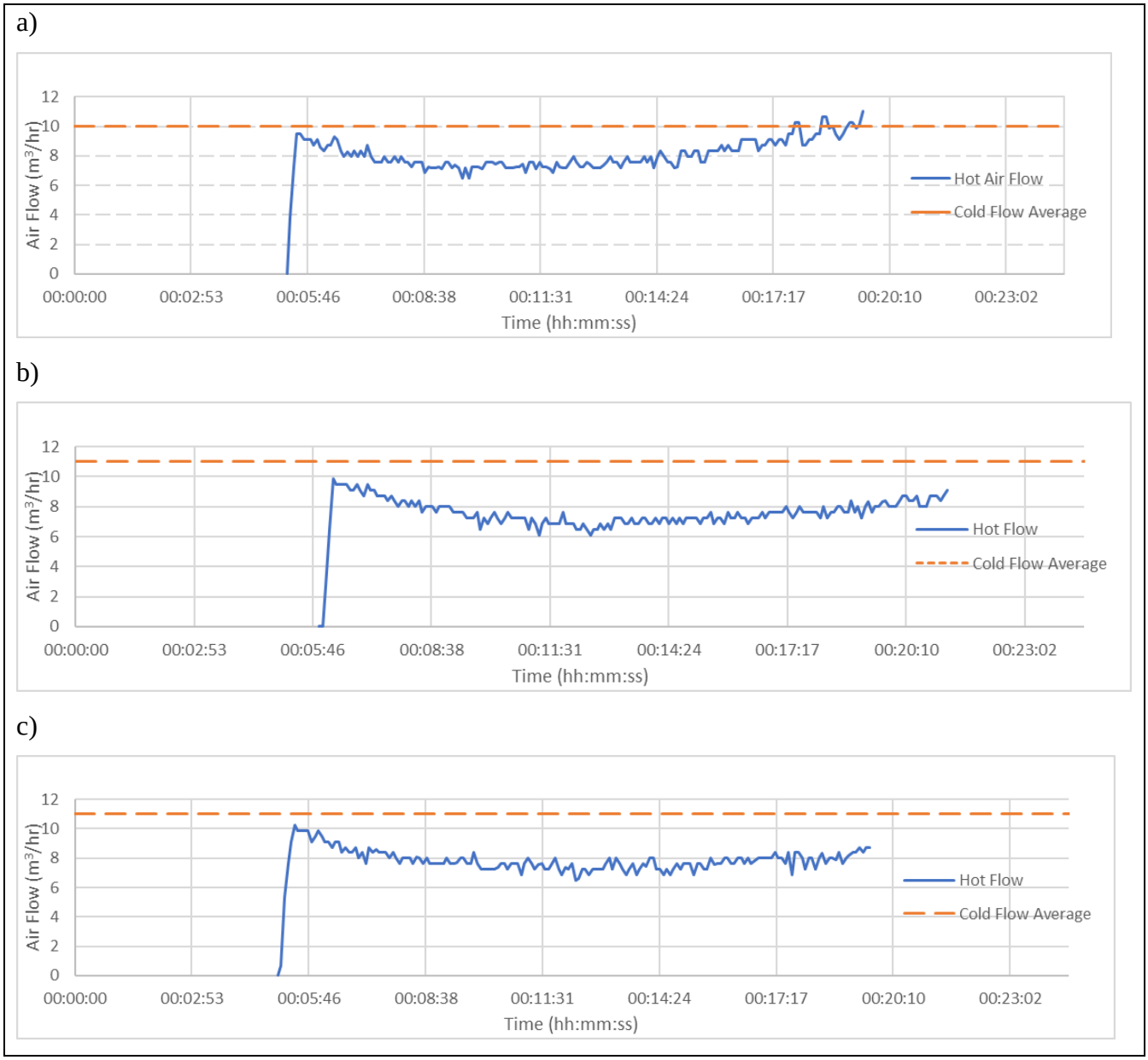

Figure 5.5 Permeability flow as a function of time for a) B2=1.4 b) 1.7 c) 3.0

5.2 Compositional and Phase Analysis

5.2.1 X-ray Fluorescence (XRF)

To provide a comprehensive understanding of the chemistry present in each sinter sample, XRF analysis was conducted, and the results were recorded in Table 5.2. Upon analysing the data, it was observed that the CaO level increased proportionally with a rise in the basicity level. On the other hand, the SiO_2 level remained constant and in line with the expected values. Moreover, it was interesting to note that the FeO content decreased as the basicity level increased, when the basicity level was 1.0 it had the highest FeO content at 7%. In contrast, the Fe_2O_3 level showed a minor variation, with a standard deviation of 2. Overall, these findings provide valuable insights into the chemical composition of the sinter samples and can be used to inform further analysis and experimentation.

Table 5.2 XRF of blends with different basicities (B2s) in terms of wt%

Compounds/B2	1.0	1.4	1.7	2.0	3.0
SiO_2	6	6	6	6	5
Al_2O_3	1	1	1	1	1
TiO_2	0	0	0	0	0
CaO	6	8	9	10	14
MgO	2	2	2	1	2
Fe_2O_3	77	71	74	72	72
FeO	7	6	6	4	4
P	0	0	0	0	0
Mn	0	0	0	0	0

5.2.1.1 X-ray Diffraction (XRD)

The XRD results are displayed for the different basicities as depicted by Figure 5.6. The results show that the major mineralogy which was observed in each of the blends was Calcium Ferrites (CF), Silico-ferrite of Calcium and Alumina (SFCA), Alumina

(A) Hematite (H) and Magnetite (M). The other mineralogy which was observed was small amounts of Magnesia (MgO), Silica (Si), Wustite (W), Calcium Carbonate (CC) and traces of Calcium Oxide (CaO). The SFCA phase was evident in all five blends, however its peak was noticeably stronger in the B2=1.4 and B2=2.0 blends. Moreover, an interesting observation is the peak for hematite and magnetite as showcased around 2θ values of 40 degrees and 75 degrees is significantly high for the B2=1.0 and 3.0 blends as opposed to the other blends

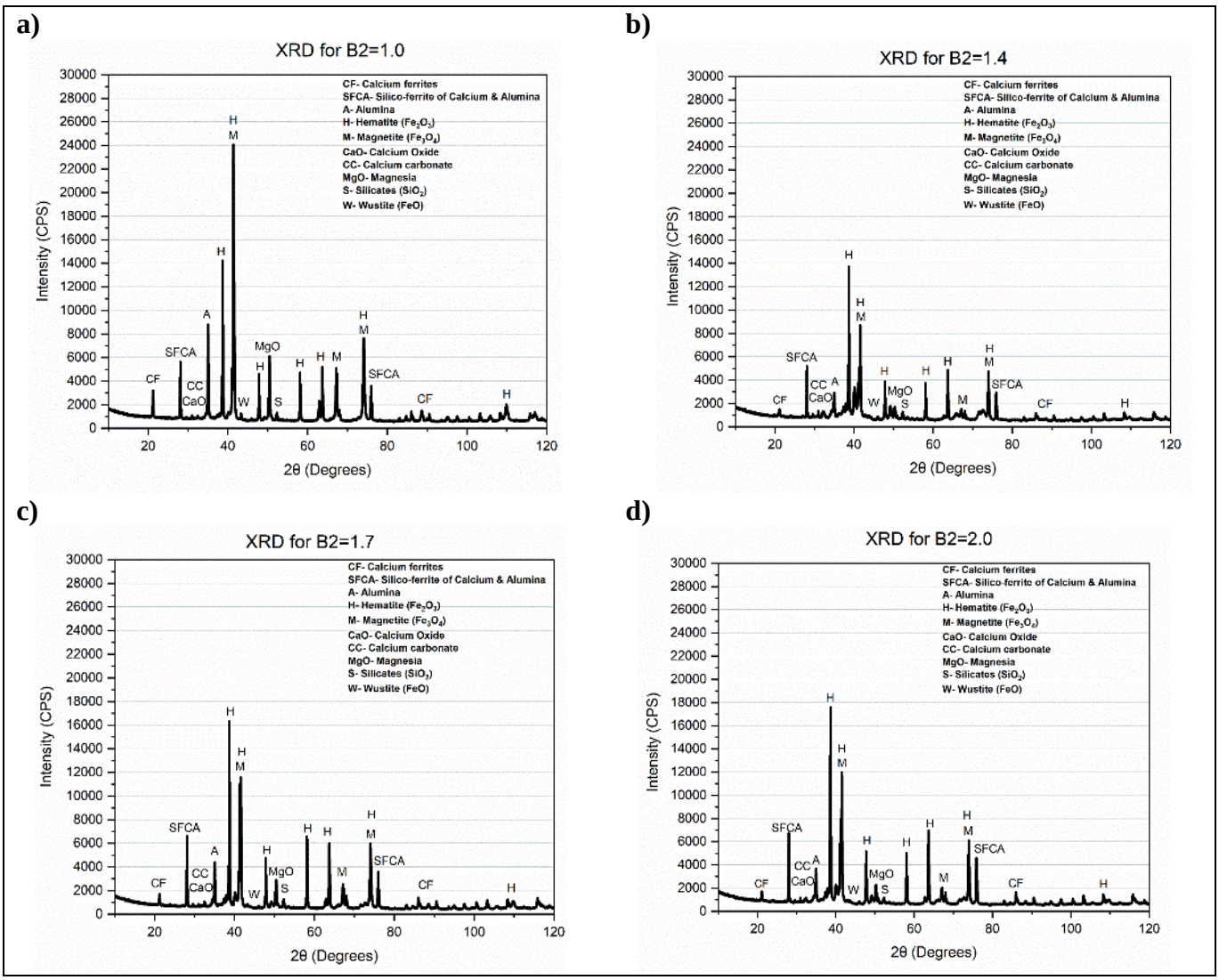

e)

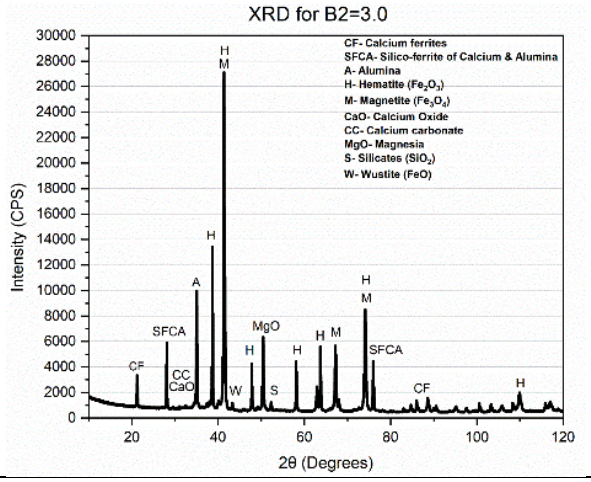

Figure 5.6 XRD patterns for different basicities (B2s). a) B2=1.0. b) B2=1.4. c) B2=1.7. d) B2=2.0 and e) B2=3.0.

The data in Table 5.3 displays the quantitative analysis of the phases that developed during the transition of basicity. The method in which this data was obtained can be found in Chapter 4.8.1.1. The data shows that as the basicity is increased the presence of SFCA's also increase, up until B2=1.7 after which the amount starts to tail off, giving the lowest value recorded for SFCA for B2=3.0. The quantitative analysis reveals that the highest SFCAs were observed at 22% when the basicity was 1.4. Similarly, comparable levels were observed at 14% and 21% when the basicity measured 1.7 and 2.0, respectively. On the contrary, when the basicity level was 3.0 it experienced the lowest SFCA content at 11%. The basicity categories 1.4, 1.7 and 2.0 also showed higher levels of calcium ferrites at 14, 10, and 17%, respectively compared to the other basicity levels. The data also shows no correlation as the basicity value increases for the Fe_3O_4 with low levels of Fe_3O_4 values for when the basicity was 1.4 and 2.0. In addition to this, it was observed the lowest Al_2O_3 level was observed when the basicity was 1.4 at 16%.

Table 5.3 XRD data for varying levels of basicity (B2)

B2/Phases (%)	Fe_3O_4	Fe_2O_3	FeO	MgO	SiO_2	Al_2O_3	$CaCO_3$	CaO	CA-F	Total SFCA
B2=1.0	28	17	0.2	15	0.5	19	2	0.5	6	12
B2=1.4	8	22	1.9	7	1.2	16	5	1.6	14	22
B2=1.7	17	26	0.4	11	0.5	18	3	1	10	14
B2=2.0	10	16	0.9	7	0.5	22	3	1.6	17	21
B2=3.0	30	15	0.2	17	0.3	19	1	0.6	5	11

5.3 Metallurgical Testing

5.3.1 Particle Size Distribution (PSD)

Table 5.4 shows the results for the PSD of the sinter after crushing and vibrating on each sinter cake. This method clearly shows how much fines are generated which as previously reported is a good way of analysing the strength of the sinter[17]. Based on the data, the general trend shows an increase in return fines as the basicity level rose. Also, when B2=3.0 it produced the most <5mm particles at 54% and the least >40mm particles at 0% in comparison to all the other basicities. When the basicity was 1.4 it had the least <5mm particles collected at 24% compared to all the other basicities, with B2=1.7 a close second at 29%. The general trend as the basicity increased was the amount of >40mm particles fell.

Table 5.4 Different PSD of sinter collected on average (2 runs) for each B2

PSD (mm)/Mass of size fraction (%)	1.0	1.4	1.7	2.0	3.0
>40	22	18	14	6	0
25-40	17	20	23	14	2
16-25	7	9	10	14	6
10-16	9	12	11	13	18
5-10	12	16	12	15	20
<5	33	24	29	38	54

Figure 5.7 displays the sinter yield for the 5 different basicity levels in this experiment where it has been taken into consideration only those particles which are larger than 5mm. Figure 5.7 illustrates that the highest yield was obtained at a basicity level of 1.4 at 76%, whereas the lowest yield was achieved at a basicity level of 3.0 at 46%. A trend can be seen which is, as the basicity level increases the particles collected which are more than 5mm generally decrease.

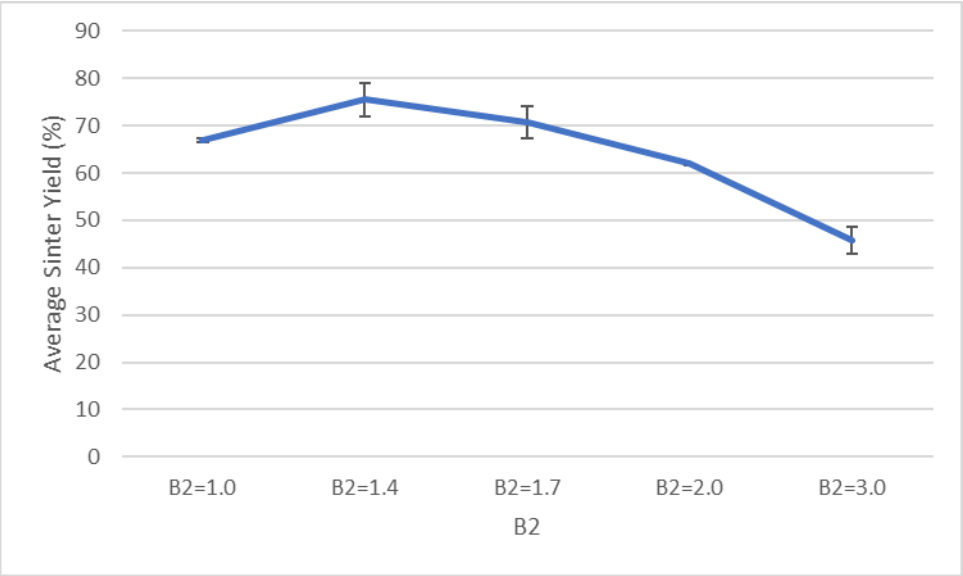

Figure 5.7 Average sinter (>5mm) yield (%) as a function of varying basicity (B2) levels.

5.3.2 Reduction Degradation Index (RDI)

Table 5.5 displays the RDI values for each iron ore sinter produced with basicity values ranging from 1-3%. The sinter produced with B2=1.4 showed the best reduction degradation characteristics with the lowest RDI value compared to the other basicity values at 25%. On the other hand, the sinter produced with B2=3.0 had the highest RDI value at 35% and can therefore be considered the weakest sinter. Although the difference between the RDI's for basicity levels 1.0-2.0 may seem insignificant, recent studies[132] have demonstrated that even slight enhancements can impact blast furnace productivity.

Table 5.5 RDI comparison at different basicities (B2s)

B2	**1.0**	**1.4**	**1.7**	**2.0**	**3.0**
RDI (%)	28	25	26	27	35

5.4 Microscopic Analysis

5.4.1 Optical microscopy & Intellesis images

In this study, Figure 5.8 displays optical images on the left and mineralogical characterisation by Intellesis on the right for each level of basicity. Observing Figure 5.8 (e), it is evident that at a basicity level of 3.0, there is minimal SFCA formation, and the SFCA crystals that form are relatively small. On the other hand, Figure 5.8 (b) and (c), representing basicity levels of 1.4 and 1.7 respectively, show an increase in SFCA content. The olive and light green colours in these figures represent SFCA and SFCA-I, respectively. The SFCAs in these blends are thicker, stripe-shaped, and columnar crystalline grains. Additionally, in Figure 5.8 (b) and (c), the hematite and magnetite phases, represented by blue and magenta colours, respectively, are uniformly distributed around the SFCA phase. However, when the basicity level was 1.0, hematite and magnetite appear more isolated, as seen in Figure 5.8 (a). The data for the average mineralogy collected by Intellesis is displayed in Table 5.6.

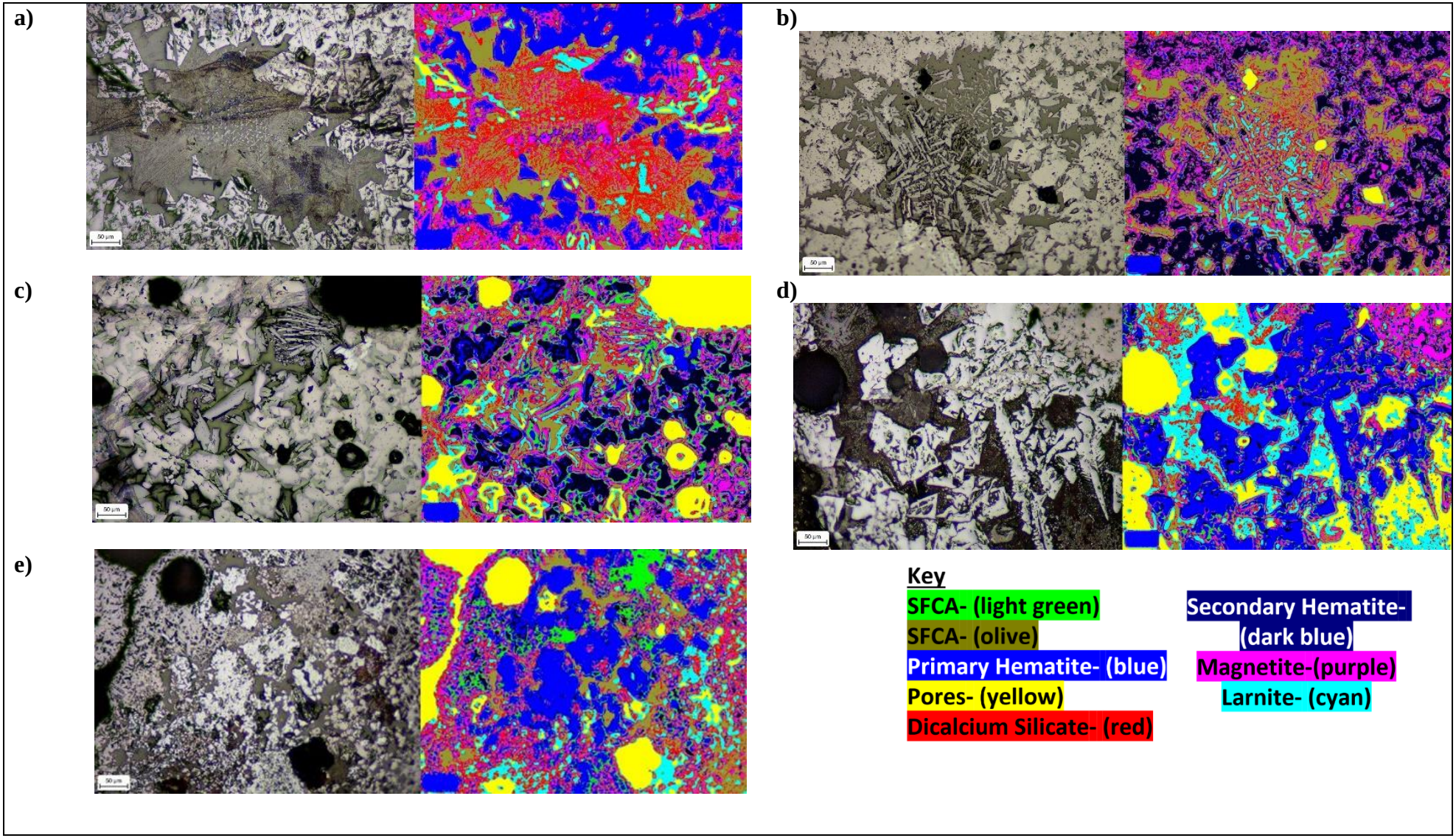

Figure 5.8 Images obtained from optical microscopy (left) whilst the images on the right are obtained from Intellesis. Images taken for basicities (B2s) a) B2=1.0. b) B2=1.4. c) B2=1.7. d) B2=2.0 and e) B2=3.0.

Table 5.6 Average phase composition (%) of each mineralogy at different basicities (B2s) according to data generated through Intellesis.

B2/Phase (%)	SFCA	Primary Hematite	Pores	Dicalcium Silicate	Secondary Hematite	Magnetite	Larnite	SFCA-I	Total SFCA's
B2=1.0	17	17	11	6	26	16	2	4	22
B2=1.4	23	16	3	7	27	14	5	6	29
B2=1.7	20	14	10	5	24	18	5	5	25
B2=2.0	18	21	13	4	16	15	7	5	23
B2=3.0	14	20	18	7	18	12	6	5	19

The comparison of total hematite captured through XRF and Intellesis analysis methods is displayed in Figure 5.9. The results generated show a difference in the two characterisation methods. The variation across the basicity values for the XRF results was 2, while for the Intellesis data, it was 3. Which shows small deviations from the mean value for both characterisation techniques.

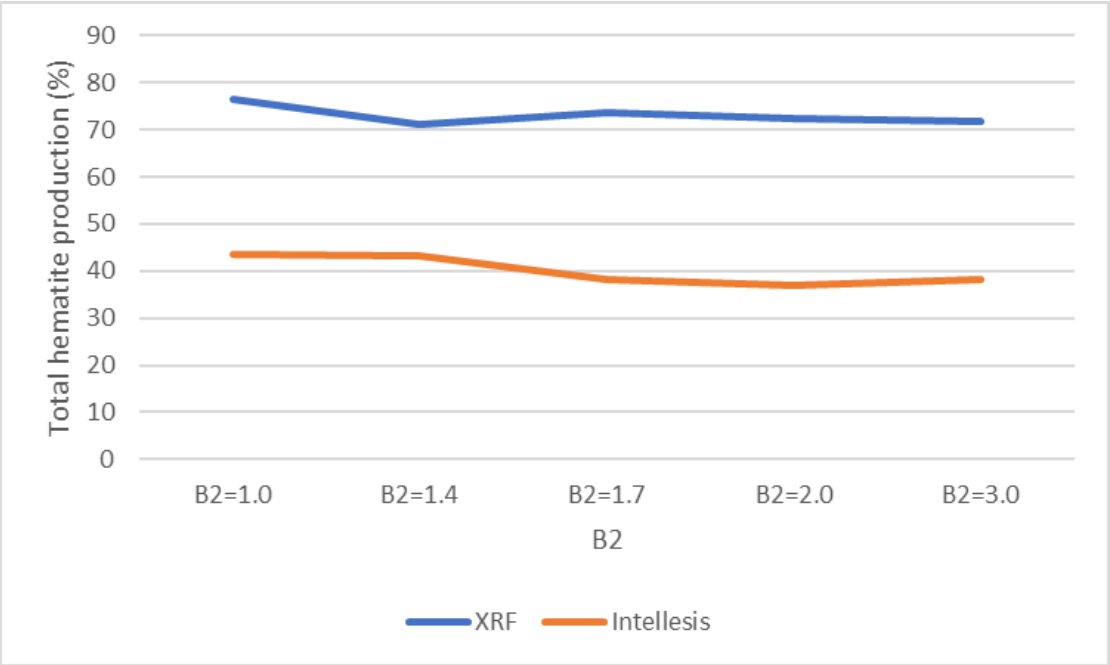

Figure 5.9 Quantitative comparison of the total hematite content found via Intellesis and XRF analysis for various B2s.

According to the information presented in Figure 5.10, the formation of SFCA has been observed over time, for the different basicity levels. The results indicate that when the basicity was 1.4 it was the most efficient blend as it yielded the highest number of SFCA's in the shortest period, which is in agreement with the hypothesis set out for this experiment.

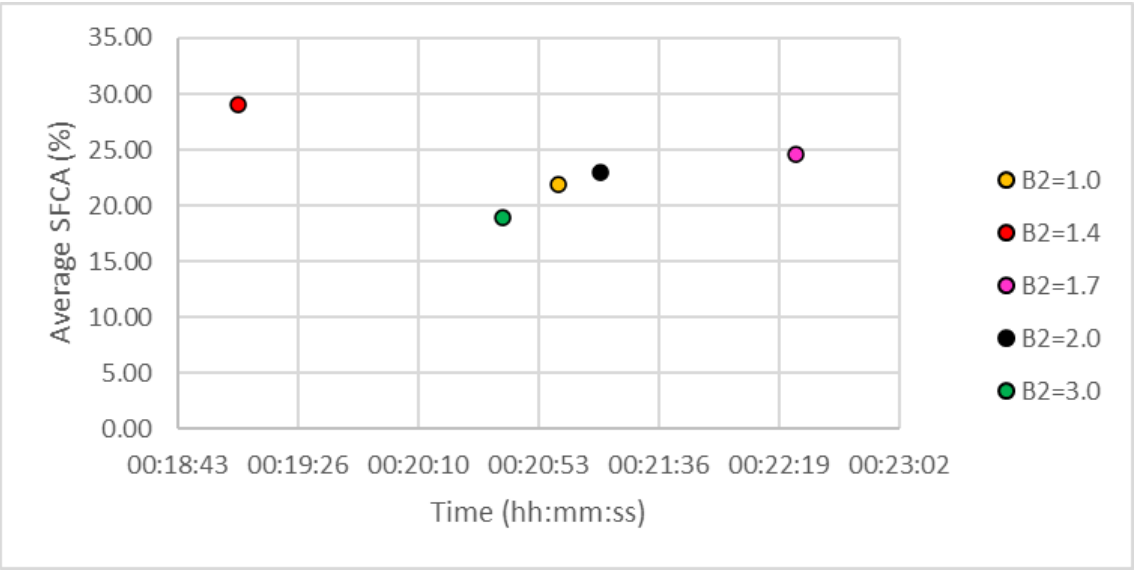

Figure 5.10 Time as a function of average SFCA formation based on data collected via Intellesis for the different basicities (B2s).

Upon reviewing Figure 5.11, it is apparent that the SFCA formation observed at different basicity levels varied based on the predictions from FactSage, a thermodynamic model, and the experimental results obtained through the Intellesis method. The FactSage model mainly considers the thermodynamic driving force and not the kinetic driving force, which is a crucial factor contributing to the variance in data between Intellesis and FactSage. FactSage predicted the highest SFCA formation at a basicity level of 3.0, while the Intellesis data indicated that the highest SFCA formation occurred at a basicity level of 1.4.

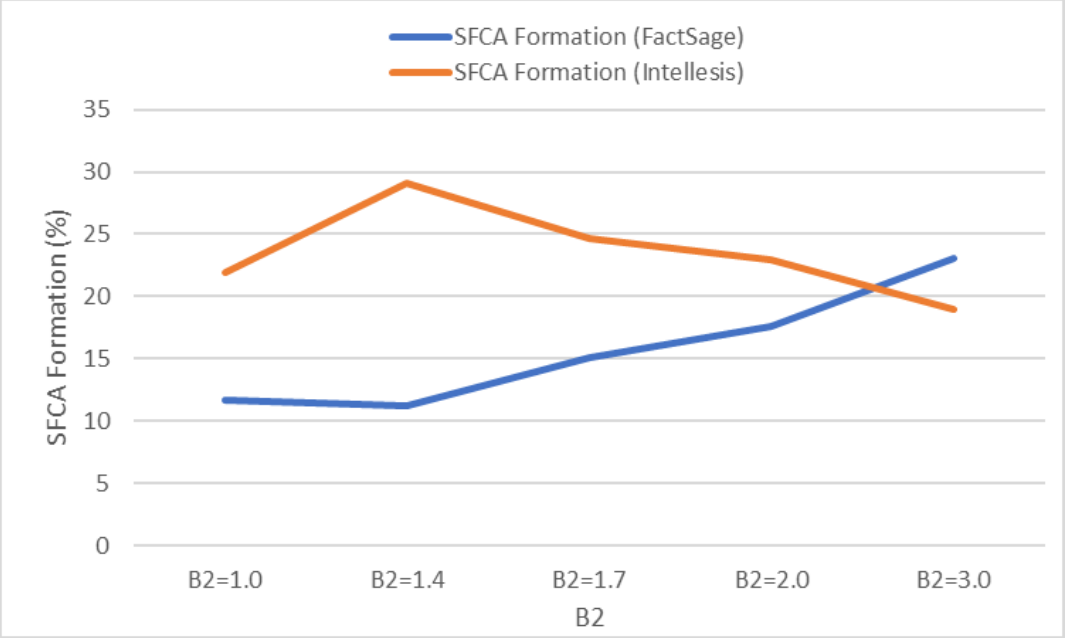

Figure 5.11 SFCA formation according to Intellesis and FactSage data for different levels of basicity (B2).

5.4.2 Scanning Electron Microscopy/ Energy Dispersive Spectroscopy (SEM/EDS)

Figure 5.12 shows the EDS mapping of the chemistry obtained by this characterisation method along with the quantification. Dominant element Fe can be seen to be reducing as the basicity is increased, which was in line with the findings from the XRF as seen in Table 5.2. In high-quality sinter, Fe bearing minerals like hematite (Fe_2O_3) and magnetite (Fe_3O_4) are predominant. Lower Fe content means fewer of these desirable phases form. As well as this a distinct difference in the level of Ca and Si can be seen between the basicities in the region 1.4-2.0 compared to when the basicity was 1.0 and 3.0, however this could just be experimental. This has been discussed further in Section 5.8.

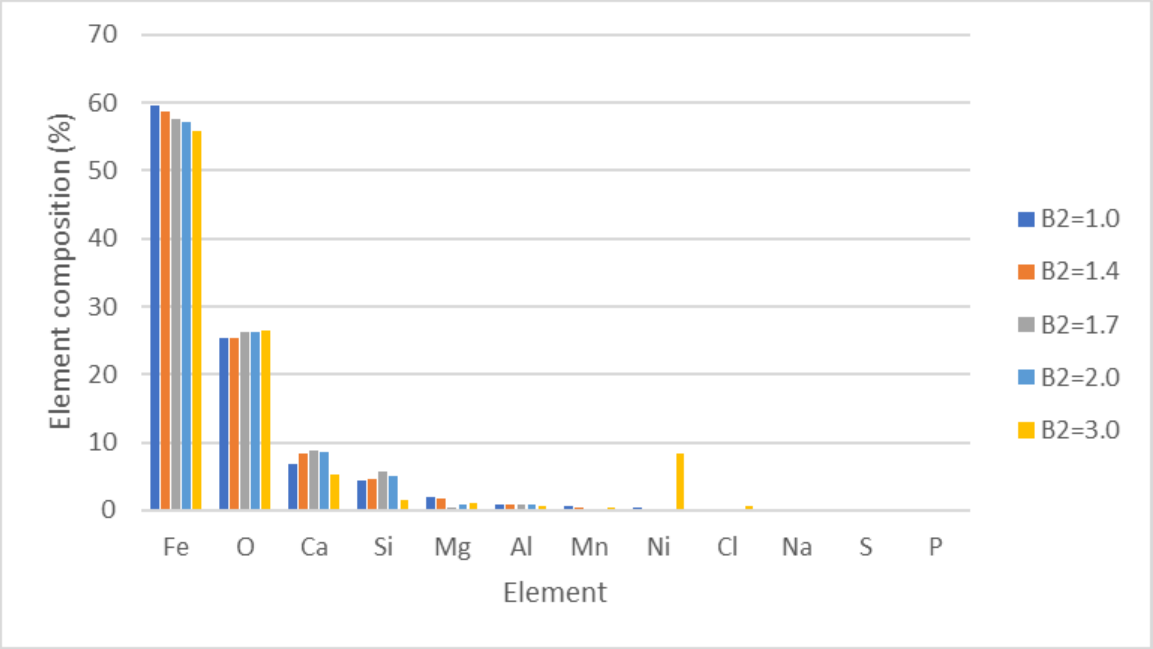

Figure 5.12 Average chemical quantification for different B2s according to data obtained from EDS.

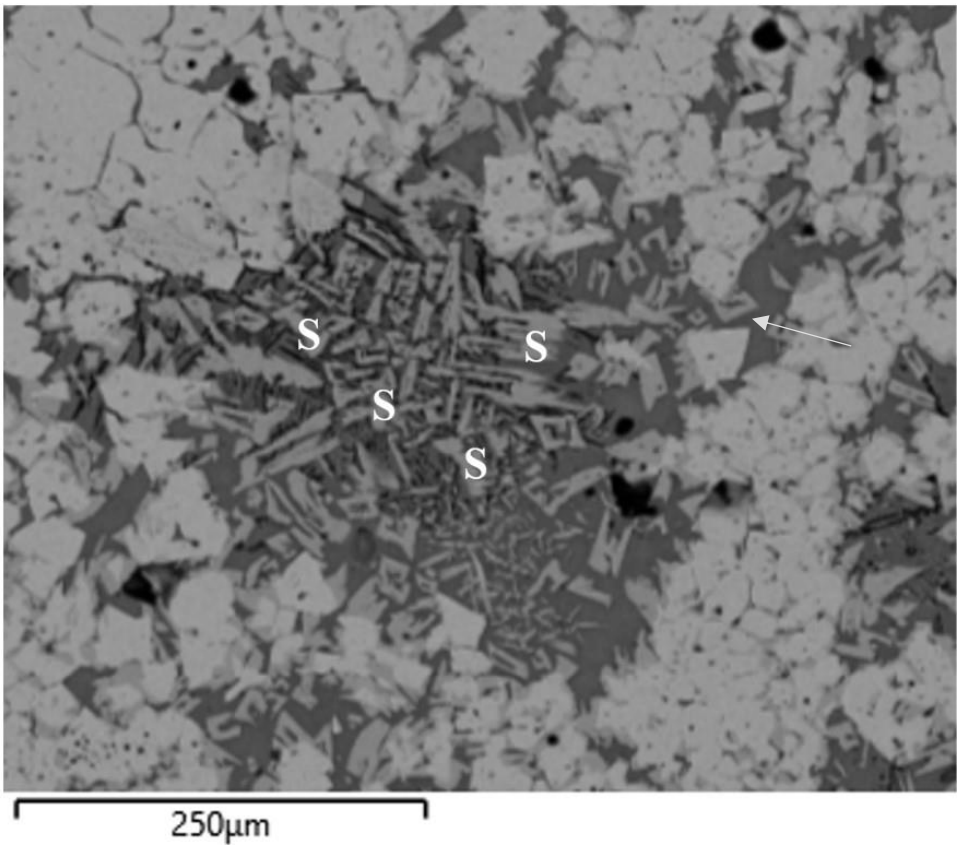

Figure 5.13 SEM image of B2=1.4 which shows SFCA's

Figure 5.13 shows precisely where the SFCA feature is present as denoted by the 'S' which is the same microstructure seen in Figure 5.8 b). Figure 5.13 is inserted here to determine the actual chemistry of what is regarded as the SFCA phase identified by the Intellesis method.

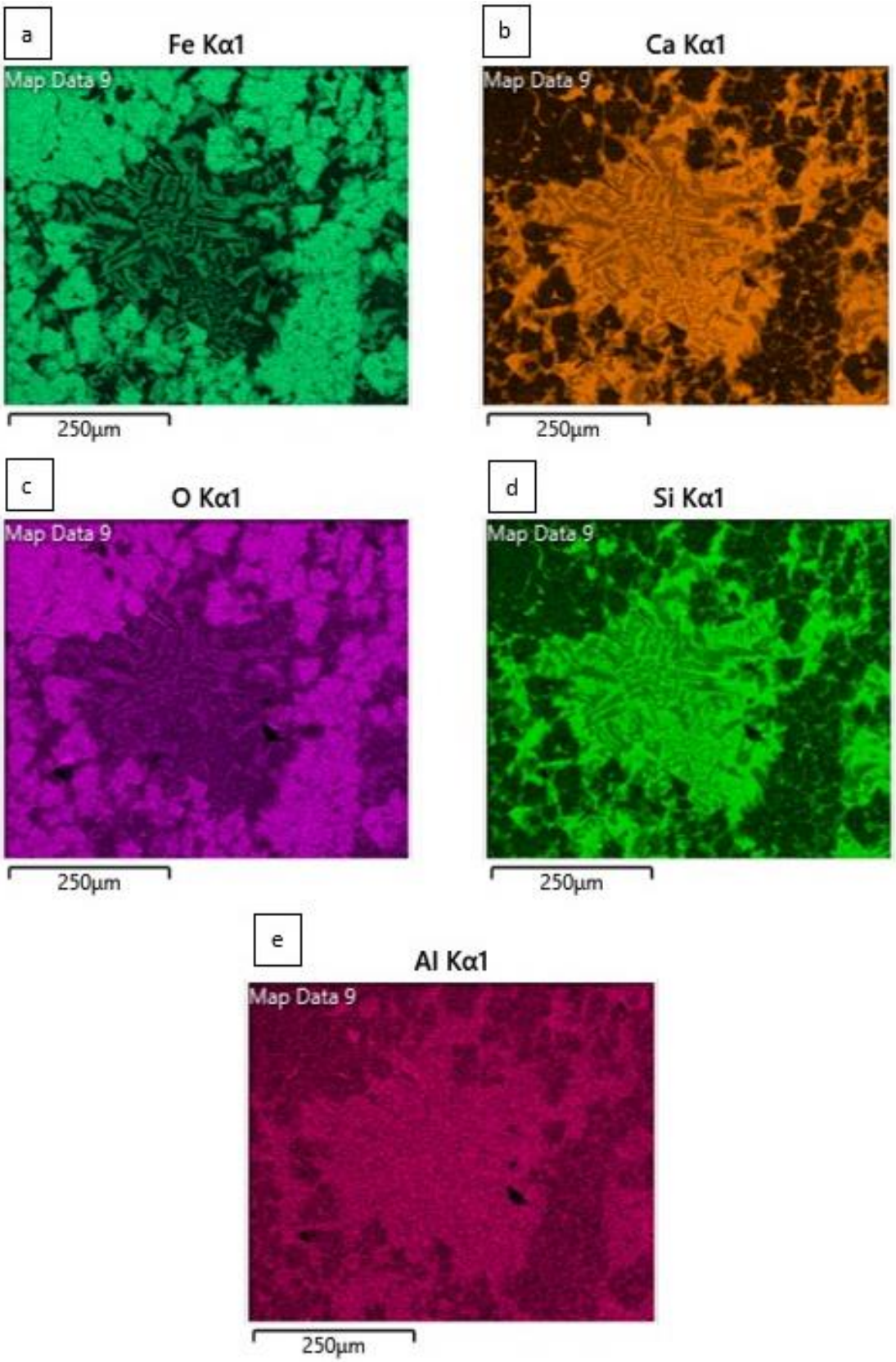

Figure 5.14 EDS mapping of the presence of SFCA's within B2=1.4. a. Fe b. Ca within B2=1.4. c. O within B2=1.4. d. Si within B2=1.4. e. Al within B2=1.4.

Furthermore, it was found that the presence of SFCA in B2=1.4 was further confirmed by SEM images and EDS data analysis as shown in Figure 5.14. The EDS mapping shown reveals the major elements: Fe, Ca, O, Si, and Al, all of which are components of SFCAs. In the images, black areas indicate where the phase of interest is absent, while other colours represent its presence. The observation that all the elements comprising SFCA are present reinforces the earlier findings from the Intellesis work package regarding the existence of SFCA.

5.5 Discussion

5.6 Influence of Basicity on Thermodynamics

In Figure 5.3 (a) and (e), the temperature profiles are inconsistent. It is observed by the stable profiles that when TC4 is in the drying and preheating zone it asymptotically finishes off and there is no sign of overlap between TC4 and TC5 on that line[26]. Whereas for both (a) and (e) the curve for TC4 touches the curve at TC5 at the drying and preheating zone point and does not have a smooth curve. Such irregularities can lead to inhomogeneous sinter production.

Figure 5.4 shows that the average maximum temperature generally decreased as a function of an increase in basicity. According to Zhang et al[5] maximum temperature and therefore the flame front temperature decreasing was due to endothermic reactions needed to calcine the extra limestone that was found in the higher basicity tests. Furthermore, the inclusion of limestone accelerated the temperature cycle and reduced the duration spent in the high temperature zone[5]. As a result, the blends with higher basicity levels fail to achieve the same peak temperatures as those with lower basicity levels.

After analysing the data depicted in Figure 5.7, a clear trend between the maximum temperatures achieved during the iron ore sintering process and the resulting yield (>5mm) of sinter product was revealed. The particle size that is less than 5mm was not considered because it would be classified as fines and would not be used in the blast furnace. Also, to accurately determine the benefits of different blends in terms of strength, this category was excluded from the analysis.

The blends tested in the experiment (effect if change in basicity on the sinter quality) revealed that the basicity level of 3.0 exhibited the lowest maximum temperature and consequently yielded the least amount of sinter. On the other hand, the basicity level of 1.4 displayed the highest maximum temperature and produced the most amount of sinter. These results emphasise the critical role of temperature in determining the success of the sintering procedure in terms of attaining the appropriate temperatures, and thus the resultant heat, consequently providing a positive impact on the yield of

the iron ore sinter produced[40]. The fuel rate remains unchanged in this experiment, pointing to either thermodynamic effects of the constituents or the efficacy of the supply of the other reactant (Oxygen and then CO). It can be inferred that temperature plays a pivotal role in determining the final output of the sintering process, and hence, it must be closely monitored and controlled. To achieve high yields, it is essential to ensure that the maximum temperature between 1200-1300°C is reached while avoiding overheating, which could cause the iron ore sinter particles to become brittle and lose their mechanical strength. Proper temperature control not only enhances the quality of the sinter but also significantly reduces production costs and energy consumption. Therefore, it is crucial to optimise the temperature conditions during the sintering process to improve the yield and overall efficiency of the process.

Studies have demonstrated that the temperature profiles in sintering play a significant role in determining the sintering time and RDI. Specifically, it has been observed by Hosotani et al.[40] that by reducing the holding time during sintering at temperatures of 1173K and above, the heat patterns in the middle and lower layers of the sinter become more uniform. This refinement ultimately leads to a shorter sintering time and an improved RDI. In this experiment, Figure 5.3 illustrates that TC3 (which measures the middle layer) at basicity level 1.0 had a holding time of 230 seconds at and above 1173K. This holding time was longer than that observed for when the basicity level was 1.4 which was at 220 seconds. Consequently, the difference in holding time may have contributed to the lower RDI and shorter sintering time for B2 level 1.4 compared to the B2=1.0 blend, as demonstrated in Table 5.5 and Table 5.1, respectively, however judging by the small difference of 10 seconds holding time it could be deemed less likely. These findings suggest that it is critical to exercise precise control over the holding time of high temperatures to optimise sintering time and produce iron ore sinter with low RDI. To do this a series of tests can be conducted to try optimising the sintering process parameters, including the holding time, under various operating conditions. These results can then be used to establish best practices and guidelines for controlling the holding time.

Recent scientific research has uncovered compelling evidence that increasing the temperature of iron ore sinter can positively impact its RDI, leading to improved structural integrity and overall quality. This is because higher temperatures make the

sinter more plastic, allowing it to better withstand expansion stress and reducing the likelihood of cracking[42], ultimately resulting in a lower RDI value. The present study supports this finding, as there has been an observation that the maximum temperature of B2=1.4 reached 1373°C as illustrated in Table 5.1 and the same blend resulted in the optimal RDI value of 25% as demonstrated in Table 5.5.

As discussed in Chapter 3.4.1 the effect of thermodynamics on the production of SFCAs has been mentioned extensively. One quality indicator which is renowned to be present when iron ore sinter blends reach high temperatures is the presence of SFCA's, they typically form around 1200-1300°C[28] [29] [30] [31] [32]. Upon careful examination of the thermodynamic data, it was determined that most of the blends in question reached a temperature above this and were therefore not significantly impacted by the change in basicity. These blends were able to maintain a temperature above 1200°C without issue. However, when the basicity was 3.0 the temperature was recorded at 1163°C. This unexpected result was found to be caused by too much of an increase in limestone content, which hindered the blend's ability to reach higher temperatures. The heat absorbed by the limestone's decomposition reduces the overall heating efficiency of the sintering process. As more limestone is present in the sinter mix, a larger portion of the energy input is diverted to heating the limestone rather than raising the temperature of the sinter bed. To maintain stable temperature profiles, it is advisable to operate within the basicity range of 1.4-2.0. Such a range provides consistent temperature patterns, while basicity levels that are too low or too high (i.e., B2=1.0 and 3.0) will most likely result in unpredictable curves and fail to deliver the necessary chemistry to attain the required high temperatures.

5.7 Influence of Basicity on Sinter Bed Permeability

In the experiment, it was observed that B2=1.4 had the shortest average sintering time. The flame front travelled from the top of the pot to the bottom at a quicker pace compared to other blends. The speed of the flame front is influenced by various factors such as fuel type, air supply, sinter bed temperature, and permeability of the bed[55]. To ensure that the speed of the flame front was not affected by fuel type and air supply, they were kept constant throughout the experiment.

When the basicity was 3.0 the average hot flow rate was at a high of 11 m^3/hr as demonstrated by Table 5.1. The reason for this was due to the introduction of additional lime. This additional lime which was added as the basicity increased most likely reacted with the iron oxides present in the ores (Fe_2O_3, Fe_3O_4) to produce calcium ferrites such as $2CaO{\cdot}Fe_2O_3$ and $3CaO{\cdot}Fe_2O_3$. These calcium ferrites have been reported to possess lower melting points when compared to the original iron oxides, which can facilitate the development of a more fluid phase within the sintering process. An increase in the liquid phase has been observed to significantly improve the bonding and agglomeration of iron ore particles, thereby promoting greater homogeneity within the bed. As a direct consequence, there is a marked improvement in the permeability of the system.[31] [149]

Upon analysing the data collected by the sinter pot (as shown in Figure 5.5) for the three blends (B2=1.4, 1.7, and 3.0), it was discovered that only B2=1.4 exceeded its respective cold air flow rate average. The remaining blends, B2=1.7 and B2=3.0, did not surpass their respective cold flow average. This can be better comprehended by examining the individual data of the hot flow and comparing it to the location of the flame front within the pot. The phenomenon of bridge formation and breaking within the sinter pot is responsible for the permeability of the pot, resulting in more porosity being created as bridges form, thereby increasing the hot flow rate. As the bridges break and the sinter solidifies, the hot flow rate increases. This is evident in the shape of each of the hot flow rate graphs, where the curve initially declines, reaches a minimum, and then rises again. At the start of the process, most of the pot is a green blend, which has good porosity, enabling smooth flow. However, as bridges begin to form, more liquid is produced, causing the flow to slow down. The flow then starts to increase again as the bridges are being broken and the sinter is solidifying, allowing more of the pot to have the porous structure formed, thus enabling smoother flow again. The permeability of level 1.4 in basicity is best as represented by Figure 5.5 a), as it surpasses the initial cold flow average and indicates good permeability. However, B2's other two levels (1.7 and 3.0) do not return to the cold flow average level, suggesting an underlying issue in the sinter production chemistry. Notably, the only variable altered in this experiment was the chemistry, which influences the resulting mineralogy as elaborated in section 5.8.

A recently conducted study by Mathur et al.[55] has revealed some noteworthy findings concerning the iron ore sintering process. The study discovered that the quantity of return fines can have a significant impact on the process, altering the sintering time due to the resulting increase in sinter porosity[55]. The current study showed that there was a clear reduction in sintering time when the amount of return fines increased from B2=1.7 to B2=3.0, as demonstrated by Table 5.1 and Table 5.4 respectively. This indicated that the modification in B2 affected the porosity of the sinter, consequently impacting its permeability. However, it is worth noting that this increase in sinter fines adversely affects the strength of the sinter[55]. Therefore, it is essential to monitor the amount of sinter fines generated to be able to rectify the overproduction and thus control the desired sintering time and the optimal strength of the sinter.

Throughout the course of the experiment, it was observed that an increase in B2 levels corresponded with a general decrease in sintering time as seen by Table 5.1. This phenomenon has been extensively studied in literature and is attributed to several factors. One of the primary reasons is that a higher B2 level leads to greater efficiency in air utilisation, resulting in a reduction in specific air requirement and subsequently contributing to shorter sintering times[67]. Another contributing factor is the improvement in preignition permeability and average permeability[68] that occurs with an increase in B2 level. This reduction in resistance in the drying zone, which is essential in water migration, alongside the increase in average permeability, works to lessen sintering time. Furthermore, as resistance in the combustion zone decreases, it further enhances average permeability and reduces sintering time.

In addition to the previously mentioned effects, it is important to note the reason for the reduction in sintering time as the B2 level rises has been reported by another recent study. From an experiment by Nyquist et al.[69] it was found that the reason for this effect was attributed to the low viscosity and high surface tension of the melt, which work together to enhance the sintering process. Moreover, the solidification process proceeds rapidly in this scenario, and the temperature coefficient of viscosity is relatively high, which further accelerates the sintering process. Therefore, for this reason it can be concluded that the increase in basicity level can have a positive impact on the efficiency and effectiveness of the sintering process, however locating an optimum is still important so the sinter does not lose its strength.

Based on the data presented in Table 5.1, it can be inferred that the bed permeability was in a favourable state when B2 was at a value of 1.4. This was supported by the observation that this blend exhibited the shortest average sintering time of 19 minutes and 30 seconds. Moreover, referring to Table 5.3 which shows the XRD results, it was observed that this blend recorded the lowest Al_2O_3 level (16%) in the final iron ore sinter compared to the other B2 levels studied. Scientific literature by Hino et al. [86] has suggested that lower levels of Al_2O_3 can mitigate the hold-up of slag melt in the pores of the iron ore sinter, thereby leading to better indirect reduction in the blast furnace[86]. Therefore, it can be recommended that operating at this specific B2 level would most likely improve reduction capabilities.

When studying the effect of B2 on bed permeability, the most suitable indicator to measure it would be the average hot flow rate. This is because it is measured during the sintering process. The experiment was conducted twice, as mentioned in Chapter 4. The two test carried out showed no variation. This suggests that the results are reliable and that the values were not significantly different, leading to the conclusion that the influence of a change in basicity on bed permeability is insignificant when using the average hot flow rate as a measurable parameter.

5.8 Influence of Basicity on the Formation of Phases

SFCA is known to be the desirable phase to obtain sinter of high quality as stated by Majumder et al[28]. Using FactSage, a thermodynamic simulation was carried out which clearly showed all the different levels of B2 in this experiment had the capacity to form SFCAs as depicted by Figure 5.1 and Figure 5.2.

As it can be seen in Figure 5.1 between the mass ranges of 0-2000g, the relevant phase present denoted by SFCA, as it can be seen it peaks at approximately 1200°C in terms of mass which means this is the temperature where the phase can be seen to be most stable, which is in the range between 1200-1300°C reported in literature[24]. The prediction model showed that as the temperature increased from 200°C to 1200°C, the rate of SFCA production increased at a rate of 0.012 %/°C. However, when the temperature rose beyond 1200°C, SFCA production appeared to slightly decrease from 12% to plateau at around 8%. Interestingly, looking at Figure 5.2 the prediction

model suggested that as the B2 level would rise, the amount of SFCA formation would rise too. This is very similar to what was seen in several studies carried out in literature,[72] [73] [30] and was attributed to the fact that the SFCA phase stabilises with an increase in B2.

The production of sinter is a complex process that can be hindered by various factors. Thermodynamic models are created with certain assumptions and simplifications to make calculations easier, but these assumptions may not capture all the complexities of the real-world system. For example, the model may assume ideal behaviour and neglect non-ideal mixing, phase transitions, and kinetic effects that can affect the sintering process. Additionally, as demonstrated in Chapter 4.8.1's FactSage simulation setup procedure, some compounds were not accurately modelled due to the limitations of the programme therefore assumptions had to be made regarding these compounds.

The FactSage model considers the thermodynamic driving force and not the kinetic driving force, which is a crucial factor contributing to the variance in data between Intellesis and FactSage, as evidenced in Figure 5.11. Thermodynamics provides insight into the equilibrium states, but reactions may not always achieve equilibrium during the timeframe of the experiment. Kinetic control, where the reaction rate predominates over equilibrium considerations, can lead to unforeseen outcomes. The formation of the product, whether it is in its most stable state or due to the pathway with the lowest energy barrier, depends on whether it is thermodynamically or kinetically controlled. In the case of thermodynamic control, the product is formed in its most stable state, while in the case of kinetic control, the product is formed because the pathway with the lowest energy barrier leads to it[150].

Table 5.6 which demonstrates the Intellesis findings, showed that the blend containing the highest amount of SFCA's was recorded at 29% when B2 measured 1.4. Additionally, comparable levels were noted at 25% and 23% when B2 measured 1.7 and 2.0, respectively. These findings are consistent with the XRD patterns quantified in Table 5.3 It is noteworthy that Intellesis (image sample) consistently yields higher numerical values for SFCA quantification compared to XRD (bulk sample) values.

As the SFCA feature is quite complex it is possible that the image samples provided a more detailed analysis of this feature within the material. This study focused on examining the intricate details within the iron ore sinter of the SFCAs, utilising 20X magnification images, which is a higher magnification level than the 5 and 10X extensively used throughout literature. These localised features exhibit different properties or characteristics compared to the bulk material, and image samples can provide a more accurate representation of those features, resulting in a higher numerical value. Additionally, the higher resolution of image samples can offer finer detail compared to bulk samples of the SFCA, leading to more precise measurements of the feature that may not be captured by bulk sampling techniques. As a result, the numerical values obtained from image samples were higher due to the ability to resolve smaller or more intricate structures.

As previously indicated, the introduction of limestone for the purpose of increasing B2 had the unintended consequence of reducing the maximum temperature reached in the test. However, it was observed that a B2 level of 3.0 had a detrimental effect on the formation of SFCA. The resultant low temperatures were responsible for the detection of low levels of SFCA by both XRD and Intellesis, as demonstrated in Table 5.3 and Table 5.6, respectively.

The effect of an increase in basicity on the level of total hematite observed is negligible as demonstrated by Figure 5.9 by both characterisation methods; Intellesis and XRF. However, there is approximately a 30% difference between the values obtained between the two methods and this difference is because the XRF method is a technique that employs bulk sampling to analyse the chemical composition of a given substance, as opposed to focusing on its phases, which is the primary objective of the Intellesis method.

Similarly, to the data captured for the average formation of SFCA, the XRF quantification data obtained through the bulk method yielded higher results compared to the Intellesis . The reason for this disparity lies in the optical microscope's ability to detect more SFCAs, which leads to the Intellesis covering less of the primary and secondary hematite areas. Conversely, the bulk measurement of the XRF provides accurate identification of hematite as a significant phase in iron ore sinter with only a

relative error typically around 1-2%[103]. Although the Intellesis also recognises this, it excels at detecting the SFCA formation due to its more prominent presence in the microstructure.

In terms of productivity of the sinter produced Figure 5.10 is a good representation to show that when the B2=1.4 the most SFCA's on average are formed as confirmed by Intellesis, it is the blend that produces the most on average and produces them approximately 3 minutes quicker than the next fastest blend. When analysing which blend is the most efficient this is the decisive factor in determining the optimum B2. The observed behaviour of B2=1.4 can be attributed to its efficient granulation process, which has resulted in notable improvements in both its permeability and flow. This heightened permeability has led to faster flow and sintering velocity, as well as optimal combustion of fuels and heat transfer between gas and solid phases[57 58]. Ultimately, these enhancements have facilitated superior productivity.

The EDS mapping illustrated in Figure 5.12 showcases the presence of Ca and Si in each of the blends used in this experiment. The SFCA compound is observed in a low-Fe, high-Si form and has a prismatic or columnar morphology. In contrast, SFCA-I exists in a high-Fe and low-Si form and presents a platy morphology[24]. The identification of Ca, Si, and Al in the EDS mapping indicates that the samples contain SFCA and calcium ferrites, which were also observed in the XRD. The colours of olive and light green in the Intellesis images confirm the existence of SFCA and SFCA-I. Moreover, the EDS quantification shows that out of all the blends there is the most Ca, Si and Al in B2=1.4, 1.7 and 2.0, which are the major elements which are contained within SFCAs. As well as this, the amount of SFCAs collected was most in this B2 region as identified by the Intellesis and XRD quantification. This is further proof of corroboration for the Intellesis work package.

Further data from the SEM/EDS analysis shows that in the specific optical microscopy image which was also simulated through Intellesis and is shown in Figure 5.8(b), upon processing the same image on the EDS, it is clear to see the elements which are present which are Fe, Ca, O, Si and Al. SFCA has been reported to be 60–76 mass% Fe_2O_3, 13–16 mass% CaO, 3–10 mass% SiO_2, 4–10 mass% Al_2O_3 and SFCA-I which is 84 mass% Fe_2O_3, 13 mass% CaO, 1 mass% SiO_2 and 2 mass% Al_2O_3[51]. In this study these

phases have been evident in each level of B2 in several different techniques including XRD, Intellesis and FactSage modelling. The SEM/EDS analysis shows how it is represented not only as a whole blend, but in the specific area noted by Figure 5.13. This specific area which was previously deemed to contain the phase SFCA denoted by the olive colour seen in Figure 5.8(b) gains further verification because of the presence of all the possible elements that comprises an SFCA through the EDS analysis shown in Figure 5.14.

The Intellesis image analysis software produced data of great value and demonstrated the capabilities for future mineralogical investigation. The trends shown within this experiment were interesting as the findings for total SFCA's on average from all the iterations from Intellesis was consistent with what was found in the quantitative data obtained from the XRD patterns as shown from Table 5.6 and Table 5.3. As well as this, the SEM/EDS results for B2=1.4 was analysed as shown in Figure 5.13 and Figure 5.14. Table 5.4 shows that for the PSD calculated for the >16 mm category, B2=1.4 had the highest amount of particles at 48% of the sinter collected at this size. This could mean that it was strong sinter and thus remained in that size and it did not proceed to further breakdown after it was subjected to crushing and shaking. This is further emphasised as it is also the blend which yielded the least <5 mm sinter on average at 24% in comparison to the rest of the blends. A reason for this could be the presence of SFCA's which was the most observed, which gave rise to this strength.

As per the findings of the previous section, it was observed that the blend containing B2 of 3.0 had a crumbly texture and was devoid of particles larger than 40 mm. This blend also had a considerable amount of fines (particles less than 5 mm) that constituted 51% of the entire blend. Despite having a diverse mineral composition that was evident from the optical microscopy images and Intellesis data, the blend's strength was noticeably low. It is worth noting that the increased presence of B2 resulted in a higher mineral content, but it also led to a considerable weakening of the sinter, making it unsuitable for use in a blast furnace. This weakness was further confirmed by the RDI value of 35%, which indicated that the sinter was not strong enough to be used for iron ore sintering purposes.

In addition, according to Table 5.6, the blend with B2=3.0 has the highest percentage of pores at 18%. This could be a contributing factor to the decrease in strength observed in the blend, which is consistent with research conducted by Loo et al.[29], as well as Lu et al.[151]. These studies found that as the pore area increased, the sinter strength decreased.

Table 5.2 displays the XRF data, which indicated a significant reduction in the FeO content with an increase in the B2 level. This is likely due to the increased phase of magnetite (Fe_3O_4), as observed in the relevant literature[38]. The data collected via XRD for the magnetite phase as shown by Table 5.3 provides confidence to this conclusion, showing a general increase in the average magnetite phase as the B2 level was increased.

During the XRF experiment as displayed in Table 5.2, a noteworthy discovery was made regarding the iron ore sinter produced. Except when the B2 level was at 1.0, the findings indicated that sinter with higher levels of FeO exhibited remarkable RDI properties[59] as shown in Table 5.5. Further research[38] unveiled that this was attributed to the presence of magnetite during the sintering process. This, in turn, resulted in the formation of a stable FeO phase.

As per recent literature, it has been observed that the presence of high levels of FeO can have an adverse impact on the reducibility of iron ore sinter. This is primarily due to the formation of fayalite which results from the reaction between FeO and SiO_2. Fayalite is a phase that is known to be challenging to reduce, and thus, a higher FeO content can lead to lower reducibility levels in the blast furnace[11]. After analysing Table 5.2, it was found that the B2 level with a value of 1.0 had the highest FeO content. This implies that when the sinter produced with this B2 level enters the blast furnace, it could react with SiO_2 and create the fayalite phase. As a result, it would have the lowest reducibility in the blast furnace. Based on this observation, it can be concluded that the blend B2=1.0 might not be advantageous and should be avoided.

The optical microscopy images displayed in Figure 5.8 were utilised to investigate the impact of B2 level on SFCA formation and crystalline grain size. The findings suggest that a B2 level of 3.0 resulted in minimal SFCA formation and smaller crystalline grains. In contrast, when the B2 level was between 1.4 and 1.7, an increase in SFCA

content was observed, as illustrated in Table 5.6, with an average total SFCA formation of 29% and 25%, respectively. Furthermore, within this B2 range, the SFCA grains exhibited a thicker, stripe-shaped columnar structure. This thicker SFCA layer enhances the binding force between the liquid-solid phase of iron oxide phases and SFCA, yielding a stronger sintered product. As SFCA serves as a critical component in the binding phase of sinter, increasing its content leads to a more robust sinter[99].

Furthermore, Figure 5.8 illustrates the quantity of iron oxide phases present within the SFCA phase, specifically hematite and magnetite. It was observed that these phases surrounded the SFCA phase when the B2 ratio was 1.4 and 1.7. However, in the case of when the B2 level was 1.0, the iron oxide containing species appeared to be more isolated, as seen in Figure 5.8 (a). These findings also suggest that the binding forces in the B2=1.4 and 1.7 blends of the liquid-solid phase were stronger[99], resulting in a higher strength of the iron ore sinter produced.

According to Debrincat et al.[13], it appears that the CaO content has a more significant impact on the sinter structure than basicity. Analysis of the Fe_2O_3-CaO-SiO_2 phase diagram indicated that exceeding a CaO level of approximately 30% leads to an increase in liquidus temperature[13]. This experiment potentially confirms this finding. Table 5.2 which shows the XRF data for this experiment illustrates that as the B2 increases, so does the CaO level in the produced sinter. Interestingly, a B2 level of 1.0 resulted in a low CaO level, while a B2 level of 3.0 caused the CaO level to be excessively high. However, it was observed that a CaO level between 8-10% appeared to be the ideal range for producing solid sinter with improved coalescence which was at B2 levels of 1.4-2.0.

5.9 Influence of Basicity on Metallurgical Testing

Improving the RDI value of iron ore sinter can significantly affect the productivity of a blast furnace. Kinnunen et al.[132] have implied that even a 1% decrease in RDI can lead to an impact on blast furnace output, potentially resulting in up to a 0.5% increase in productivity.

It has been established that the RDI values were at their highest, measuring at 28% and 35%, when the basicity levels were at 1.0 and 3.0, respectively. This outcome can

be attributed to the temperature profiles outlined in Figure 5.3. However, maintaining operations within the range of 1.4 to 2.0 shows an RDI enhancement of at least 1%, thus operating in this region will enable at least a 0.5% increase in blast furnace productivity[132].

As per the findings of literature[45], any fluctuation in the temperature profile can significantly impact the sinter reducibility. In particular, when B2=3.0, the thermal efficiency in the sinter bed was not uniform as the permeability of the sinter decreased due to endothermic reactions necessary for calcining the additional limestone present in the higher B2 tests[5]. These temperature irregularities can result in inconsistent sinter production with lower reducibility.

The additional inclusion of limestone into the production process as the B2 level rises has accelerated the temperature cycle and reduced the periods of exposure to high temperature areas. As a result, there has been a significant increase in the production of slag bond generated[5], this slag bond is typically small in particle size and could be majority of what is seen in Table 5.4 for the <5mm category. Generally, the data shows an increase in the overall quantity of particles collected less than 5mm in size as the B2 level rises.

Recent research[18] suggests that the presence of stronger needle shaped SFCA phases enhance sinter RDI. It is therefore possible that the increased presence of SFCA-I detected by Intellesis in the 1.4-2.0 B2 range as demonstrated by Table 5.6, compared to that found in the 1.0 and 3.0 B2 regions, is a contributing factor to this enhancement.

Based on the PSD data, it was observed that as B2 increased, the size of bigger particles decreased while the size of smaller particles increased. This observation was attributed to the contents of the reactants charged into the sinter pot. From biggest to smallest the sizes were nuclei, adhering and then non-adhering. Additional NTLR data obtained by Tata Steel UK revealed that as the B2 increased, the number of nuclei particles increased while the amount of non-adhering particles decreased along with the number of adhering particles. This resulted in bigger particles with less adhesion ability as the number of adhering particles decreased. This explains why B2=3.0 produced a "crumbly" sinter blend with the most <5 mm fines collected on average as shown in Table 5.4.

Another reason as to why these fines in the sinter produced were more prominent when the B2 level was 3.0 may have been due to the presence of weakened areas within the structure of the sinter bed or higher residual stresses[41], which most likely formed due to non-uniform expansion and contraction as the sinter cools. This non-uniform expansion and contraction can result in the generation of a greater number of fines.

The current study has revealed that the RDI value was marginally higher when the B2 level was 2.0, in contrast to when it was 1.4. This finding can be attributed to the fact that it has been reported in a recent study that when the B2 level of iron ore sinter is 2.0, mineralogical examination has revealed that the sinter's structure becomes more heterogeneous. This heterogeneity causes both acidic and basic phases to coexist within the sinter[65], leading to the formation of small cracks in the material. The RDI was affected by these cracks, as they contributed to a reduction in the sinter's structural integrity[66].

Based on the experimental data, it has been found that sinter made with B2 levels between 1.4-2.0 resulted in strong sinter with low RDI. A recent study reported that an acceptable RDI value for the blast furnace is 27%[18]. Therefore, Table 5.5 which shows the RDI values for each B2 level indicated that sinter with B2 levels between 1.4 and 2.0 fell within the acceptable range, while B2 levels between 1.0 and 3.0 did not. The mineralogy of the sinter was found to have changed between 1.4-2.0, resulting in an increase in magnetite and decrease in total hematite phase, as shown in Table 5.6 from collected Intellesis data. This change is responsible for the improvement in RDI, as reported in literature[106].

The RDI level reached its peak when the B2 level was set at 1.4. The reason behind this outcome can be observed in Figure 5.5, which displays the minimum and maximum levels of hot flow through the bed during the sintering experiments conducted for B2 levels 1.4, 1.7, and 3.0. The B2 level of 1.4 showed a difference of 4.50 m3/hr between the lowest and highest hot flow rates, with a minimum of 6.50 m3/hr and a maximum of 11.00 m3/hr. Similarly, the B2 level of 1.7 had a difference of 3.43 m3/hr, with a minimum of 6.11 m3/hr and a maximum of 9.54 m3/hr. In contrast, the B2 level of 3.0 showed a difference of 2.28 m3/hr, with a minimum of 6.47 m3/hr and a maximum of 8.75 m3/hr. The final hot flow rate recorded for each

of the tests was the hot flow through the produced sinter cake. The minimum hot flow rate revealed the worst of the bridge forming and how the pores closed to slow down the flow of air. It is essential to quantify the difference between the minimum and maximum hot flow rates to evaluate the improvement in permeability between the bridges forming and breaking. This improvement can be attributed to the uniformity of phases and their distribution. This conclusion is supported by Table 5.5 and Figure 5.4, which represent the RDI level for each of the different B2 levels and the maximum temperature reached on average for these B2 levels respectively. The results reveal that B2 level 1.4 had the best RDI at 25% and reached the highest maximum temperature at 1373°C , while B2 level 3.0 had the worst RDI at 35% and the lowest maximum temperature reached at 1163°C.

Ultimately the aim of the iron ore sintering process as mentioned before is to create sinter with a high cold strength and low RDI, in a very limited range of chemical variation, and with the lowest fines content feasible. Table 5.5 and Table 5.4 shows that B2=1.4 has an RDI value of 25% and fines content value of 24% which means operating at this B2 ensures the presence of these attributes the most compared to all the B2s.

5.10 Chapter Conclusions

The key points from this study are as follows:

i. Maximum temperature data for this experiment suggested that at any B2 apart from B2=3.0 is a sufficient level to obtain stable SFCA production.

ii. To gain a stable temperature profile that also reaches desired temperatures operating in the 1.4-2.0 B2 is ideal.

iii. RDI tests show that operating between B2=1.4-2.0 has the lowest RDI values at 25, 26 and 27% respectively.

iv. PSD tests show that the least fines content observed at B2=1.4 and 1.7 at 24 and 29% respectively compared to the rest of the B2s. Therefore, operating at this B2 will help to understand the mineralogical features of sinter that contribute to achieving sinter of the correct optimised quality for a given blast furnace burden.

v. According to XRF data analysis, as B2 increases, the amount of FeO decreases until it reaches an optimal level of 6% for B2 values of 1.4 and 1.7. This leads to the creation of stronger sinter with superior disintegration properties.

vi. XRD analysis shows that when the B2 was between 1.4 and 2.0 the highest number of SFCA's was recorded. This shows operating in this region is beneficial as we know SFCA's are known to influence the mechanical strength, reduction degradation as well as reducibility.

vii. A new approach developed by Intellesis has been developed. The results were validated through XRD, SEM, and EDS analysis, which confirmed that operating within the B2 range of 1.4-2.0 would facilitate the creation of SFCA in a greater quantity and more evenly distributed alongside iron oxide phases, resulting in a robust sinter.

viii. Images from Intellesis have been produced which clearly show the progressive occurrence of the key SFCA phase as the B2 is in the range 1.4-2.0. This is backed up by quantification from multiple iterations of these B2 levels.

ix. The findings suggest that a B2 level of 3.0 resulted in minimal SFCA formation and smaller crystalline grains.

x. When the B2 level was between 1.4 and 1.7, the SFCA grains exhibited a thicker, stripe-shaped columnar structure. Literature[99] has shown that this thicker SFCA layer enhances the binding force between the liquid-solid phase of iron oxide phases and SFCA, yielding a stronger sintered product.

xi. Based on the data analysis of sinter pot blends B2=1.4, 1.7, and 3.0, it appears that B2=1.4 has a superior cold air flow rate average. This suggests that its granulation process is more efficient and allows for better permeability. The dynamics of bridge formation and breaking affect hot flow rates, with B2=1.4 exhibiting the most efficient granulation process and higher productivity. The RDI peak at B2=1.4 implies optimal permeability, which is further supported by the uniformity of phases and their distribution. On the other hand, B2=3.0 displays inferior RDI and lower maximum temperature, indicating compromised sinter quality. This emphasises the significant role that chemistry plays in determining the outcomes of sinter production.

6 Impact of Flux Particle Size on Sinter Quality

6.1 Introduction

This investigation was designed to observe the changes in particle size of flux (PSF) to determine sinter quality. The study was novel for the inclusion of magstone as well as limestone. The reason for this inclusion is due to historical knowledge of benefits from the chemistry of the magstone which has been deduced by Tata Steel UK. Fluxing the sinter mix with magstone also has benefits for the blast furnace as it positively impacts the blast furnaces slag properties, by increasing the ability to absorb and retain impurities and viscosity which have direct impact on the process stability[111].

This investigation was carried out at the pilot pot facility located in Port Talbot as shown in Chapter 4, with the help of Tata Steel. The initial motivation for this experiment was a business benefit, after evidence was discovered in the finally produced sinter of a "white relict". A relict can be defined in this scenario as a surviving species after the sinter test was carried out. For this experiment it was likely to be either Magstone or Limestone flux. One hypothesis for its presence was that the flux particles in that blend could have been too large. Thus, this experiment was designed as a result. The intended deliverable of this experiment was to be able to quantitatively determine the relation between particle size, productivity, and presence of remaining raw flux.

It is important to note that changing the size of the flux alone would only shift the focus to how the other raw materials react with these different sizes of flux. Therefore, interesting observations were made on how the other raw materials behaved and what phases were produced as the PSF increased.

A possible hypothesis for this experiment based on current understanding in the literature is that using smaller particle sizes of fluxes will result in improved RDI, reducibility, and reduced fines content. This is because smaller particles will not have relicts present and thus the flux would be assimilated into the melt.

With the aid of SEM, EDS, XRD, XRF, RDI and Intellesis, the research will try to prove or disprove this hypothesis by:

1.) Observing how the sinter is seen visually when the particle size of the flux (PSF) is changed, assisted by optical microscopy images and consequential intellesis images to see the different phases present.

2.) Confirming the existence of SFCA's with the help of XRD & EDS mapping therefore corroborating the existence of sinter quality.

3.) Quantitatively analysing the different mineralogy, specifically SFCA's to prove the theory of the more SFCA's that are present the better the quality of the sinter. Quality metrics used here will be RDI and particle size distribution (PSD) analysis.

4.) Understanding more about the influence of PSF changes on, thermodynamics, sinter bed permeability, formation of different phases and metallurgical testing.

6.2 Results

6.2.1 Sinter pot parameters

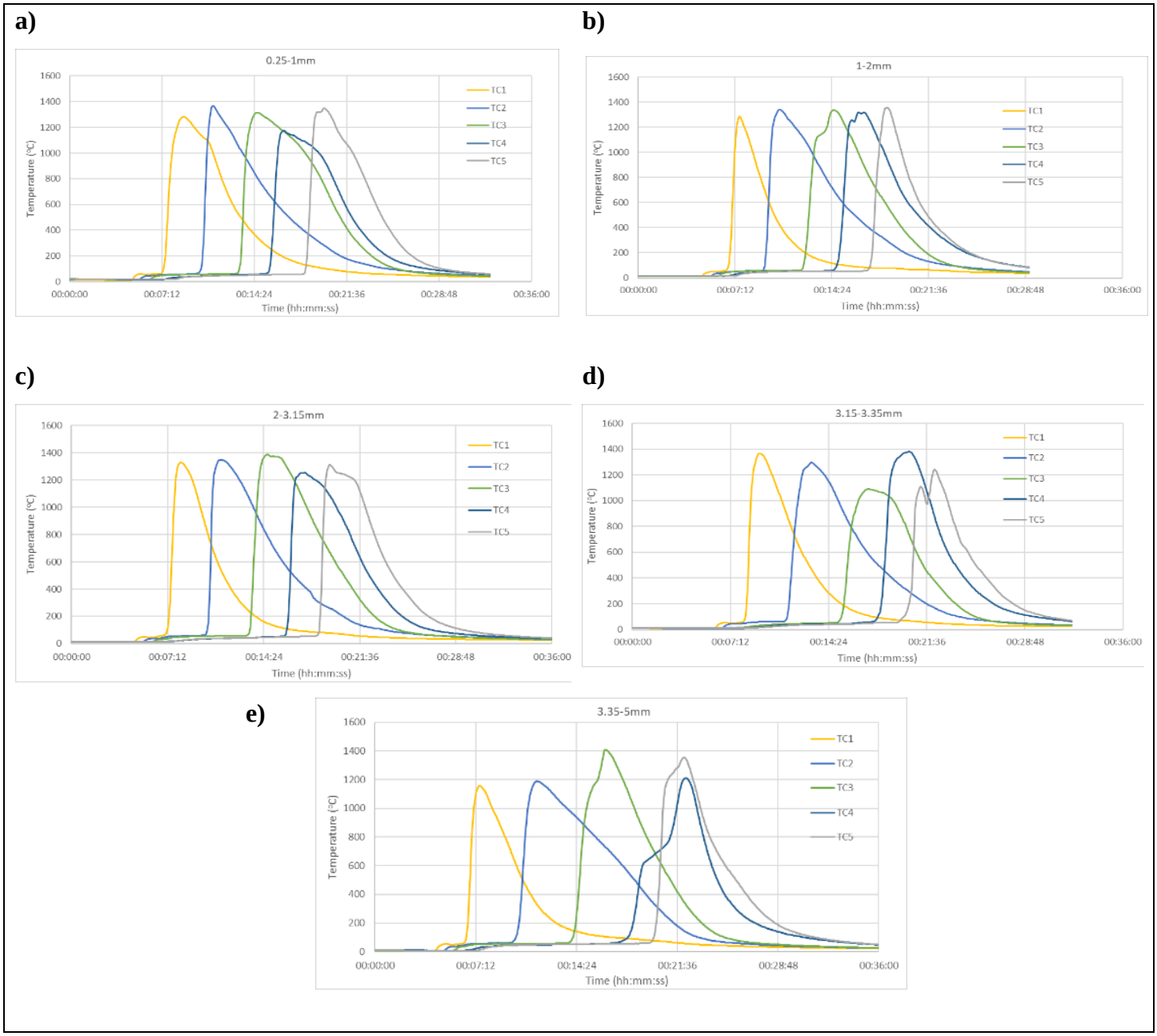

Figure 6.1 Temperature profiles for each blend as a function of flux particle size. a) 0.25-1mm b)1-2mm c) 2-3.15mm d) 3.15-3.35mm and e) 3.35-5mm

In Figure 6.1, the thermodynamic progression of each blend is shown. Within the subplots b) and c), which represent PSFs 1-2mm and 2-3.15mm, respectively, a consistent pattern is observed. All five thermocouples (TC's) sequentially reach and surpass 1200°C. However, subplots a), d), and e), which display temperature profiles for 0.25-1mm, 3.15-3.35mm, and 3.35-5mm, respectively, showcase unpredictable trends. In these subplots, one or more peaks do not occur in a sequential arrangement, or all five TC's are unable to surpass 1200°C. One other observation calculated that TC3 at the PSF of 0.25-1mm depicted by Figure 6.1 a) had a holding time of 320 seconds at and above 900°C, which was significantly longer than the holding time for the 1-2mm PSF as demonstrated in Figure 6.1 b), which is attributed by the wider TC3 peak.

Table 6.1 Contrast of parameters at different flux particle size

Parameters/Flux size (mm)	**0.25-1**	**1-2**	**2-3.15**	**3.15-3.35**	**3.35-5**
Average Max Temp (°C)	1383	1373	1384	1383	1398
Average Sintering Time (hh:mm:ss)	00:18:25	00:15:00	00:16:17	00:16:30	00:18:22
Average cold flow rate (m3/hr)	9	10	11	11	10
Average hot flow rate (m3/hr)	7	9	8	8	7

Table 6.1 displays the max temperature, sintering time, cold flow rate and hot flow rate. The average value has been calculated and shown based on 2 repeats that were carried out for each test. The recorded sintering times for each blend in relation to the particle size of flux (PSF) show that when the PSF was 1-2mm the shortest average sintering time of 15 minutes was noted. In the experiment carried out, it was found that the blend in the PSF range of 0.25-1mm obtained the longest average sintering time at 18 minutes and 25 seconds. Interestingly, the difference in average sintering

time was not significant when using a PSF range of 3.35-5mm, with an average sintering time of 18 minutes and 22 seconds.

Based on the average maximum temperature data collected during the experiment, it appears that the highest average maximum temperature was achieved at 1398°C when the PSF ranged between 3.35-5 mm. Furthermore, there was a noteworthy difference of 25°C in the average maximum temperatures across the five different blends. The lowest recorded maximum temperature occurred when the PSF was 1-2 mm at 1373° C.

Based on the data collected regarding average cold air flow rates, it was discovered that the blend with the highest rate occurred when the PSF was between 2-3.35 mm and the flow rate was 11m^3/hr. Conversely, the lowest average cold air flow rate was recorded when the PSF was between 0.25-1 mm and the flow rate was 9m^3/hr. With regards to average hot air flow rates, the data indicated that the highest flow rate was observed when the PSF was between 1-2mm, and the flow rate was 9 m^3/hr. The lowest hot air flow rates were recorded when the PSF was between 0.25-1 mm and 3.35-5 mm, as compared to all other PSF's.

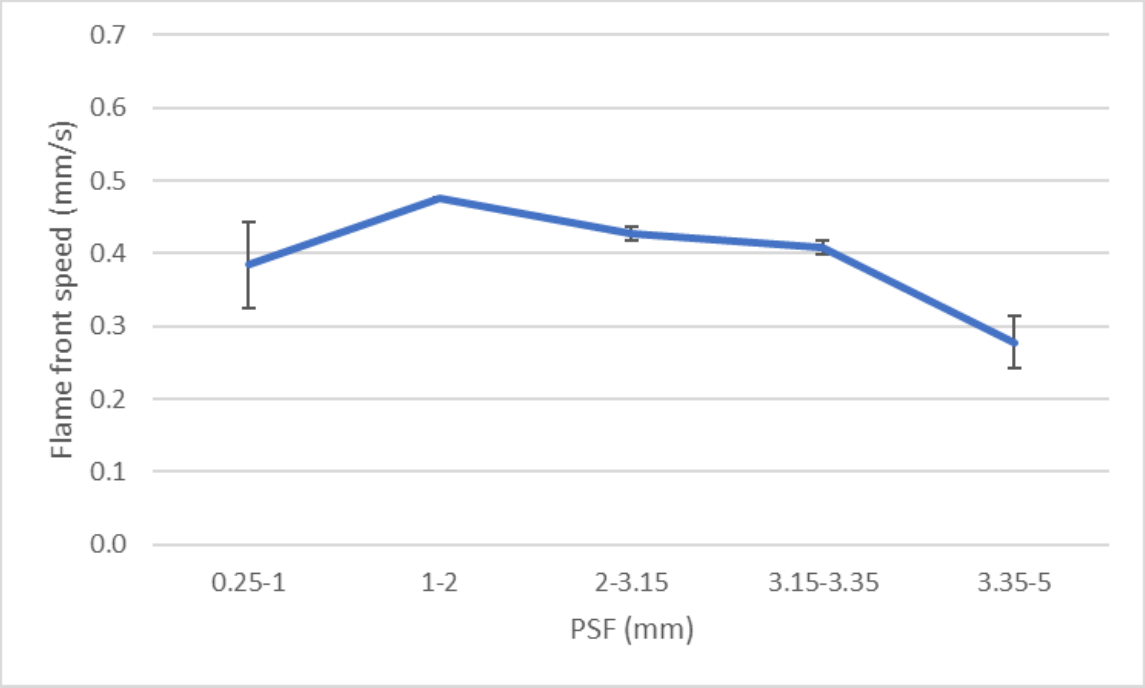

Figure 6.2 Average flame front speed as a function of PSF.

According to the data depicted in Figure 6.2, it is apparent that the average flame front speed attains its maximum value within the PSF range of 1-2mm. On the other hand, the average speed of the flame front is found to be the slowest in the 3.35-5mm range.

6.2.2 Metallurgical Testing

6.2.2.1 RDI

In accordance with Table 6.2, it is evident that the RDI values vary for each PSF. The PSF in the 2-3.15 mm range demonstrated the most effective reduction degradation capability at 44%, with the 1-2mm size range following closely at 45%. However, the 0.25-1 mm PSF exhibited the weakest reduction degradation ability with an RDI value of 57%. As mentioned previously literature has suggested even small changes in RDI of 1% can have a significant effect on the quality of the sinter produced.

Table 6.2 RDI comparison at different PSFs

Flux size (mm)	0.25-1	1-2	2-3.15	3.15-3.35	3.35-5
RDI	57	45	44	47	50

6.2.2.2 PSD

Table 6.3 shows the results for the post analysis on each sinter cake which has been carried out to observe the analysis of the sinter in terms of PSD. Analysing the strength of the sinter in this way proves to be an effective method. When the PSF was between 3.15-5 mm the amount of <5 mm particles that were collected were the most out of the PSF's at 20%. On the other hand, when the PSF was between 1-2mm the least <5mm particles were collected at 15%.

Table 6.3 Percentages for different PSF for each blend collected for each PSD

PSD/PSF(mm)	0.25-1	1-2	2-3.15	3.15-3.35	3.35-5
>40	5	4	4	20	1
25-40	20	22	24	12	24
16-25	15	25	22	14	18
10--16	20	19	18	16	21
5--10	20	16	15	18	16
<5	19	15	17	20	20

6.2.3 Compositional and Phase Analysis

6.2.3.1 XRF

As shown in Figure 6.3 the chemical analysis of each sample was conducted using XRF. Since this experiment is focused on repeatability across various PSFs, it is apparent that the chemical analysis is consistent across all the species involved, with only a small margin of error (maximum variation of 2 for any of the compounds). Some differences which are visible are a general increase in FeO as the PSF is increased, as well as a slight increase in the FeO value from the 0.25-1mm to 1-2mm region.

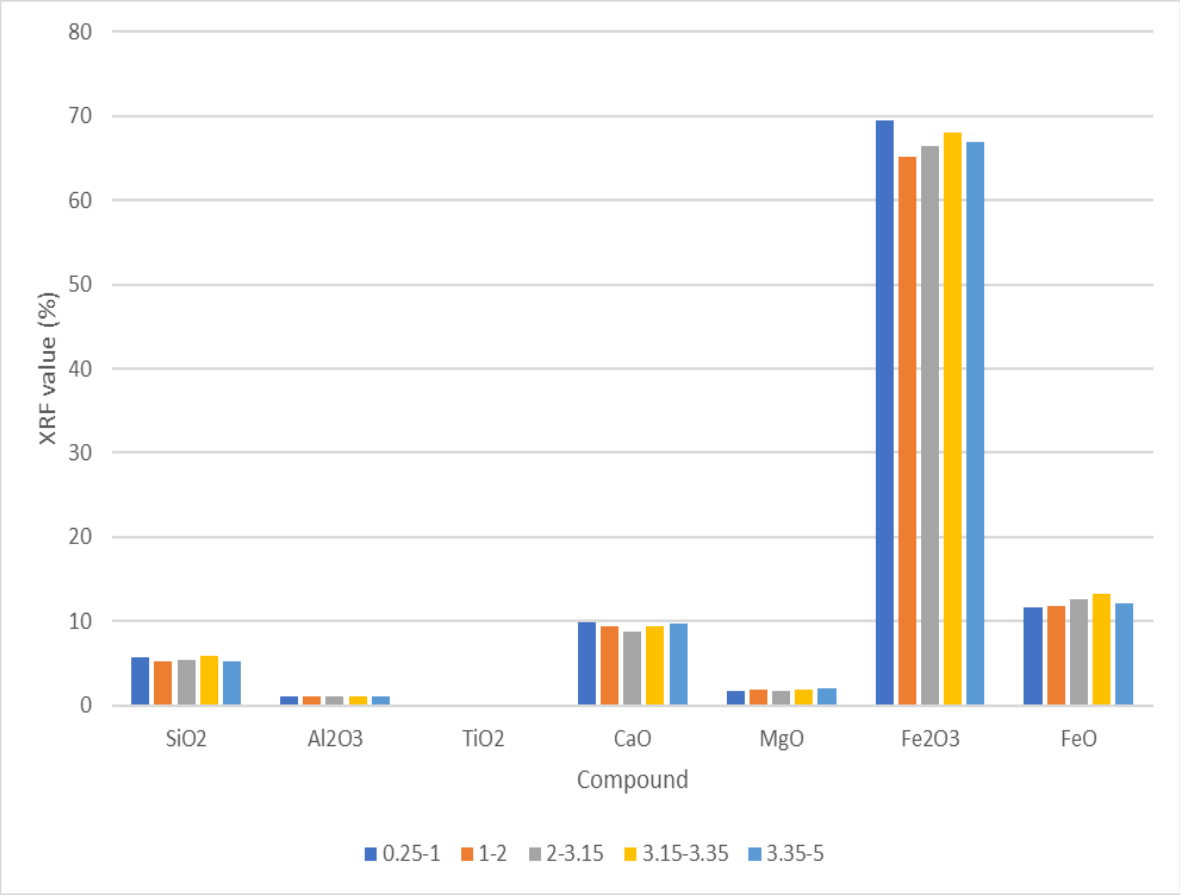

Figure 6.3 XRF for experiment with differing particle size of flux

6.2.3.2 XRD

Table 6.4 shows the quantitative analysis of the phases formed as the PSF was changed according to XRD data. The data shows that the major mineralogy which was observed in each of the blends was Calcium Ferrites (CF), Silico-ferrite of Calcium and Alumina (SFCA), Alumina (A) Hematite (H) and Magnetite (M). The other mineralogy which was observed was small amounts of Magnesia (MgO), Silica (Si), Wustite (W), Calcium Carbonate (CC) and traces of Calcium Oxide (CaO). It has been noted that the 2-3.15mm PSF category exhibited the highest concentration of Al_2O_3 at 28%. The total sum of the SFCA's and CF's observed generally decreased as the PSF was increased. The data displays very minimal changes in the percentage for Fe_3O_4, Fe_2O_3, FeO, MgO, SiO_2, Al_2O_3, $CaCO_3$, and CaO, which was parallel to the data obtained by XRF as shown in Figure 6.3.

Table 6.4 Quantitative analysis of the phases formed as the PSF varies according to the XRD data

Flux PSF (mm)/ Phase (%)	Fe_3O_4	Fe_2O_3	FeO	MgO	SiO_2	Al_2O_3	$CaCO_3$	CaO	CF	SFCA
0.25-1	24	11	0.6	12	0.2	26	5	0.6	4	19
1-2	26	10	0.6	13	0.5	25	3	0.7	4	17
2-3.15	24	10	0.6	12	0.3	28	3	0.8	4	17
3.15-3.35	23	13	0.6	11	0.7	25	3	0.7	6	17
3.35-5	26	11	0.6	12	0.5	24	3	0.8	5	17

6.2.4 Microscopic Analysis

6.2.4.1 Optical microscopy & Intellesis

Based on Figure 6.4, it is noticeable that as the particle size range increases, the light green and olive phase, which is controlled by the SFCA phases, decreases significantly. Another observation is that the hematite phase, which is represented by the light and dark blue colours, also decreases as particle size increases. At the same time, the magnetite phase, characterised by the magenta colour, appears to increase. It is clear to see for the PSF's between 1-3.35 mm which is depicted by Figure 6.4 (b), (c) and (d), the columnar SFCAs are uniformly distributed with other phases like magnetite and hematite.

Table 6.5 displays the average conclusions of the mineralogy. The random images for each PSF, as shown in Figure 6.4, provide a good representation of the trend observed in Table 6.5. The total number of SFCAs generally decreased as the PSF increased, which aligns with the trend observed in the XRD data displayed in Table 6.4. As the PSF increased, the secondary hematite content generally decreased. The data shows that the categories of PSF between 0.25-1mm and 2-3.15mm exhibited the highest concentration of secondary hematite at 28%, compared to the other PSFs. An interesting finding is that the total levels of hematite and magnetite displayed an inversely proportional relationship during this experiment. The highest number of pores can be observed in the 1-2mm and 3.15-3.35mm PSF categories at 13%, which is the highest among all the PSFs.

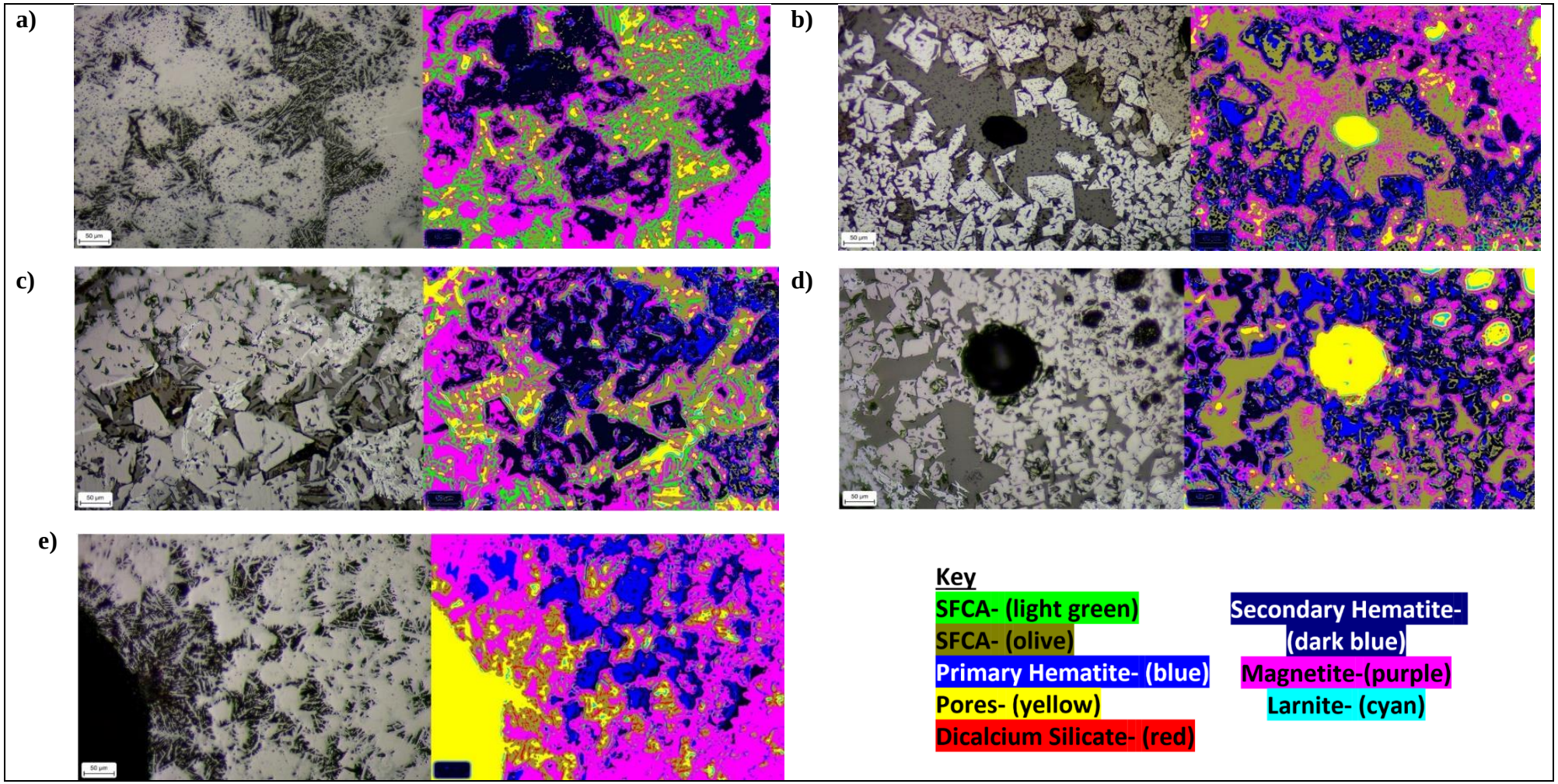

Figure 6.4 Images obtained from optical microscopy (left) whilst the images on the right are obtained from Intellesis. Images taken for particle sizes of flux a) 0.25-1mm b)1-2mm c) 2-3.15mm d) 3.15-3.35mm and e) 3.35-5mm

Table 6.5 Average phase composition (%) of each mineralogy at different PSF's according to data generated through Intellesis

Blend/Phase (%)	SFCA	Primary Hematite	Pores	Dicalcium Silicate	Secondary Hematite	Magnetite	Larnite	SFCA-I	Total SFCA
0.25-1	12	9	8	2	28	28	1	13	25
1-2	11	12	13	3	25	27	1	8	19
2-3.15	10	12	10	2	28	27	1	10	19
3.15-3.35	13	17	13	2	19	34	0	3	16
3.35-5	10	15	12	2	13	45	1	3	13

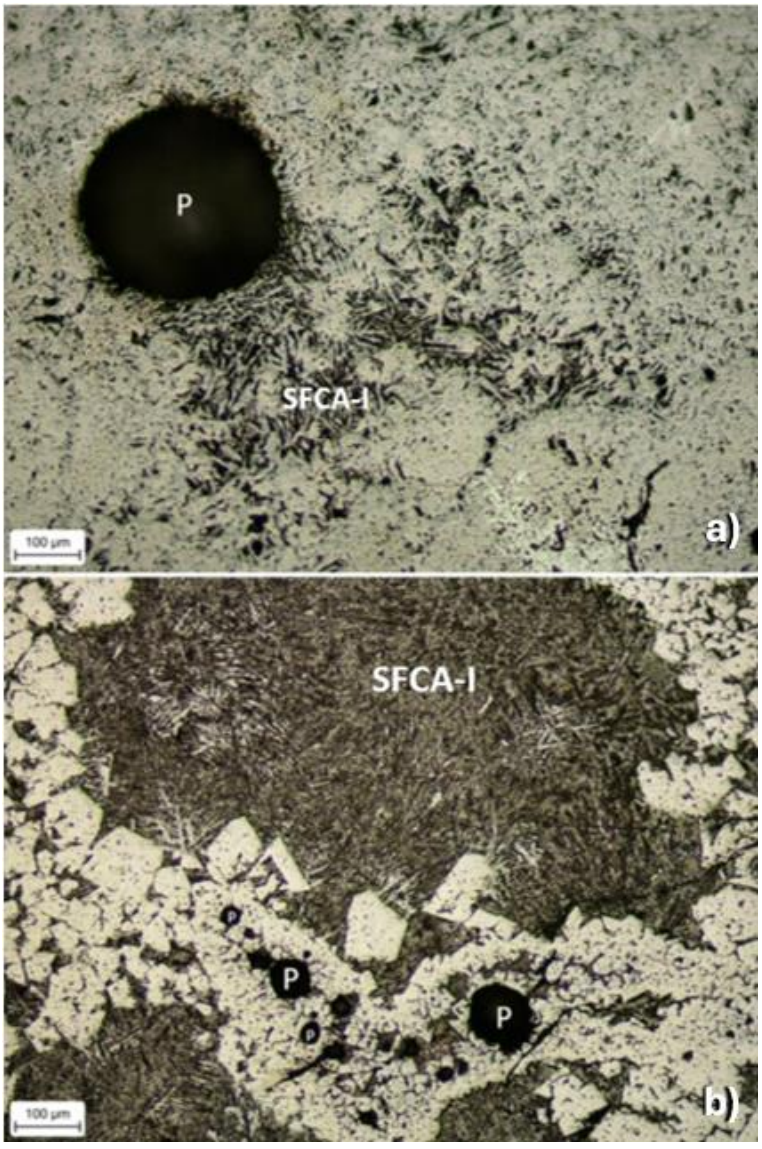

Figure 6.5 Optical microscopy images of the comparison of the arrangement of the pores & SFCA-I (indicated by white P & SFCA-I respectively) in blends with flux size a) 0.25-1mm and b) 1-2mm at 10X

Figure 6.5 illustrates two optical microscopy images which were taken at a 10X magnification level to observe pore SFCA-I behaviour. The images show that the pore size is larger when the PSF is between 0.25-1mm. In contrast, when the PSF is between 1-2mm, the pore size is more uniform, they are more dispersed and there are more pores present. It is also noticeable that from the PSF 0.25-1mm to 1-2mm, there is a corresponding reduction in the size and an increase in the amount of SFCA-I grains.

6.2.4.2 SEM/EDS

A backscattered image shown by Figure 6.6 and consequential EDS map were captured for when the flux size was between 1-2 mm. The image in Figure 6.4 b) has been copied in as seen by Figure 6.7 for comparison. The purpose of including the image is to corroborate the findings of Intellesis. The feature which has been regarded as SFCA, which was identified in Figure 6.7 was examined using EDS. This examination aimed to confirm whether the SFCA was present and lend further credence to the Intellesis work package, thereby strengthening the validation process.

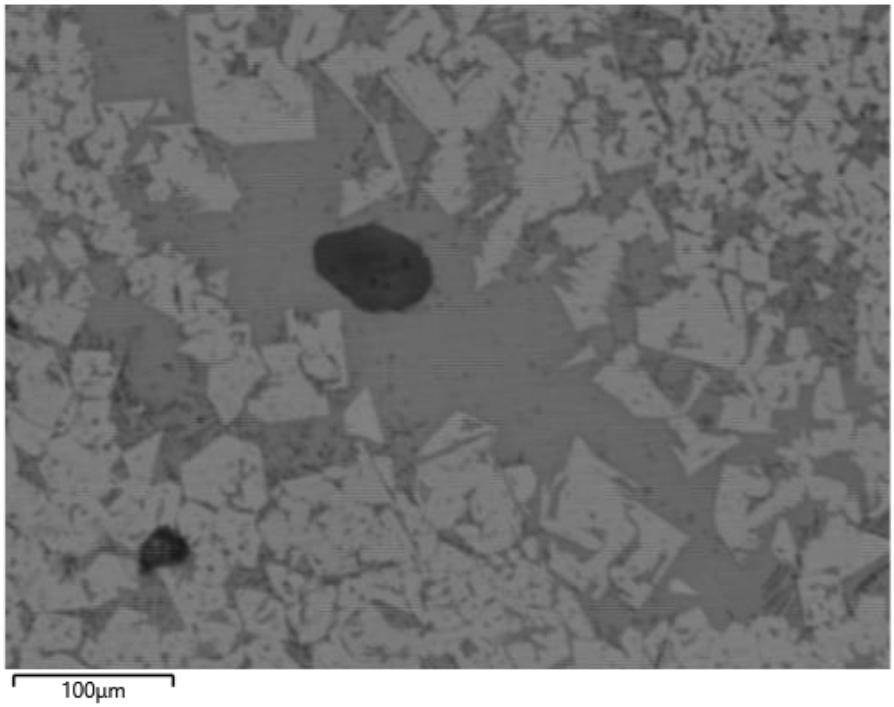

Figure 6.6 Backscattered image using scanning electron microscopy (SEM) of flux size 1-2mm

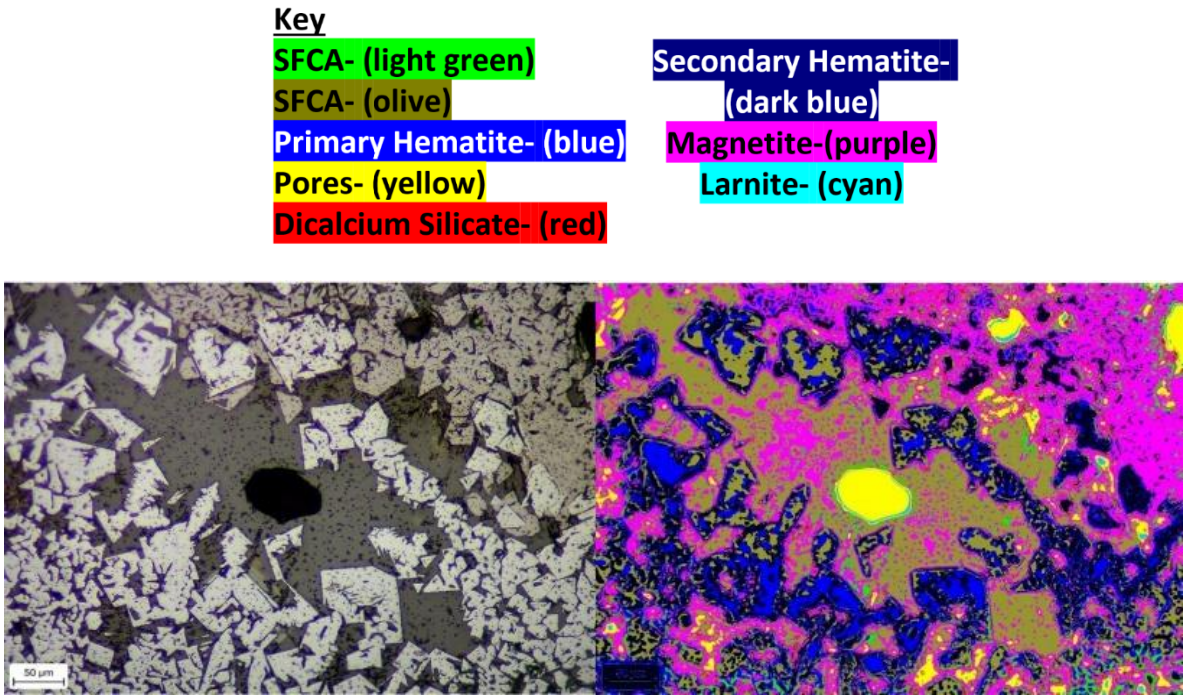

Figure 6.7 Copy of image obtained from optical microscopy (left) whilst the images on the right was obtained from Intellesis. Images taken for particle sizes of flux 1-2mm

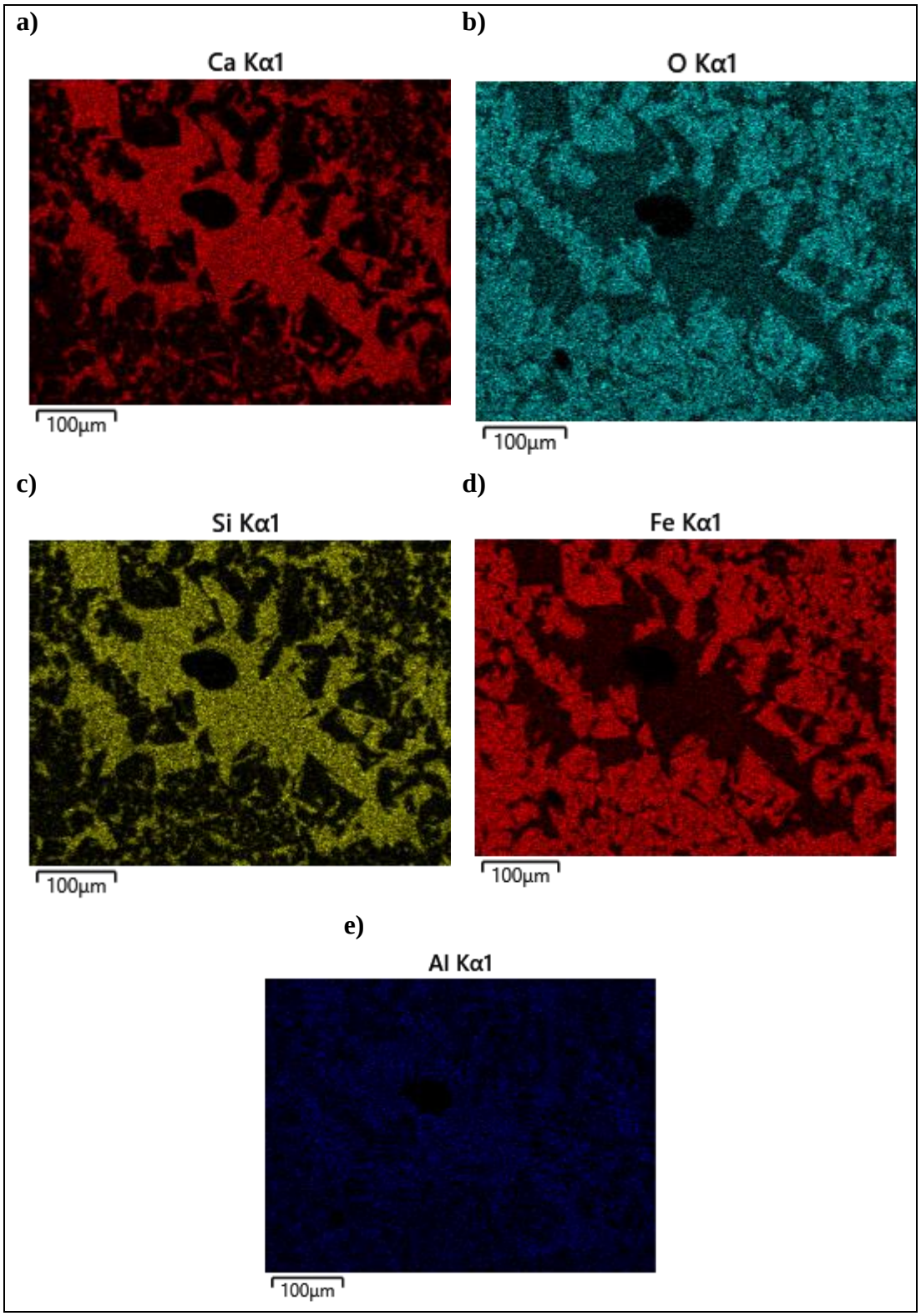

Figure 6.8 EDS mapping of the presence of SFCA's for the PSF 1-2mm a) Ca b) O c) Si d) Fe e) Al

In Figure 6.8, EDS maps that showcase the simulated backscattered image displayed in Figure 6.6. The maps highlight a significant presence of various elements, including silicon, iron, calcium, oxygen, aluminum, and pores presented as black voids. The presence of these elements is crucial because it is known that the SFCA phase, which contains these key elements, is present. Therefore, the EDS maps corroborate the Intellesis images' observation of SFCAs previously defined in Chapter 6.2.4.1.

6.3 Discussion

6.3.1 Influence of Particle Size of Flux (PSF) on Thermodynamics

During the process of sintering, approximately 80% of the heat necessary to create a strong sinter comes from the combustion of coke. This heat is crucial in generating enough melt for the sinter to form with good strength[36]. The rest of the heat has been reported to come from the radiation from the sinter bed. The sinter bed itself emits heat through radiation. As the sinter bed is heated, it emits thermal energy, which contributes to the overall heat input. In this experiment, the fuel level was kept constant. However, the manipulation of the fuel (coke breeze) with the rest of the blend (different PSF) for example how the coke breeze particles engage with the different size of flux or the lack of engagement due to hindrance of the flux particles was deemed to cause temperature differences between each blend.

As a result, the coke breeze that was used was randomly selected and below 3.15mm as stated in Chapter 4.1.2. It is known that in the larger PSF blends with particle sizes between 3.35-5mm, the flux will act as the nuclei particles and the coke breeze will act as the adhering particles in the sinter mix. This should theoretically lead to a more favourable combustion reaction through kinetically controlled reactions and thus higher temperatures throughout the blend. However, literature also suggests that the accessibility of oxygen to these coke particles has an impact on their combustion rate[48]. Therefore, for the bigger PSF the flux will hinder the ability for the coke particles to reach the oxygen.

It was found that as the PSF decreases accessibility of oxygen to these coke particles becomes easier. This is because the coke particles have a greater surface area to reach the oxygen, making ignition a simpler process[48]. Additional data from the sinter pot revealed that the bottom thermocouples recorded the maximum temperature achieved during the experiment for large PSFs. However, for smaller PSFs, the top two thermocouples recorded the highest temperature. This may be because the top of the sinter pot experiences the highest temperature for the smaller PSFs as the small flux particles provide more accessibility to oxygen for the coke particles to ignite quickly. On the other hand, larger PSFs hinder the ability for the coke particles to reach the oxygen and thus the combustion reaction does not occur as easily.

Throughout the course of the experiment, close attention was paid to the duration of high temperature exposure. The findings of a study conducted by Hosotani et al. [40] revealed that reducing the holding time during sintering at temperatures exceeding 900°C led to the formation of more refined heat patterns in the middle and lower layers. This refinement in heat patterns is thought to play a crucial role in decreasing the overall sintering time and enhancing the RDI.

During this experiment, as can be seen by Figure 6.1 (a) it was observed that TC3 (the TC which measures the middle layer) at the PSF of 0.25-1mm had a holding time of 320 seconds at and above 900°C, which was significantly longer than the holding time for the 1-2mm PSF depicted in Figure 6.1 (b). This disparity in holding time may be a contributing factor to the lower RDI for the 1-2mm PSF which is 45% as opposed to 57% for the 0.25-1mm category. Also, shorter sintering time which was 15 minutes for the 1-2mm PSF as opposed to 18 minutes and 25 seconds for the 0.25-1mm region as displayed in Table 6.1 and Table 6.2 respectively. These results suggest that the holding time of high temperatures is a critical variable for optimising sintering outcomes and that precise control of this parameter is necessary to produce high strength iron ore sinter.

As the temperature in the sinter bed decreases, which is evident by Table 6.1 which demonstrates the maximum temperature falling from PSF 0.25-1mm to 1-2mm. There was a corresponding reduction in the size of SFCA-I grains as evidenced by Figure 6.5 (b) which demonstrates a microscopic image taken of the 1-2mm PSF which shows

the SFCA-I grains are observed in greater amounts in comparison to that seen in Figure 6.5 (a) which represents the optical microscopy image taken for the 0.25-1mm PSF, whilst occupying the same volume which shows they have gone smaller.

Also seen by Figure 6.5 (b) the fine pores are further dispersed. These pores play a crucial role in mitigating the negative effects of pore closure that can occur during the reduction process, particularly at high temperatures of 1000°C and above. The presence of these small pores enhances the sinter's ability to undergo reduction at high temperatures. This will restrict the expansion of the temperature pattern in the sinter bed, thereby maintaining the integrity of the smaller pores and ensuring optimal sinter reduction[40]. Based on this image, it can be inferred that the 1-2mm PSF has superior reducibility compared to 0.25-1mm PSF as shown by Figure 6.5 (a).

Ultimately, each of the blends reach beyond 1300°C, which according to literature[33] is in the range for the best sintering maximum temperature to ensure iron ore sinter with high quality can be produced in terms of optimum Total Iron (TFe), CaO/SiO_2 ratio, FeO (%), Sulphur (%), RDI (%), Degree of Reduction (%). Therefore, in terms of sinter quality produced the maximum temperature of the blends had a negligible effect. Additionally, the average cold and hot flow rates generated for each blend did not significantly impact the quality of the sinter obtained. This is evidenced by the standard deviation of 1% between the results, indicating small variation amongst them.

6.3.2 Influence of Particle Size of Flux (PSF) on Metallurgical Testing

The RDI values for each of the blends were similar in the range 1-3.35 mm between 45% and 47%, seeing large increases for the 0.25-1 mm and 3.35-5 mm range to values of 50% and 57% respectively. Based on the information presented in Figure 6.1, it is evident that Figure 6.1 (b) and (c) show consistent temperature patterns. This is likely due to the appropriate size of the PSF, which allows for a smooth passage of the flame front. These PSF levels are associated with significantly low RDI values. It is important to note that this may be temperature-dependent, as only these tests recorded temperatures exceeding 1200°C across all TC's 1-5. Previous research supports this claim, as it has been discovered that a flame front temperature profile that peaks above 1200°C results in a uniformly sintered product[24 25].

On the other hand, it is clear to see from Figure 6.1 (a), (d) and (e) TC4, TC3 and TC4 respectively does not reach the desired 1200°C. This shows an unstable temperature profile which therefore implies the flame front that progresses down the sinter pot is also unstable and not reaching the desired temperature thus leading to the production of inhomogeneous sinter with significantly worse RDI values compared to when the PSF was between 1-3.15mm.

In Figure 6.1 (d) and (e), the flame fronts are erratic and not sequential, with TCs containing double peaks. This instability greatly affects the reducibility of the sinter[45] and is particularly noticeable in (d) when TC5 was in the melt zone, then moved to the drying and preheating zone before returning to what appears to be the sintered zone, thus has a double peak[26]. Such irregularities in temperature history within the sinter bed can result in inhomogeneity in the sinter produced. This can also lead to issues such as inconsistencies in gas flow[43 44]. Similarly, (e) is also highly erratic, with two TCs peaking at the same time (TC 4 and 5), which is irregular and affects reducibility, consequently, sinter produced of this PSF will result in a decrease in productivity and increase in the running cost for the blast furnace.

As per the findings presented in Table 6.3, the PSF range of 1-2 mm demonstrated the lowest particle fines content, with a percentage of 15%, for particles under 5mm. The range of 2-3.15mm was very similar, with a yield of fines of 17%. The data in Table 6.3 shows that when the PSD was < 10 mm the most amount of sinter was collected when the PSF was between 0.25-1mm at 39%. Based on the data analysis, it was determined that the PSF with the smallest size yielded a larger quantity of small particles. It is important to note that this specific blend was also found to have the highest recorded maximum temperature. Figure 6.1 (a) provides a visual representation of this phenomenon occurring at TC2. Due to this temperature not being maintained throughout each of the TC's the sinter does not maintain its homogeneity and because of the presence of excess fines (the excess fines being the flux particles) they weaken the thermal efficiency[107] and thus the structure was not fused throughout the whole sinter cake. This therefore supports the observation of an increase in the fines content observed, further emphasised in the data gathered via RDI. Where the PSF was between 0.25-1mm the RDI was the highest out of all the blends at 57%, meaning it also produced the weakest sinter.

It is clearly visible from Figure 6.4 (b), (c) and (d) that the PSFs ranging from 1-3.35mm exhibit a uniform distribution of SFCA with other phases such as magnetite and hematite. The hematite observed in these PSF regions demonstrates the integration of the fluxes at these sizes were better than at the 0.25-1mm or 3.35-5mm categories depicted by Figure 6.4 (a) and (e). This assimilation of hematite has been reported in literature to give the sinter good mechanical strength and fewer return fines[114]. This is confirmed with data from the metallurgical testing which shows in the region 1-3.35mm the RDI is the lowest and between 1-3.15mm less fine generation is seen than any other category.

Moreover, it has been noted that in the XRD analysis, the 2-3.15mm PSF category exhibited the highest concentration of Al_2O_3 at 28%, as indicated in Table 6.4. Additionally, this category also displayed the highest amount of secondary hematite compared to the other PSFs, as evidenced by the Intellesis data produced in Table 6.5 at 28%. According to relevant literature[87], the presence of Al_2O_3, whether as an inclusion or solid solution, plays a crucial role in the disintegration of secondary hematite. This is because the difference in expansion between hematite and Al_2O_3 leads to internal tension, ultimately resulting in the formation of cracks and brittleness in the sinter. Although the RDI in this region is not the most unfavourable among all the PSFs, it is still a relevant factor to consider when selecting the PSF to operate at to achieve maximum strength in the produced iron ore sinter.

To operate efficiently, the blast furnace requires sinter that possesses high cold strength and a low RDI. The sinter must have a specific chemistry variation within a narrow range and low fines content.[152]. After analysing the data presented in Table 6.3, it is evident that sinter produced within the PSF between 1-2 and 2-3.15mm exhibits a significantly lower average fines content (<5mm) of 15 and 17% compared to the other blends.

In analysing the percentage of particles collected for the >5mm PSD for the 1-2 and 3.15mm PSF, it has been found that a remarkable 85 and 83% of these particles were observed respectively. This characteristic serves as a clear indicator of the PSF's exceptional cold strength. Furthermore, when considering sinter production, it has been observed that utilising particle size fractions ranging from 1-2 and 2-3.15mm of

PSF results in the lowest RDI values of 45% and 44% respectively, as noted in Table 6.2. Therefore, operating in the 1-3.15mm PSF range stands out as the most favourable option for sinter pot operators aiming to achieve a low RDI value, high cold strength and lower fines content generation to fulfil the blast furnaces requirements.

6.3.3 Influence of Particle Size of Flux (PSF) on Formation of Different Phases

XRD patterns were produced for each of the blends. Table 6.4 shows the phases that were present and the percentage of each accordingly. Firstly, it is important to note, the chemistry of the successive blends was unchanged. Therefore, seeing changes in most of the chemical compounds was not expected, as seen by Table 6.4. The illustration displays very minimal changes in the percentage for Fe_3O_4, Fe_2O_3, FeO, MgO, SiO_2, Al_2O_3, $CaCO_3$, and CaO, which was parallel to the data obtained by XRF. The phase and morphology change i.e., changes in the SFCA and CF however was clear because of the change in PSF. The total sum of the SFCA's and CFs observed increased as the PSF was decreased. This is in harmony with what was found from the intellesis findings, as the total SFCA's on average increased as a function of decreasing PSF. This provides more confidence in the intellesis work package as the results agree. The reason for these increases in SFCA's and CF's as the PSF was decreased according to literature[105] was due to the presence of more uniform distribution of flux particles as a result leading to a better bed permeability which favours easy integration and effective distribution of the desired CF and SFCA phases.

To enhance the reliability and efficacy of the intellesis work package SEM/EDS was used to verify that the visible particles in the 1-2mm range belonged to the SFCA category. This had been previously determined via optical microscopy and intellesis work. The EDS mapping technique confirmed the existence of a phase with a columnar arrangement, which had previously been identified as SFCA in Figure 6.4 (b) through optical microscopy. The considerable amounts of Ca, O, Si, Fe, and Al elements observed in Figure 6.8 are well-documented constituents of SFCA, as per existing literature[95]. Therefore, moving forward in addition to the SEM/EDS corroboration seen in Chapter 5 this was evidence to suggest the Intellesis work had been further corroborated.

The level of hematite and magnetite had an inversely proportional relationship in this experiment according to data shown in Table 6.5 via intellesis. When the PSF was small, the level of magnetite was low, and the level of hematite was high. However, as the PSF grew, the level of hematite decreased while the level of magnetite increased. A good representation of this is further shown in Figure 6.4 as it can visually be seen how the colour of magenta which represents magnetite increases, and the blue colours (light and dark) which represent hematite (primary and secondary respectively) progressively falls as the images advance from Figure 6.4 (a) to (e).

Recent research has shed light on the relationship between PSF and sinter strength. Specifically, it has been found that limestone and magstone particles that are too coarse have a smaller surface area, which leads to reduced contact between hematite particles and CaO[105]. This, in turn, hinders the formation of sufficient bonding phases such as SFCA that are crucial for creating a strong and cohesive sinter structure. The importance of these bonding phases cannot be overstated, as they play a significant role in determining the mechanical strength of the sinter. The current study provides further evidence of this, with Table 6.4 and Table 6.5 clearly showing that the SFCA phase is more present in the PSF 0.25-1mm category (fine PSF) than in the 3.35-5mm category (coarse PSF), according to XRD and Intellesis data, respectively.

According to Table 6.2, the RDI value has decreased while the PSF has increased. This phenomenon can be attributed to the decrease in the skeletal hematite phase, which is also known as secondary hematite. This phase has been reported[4] to have a less crystalline structure and more porous or amorphous, leading to lower density and strength whereas primary hematite is generally dense, stable, and well-crystallised. It contributes to the strength and reducibility of the sinter. This reduction in secondary hematite has been observed in previous studies[115] and is often associated with a coarser flux size. It is worth noting that the data from Intellesis presented in Table 6.5 corroborates this observation by exhibiting a reduction in average secondary hematite levels from 28% in the 0.25-1mm PSF range to 13% in the 3.35-5mm PSF range.

Based on a recent study[40], it was reported that the size of FeO particles experienced a decrease while their quantity increased during reduction. This reduction process led to the fragmentation of the FeO network into smaller fragments. The reason behind this

phenomenon was attributed to the formation of a greater number of fine pores that were dispersed. These fine pores resulted in an increase in the number of pores that were not closed by the melt during high-temperature reduction. This, in turn, could be a potential explanation for the increase in finer pores observed when comparing 0.25-1mm PSF illustrated by Figure 6.5 (a) to 1-2mm PSF as shown in Figure 6.5 (b) in this investigation. As it can be seen from Figure 6.3, a small increase in the FeO value from the 0.25-1mm category (11.62%) to the 1-2mm (11.75%) region may have indicated a slight chance of more FeO due to the broken FeO network. However, based on the data presented in Figure 6.3 which shows the XRF results for this experiment, it may be considered that the difference between the PSFs are not statistically significant. In addition to this, the XRD values for FeO are identical in both cases represented by Table 6.4, leading to the possibility that the size of the flux may not have had a significant impact on the resulting FeO content.

It has been observed that the RDI test yielded improved results when the PSF was within the range of 1-2mm, as opposed to when it was within the range of 0.25-1mm. This enhancement can be attributed to the formation of the SFCA-I phase, which is clear in Figure 6.5. Upon closer examination, it is apparent that there are considerably more SFCA-I's present in Figure 6.5. (b) in comparison to Figure 6.5. (a). This phase has been found to effectively absorb energy and reduce the mechanical damage during impact that occurs during the RDI test[41], thus serving as a key factor in preventing degradation.

According to the data gathered from Intellesis for the present study, Table 6.5 revealed that the 1-2mm PSF demonstrated the highest average pore count. This finding carries significant implications, as previous research has established that there is a positive correlation between iron ore sinter reducibility and an increase in pore specific area, coupled with a decrease in the range of pore co-variance[124]. Consequently, the observed increase in the pore amount for the 1-2mm PSF suggests that its reducibility would likely be more favourable compared to other PSFs.

Based on the research outlined in literature[41], it has been noted that the sintering process can be greatly influenced by the prevention of micro pores from coalescing. This, in turn, can have a significant impact on the surface area and the enhancement

of the reducibility of iron ore sinter. Upon closer examination of Figure 6.5, it is evident that the 1-2mm PSF, which is characterised by a high frequency of pores which is uniformly distributed, exhibits superior reducibility. This claim is further supported by the data obtained from intellesis, as presented in Table 6.5. The data clearly shows that this blend has the highest average number of observed pores in this experiment. Therefore, it can be inferred that the presence of micro pores and their optimal distribution can greatly contribute to the success of the iron ore sinter produced in terms of becoming more reducible.

This study was motivated by the presence of a material, known as a "relict," that was discovered on the surface of the produced industrial iron ore sinter. The substance in question appeared to be either limestone or magstone, and a possible reason for its appearance may have been due to it not undergoing the calcination reaction completely during the sintering process. This is likely attributed to its larger particle size, as previous research has demonstrated that coarser flux particles are more challenging to calcinate during sintering. In fact, some studies have suggested that these particles should be extracted entirely[112]. During the sintering process, the calcination reaction occurs at the surface of the limestone particles[109]. Larger flux particles have less total surface area exposed to the reacting gases in the sintering furnace. Calcination primarily occurs at the surface of the flux particles, where carbon dioxide (CO_2) is released, and calcium oxide (CaO) is formed. With larger particles, there is less surface area available for these reactions to take place. This results in a slower calcination rate for the larger flux particles.

6.3.4 Influence of Particle Size of Flux (PSF) on Bed Permeability

Literature suggests the sintering time and thus the productivity of the sinter relies on how permeable the green blend is[18]. This is evident from Table 6.1 as the PSF is decreased the sintering time is seen to generally fall. However, when ‘excess fines’ in the form of 0.25-1 mm flux size is introduced, it is seen to widen the temperature profile and worsen the bed permeability and increase the sintering time as a result.[40]

After analysing the data presented in Table 6.1, it was observed that the PSF with a particle size ranging from 0.25-1mm exhibited the longest sintering time and the lowest average hot flow rate when compared to the other blends. This phenomenon

can be attributed to the impact of the PSF on the bed's permeability. Similarly, Bhagat et al.[107] conducted a study on the negative impact of excess fine like (-0.5mm) limestone particles on the thermal efficiency of the iron ore sintering process, and their findings are in line with the trend observed in this study. They discovered that the presence of such fines adversely affected the calcination of limestone and its assimilation into hematite and other mineral phases, leading to a decrease in thermal efficiency. Moreover, they suggested that the sinter mix was compacted due to the higher quantity of finely sized flux, resulting in reduced permeability.

Recent research[18] has identified two factors that heavily impact the success of the sintering process: airflow rate and flame front speed. These factors play a critical role in determining the efficiency of the sintering process and the permeability of the green sinter bed. This study has found that sinter productivity significantly increased when operating at a PSF of 1-2mm due to the increased average flame front speed a shown in Figure 6.2. Figure 6.2 shows that the highest average speed occurred at 0.48mm/s in the 1-2mm PSF region. Consequently, there has been an observed improvement in bed permeability in this range. The findings are supported by Table 6.1, which indicated that sintering time was the lowest when the PSF was between 1-2mm. The observations of a higher flame front speed and lower sintering time point towards the significance of maintaining optimal PSF levels to achieve higher productivity and efficiency in the sintering process.

The results showed that when the PSF increased to 2-3.35mm from 1-2mm, the permeability only decreased by an average of 0.09mm/s. This finding suggests that the flame front speed in these categories was not significantly affected. The values obtained from the 1-3.35mm range of PSF had negligible standard deviation, as demonstrated in Figure 6.2. However, when the PSF was either 0.25-1 or 3.35-5mm, the standard deviation was much higher, indicating instability caused by the PSF. Temperature profiles also exhibited instability at both high and low PSF, as illustrated in Figure 6.1. This instability could be a contributing factor to the larger flame front speed deviation. As a result of these unstable characteristics, these PSFs may not be optimal for operation.

It is important to note that the speed of the flame front and thus the porosity of the bed were the lowest for the range of PSF 0.25-1mm. This can be attributed to an increase in the number of macro-pores and a decrease in the number of micro-pores which was also agreed with in a recent study by Hosotani et al.[40], as depicted in Figure 6.5. Conversely, the 1-2mm range exhibited a higher number of finer and more dispersed pores. Consequently, the reducibility of the sinter in this range was higher compared to the 0.25-1mm range. It is imperative to have a thorough understanding of the scientific evidence that indicates the crucial role of pores larger than 0.01 μm in facilitating the penetration of reducing gas. Such pores are instrumental in optimising the reduction of sinter[60], and must be taken into account when developing strategies to improve this process.

Moreover, another reason why the blend with a 1-2mm PSF had a better permeability than the 0.25-1mm blend may have been due to an increase in the PSF which led to a delay in the decomposition of limestone and magstone. This delay meant that the heat pattern was improved[106]. This trend is supported by Figure 6.1(b) which shows the temperature profile for the 1-2mm PSF which is observed to be more stable than that seen for Figure 6.1(a) which shows the temperature profile for 0.25-1mm PSF.

Bhagat et al.[59] has uncovered a significant correlation between the duration of the sintering process and the RDI of iron ore sinter. Bhagat et al. revealed that prolonged sintering lead to worsened RDI levels, resulting in a weakened sinter. The findings of the current study agree with this as is indicated that the blend with a PSF of 0.25-1mm demonstrates the longest sintering time on average as displayed in Table 6.1 and has the corresponding highest RDI value of 57%, as specified in Table 6.2. From this study it has been found the reason why this happened is attributed to the permeability of the bed, which has a significant impact on the RDI of the sinter. In other words, a longer sintering duration directly correlates with a higher RDI, ultimately affecting the strength and porosity of the iron ore sinter that is produced.

6.4 Chapter Conclusions

During the experiment, the business problem of the presence of a "white relict" on a piece of sinter was identified. This material was not completely calcinated during the sintering process, which resulted in its presence. The reason for this can be attributed to the material's larger PSF. The present study has shown that coarser flux particles are more difficult to calcinate during sintering.

As well as this, the following gaps in knowledge were concluded. It was discovered that the size of the flux particles has a significant impact on the combustion rate. Smaller particles (1-3.15mm) allow for easier oxygen accessibility to the coke particles, leading to faster combustion rates and higher temperatures. In contrast, larger particles hinder the coke particles' ability to access the oxygen, leading to slower combustion rates and lower temperatures.

Moreover, larger PSF resulted in reduced contact between hematite particles and CaO due to the smaller surface area of coarser PSF, leading to the production of insufficient bonding phases such as SFCA, which are essential for creating a strong and cohesive sinter structure. On the other hand, smaller particle sizes (1-3.15mm) resulted in a higher proportion of SFCA phases, as observed through quantitative analysis by Intellesis.

In the 1-3.15mm range, optical microscopy images indicated that SFCA is uniformly distributed with other phases like magnetite and hematite. When this occurred, it produced a sinter with good mechanical strength and fewer return fines, resulting in a more homogeneous sinter between this particle size range. This is due to the granulation process being more efficient because the smaller PSF allowed for more unform mixing and granulating as opposed to the larger PSF's, and therefore allowing for better permeability within the green blend. Additionally, when the sinter pot test was being carried out the bridge formation mechanism in these sinter cakes occurred more quickly due to the size of the flux, resulting in a faster propagation of the flame front, as evidenced by the calculated flame front speed. As a result, the breaking of the bridge also occurred more quickly, as evidenced by the hot flow average for this range of particle size distribution.

The uniform distribution of iron oxide phases and SFCAs resulted in stronger bonds between the particles that held the sinter together, yielding better RDI values of 45% and 44% for 1-2mm and 2-3.15mm particle sizes, respectively. Additionally, the 1-2mm particle size had the lowest particle fines content, with only 15% of particles under 5mm. Lastly, the particle size distribution of >5mm PSD for the 1-2mm and 3.15mm particle sizes had the most particles collected at 85% and 83%, respectively.

The best RDI was taken at the 1-2mm range which implied optimal permeability and the correct assimilation of the mineralogy, which is further supported by the uniformity of phases and their distribution as observed in the images obtained by Intellesis. On the other hand, 3.35-5mm displayed inferior RDI, did not obtain the best permeability or assimilation of mineralogy and this was supported by the lack of SFCA formation and distribution amongst the hematite and magnetite phases observed in the Intellesis images.

According to various sources[61 88 103] SFCA has a platy shape. Using Intellesis, multiple simulated images with a PSF of 1-2mm revealed that approximately 11% of SFCA was detected. The optical image of SFCA, which appeared as olive-coloured in the programme, underwent additional analysis in the EDS. The results were conclusive as the elements detected by EDS matched those that compose SFCA, thus supporting the findings of the Intellesis work package.

Through the results of this experiment, we have gained a deeper understanding of the underlying mechanism responsible for the changes in permeability that occur over time due to the hot flow. This discovery is novel and has not been previously documented in literature. As such, it can be deemed a highly significant finding.

7 Impact of Sinter Basicity (B2), MgO and SiO_2 on Sinter Quality

7.1 Introduction

In this chapter the investigation at hand is driven by the paramount importance of enhancing critical domains: thermodynamics, SFCA production, RDI, fines content, and bed permeability. Considering the pivotal role these factors play in efficient iron and steel production; this study will seek to uncover the intricate relationship between fundamental factors influencing sintering processes.

While existing literature[62 79 80] has explored the effect of B2, MgO and SiO_2 on the sintering process and parameters, a comprehensive understanding of the synergistic impact of all three levels on the aforementioned parameters remains limited. This study aims to fill this gap, utilising the Taguchi method for robust experimental design. The orthogonal array for this experiment is featured in Chapter 4.8.3 Table 4.7 where it can be located for reference.

By systematically varying B2, MgO, and SiO_2 levels, the aim is to decipher their collective influence on sinter quality. B2, a crucial ratio of CaO to SiO_2, is widely recognised for shaping sinter mineralogy and thermodynamics[27 99]. The addition of MgO and SiO_2, which are naturally occurring in fluxes and other materials, adds complexities to the sintering process. Through analysing the interactions between these variables, this research will attempt to reveal a complete understanding of how they impact various quality indicators such as RDI and produced fines content.

Based on a review of literature and previous experiments outlined in this thesis, a potential hypothesis for this experiment would be that when sinter was produced with lower RDI and fines content, a B2 range of 1.5-2.0% will perform better. Additionally, an increase in SiO_2 percentage would improve the resulting sinter. Lastly, lower percentages of MgO, around 1.5% would produce the best results.

With the aid of XRD, XRF, RDI and Intellesis, this chapter investigates this hypothesis by:

1.) Observing how the RDI and fines content is changed as the different factor levels are investigated.

2.) How the XRD and Intellesis quantification effects the different phases present as the factor levels are changed.

3.) Understanding more about the influence of B2, SiO_2 and MgO changes on, thermodynamics, sinter bed permeability, formation of different phases and metallurgical testing.

7.2 Results

7.2.1 Statistical Analysis

7.2.1.1 Regression Analysis

In this section, the most important factor levels from the regression analysis performed are analysed. Various analyses were carried out, and based on the results of the regression analysis, a probability value (p-value) was assigned to each independent variable. The p-value indicates the probability of a particular independent variable being the most significant contributor to the dependent variable, which is the factor being measured. A low p-value suggests that the variable in the regression model is a significant contributor to explaining the variation in the dependent variable, while a high p-value suggests that the variable may not serve as a statistically significant predictor of the dependent variable. To facilitate the discovery of potential relationships, an exploratory analysis was carried out, whereby the threshold was set at a more lenient level than usual regression analyses (0.05). This approach was adopted to lay the groundwork for subsequent investigations. The experiment's significance level was set at 0.20 to accommodate the exploratory nature of the analysis, acknowledging that this threshold is less stringent than the conventional 0.05 level and may require further statistical validation to ensure robustness. An article written by Rubin et al.[153] delved into the question of whether the p-value loses its significance during exploratory analyses. Their research revealed that the p-value retains its meaning even when conducting exploratory analyses.

Table 11.2 to Table 11.8 in Appendices Chapter 11.3 have been plotted in order of significance for the context of this experiment, with the tables at the end showing no significant contributor from the dependent variables. The main idea behind carrying out the regression analyses is that the statistical analysis is primarily influenced by certain chemicals, including SiO_2, MgO, and basicity. These materials have demonstrated their significance by exhibiting low p-values. However, if any dependent variables do not show low p-values for these chemicals, there might be another mechanism responsible for this, like particle size distribution or permeability.

From Table 7.1 the following deductions can be made. For the average maximum temperature each of the independent variables have low p-values and thus it can be argued that they all could be significant contributors. A similar trend is seen for the average yield as both basicity and MgO demonstate low p-values, showing both could be argued to being statistically significant contributors. In the context of XRD-based analysis, MgO plays a vital role in explaining the variation in the average SFCA formation, in comparison to other independent variables. SiO_2 is observed to be the most significant contributor to explaining the variation in RDI, in contrast to basicity and MgO. MgO is the most influential factor when explaining the average hot flow, outperforming other independent variables. It is important to note that a reported p-value of exactly 0 is often rounded down from a very small value, rather than being precisely zero.

Table 7.1 Conclusion of P-values for different dependent variables with respect to SiO_2, Basicity and MgO (statistically significant results highlighted in green)

P-Value	SiO_2	Basicity	MgO
Average Maximum Temperature	0.002	0.120	0.000
Average Yield > 5mm	0.817	0.013	0.006
Average SFCA formation according to XRD data	0.621	0.703	0.012
RDI	0.120	0.706	0.815
Average hot flow rate	0.484	0.850	0.157
Average time	0.906	0.223	0.373
Average SFCA formation according to Intellesis data	0.271	0.590	0.912

7.2.1.2 Pearson Correlation Analysis

Figure 11.11 to Figure 11.17 in Appendices Chapter 11.3 show the different Pearson correlation graphs which were determined by Minitab. These plots were created to examine potential relationships between system performance measurements (SPMs), regardless of SiO_2, MgO, and basicity levels. It is of importance to establish the correlation of dependent variables and to identify the underlying reasons for such dependencies. This is essential for establishing statistically significant relationships between variables and for determining the impact of one variable on another. In cases where dependent variables are not reliant, it is crucial to investigate the factors contributing to their independence. This knowledge can help improve the accuracy and reliability of research outcomes and provide valuable insights for future decision-making processes.

Most of the graphs can be deemed to have no correlation, which is evident because the Pearson coefficient (r) does not fall in the corresponding 95% confidence interval (CI) range. However, some of the graphs and thus r values are in the CI range and thus it can be observed that with 95% confidence the probability of getting that r value is possible. Each of the system performance measurements (SPM) conducted in this experiment have been plotted against each other with the correlation coefficient as depicted by Table 7.2, the key was also obtained from literature[154] which also mentioned most researchers would probably agree.

Table 7.2 Pearson coefficient correlations for each system performance measurement (SPM) [154]

SPM	RDI	Time	Formation of SFCA (Intellesis)	Formation of SFCA (XRD)	Average Yield	Max Temp	Average Hot Flow
RDI	-	-	-	-	-	-	-
Time	0.390	-	-	-	-	-	-
Formation of SFCA (Intellesis)	-0.108	-0.150	-	-	-	-	-
Formation of SFCA (XRD)	0.148	-0.076	-0.074	-	-	-	-
Average Yield	-0.104	0.411	0.220	-0.196	-	-	-
Max Temp	-0.092	-0.036	-0.171	-0.374	0.187	-	-
Average Hot Flow	-0.509	-0.794	0.020	0.218	-0.232	-0.060	-

Key		
0.00-0.39	Negligible/weak correlation	
0.40-0.69	Moderate correlation	
0.70-1.00	Strong correlation	

7.2.2 Sintering Parameters

After conducting a thorough statistical significance analysis in Chapter 7.2 it became apparent that the independent variables did not bear a significant impact on the average sintering time according to the regression analysis. Nevertheless, a strong correlation between the average time and the RDI was evident through the Pearson coefficient correlation, indicating their interdependence.

The figures shown in section 7.2.2 with an orange curve can be used for visual purposes to compare all the other factor levels to the base blend of this experiment which was at 5.5% SiO_2, 2.0% MgO and B2=1.6.

There were some key individual results shown in Figure 7.1 which were as follows. The results presented in Figure 7.1 showed that the blends performed exceptionally well when the SiO_2 level was maintained at 7.0%. The average sintering time for this level was 13 minutes and 23 seconds. It was discovered that the blend with the quickest sintering time had a SiO_2 level of 7%, MgO level of 2.0%, and B2 of 1.5, taking only 13 minutes to sinter, significantly faster than other factor levels. On the other hand, when the SiO_2 level was 6.5%, the average sintering time was 16 minutes and 27 seconds, with the slowest sintering time of 17 minutes and 55 seconds found in the blend with a SiO_2 level of 6.5%, MgO level of 1.5%, and B2 of 2.0. It is noteworthy that there was a 40% difference between the slowest and fastest blends. Regarding the fastest time to sinter at different MgO levels, the average fastest sintering time was 14 minutes and 24 seconds when the MgO level was 2.5%. When the B2 level was 2.5, it had the fastest average time to sinter at 14 minutes and 32 seconds compared to all the B2 levels.

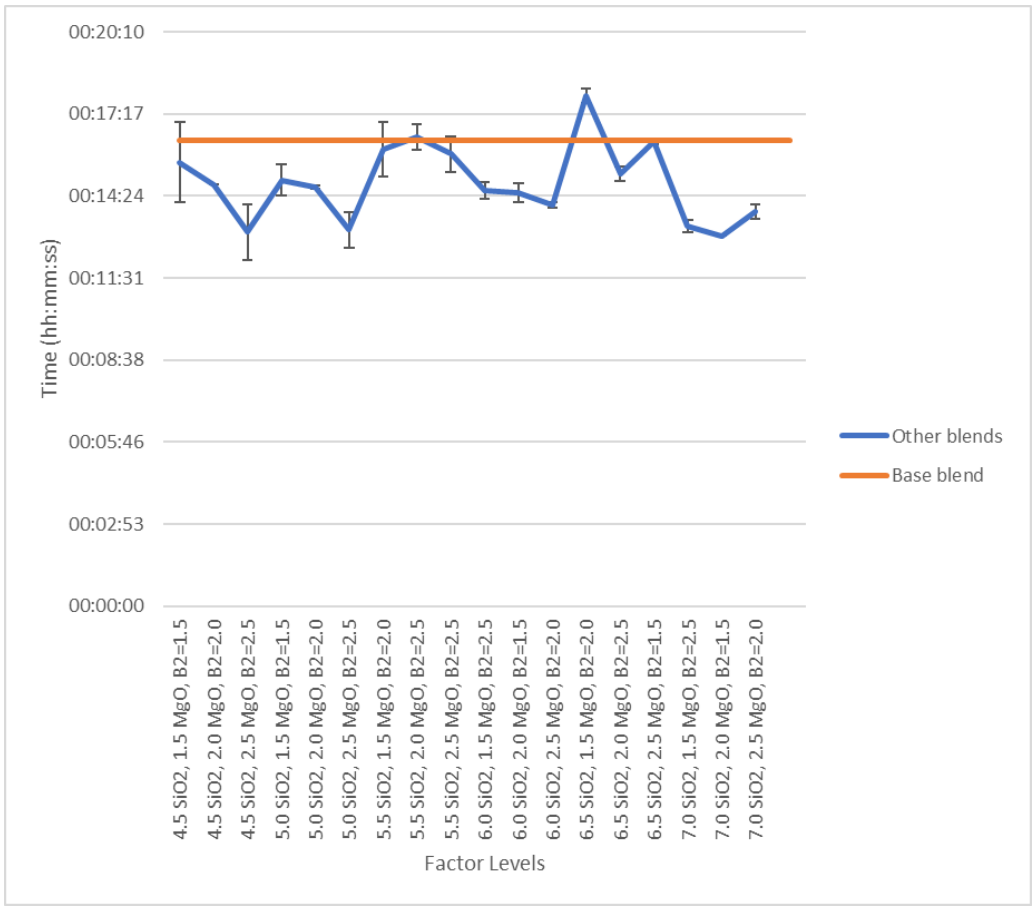

Figure 7.1 Average sintering time as a function of different factor levels.

In Chapter 7.2 a statistical significance analysis was conducted which revealed that all the independent variables had a notable impact on the average sintering maximum temperature as per the regression analysis. However, it was observed that there was a weak correlation between the average sintering maximum temperature and the rest of the SPM's, suggesting that they are not interdependent.

During the experiment the sintering maximum temperature was recorded for each of the different factor levels as demonstrated in Figure 7.2. The highest maximum temperature of 1449°C was achieved when the blend had a SiO_2 level of 5%, MgO level of 1.5%, and B2 of 1.5. Conversely, the lowest maximum sintering temperature was observed when the blend had a SiO_2 level of 7%, MgO level of 1.5%, and B2 of 2.5, reaching only 1333°C. When calculating the average maximum temperature for MgO, SiO_2, and B2, it was found that when the MgO level was 2.0%, the highest maximum temperature was obtained compared to all the other MgO levels. Similarly, when the SiO_2 level was 5.0%, it had the highest maximum temperature observed

compared to all the SiO_2 levels. Additionally, when the B2 was 1.5, the highest maximum temperature was observed compared to all the B2 levels. However, in general, all the blends reached a sufficient maximum temperature, as they all reached above 1250°C.

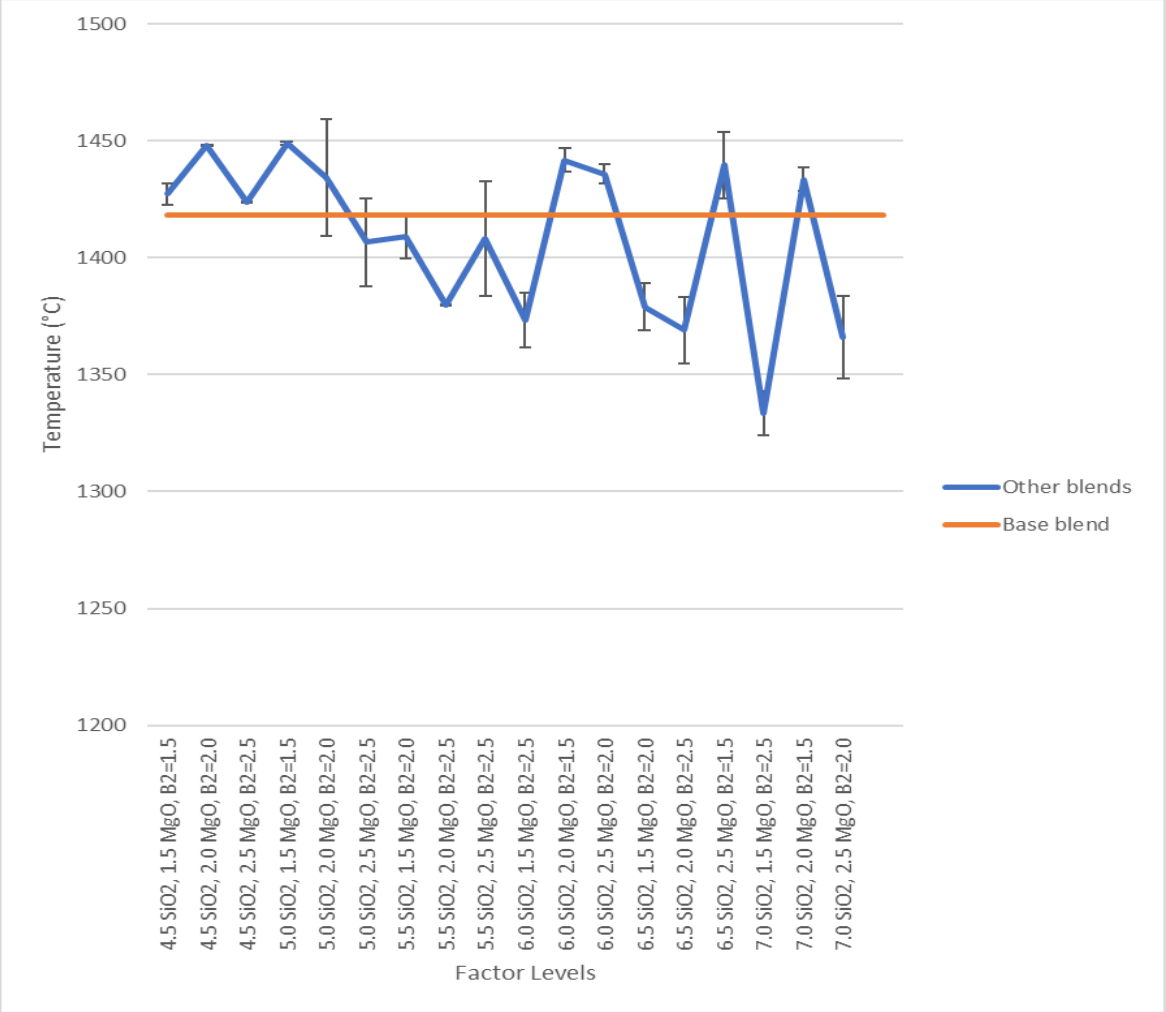

Figure 7.2 Average sintering maximum temperature as a function of different factor levels.

In Chapter 7.2 a statistical significance analysis was conducted which revealed that out of all the independent variables the MgO had a notable impact on the average hot flow rate temperature as per the regression analysis. As well as this, it was observed that there was a moderate correlation between the average hot flow and the RDI which was evident through the Pearson coefficient correlation, indicating there was some interdependence.

The chart in Figure 7.3 depicts the average hot flow rate and shows that the greatest hot flow was achieved when SiO_2 levels were at 7%, MgO levels were at 1.5%, and B2 levels were at 2.5, resulting in a flow rate of 19 m^3/hr. On the other hand, the lowest hot flow rate was observed when SiO_2 levels were at 6.5%, MgO levels were at 1.5%, and B2 levels were at 2.0, resulting in a flow rate of 8m^3/hr. When looking at the average hot flow rate for MgO, SiO_2, and B2, the MgO levels remained constant at 12m^3/hr, indicating that it was not affected by varying levels. The highest hot flow rate was observed when SiO_2 levels were at 7.0%, outperforming all other SiO_2 levels. Additionally, the highest hot flow rate was observed when B2 levels were at 2.5, surpassing all other B2 levels.

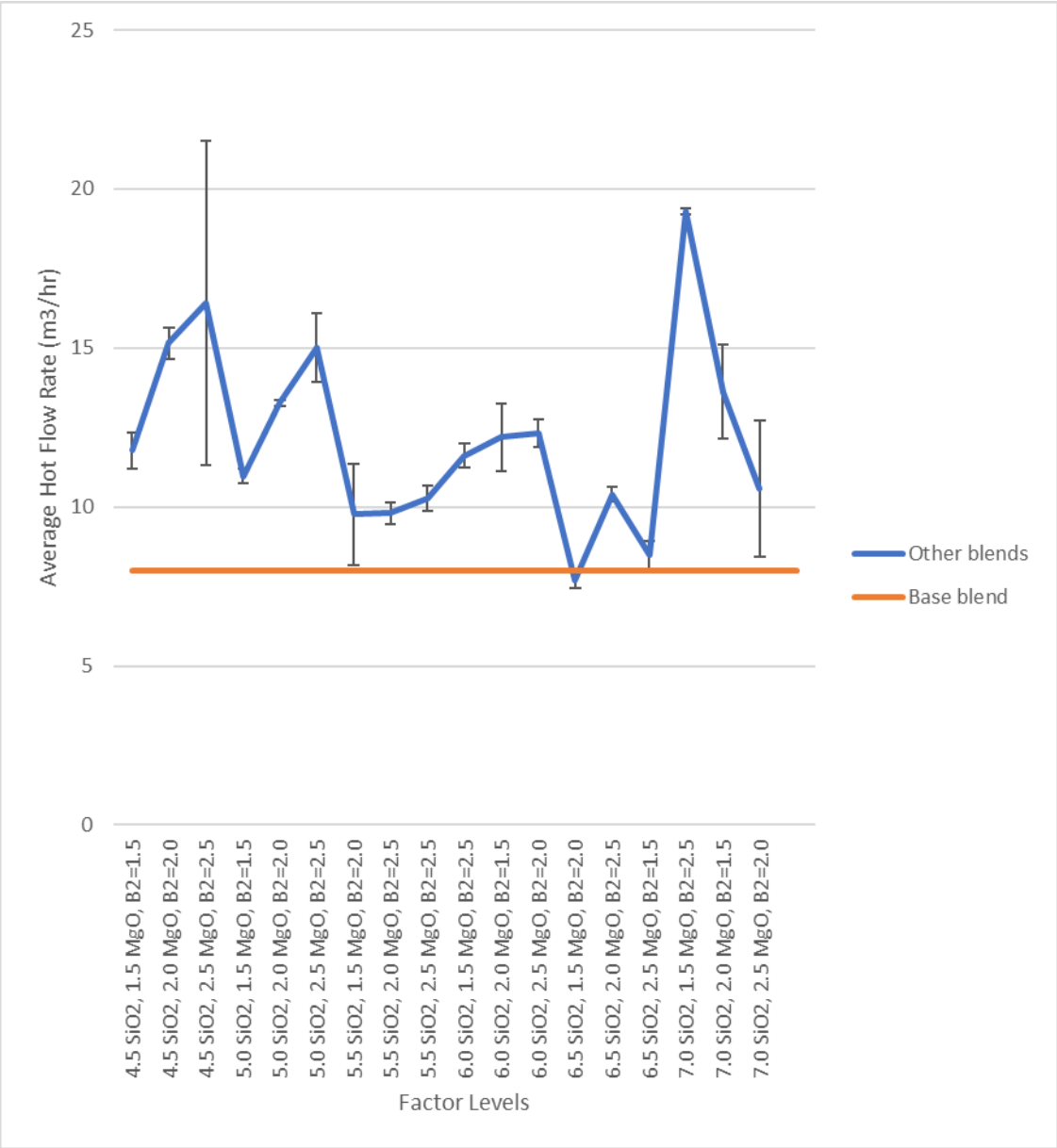

Figure 7.3 Sintering average hot flow rate as a function of different factor levels.

7.2.3 Metallurgical Testing

7.2.3.1 PSD

The results for the PSD of the sinter after crushing and vibrating on each sinter cake are shown in Figure 7.4. This method is an effective way of analysing the strength of the sinter by measuring the amount of fines generated. It was observed that the highest percentage of <5mm particles (25%) was produced when the levels of SiO_2, MgO, and B2 were at 4.5%, 2.5%, and 2.5, respectively. On the other hand, the most >40mm

particles (17%) were collected when the levels of SiO_2, MgO, and B2 were at 6.5%, 1.5%, and 2.0, respectively. When considering the average <5mm fines collected for all the MgO, SiO_2, and B2 levels, it was found that the fines collected were less at MgO levels of 1.5% and 2.0% compared to all other MgO levels. The lowest <5mm fines were observed when SiO_2 levels were at 5.5%, outperforming all other SiO_2 levels. Similarly, the lowest <5mm fines were observed when B2 levels were at 1.5, surpassing all other B2 levels.

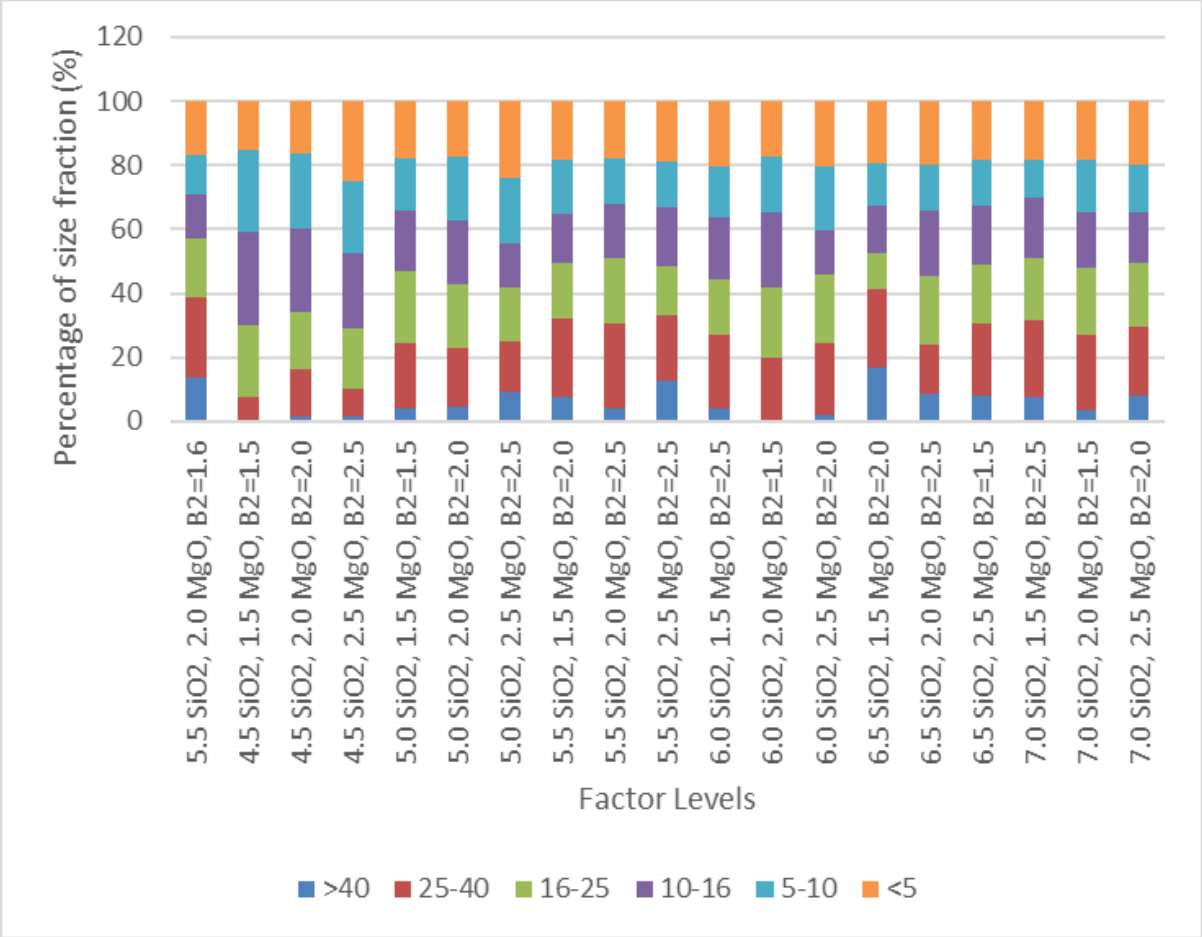

Figure 7.4 Particle size distribution (PSD) as a function of the factor levels.

In Chapter 7.2 a statistical significance analysis was conducted which revealed that out of all the independent variables the basicity and MgO had a notable impact on the average yield as per the regression analysis. However, it was observed that there was a weak correlation between the average yield and the rest of the SPM's, suggesting that they are not interdependent.

According to the information presented in Figure 7.5, the average yield for each blend was analysed (>5mm). The data shows the blend with the highest yield contained 4.5% SiO_2, 1.5% MgO, and B2=1.5 at 85%. On the other hand, the blend with the lowest yield comprised 4.5% SiO_2, 2.5% MgO, and B2=2.5 at 75%.

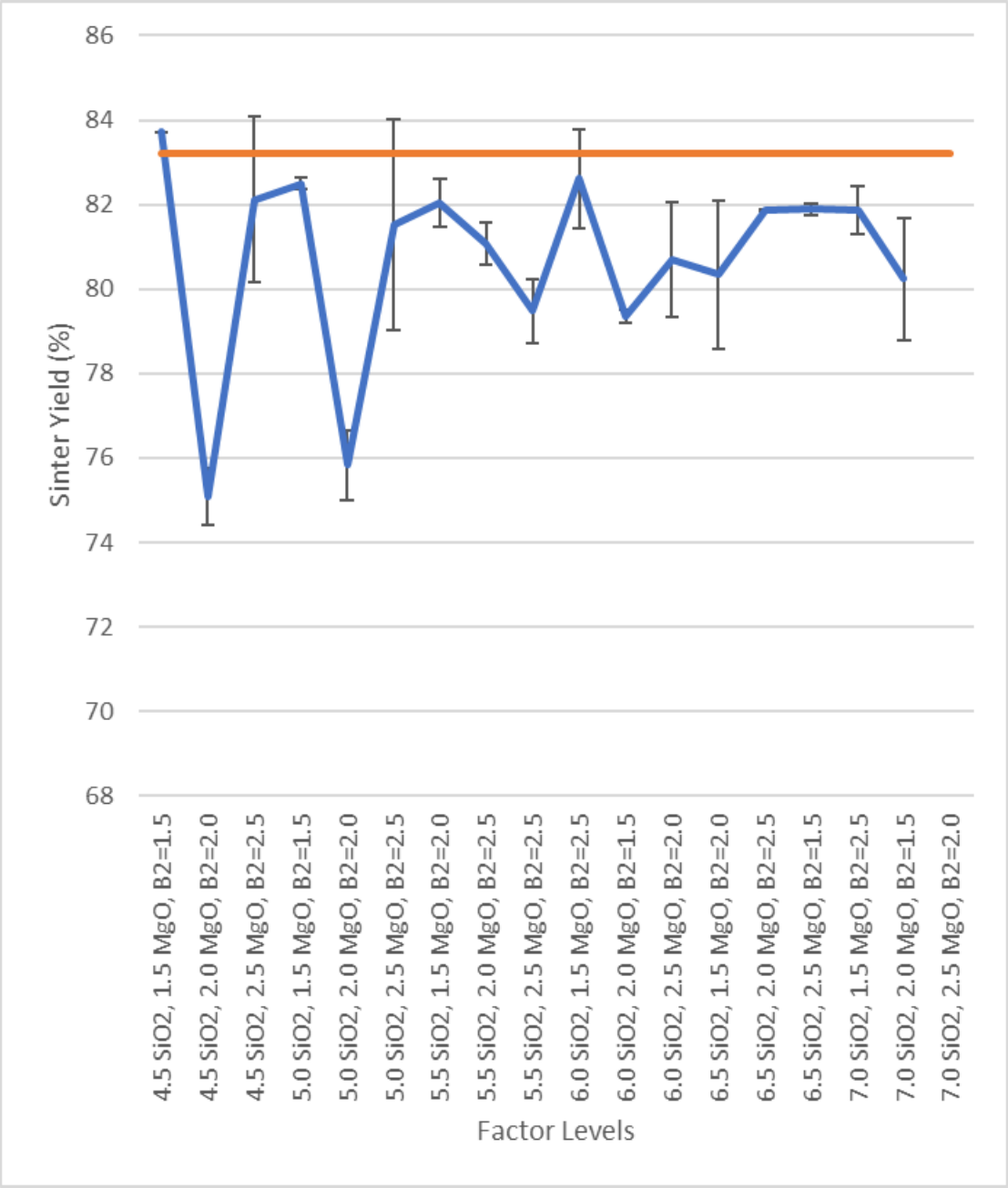

Figure 7.5 Average sinter yield (>5mm) as a function of the different factor levels.

In Chapter 7.2 a statistical significance analysis was conducted which revealed that out of all the independent variables the SiO_2 had a notable impact on the RDI as per the regression analysis. As mentioned previously, it was observed that there was a

moderate correlation between the RDI and the average hot flow, which was evident through the Pearson coefficient correlation, indicating there was some interdependence.

The RDI value of each iron ore sinter made in this experiment is showcased in Figure 7.6. It can be evidently seen that when the SiO_2 levels were at 7.0%, MgO at 1.5%, and B2 at 2.5 it had the best reduction characteristics as displayed by the lowest RDI value compared to the rest of the values used at 12%. On the contrary when the SiO_2 levels were at 6.5%, MgO at 1.5%, and B2 at 2.0 the highest RDI was recorded at 55%. It is clear to see from Figure 7.6 the highest RDI values were observed between the levels of SiO_2 of 6-6.5%. Additionally, the low values of RDI were seen at the low SiO_2 levels of 4.5-5.5% and at the very high values of 7.0% SiO_2.

1.1.1.1 RDI

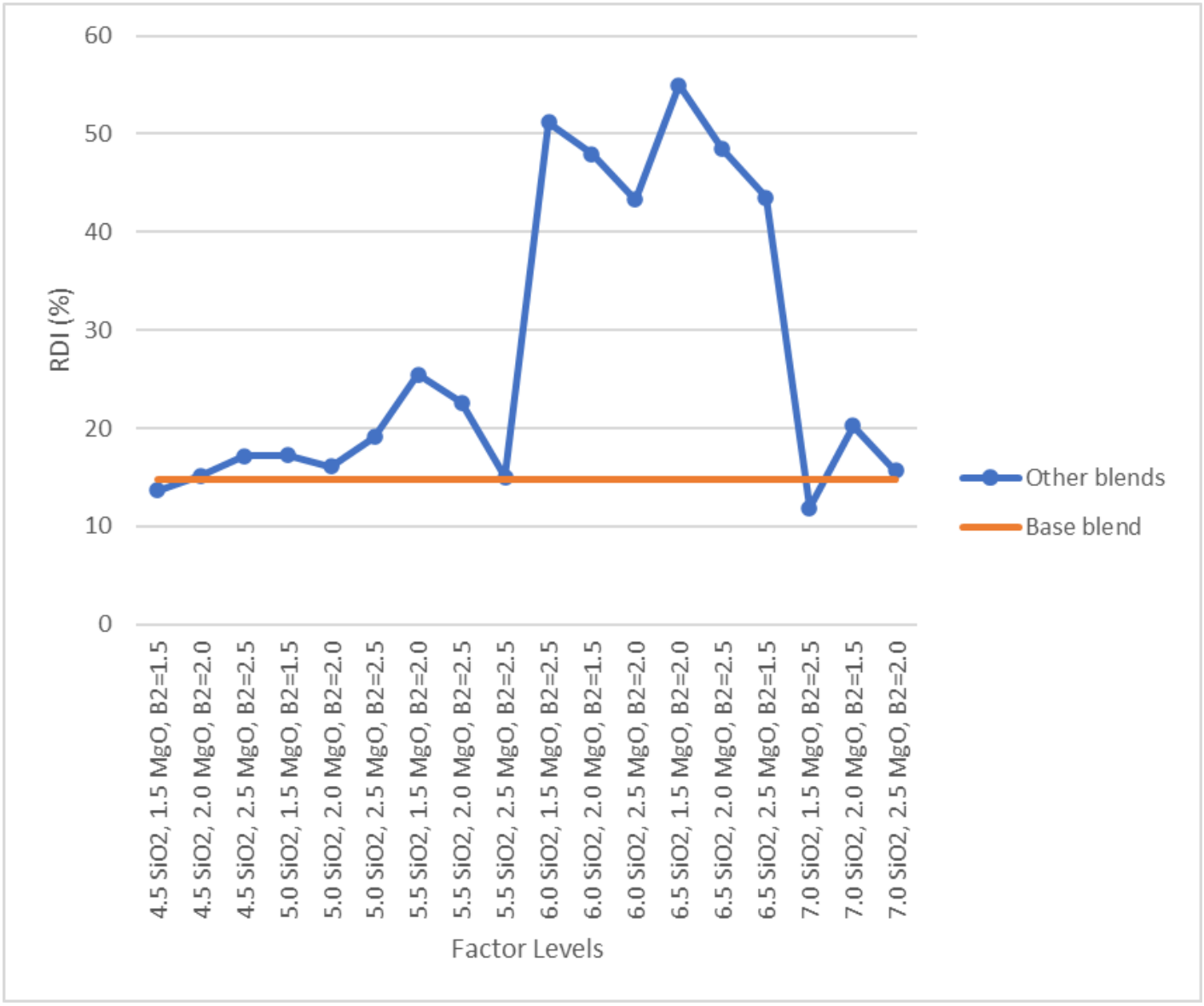

Figure 7.6 RDI as a function of factor levels

7.2.4 Phase and Mineralogical Analysis

7.2.4.1 XRD

The XRD data was collected and Figure 7.7 provides a quantitative analysis of the phases formed as the different factor levels were implemented. The major mineralogy observed in each of the blends consisted of Calcium Ferrites (CF), Silico-ferrite of Calcium and Alumina (SFCA) (which consists of both SFCA and SFCA-I), Alumina (A), Hematite (H) (which consists of both primary and secondary hematite), and

Magnetite (M). Small amounts of Magnesia (MgO), Silica (Si), Wustite (W), Calcium Carbonate (CC), and traces of Calcium Oxide (CaO) were also observed. When the SiO_2 levels were at 7.0%, MgO at 1.5%, and B2 at 2.5 the highest CF's were recorded and when the SiO_2 levels were at 6.5%, MgO at 2.0%, and B2 at 2.5 the highest total SFCA's were noted.

In Chapter 7.2 a statistical significance analysis was conducted on the average SFCA formation in particular which has been heavily regarded as a quality indicator in iron ore sinter. This revealed that out of all the independent variables the MgO had a notable impact on the average SFCA formation according to XRD as per the regression analysis. However, it was observed that there was a weak correlation between average SFCA formation according to XRD and the rest of the SPM's, suggesting that they are not interdependent.

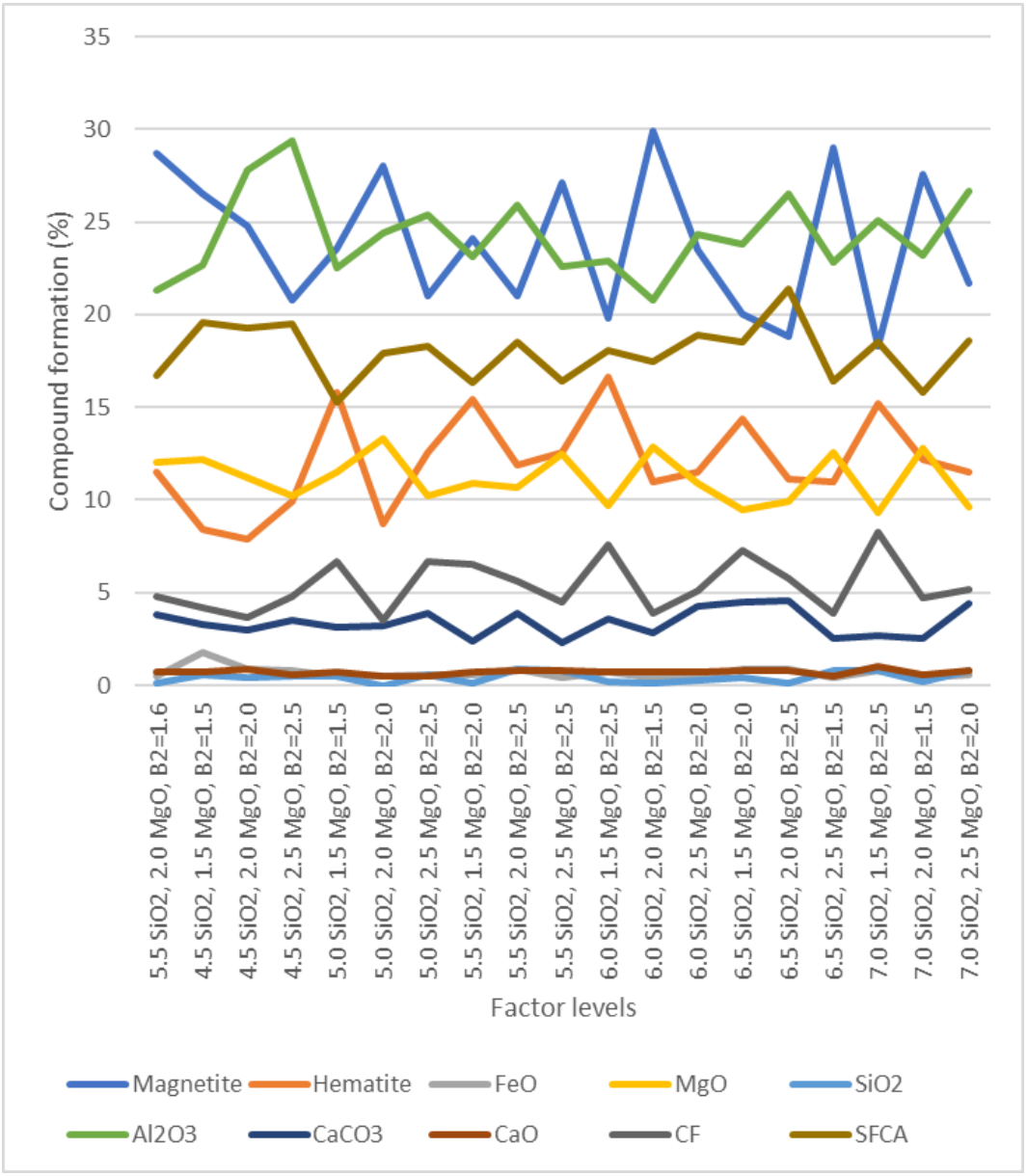

Figure 7.7 Phase formation according to XRD data collected.

1.1.1.2 Optical Microscopy/Intellesis

Figure 7.8 shows the average mineralogy conclusions calculated after analysing 13-57 images simulated through intellesis for each factor level in the phase analysis. It illustrates the individual phases such as SFCA, primary hematite, pores, dicalcium silicate, secondary hematite, magnetite, larnite, and SFCA-I, but also presents the total SFCA, calculated as the sum of SFCA and SFCA-I, as well as the total hematite, which

is the combined amount of primary and secondary hematite (this explains why the y-axis exceeds 100%).

The SiO_2 levels of 5.5%, MgO at 2.0%, and B2 at 1.6 recorded the most SFCA's, while the least SFCA's were observed when the SiO_2 levels were at 6.5%, MgO at 1.5%, and B2 at 2.0.

In Chapter 7.2 a statistical significance analysis was also conducted on the average SFCA formation according to intellesis. This revealed that no independent variable had a notable impact on the average SFCA formation according to intellesis as per the regression analysis. As well as that, it was observed that there was a weak correlation between average SFCA formation according to Intellesis and the rest of the SPM's, suggesting that they were not interdependent.

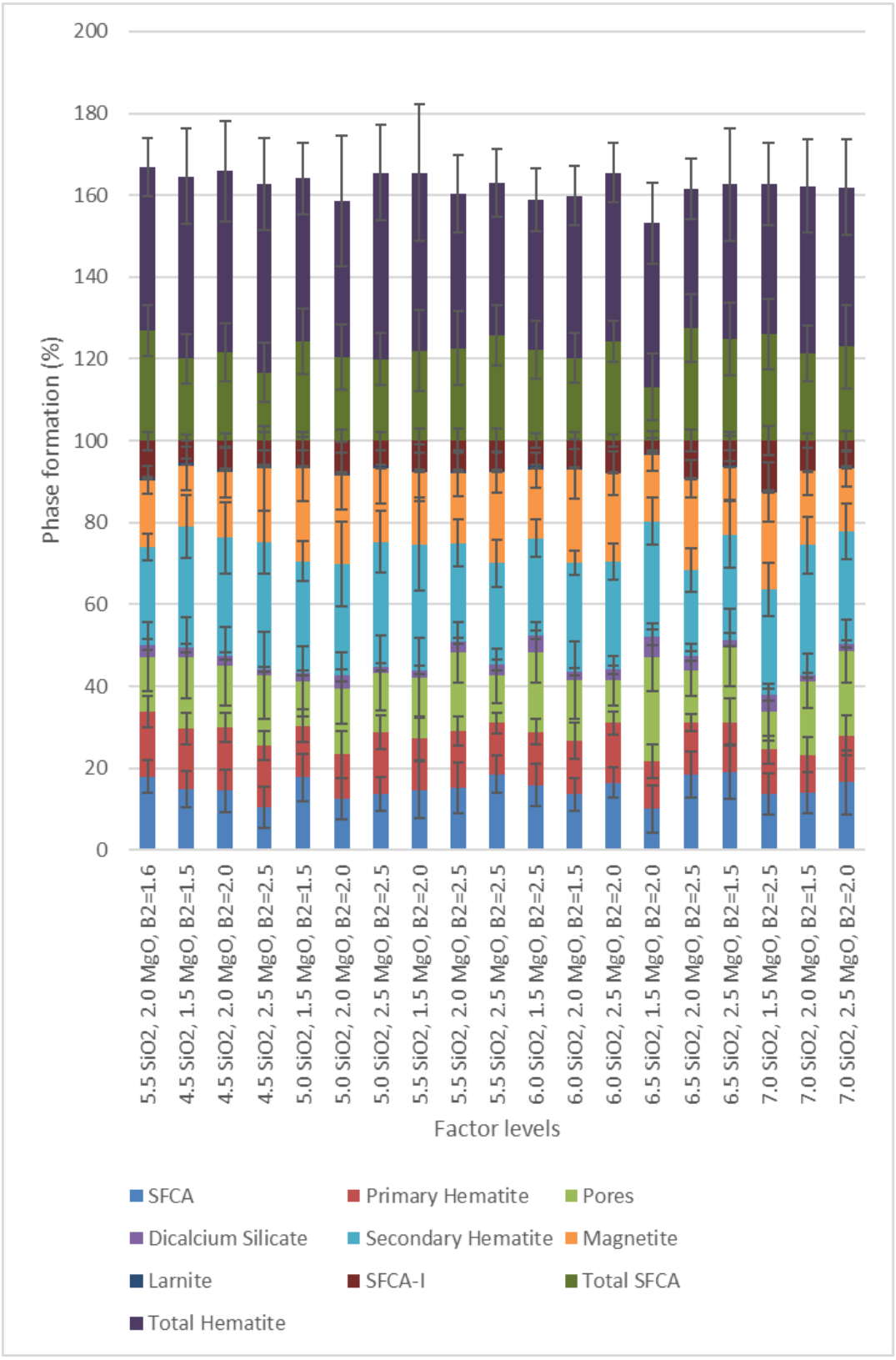

Figure 7.8 Phase formation according to Intellesis data collected.

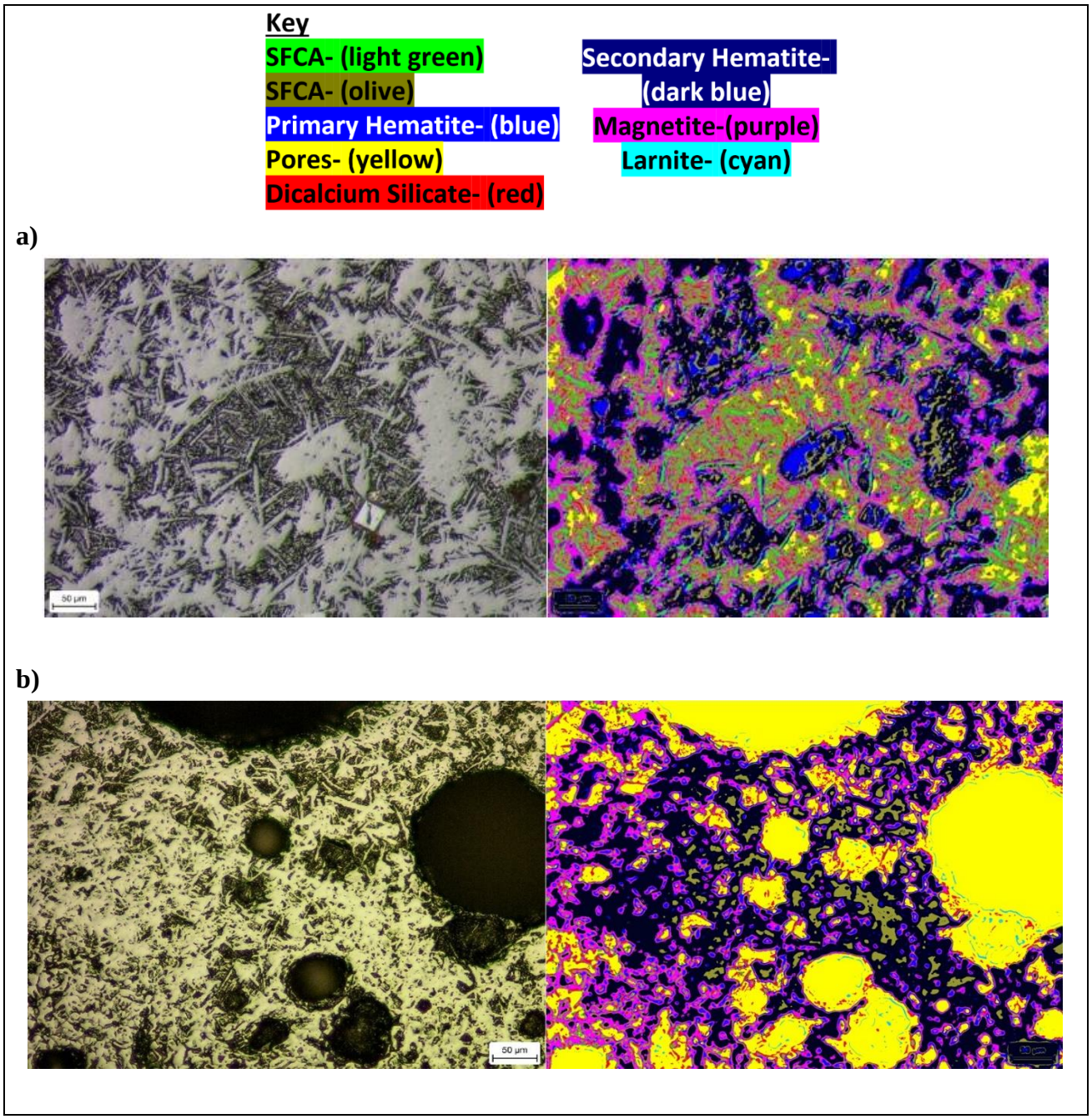

Figure 7.9 Images obtained from optical microscopy (left) whilst the images on the right are obtained from Intellesis. Images taken for a) 7.0 SiO_2, 1.5 MgO, B2=2.5 b) 6.5 SiO_2, 1.5 MgO, B2=2.0

Observing Figure 7.9 shows the optical microscopy images along with its corresponding intellesis images. It is evident that the SFCA-I, represented by the light green colour, is prevalent in (a). Both primary and secondary hematite, illustrated by the light and dark blue shades respectively, are uniformly distributed. However, in (b),

SFCA-I is not as dominant, and only small quantities of SFCA, characterised by the olive color, are apparent and the primary and secondary hematite phases are not uniformly distributed

Table 7.3 Most optimum blend according to this experiment

Factor Level	RDI	Average Sintering Time (hh:mm:ss)	Average Sinter Yield (%)	Average Hot Flow (m3/hr)	(Intellesis) SFCA production (%)	(XRD) SFCA production (%)	PSD >16 (mm)
7.0% SiO_2, 1.5% MgO, B2=2.5	12	00:13:20	82	19	26	19	51

Table 7.3 shows the outcome of this particular experiment which shows to get a balance of the best system performance measurements operating at 7.0% SiO_2, 1.5% MgO and B2=2.5 will ensure this the most. This has led to the identification of the most effective factor level. These results have helped determine the optimal factor level for achieving a low RDI, low sintering time, high yield, high hot flow, high SFCA formation and larger particle size generation.

7.3 Discussion

7.3.1 Influence of Factor Levels on the Mechanism & Statistical Analysis

From the statistical analysis carried out in Chapter 7.2 the following trend was established. To facilitate the discovery of potential relationships, an exploratory analysis was carried out, whereby the threshold was set at a more lenient level than usual regression analyses (0.05)[153]. This approach was adopted to lay the groundwork for subsequent investigations. The experiment's significance level was established at 0.20, indicating that any value below this threshold was deemed significant. It is clear to see that some of the independent variables in this experiment were more significant than others when being varied to some of the SPM's being measured evident by small p-values being established. However, for some of the SPM's being measured the independent variables had no significant contribution evident by its large p-value. Therefore, for the non-significant contributors it could be deduced that there was another mechanism which was the driving force for the change in the SPM.

During the literature review, Scarlett et al.[31] discovered that the composition of the chemistry used to generate SFCA's was significant. This suggests that varying the composition of the chemistry could impact the production of SFCA's. However, the data gathered via Intellesis for the regression analysis showed that none of the independent variables were significant as seen by Table 7.1. This proved that to produce SFCA's, the composition of the chemistry may not be the most important factor. The data collected throughout the project revealed that the most significant factor in producing SFCA's is the production of a green blend that is highly permeable and uniformly distributed. This blend creates a porous sinter cake where the flame front was able to propagate with ease, producing the necessary mineralogy, including the iron oxide phases that are crucial to the production of SFCAs.

Starting with the RDI, when changing the different levels of basicity, SiO_2 and MgO it was evident from the p-values obtained that the SiO_2 was the most significant contributor to the change in RDI. In this experiment, it was observed that the blend containing 7.0% SiO_2, 1.5% MgO, and B2=2.5 had the lowest RDI at 12% compared to any other blends. Pownceby et al.[97] has shown that having SFCA-I which appears

in a needle-like morphology improved the strength and reducibility of the blend. The data from Intellesis showed that the highest level of SFCA-I was recorded at this factor level at 12%, which agrees with this finding. This information is available in Figure 7.8. This means the SiO_2 content gave rise to the SFCA formation which in turn produced sinter of high strength and therefore low RDI.

It was interesting to note that the RDI of iron ore sinter was found to be above the threshold of 33%, ensuring low-quality sinter production[11], when the SiO_2 level was between 6 and 6.5%. Bhagat et al.[59] have also observed a correlation between the duration of sintering and the RDI of iron ore sinter. Their study found that an increase in sintering time led to a worse RDI, resulting in weaker sinter. Although the statistical analysis conducted in this experiment did not evaluate this correlation, it did show moderate correlation between RDI and average hot flow, and strong correlation between time and average hot flow. Therefore, indirectly, it can be said that this experiment supported the findings of Bhagat et al.[59] and shows a moderate indirect correlation between sintering time and RDI. The Pearson coefficient analysis also revealed a strong correlation between average hot flow and average sintering time, indicating that the prolonged sintering times for the 6-6.5% SiO_2 level were due to the hot flow through the bed. This confirms the findings of Bhagat et al. [59] and further supports the moderate indirect correlation between sintering time and RDI.

Upon examination of the 6-6.5% SiO_2 blends, it appears that these mixtures encounter some difficulty at this level. Due to the relatively slow flow of hot material through the pot, the sintering time for these blends is comparatively long. This raises the question of what sets this blend apart from all others. Lower SiO_2 percentages appear to perform adequately, while higher percentages excel. What could be causing slow sintering and subpar sinter production within this SiO_2 range? The only plausible explanation is that the 6-6.5% SiO_2 blend was not achieving the correct composition. If this is not the case, then additional testing must be conducted at these levels to eliminate any potential errors, despite multiple runs having been performed for each blend.

In this analysis, the average hot flow rate (an SPM) which influences the permeability of the bed was observed. After regression analysis, it was found that MgO played the

most significant role for the average hot flow rate as seen in Table 7.1 and thus determining how permeable the sinter cake was, compared to basicity and SiO_2 levels. During this test, three levels of MgO was used: 1.5%, 2.0%, and 2.5%. Each level of SiO_2 was divided into 4.5, 5, 5.5, 6, 6.5, and 7%, and each trend was observed as can be seen in Figure 7.3. The results showed that the increase in MgO levels led to an increase or no change in the flow rate for each SiO_2 level. However, when the SiO_2 level reached 7%, the average hot flow rate decreased from 19m3/hr to 14m3/hr, and then further to 11m3/hr. Based on the regression analysis, since MgO was the significant factor for the average hot flow rate, it can be said with statistical confidence that the cause of the reduction was the MgO level. This may be associated with the sharp increase in SiO_2 level mixed with the increase in the MgO level, which negatively impacted the flow rate.

Some SPMs did not have a low p-value and thus had no significant contributors for instance average SFCA formation according to Intellesis. This means that another mechanism was responsible for this. Judging by previous experiments it can be deduced that it may be the particle size of the flux which was the significant contributor to changes in the SFCA formation data according to Intellesis. It has been established that smaller particle sizes of flux (1-3.15mm) resulted in a higher SFCA phase, as observed through quantitative analysis by Intellesis. The bridge formation mechanism in these sinter cakes occurred more quickly due to the size of the flux, resulting in a faster propagation of the flame front, as evidenced by the calculated flame front speed. As a result, the breaking of the bridge also occurred more quickly, as evidenced by the hot flow average for this range of particle size distribution.

In this experiment, the regression analysis of the RDI versus the SiO_2, MgO and Basicity as shown in

Table 11.5 calculations demonstrated that SiO_2 had the most significant impact on RDI compared to MgO and Basicity. This is evident from the smallest p-value (0.120), indicating statistical significance and ruling out random variation. To facilitate the discovery of potential relationships, an exploratory analysis was carried out, whereby the threshold was set at a more lenient level than usual regression analyses (0.05). This approach was adopted to lay the groundwork for subsequent investigations. The

experiment's significance level was established at 0.20, indicating that any value below this threshold was deemed significant. This is supported by the observation that at a SiO_2 level of 7.0%, the RDI was the lowest among all factor levels, emphasising the crucial role of SiO_2.

In Table 7.2, a Pearson coefficient correlation assessment was conducted between time and hot flow rate, revealing a strong negative linear relationship. The Pearson correlation coefficient (r) value of -0.794 indicated a robust negative association between these two variables. In simpler terms, as the hot flow rate increased, the sintering time decreased, and vice versa, consistently moving in opposite directions. The magnitude of the correlation coefficient (|-0.794|) indicated a strong negative correlation. The closer this absolute value is to 1 (positive or negative), the stronger the correlation. Therefore, a value of -0.794 confirmed a significant negative relationship between the two variables, suggesting that changes in hot flow rate could explain a substantial variation in sintering time. Knowing the hot flow rate provided valuable information about the likely sintering time, with the relationship strong enough for meaningful predictions. This statistical proof confirmed that the average hot flow rate was significantly affected by bed permeability, supported by Mathur et al[55] indicating a negative correlation between porosity, permeability, and sintering time.

When comparing the RDI and average hot flow results, a Pearson coefficient value of -0.509 as shown in Table 7.2 indicated a moderate negative correlation between these two variables. Specifically, as the average hot flow increased and sintering time decreased, RDI also decreased, resulting in a shorter sintering process.

In general, various phases are found around the pores, including hematite, magnetite, wustite, calcium ferrite, silicate phases, slag phases, alumina-silicate phases, and SFCA phases. Literature[155] [156] [157] reports a reduction order of hematite > SFCA > magnetite. The Pearson correlation for RDI and SFCA formation (intellesis) which is displayed in Table 7.2 yielded an r value of -0.108, falling outside the 95% confidence interval range, suggesting no correlation. This implies another factor was influencing the sinter strength. Examining the Pearson data for average hot flow and RDI, it becomes evident that porosity and permeability significantly affect sinter strength. The

distribution of porosity plays a crucial role in sinter strength. The reduction degradation process indicated that phases surrounding the pores are important during RDI measurement and influence the sinter's pore structure. The size and distribution of pores within the sinter can impact gas diffusion and iron reduction pathways. A well-distributed and homogeneous microstructure is generally associated with good reducibility and a lower RDI[24].

7.3.2 Influence of Factor Levels on Thermodynamics

In Chapter 7.2 a statistical significance analysis was conducted which revealed that all the independent variables had a notable impact on the average sintering maximum temperature as per the regression analysis. This means they were all equally accountable for the results that were obtained. This is also reflected and agreed with the results of this experiment and literature. According to research, it has been revealed that temperatures ranging from 1250-1300°C are favourable to the formation of SFCA[28], but the lowest maximum temperature achieved in the experiment was 1333°C. Taking into account the standard deviation, the lowest possible temperature that could have existed was 1328°C in all blends, which still guarantees the formation of SFCA's. Therefore, it can be concluded that the average maximum temperature was not compromised in any of the blends tested, as they all exceeded the required temperature to produce SFCA's and improve sinter quality[33]. A weak correlation was detected between the average sintering maximum temperature and the other SPM's. This can be attributed to the fact that the maximum temperature is not impacted by the quantity of SiO_2, basicity, and MgO utilised in the experiment. The fuel rate, which remained consistent throughout the experiment, was found to have a significant influence on the temperature. These findings reinforce the notion that has been widely documented in existing literature and previous chapters of this thesis.

Upon conducting a comprehensive analysis, it has become evident that the blend comprising of 7.0% SiO_2, 1.5% MgO, and B2=2.5 has demonstrated the lowest attainable maximum temperatures while simultaneously producing the highest count of SFCA's according to intellesis, as depicted in Figure 7.8. Kalenga et al.[101] has disclosed that lower temperatures are favorable to a greater accumulation of SFCA's, which can be attributed to the decomposition of carbonates and a consequent reduction

in sintering temperatures. This finding suggests that the blend encompassing 7.0% SiO_2, 1.5% MgO, and B2=2.5 may prove to be a more viable alternative for obtaining higher concentration of SFCA's during the sintering process.

The presented data in Figure 7.5 provides evidence that the yield of iron ore sinter product is adversely affected when maximum temperatures are not achieved[40]. Among the different blends tested, the blend containing 7.0% SiO_2, 1.5% MgO, and B2=2.5 had the lowest maximum temperature and was amongst the blends that generated the least yield. This observation emphasises the significance of attaining high temperatures during the sintering process to obtain a greater yield. Therefore, it can be concluded that temperature plays a crucial role in determining the final output of the sintering process and should be carefully monitored and controlled.

7.3.3 Influence of Factor Levels on Bed Permeability

Upon analysing Figure 7.1 and Figure 7.3, which displays the average sintering time and hot flow rate, it is evident that the blends performed well when the SiO_2 levels were at 7.0%. This suggests that the iron ore sinter had the ideal permeability at this SiO_2 level and corresponding highs of 19, 14 and 11 m^3/hr for the hot flow rates, making it possible for the flame front to propagate through the bed most quickly[37]. Consequently, this resulted in the most efficient and productive outcomes of the lowest average sintering time recorded throughout this experiment.

In addition, it was observed that with SiO_2 levels at 6.5%, MgO at 1.5%, and B2 at 2.0, the flamefront propagation was hindered, resulting in the lowest hot flow rate of 8m^3/hr compared to other levels. This blend also took the longest time to sinter, approximately 18 minutes, which was considerably longer than the next slowest blend which was 2 minutes quicker. This highlights the poor permeability of the bed, which hindered the flamefront's ability to propagate quickly.

Furthermore, a clear correlation can be observed between achieving efficient sinter production and maintaining a 2.5% MgO level. A total of three trials out of six have demonstrated that sinter can be produced in approximately 13 minutes when the MgO level is at 2.5%. It is clear that a MgO level of 2.5% accelerates sintering time, resulting in improved productivity. In fact, sintering occurred within 14-16 minutes in the other three instances as well, which is still reasonably quick.

At a SiO_2 content of 7.0% and a MgO content of 1.5%, with a B2 factor of 2.5, the addition of 0.5% MgO resulted in a shift to 7.0% SiO_2, 2.0% MgO, and a B2 factor of 1.5. This led to a reduction in permeability, as evidenced by the decline in average hot flow rate from 19 to 14 m^3/hr, as depicted in Figure 7.3. Recent studies suggest that this may be attributed to excessive fluidity arising from the elevated MgO content, which can cause poor granulation, decreased permeability, and irregular sinter structure formation[75].

The observed data collected on the effect of varying factor levels of 6.5% SiO_2 and 1.5% MgO, with B2 level 2.0 to 7.0% SiO_2 and 1.5% MgO, with B2=2.5, reveal a noticeable distinction. It is noteworthy that increasing SiO_2 by 0.5% yields a significant impact, as it promotes the creation of a liquid phase and influences bed permeability, leading to greater mechanical strength[74], as demonstrated by the RDI values presented in Figure 7.6.

Recent research has uncovered a significant correlation between the duration of the sintering process and the RDI of iron ore sinter. The study reveals that prolonged sintering leads to worsened RDI levels, resulting in a weakened sinter[59]. The findings indicate that the blend with a 7.0% SiO_2, 1.5% MgO and B2=2.5 demonstrated the lowest RDI value of 12, as specified in Figure 7.6. This pattern is attributable to the permeability of the bed, which has a significant impact on the RDI of the sinter. In other words, a shorter sintering duration as seen in this factor level by Figure 7.1 at 13 minutes directly correlates with a lower RDI, ultimately affecting the sinter's quality.

Recent studies have demonstrated that the duration of the sintering process is a critical factor in the quality of iron ore sinter. Specifically, the research revealed that longer sintering periods can lead to reduced RDI levels, which in turn can result in weaker sinter[59]. The study's findings indicated that the blend featuring 7.0% SiO_2, 1.5% MgO, and B2=2.5 yielded the most desirable results, with the lowest RDI value of 12%, as outlined in Figure 7.6. This outcome is largely due to the significant influence of the bed's permeability on the RDI of the sinter.

To summarise, the data presented in Figure 7.1 indicated that shorter sintering periods, such as those lasting only 13 minutes, are associated with lower RDI levels and thus higher strength sinter. Conversely, the longest sintering time of 18 minutes was

observed when the factor level was 6.5 SiO_2, 1.5% MgO, and B2=2.0. This outcome corresponds with the finding that the iron ore sinter test with the longest average duration also had the highest RDI value of 55%, as demonstrated in Figure 7.6. These results suggest that optimising the sintering process can have a significant impact on the quality of the final product.

The data in Figure 7.1 showed a correlation between higher B2 levels (ranging from 1.5-2.5) and shorter sintering time during the experiment. This relationship has been extensively studied and is thought to be influenced by multiple factors. One of the key factors contributing to this phenomenon is the correlation between a higher level of B2 and improved air utilisation. As a result, less air is required, leading to shorter sintering times[67]. Additionally, an increase in B2 level enhances pre-ignition permeability and average permeability[68]. This results in a decrease in resistance in the drying zone, which is crucial in water migration, and an increase in average permeability, which helps to reduce sintering time. Furthermore, as resistance in the combustion zone decreases with an increase in B2 level, it further enhances average permeability and reduces sintering time.

Another source has reported that increasing the B2 level results in a shorter required sintering time due to the low viscosity and high surface tension of the melt. These factors work together to improve the sintering process. Moreover, solidification occurs quickly in this situation, and the temperature coefficient of viscosity is high, which further speeds up the sintering process[69].

7.3.4 Influence of Factor Levels on Metallurgical Testing

Previous research[18] on PSD indicated that the amount of fines (<5mm) collected can determine the strength benefits of a blend. According to Figure 7.4, the collection of fines was highest when the SiO_2 level was at 4.5%, MgO at 2.5%, and B2 at 2.5, at a total of 25%. Furthermore, this blend only had 2% of sinter collected in the >40mm category. These results indicated that this factor level is not optimal for the purpose of sinter strength as it resulted in an excess of fines being collected and insufficient collection of larger particle sizes. Consequently, the sinter produced by this blend was weaker than that of other blends.

Interestingly, the blend with the lowest amount of fines was achieved when the SiO_2 level was at 4.5%, MgO at 1.5%, and B2 at 1.5, at a concentration of 15%. It is worth noting that the highest amount of fines were collected with the same SiO_2 level of 4.5%, suggesting that SiO_2 is not the determining factor. Additionally, the third blend, which had 4.5% SiO_2, had a fine content of 16%, which was closer to the fine content of the blend with the least amount of fines. This indicated that an MgO concentration of 1.5-2.0% and a B2 concentration of 1.5-2.0 are optimal if the target is to minimise fines production. However, increasing MgO and B2 to 2.5% and 2.5, respectively, hinders the effect of the PSD, resulting in more fines being collected. This weakens the sinter and makes it more susceptible to breakdown when force is applied, which does not meet the requirements of blast furnaces.

However, the >20mm fraction size is the range of particle size which is submitted to the blast furnace[14]. So, for this experiment the >16mm category can be observed as being close enough to this range. Upon analysis on this range it is seen that when the SiO_2 level is 4.5% it has some of the lowest amounts collected, so although the fines generation is low, so is the yield for the range >16mm, which is also not desired for the blast furnace, and therefore it can be noted that a lack of SiO_2 (ie 4.5%) is not ideal for this reason.

The collected data was analysed and the standard deviation was calculated for all the PSD categories. It was observed as can be seen by Figure 11.19 that the >40 and 25-40mm categories had the joint highest standard deviation results at 5 and provided reason to suggest this is the category where the factor levels are behaving very different. This indicated a need for further investigation to determine the cause of such significant differences in collection amounts. The >40mm particle range was between 0-17%. Splitting the categories into low, medium, and high strength showed that sinter with SiO_2 levels between 4.5-5% had the most low-strength sinter collected, supporting previous findings. Additionally, sinter with 6.0% SiO_2 levels displayed weak behavior in collecting particles between 16-40mm. For the 25-40mm range, the low and high-strength sinter had a clear overlap despite the anomalous result for SiO_2 level at 5.0%, MgO level at 1.5%, and B2 at 1.5. It was also observed that the SiO_2 level between 4.5-5.0% yielded the least amount of bigger particles, further suggesting that this level of SiO_2 is not ideal in terms of collection of bigger sized particles.

After conducting a thorough analysis of the data, it is evident that the SiO_2 levels between 4.5-5.0% do not exhibit the required strength for iron ore sinter to progress to the blast furnace. Additionally, even at a SiO_2 level of 6.0%, weak sinter is produced that tends to break down under force. Consequently it would be recommended to avoid producing sinter within this range, if the target is to achieve sinter strong sinter to create a stable burden structure in the blast furnace, allowing gases to pass through and react with the iron ore effectively then this level of SiO2 will not be appropriate. However, any other SiO_2 level appears to be suitable for use in the blast furnace for this purpose. To ensure less disintegration when subjected to force, it is advisable to focus on producing sinter with SiO_2 levels between 6.5-7%, which is ideal for the blast furnace to avoid breakages when a force is applied.

To ensure high-quality iron ore sinter, it's important that the RDI does not exceed 33%[11]. According to Figure 7.6, the RDI data for this experiment revealed weak sinter formation at SiO_2 levels between 6.0-6.5%, which produced RDI values between 43-55%, indicating that the iron ore sinter will not perform well in the lower blast furnace. However, all other blends have RDI values below 33%, making them good enough and suitable for use in the lower blast furnace.

Recent research[78] has seen that adding MgO reduces the amount of hematite and increases magnetite formation from MgO and hematite in the sinter. There are circumstances shown in this experiment as seen in Figure 7.6 which shows the RDI value was seen to fall as MgO is added when the SiO_2 level was 5, 5.5,6 and 6.5%. The reason for this was upon observance of the XRD data shown in Figure 7.7 the addition of MgO at 5.0% SiO_2 by going from 1.5 to 2.0% MgO, shows the amount of hematite falls by more than half of its percentage, consequently the amount of magnetite rises and a decrease by 1% is observed in the RDI value, which has proven to be significant in past literature[132]. A similar trend is noticed at 5.5, 6.0 and 6.5% SiO_2. Therefore, this agrees with what was found in literature.

A modification was made to the blend composition, resulting in a change from 7.0% SiO_2, 1.5% MgO, and B2=2.5 to 7.0% SiO_2, 2.0% MgO, and B2=1.5, leading to a 0.5% increase in MgO. This change had an impact on the RDI as seen in Figure 7.6, which increased by 8%. Analysis of the XRD data in Figure 7.7 indicated that the

increase in MgO caused a shift from 15% hematite and 18% magnetite to 12% hematite and 28% magnetite. This indicated that there was a decrease in hematite availability, leading to less reduction[74].

According to recent studies, the addition of MgO has been found to accelerate the thermal decomposition of hematite and result in the formation of a Fe_3O_4($FeO.Fe_2O_3$)-Mg phase. This phase is known to exhibit reduced reducibility[79]. In this experiment, an increase in MgO by 0.5% from a factor level of 7.0% SiO_2, 1.5% MgO, and B2=2.5 to 7.0% SiO_2, 2.0% MgO, B2=1.5 may lead to the production of this phase. The reduction ability of the sinter is a critical factor in the successful operation of the blast furnace. When this ability is lost, the negative effects of the sinter in the blast furnace is exacerbated, resulting in a decrease in productivity and potential increase in costs.

The incorporation of MgO during the sintering process can have a significant impact on overall productivity. Previous research indicates that magnesium minerals are often difficult to assimilate, and in compositions with high flux, MgO can act as a refractory phase[77], causing magnesium to remain in relicts or reaction zones. The addition of MgO to the mixture can create a melt with SiO_2 at temperatures above 1350°C and with Fe_2O_3 at temperatures above 1600°C. This results in an increase in the liquidus temperature of the melt, which consequently slows down the sintering rate[78] [79], ultimately leading to an increase in return fines and reduced productivity.

This experiment explores this phenomenon further, whereby when there was an increase in MgO by 1% from a factor level of 7.0% SiO_2, 1.5% MgO, and B2=2.5 to 7.0% SiO_2, 2.5% MgO, B2=2.0. The findings of this experiment indicated a small increase in return fines from 18% to 20%, as depicted in Figure 7.4. These results may highlight the critical role of MgO in the sintering process and emphasise the importance of closely monitoring its presence to optimise productivity and minimise fine generation.

After conducting a thorough analysis of the yield data presented in Figure 7.5, it is important to note that each blend displays an acceptable yield, with the lowest recorded at 75% and a standard deviation of 2 between them. This observation suggests that the factor levels did not have a significant impact on the yield, and there may be another factor that is influencing the results of the yield, such as a constant

factor, like fuel level. Therefore, further investigation is highly recommended to identify which other factor is affecting the yield.

7.3.5 Influence of Factor Levels on Formation of Different Phases

In this experiment, it was observed that the blend containing 7.0% SiO_2, 1.5% MgO, and B2=2.5 had the lowest RDI at 12% compared to any other blends. Research[97] has shown that having SFCA-I which appears in a needle-like morphology improved the strength and reducibility of the blend. The data from Intellesis showed that the highest level of SFCA-I was recorded at this factor level at 12%, which agrees with this finding. This information is available in Figure 7.8.

From the XRD data, the SFCA levels were highest at a SiO_2 level of 6.5% and lowest at 5.0%, within the range of 4.5 to 7.0% SiO_2. However, it's important to note that the standard deviation for this data set is 1, indicating that the differences between the values are not significant enough to draw strong conclusions.

After examining the data provided by Intellesis, it is possible to draw more definitive conclusions. The AI software shows a significant variation in total SFCA content, ranging from 13 to 27 in this experiment. It is worth noting that when the averages of total SFCA formation at each SiO_2 level are taken, there is a noticeable increase in SFCA formation as SiO_2 levels increase. Previous literature has indicated that higher SiO_2 content can lead to the formation of additional silicate phases, which may explain this increase in the SFCA phase[82].

The microstructure of sinter products plays a crucial role in determining their properties. As depicted in Figure 7.9 (b), sinter that contained 6.5% SiO_2, 1.5% MgO, and B2=2.0 exhibited a lower presence of SFCA-I and a higher concentration of non-melted hematite and magnetite particles. Conversely, when the SiO_2 content was increased by 0.5% to 7.0% SiO_2, 1.5% MgO, and B2=2.5, as seen by Figure 7.9 (a) there was a noticeable increase in the amount of SFCA-I, resulting in the formation of a dense and homogeneous structure of SFCA-I that held the solid particles of hematite and magnetite together. This, in turn, contributed to the development of high mechanical strength and superior quality of iron ore sinter[80]. Therefore, it is crucial to produce enough SFCA-I as the primary binding phase, which necessitates ensuring a

sufficient level of SiO_2 to guarantee the mechanical strength and performance of the sinter.

The data presented in Figure 7.7 shows that a blend composed of 4.5 SiO_2, 2.5 MgO, and B2=2.5 had the highest level of Al_2O_3, as determined by the XRD analysis. This suggests that the inclusion of these specific components had a notable impact on the Al_2O_3 content of the blend. Additionally, examination of the results shown in Figure 7.8 reveals that the level of secondary hematite detected by Intellesis was also among the highest in this experiment, at 31%. Previous research has indicated that Al_2O_3 has a tendency to accumulate in secondary hematite when primary hematite is converted[11]. This may explain the higher levels of Al_2O_3 found in the blend containing 4.5 SiO_2, 2.5 MgO, and B2=2.5. It is also noteworthy that this increased amount of Al_2O_3 may have contributed to the poorer RDI results observed in comparison to the other 4.5 SiO_2 blends shown in Figure 7.6. Overall, these findings provide valuable insights into the complex interaction between the various components present in the blend and their impact on the resulting properties of the material.

As previously mentioned, the blend composed of 7.0% SiO_2, 1.5% MgO, and B2=2.5 can be a choice operators go for due to the positive outcomes for various system performance measurements mentioned. However, one drawback that may hinder its effectiveness in achieving the desired outcomes. While no specific tests have been conducted, the reducibility of this blend can be inferred based on several factors. According to literature, the reducibility of sinter can vary depending on the type of hematite present. Primary hematite is more porous and therefore more reducible compared to secondary hematite[11]. In this experiment, it was observed that the level of primary hematite present in the blend in question is not as high as in other blends, with an average of only 11% compared to 16% in other blends. This suggests that the porosity associated with primary hematite may be lacking in this blend, making it less reducible and, therefore, less efficient in reducing gases in the blast furnace. It is important to consider this limitation when determining the suitability of this blend for specific applications. While it may be appropriate for some purposes, it may not be the best choice for others that require higher reducibility. Therefore, it is advisable to conduct further tests and evaluations to determine the most appropriate blend for specific use cases.

The XRD data, presented in Figure 7.7, allowed for the calculation of the amount of calcium ferrites produced at three different levels of MgO (1.5%, 2.0%, and 2.5%). The data analysis revealed that the average amount of calcium ferrites for each level of MgO was found to be 7%, 5%, and 5%, respectively. These results indicate that the level of MgO in the iron ore sinter significantly affects the resulting calcium ferrites production. The literature suggests that this is mainly due to higher percentages of MgO, which can lead to the replacement of Fe^{2+} by Mg^{2+} in the magnetite crystal lattice and subsequently result in the formation of magnesium-containing magnetite and magnesium ferrite during sintering experiments. This, in turn, hinders the oxidation of magnetite to hematite and limits the production of calcium ferrite[74]. Therefore, it is crucial to consider the MgO level in iron ore sinter production to enhance the production of calcium ferrites.

7.4 Chapter Conclusions

During this test, a novel approach was used to analyse the data gathered. A Taguchi approach was adopted with the aim of discovering new insights into the sintering process mechanism. As a result of this experiment, the following conclusions were drawn.

It can be said with statistical evidence that the RDI of sinter is significantly dependent on the SiO_2 content inside the produced sinter out of SiO_2, MgO and basicity. Also, the MgO content dictates the average hot flow which was the most out of the independent variables used in this experiment. This means the permeability of the sinter bed is dependent on the MgO content. Furthermore, for the SFCA observed via intellesis this is not dependent on the SiO_2, MgO or basicity, which means that it is dependent on another mechanism. The mechanism on which it may be dependent on could be the particle size distribution or permeability of the sinter bed.

In conclusion, it was observed that as the SiO_2 level increased the resultant system performance measurements improved.

i. RDI measurement was low in two places when the SiO_2 level was 4.5% (average value of 15%) and when the SiO_2 level was 7.0% (average value of 16%).
ii. Sinter yield for the >16mm particles collected generally increased. For the 7.0% SiO_2 level it was substantially high at an average of 49% relative to the other levels of SiO_2.
iii. For the 7.0% SiO_2 the SFCA formation, as reported by Intellesis, was also high at 23% on average (highest average recorded for this whole experiment).
iv. For the 7.0% SiO_2 The sinter yield rate at this level was 81%
v. For the 7.0% SiO_2 the sintering time and average hot flow rate were favourable, resulting in an ideal productivity rate for this level.

The experiment indicates that a 1.5% MgO level is the most optimal choice. This conclusion is supported by:

i. Average RDI value of 29%, satisfying the desired criteria.

ii. Average percentage of particles collected in the >16mm category was 46%, which was a positive outcome.
iii. Intellesis calculated that the total production of SFCA was 21%, which was a respectable level compared to other MgO levels.
iv. Least <5mm particles collected at 18%.

After careful analysis of the B2 data, it is evident that the system performance measurements do not exhibit any significant difference between B2 levels of 1.5-2.5. This conclusion is backed up by the fact that the standard deviation remains at a maximum of 1 for all performance measurements.

Based on the results, the optimal blend for high-quality sinter production would include 7.0% SiO_2, 1.5% MgO, and a B2 between 1.5-2.5. In this experiment, a blend with 7.0% SiO_2, 1.5% MgO, and a B2 of 2.5 was used and produced excellent results, as shown in Table 7.3. These measurements demonstrate that the resulting iron ore sinter is of high quality and meets the requirements of the blast furnace.

8 Conclusion

In conducting three experiments, various aspects of the sintering process were explored, leading to distinct conclusions and valuable insights. Above all, a novel method of characterising the mineralogy within iron ore sinter on the software Intellesis was established with corroboration from multiple globally recognised characterisation techniques such as XRD, SEM, EDS and XRF. The fast simulating colour characterising AI helped to easily observe the different mineralogy within iron ore sinter and quantify them.

The first set of findings focused on optimising the B2 parameter, providing crucial information for achieving stable SFCA production and enhancing sinter quality. The experiment revealed that operating within the B2 range of 1.4-2.0 proved optimal for multiple factors. Maximum temperature data indicated that any B2 apart from 3.0 is sufficient for stable SFCA production. This range not only facilitated a stable temperature profile but also resulted in the lowest RDI values and the least fines content, indicating improved sinter quality. XRF analysis emphasised the importance of maintaining an optimal FeO level for stronger sinter, while XRD analysis highlighted the abundance of SFCA at B2 levels between 1.4 and 2.0, crucial for mechanical strength and reduction properties.

The incorporation of Intellesis's innovative approach further reinforced the significance of the B2 range (1.4-2.0) in facilitating SFCA creation. The method, validated through XRD, SEM, and EDS analysis, showcased impressive outcomes, emphasising the importance of Intellesis's contribution. The images produced by Intellesis, and subsequent quantification demonstrated the progressive occurrence of key SFCA phases within the specified B2 range.

Contrastingly, a B2 level of 3.0 resulted in minimal SFCA formation and smaller crystalline grains, underscoring the importance of the chosen operational range. The columnar structure of SFCA grains between B2 levels of 1.4 and 1.7, as observed in the Intellesis images, further supported the idea that this thickness enhances binding force, resulting in a stronger sintered product.

The second set of conclusions addressed a practical issue, the presence of "white relict" on sinter pieces. The study identified that coarser flux particles with larger PSF posed

challenges during the sintering process, leading to incomplete calcination and the presence of the undesired material. This highlighted the critical impact of flux particle size on combustion rates, oxygen accessibility, and the formation of essential bonding phases like SFCA.

Furthermore, a gap in knowledge emerged, revealing that smaller flux particles (1-3.15mm) allowed for faster combustion rates and higher temperatures. Additionally, smaller particles resulted in a higher SFCA phase, contributing to a more homogeneous sinter structure with superior mechanical strength.

The third experiment adopted a novel Taguchi method, providing statistical evidence of the dependencies within the sintering process. Currently in literature there is work on prediction models, however this study is different as it focusses on what is statistically significant when it comes to composition of input chemistry into the sintering process. SiO_2 content significantly affected RDI, while MgO content dictated hot flow, emphasising the role of permeability. The SFCA formation, observed through Intellesis, was independent of SiO_2, MgO, or basicity, suggesting a potential dependence on particle size distribution or permeability.

In summary, these three experiments collectively show operating within the B2 range of 1.4-2.0 will lead to optimal sinter production. As well as this operating with particle sizes of flux at 1-3.15mm is highly beneficial. The findings highlight when operating at the optimum levels one key thing happened to the process of the sintering mechanism, the way in which the flame front generally went down the pot was with ease and the correct assimilation of the mix occurred. Having the right particle size of flux enabled the oxygen to access the fuel and thus produce a stable temperature was key to this. The basicity ratio was also fundamental and achieving the optimum CaO to SiO_2 ratio facilitated the formation of the molten phase, which enhanced the adhesion and bonding of particles. The permeability of the sinter bed was influenced by basicity. Optimum basicity maintained porosity and permeability within the sinter bed. Proper permeability ensured efficient gas flow during the sintering process. The level of SiO_2 has been statistically proven to impact the RDI and thus the strength of the sinter. As well as this the addition of MgO has a high statistical probability to enhance the hot flow and thus the permeability.

9 Recommendations/Future Work

i. Enhancing the quality of iron ore sinter production is a critical objective for optimising blast furnace operations. One approach to achieving this goal is by improving the reducibility of iron ore sinter, which can reduce the need for carbonaceous reducing agents (such as coke). This can significantly lower operating costs and minimise the environmental impact associated with coke production. While in this project the reducibility could be inferred in some cases, for example in the test when varying the level of basicity, it was inferred from literature that, any fluctuation in the temperature profile could significantly impact the sinter reducibility. In particular, when the B2 was 3.0, the thermal efficiency in the sinter bed was not uniform as the permeability of the sinter decreased due to endothermic reactions necessary for calcining the additional limestone present in the higher B2 tests[5]. These temperature irregularities can result in inconsistent sinter production with lower reducibility. If a quantifiable measure of reducibility was carried out, such as the ISO Relative Reducibility Test, it could confirm this discovery and anticipate future experiments at this level of basicity. It is acknowledged that conducting tests like the ISO Relative Reducibility Test would yield more dependable outcomes.

ii. Further investigation into the SFCA phases is crucial for producing high-quality sinter. By focusing on this area in future work, operators can gain a deeper understanding of the SFCA phases and learn how to control them. The Intellesis model can be improved to better identify the SFCA phases and detect changes in its phase distribution. This will allow for more effective management of the SFCA phases.

iii. In this study, the ability of FactSage to predict the SFCA formation as a function of temperature was predicted in relation to the "varying basicity" experiment. The aim was to understand how thermodynamic phase stability was affected. To expand on these findings, all the studies in this project and future research could benefit from this computational thermodynamics to support the practical experiment carried out. It may also be useful to validate these results using other established thermodynamic software like Thermo-Calc.

iv. Expanding on the promising results achieved with Intellesis for XRD analysis, which helped to identify phase distribution linked to sinter quality in this project, the next logical step would be to enhance the methodology using Rietveld analysis. While Intellesis showed potential, the absolute values lacked consistency. Therefore, Rietveld analysis would provide unambiguous clarity on the specific benefit, ensuring more robust conclusions regarding phase distribution and its implications for sinter quality. Furthermore, this approach would allow for a better understanding of variations in basicity, flux particle size, MgO, and SiO_2 on the amount of the different phases which are formed, thereby further strengthening the reliability and depth of the findings.

10 Impact

The following examines the impact of this research project on each of the stakeholders and the environmental impact in the steel industry.

10.1 Steel Manufacturers and Producers

i. Efficiency Improvement: Manufacturers can benefit from improved efficiency in the sintering process as recent research[18] has identified two factors that heavily impact the success of the sintering process: airflow rate and flame front speed. These factors play a critical role in determining the efficiency of the sintering process and the permeability of the green sinter bed. The control of PSF which was varied in this project has found that sinter productivity significantly increased when operating at a PSF of 1-2mm due to the increased average flame front speed during the sinter test from better permeability. This ultimately leads to reduced production costs and higher output rates. This can positively impact their profitability and competitiveness.

ii. Enhanced Product Quality: Higher-quality sinter from ensuring maximum temperature reaches between 1200-1300°C while avoiding overheating, could cause the iron ore sinter particles to have a strong bond between each other and thus improve their mechanical strength. Proper temperature control allows smoother transition of the flame front down the sinter pot with the appropriate mineralogy being formed, this will mean better iron ore sinter will be formed with the requirments to fulfill the blast furnaces needs which in turn can lead to improved steel quality, allowing manufacturers to produce premium-grade steel products that fetch higher prices in the market.

iii. Long-Term Viability: This experiment yielded impressive results. Utilising a B2 range of 1.4 to 2.0 and a precise PSF size between 1 and 3.15mm can significantly enhance sinter quality in the steel industry. This affirms previous knowledge from literature and instils steel manufacturers with greater assurance if they do adopt these recommendations.

10.2 Research and Development Community

i. Building on Findings: The research in this project can serve as a valuable foundation for future studies and innovations related to sinter production, attracting further research investment and collaboration.

ii. Technology Development: Technology providers might develop solutions that enable steel manufacturers to implement the findings found in this research effectively, leading to new business opportunities. In particular, the Intellesis method offers a faster way to identify different mineralogy within iron ore sinter compared to many existing practices.

10.3 Labour Force

i. Stability and Growth: As the industry becomes more efficient and competitive, the labour force can benefit from job stability and potential growth opportunities, particularly if the industry expands due to improved profitability.

10.4 Environmental Impact

The off gases in the sintering process can be harmful and even toxic in some circumstances. One study showed that in the production of a ton of sinter ore; 242 kg CO_2, 23 kg CO, 0.3 kg SO_2, 0.6 kg NO_x, 0.5 kg dust and 1.2 micrograms dioxin were released into the atmosphere[158]. This is highly dangerous and contributes to the amount of carbon emissions emitted and could even lead to global warming. Moreover, surrounding residential areas can be negatively affected by the fumes given off in the sintering process by the above-mentioned as well as particulate matter emissions that are given off because of the process. In addition to this, noise pollution is also a problem from the sintering process, mainly from the sinter waste gas fans, sinter cooling fans and sinter crushing, it is especially a problem for the sinter plant operators[159].

i. Reduced Emissions: Improved efficiency and energy savings especially from the usage of more sinter in the blast furnace can lead to reduced greenhouse gas emissions per unit of steel produced, contributing to a more environmentally friendly image for the industry. This is mainly due to the highly endothermic calcination of limestone taking place in the sinter test thus does not need to take place in the blast furnace.

ii. Sustainable Practices: The adoption of the research's recommendations can align with sustainability goals, demonstrating the industry's commitment to responsibly manage resources. This is notably true for the usage of particle size of flux between 1 and 3.15 mm, which allows for less energy required for the calcination reaction and thus energy usage. Furthermore, the utilisation of a minimal quantity of raw materials for the sinter pot tests, in contrast to what would have been utilised on the strand, resulted in substantial cost savings for the sinter production team. By conducting these tests, the sinter operators could effortlessly determine the optimal blends for achieving the best sinter production, while also avoiding any suboptimal blends. Additionally, this approach mitigated wastage, minimised operator costs, and reduced emissions into the atmosphere.

11 Appendices

11.1 Preliminary Experiment

This test was carried out as a means of completing a competency. However, due to tracking the particle sizes which went into each blend subsequent conclusions could be found. The figures below show the results obtained when a random amount of Magstone and Limestone was poured out of a bucket and the consequent blends were then sintered to show some interesting findings. From the figures below there was a similarity observed, as it can be seen blends 2 and 3 were similar in the fact that the amount of PSD of Magstone between 3.35-5mm outweighed that of PSD of Magstone in the region 2-3.15mm. Whereas for blend 1 the PSD for 2-3.15mm outweighed that of 3.35-5mm. The ratio of the total PSD between 0-3.15: 3.15-5 for blend 1 was ~ 69:31. Whereas for blends 2 and 3 was ~ 58:42 and 57:43 respectively. A similar trend was established for limestone too, as blends 2 and 3 were more similar, and blend 1 was a little different, this is because the PSD of limestone in the region 1-2mm for blends 2 and 3 are far greater than the PSD between 0.25-1mm. However, this is not the case for blend 1 as the PSD for the 0.25-1mm is marginally greater than the 1-2mm. The ratio of the total PSD between 0-1: 1-5 for blend 1 is ~ 36:64. Whereas for blends 2 and 3 is ~ 25:75 and 24:76 respectively. Acknowledging these similarities and differences meant that the resulting sinter cakes would have to be different. Table 11.1 shows the results obtained for these blends successively, and as it can be seen the same trend continues as blends 2 and 3 are more similar as opposed to blend 1. Figure 11.7 shows the actual chemistry of each of the blends and references the predicted blend chemistry, as it can be seen all the results somewhat align with some margin of error. This meant the test was a success, and there was some reason to believe the particle size of the flux effects the sinter parameters and thus the sinter quality, without necessarily effecting the sinter chemistry.

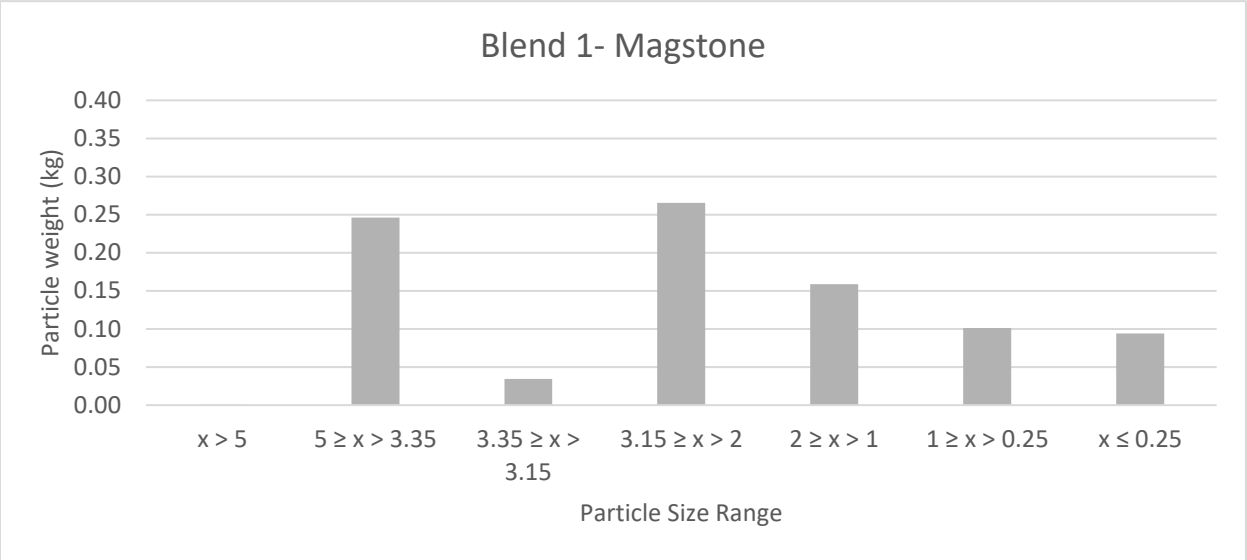

Figure 11.1 From a random amount of 0.9KG from a bucket of max particle size 5mm of Magstone the PSD as a function of particle weight blend 1

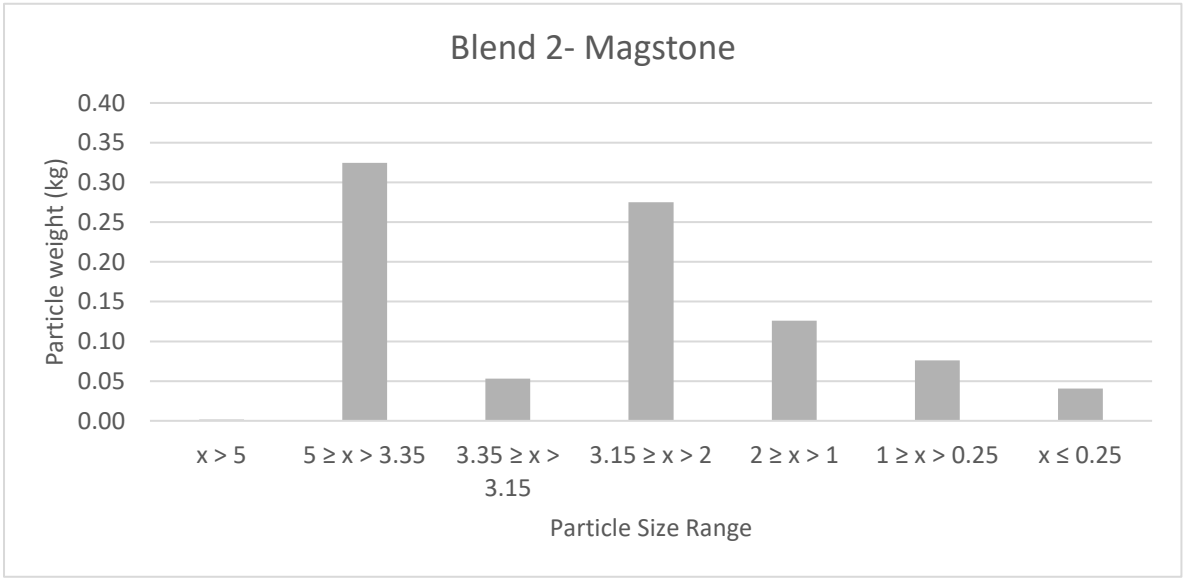

Figure 11.2 From a random amount of 0.9KG from a bucket of max particle size 5mm of Magstone the PSD as a function of particle weight blend 2

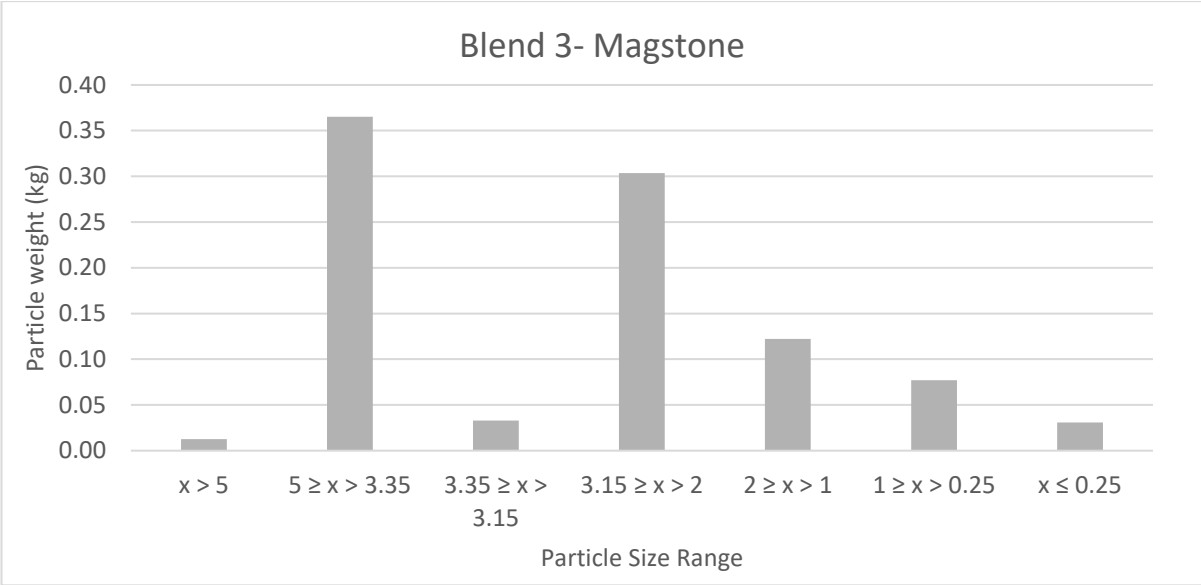

Figure 11.3 From a random amount of 0.9KG from a bucket of max particle size 5mm of Magstone the PSD as a function of particle weight blend 3

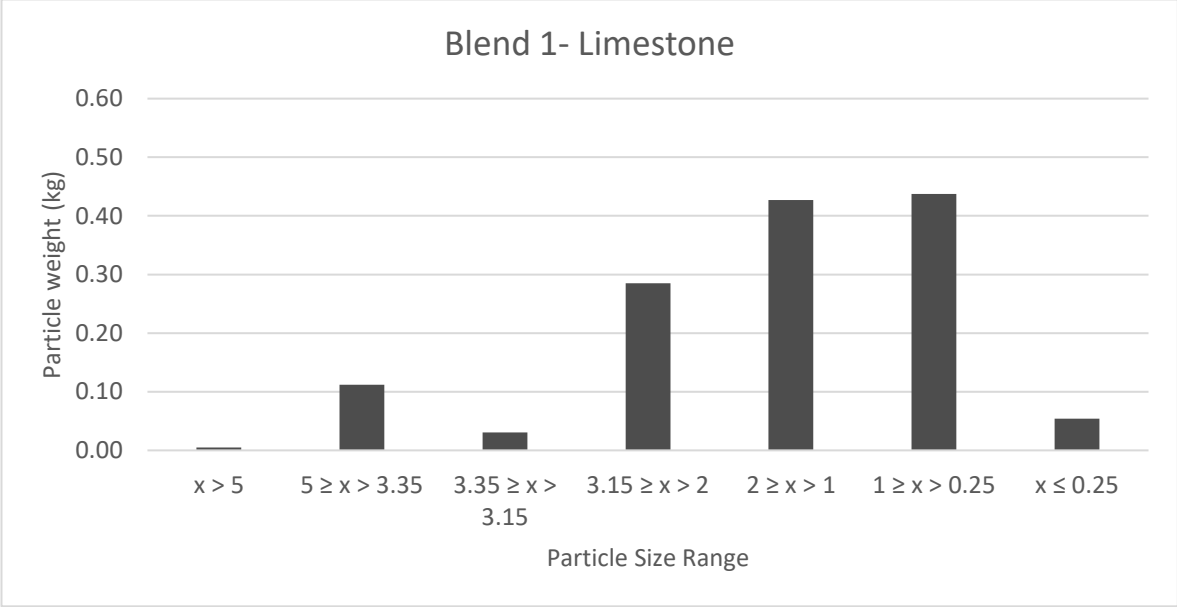

Figure 11.4 From a random amount of 1.35KG from a bucket of max particle size 5mm of Limestone the PSD as a function of particle weight blend 1

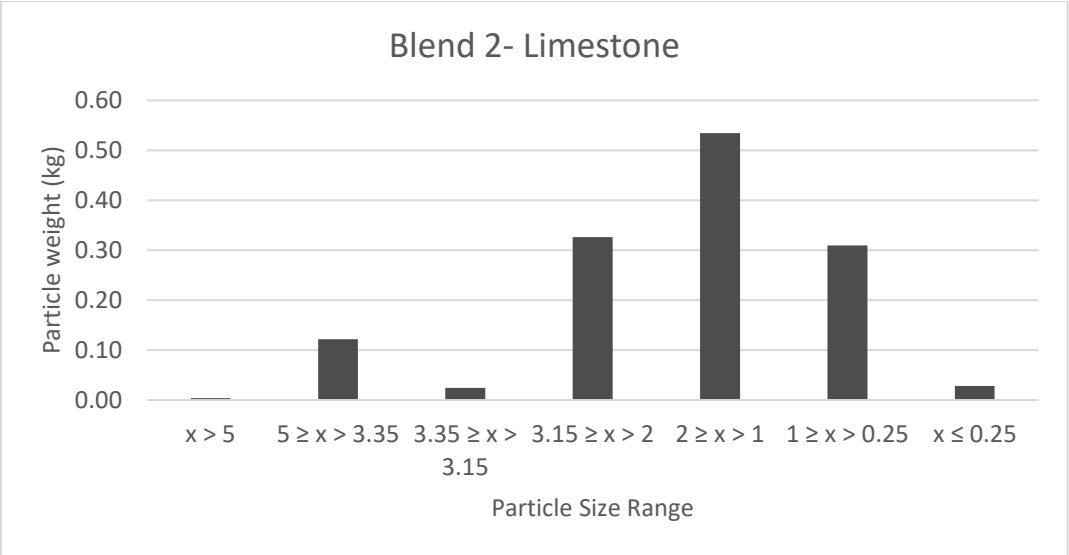

Figure 11.5 From a random amount of 1.35KG from a bucket of max particle size 5mm of Limestone the PSD as a function of particle weight blend 2

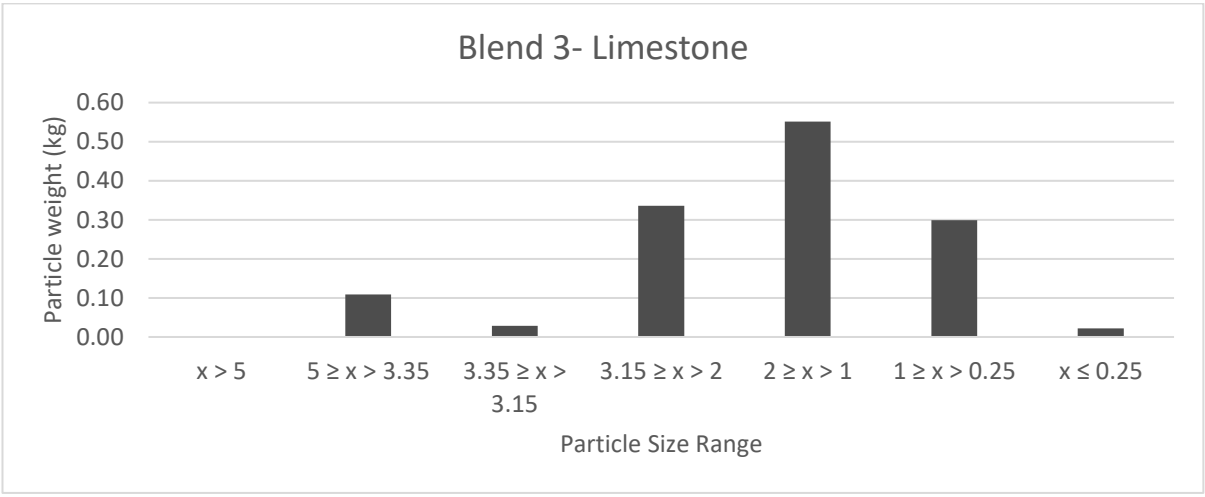

Figure 11.6 From a random amount of 1.35KG from a bucket of max particle size 5mm of Limestone the PSD as a function of particle weight blend 3

Table 11.1 Process parameters for Blend 1, 2 and 3 after being sintered

Process Parameter/Blends	**1**	**2**	**3**
Hot Flow Average (m3/hr)	6.68	7.69	7.37
Cold Flow Average (m3/hr)	8.69	8.78	9.08
Max Sintering Temperature (°C)	1300.91	1348.36	1316.31
Sintering Time (mm:ss)	00:20:05	00:17:40	00:17:55
Sintered Air Flow (m3/hr)	52.38	61.08	55.80
Flame Front Speed Average (mm/s)	0.40	0.52	0.77
Max off-gas temperature (°C)	445.99	447.73	477.68
Fraction of sinter >5mm (%)	80.49	81.44	82.55
Avg Flame Front Width (mm)	27.71	21.30	21.42
Avg Sinter Cooling Rate (°c/s)	2.81	3.27	3.00

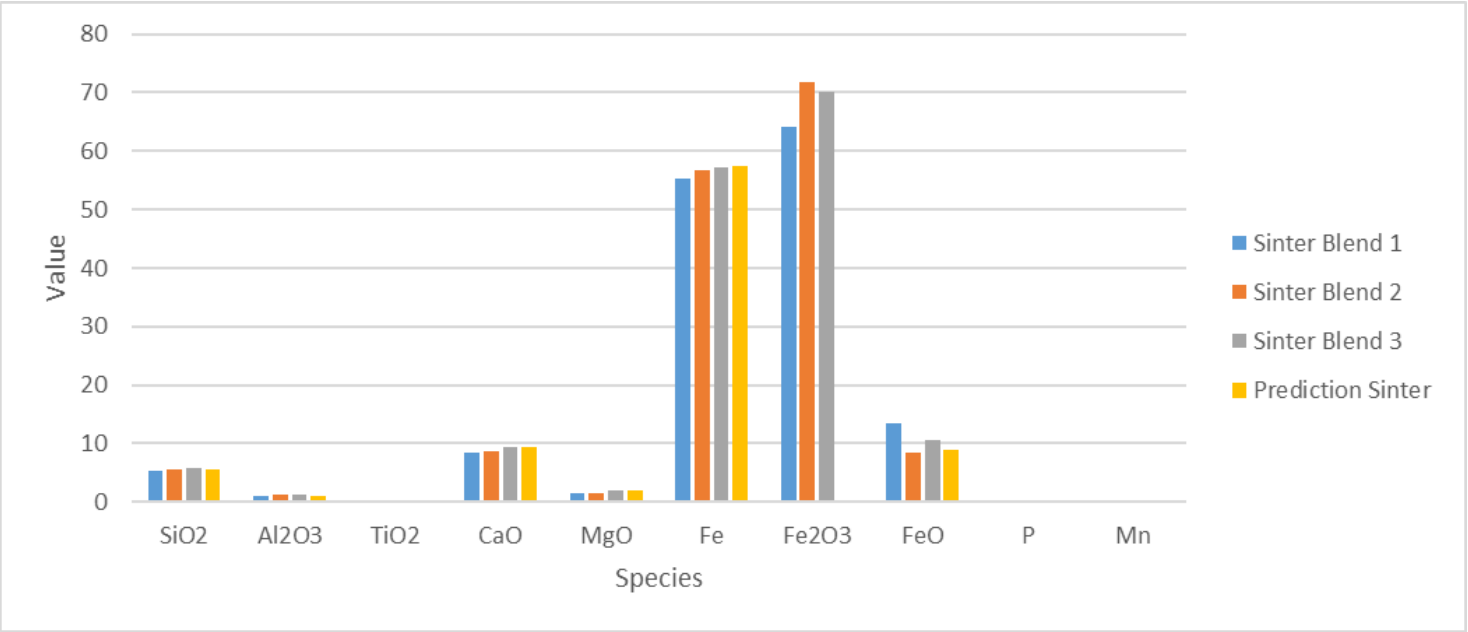

Figure 11.7 XRF of Blends 1,2 and 3 showing the similarities in the 3 blends chemistry as well as what was predicted

Following on from the repeatability study there was good indication that meant that the PSD played an instrumental role in determining many of the sinter process parameters i.e., sintering time, max sintering temperature, air flow etc. Therefore, the follow-up experiment was inspired by this and so the flux (Limestone and Magstone) particle size effect was further delved into in this consequent experiment.

	1	2	3	5	6	7	8	9	10		Error	
Process parameters												
Pressure drop:	100	100	100	100	100	100	100	100	100	mbar	0	mbar
Ignition time:	01:00:00	01:00:00	01:00:00	01:00:00	01:00:00	01:00:00	01:00:00	01:00:00	01:00:00	m s	00:00:00	m s
Cold permeability flow rate	11.49	13.98	12.16	12.92	13.76	15.85	15.74	14.98	14.07	m3hr	1.51	m3hr
Hot Permeability flow rate:	7.973684	8.987918	8.34735	8.290319	8.574181	8.62905	9.54603	9.50647	8.247217	m3hr	0.56	m3hr
Sintering time:	00:17:35	00:16:20	00:16:55	00:17:15	00:17:00	00:17:25	00:16:35	00:16:35	00:16:50	m s	0.00	m s
Max sintering temp:	1393.87	1365.77	1410.74	1427.11	1421.53	1428.10	1441.95	1441.49	1407.59	C	24.32	C
Peak temperatures												
thermocouple 1	1243.13	1359.29	1331.31	1374.73	1331.27	1367.96	1277.03	1274.06	1242.66	C	52.75	C
thermocouple 2	1322.58	1363.46	1362.80	1346.76	1385.10	1337.75	1334.20	1331.29	1329.92	C	20.45	C
thermocouple 3	1315.96	1359.83	1410.74	1397.15	1387.70	1300.44	1317.17	1287.91	1395.72	C	47.45	C
thermocouple 4	1393.87	1365.77	1366.78	1427.11	1400.97	1377.48	1441.95	1441.49	1397.04	C	29.64	C
thermocouple 5	1365.73	1321.21	1388.31	1388.76	1421.53	1428.10	1393.40	1328.47	1407.59	C	37.72	C
max off gas temp 1	534.54	642.61	489.68	539.42	640.10	635.49	564.42	557.05	558.11	cm/s	54.02	C
max off gas temp 2	161.84	164.57	163.64	151.35	171.49	173.96	178.63	176.65	161.53	s	8.77	C
sintered airflow	58.84	58.83	59.97	55.02	57.69	59.58	62.61	54.66	55.03		2.69	m3hr
Time above 1000C												
Thermocouple 1	01:30:00	01:45:00	01:55:00	01:50:00	01:40:00	01:45:00	02:00:00	01:30:00	01:05:00	mm:s	00:16:35	mm:s
Thermocouple 2	03:25:00	02:35:00	02:25:00	02:40:00	02:00:00	02:55:00	02:40:00	02:45:00	02:05:00	mm:s	00:25:37	mm:s
Thermocouple 3	03:25:00	03:05:00	03:05:00	03:10:00	03:00:00	03:10:00	03:40:00	03:05:00	02:45:00	mm:s	00:15:30	mm:s
Thermocouple 4	02:40:00	02:00:00	02:50:00	02:30:00	03:35:00	03:15:00	03:45:00	02:35:00	03:15:00	mm:s	00:33:53	mm:s
Thermocouple 5	01:40:00	01:45:00	02:30:00	02:30:00	02:35:00	03:30:00	03:15:00	01:50:00	02:20:00	mm:s	00:38:18	mm:s
Flamefrontspeed												
TC1-2	0.29	0.33	0.34	0.30	0.35	0.25	0.32	0.30	0.30	mm/s	0.03	mm/s
TC2-3	0.31	0.25	0.29	0.32	0.29	0.29	0.30	0.30	0.32	mm/s	0.02	mm/s
TC3-4	0.36	0.52	0.44	0.52	0.41	0.78	0.67	0.45	0.33	mm/s	0.14	mm/s
TC4-5	0.42	0.64	0.40	0.44	1.27	0.64	1.17	0.58	0.82	mm/s	0.32	mm/s
Flamefront width												
TC1-2	20.42	23.33	23.90	20.85	24.50	17.19	22.27	21.30	21.30	mm	2.20	mm
TC2-3	40.44	32.50	37.92	41.36	37.14	37.14	38.72	38.72	41.36	mm	2.74	mm
TC3-4	48.46	70.00	59.06	70.00	55.59	105.00	90.00	60.97	45.00	mm	19.52	mm
TC4-5	67.88	101.82	64.00	70.00	203.64	101.82	186.67	93.33	131.76	mm	51.13	mm

Figure 11.8 Errors for different process parameters in the sinter pot carried out by Al-Haji et al.[126]

11.2 Error Calculations

This section looks at the errors which were present in the sinter pot which was used in this project. When conducting scientific research, it is important to be thorough and transparent. That's why researchers often include errors encountered during their experiments. While the main text (see Chapter 4.4) outlines known errors associated with specific tests, this additional chart sheds light on additional errors that may be associated with the sinter pot. Figure 11.8 shows the errors for each of the process parameters. This was taken from Al-Haji et al.[126] and was based on a repeatability study with a representative blend. This chart plays a critical role in providing an overview of the various types of errors that can occur during sinter pot experiments.

11.3 Impact of Sinter B2, MgO and SiO_2 on Sinter Quality

11.3.1 Statistical analysis graphs/tables for the Taguchi Experiment

Table 11.2 Regression analysis: Average maximum temperature versus SiO_2, Basicity, MgO

Term	P-Value
Constant	0.000
SiO_2	0.002
Basicity	0.120
MgO	0.000

Table 11.3 Regression analysis: Average yield > 5mm versus SiO_2, Basicity, MgO

Term	P-Value
Constant	0.000
SiO_2	0.817
Basicity	0.013
MgO	0.006

Table 11.4 Regression analysis: Average SFCA formation according to XRD data versus SiO_2, Basicity, MgO

Term	P-Value
Constant	0.000
SiO_2	0.621
Basicity	0.703
MgO	0.012

Table 11.5 Regression analysis: RDI versus SiO_2, Basicity, MgO

Term	P-Value
Constant	0.775
SiO_2	0.120
Basicity	0.706
MgO	0.815

Table 11.6 Regression analysis: Average hot flow rate versus SiO_2, Basicity, MgO

Term	P-Value
Constant	0.169
SiO_2	0.484
Basicity	0.850
MgO	0.157

Table 11.7 Regression analysis: Average time versus SiO_2, Basicity, MgO

Term	P-Value
Constant	0.000
SiO_2	0.906
Basicity	0.223
MgO	0.373

Table 11.8 Regression analysis: Average SFCA formation according to Intellesis data versus SiO_2, Basicity, MgO

Term	P-Value
Constant	0.119
SiO_2	0.271
Basicity	0.590
MgO	0.912

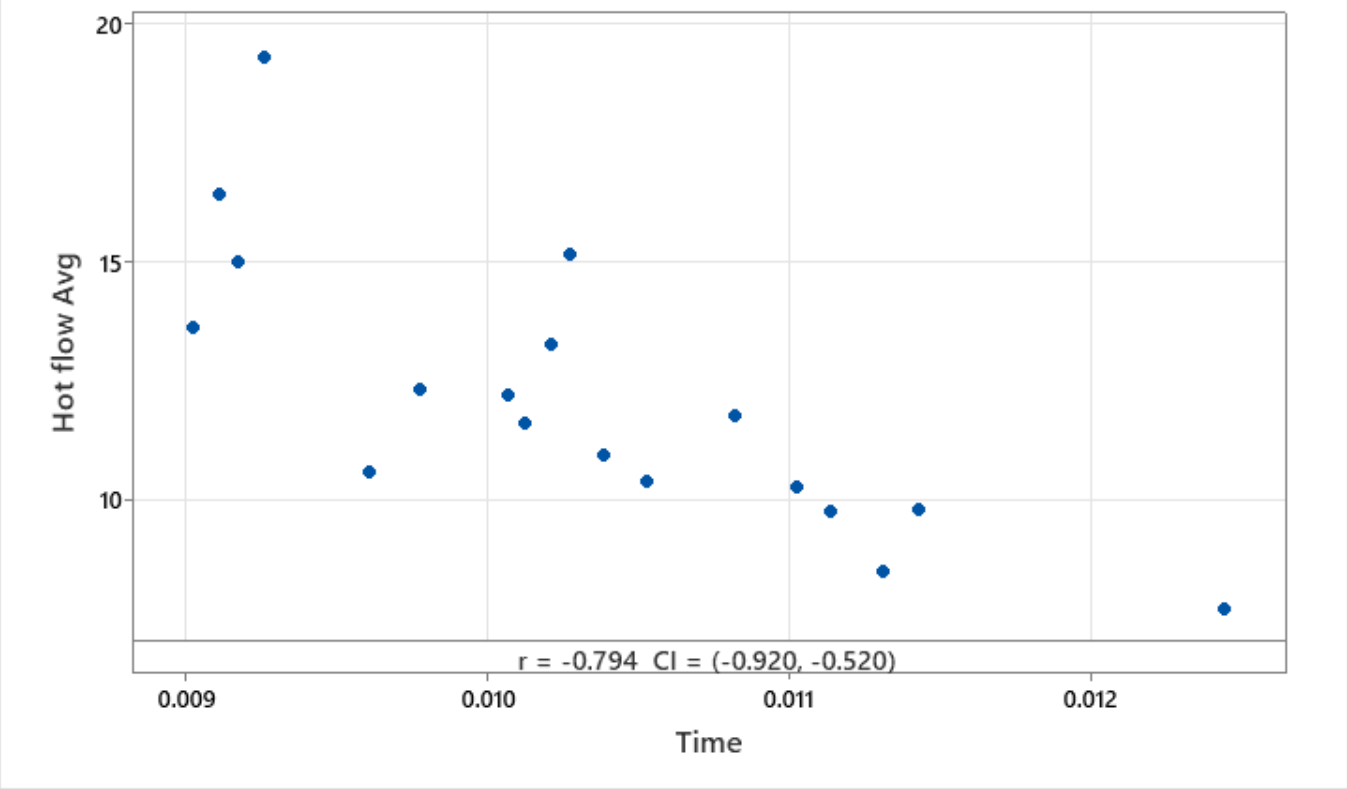

Figure 11.9 Pearson Correlation for Time vs Hot Flow Average

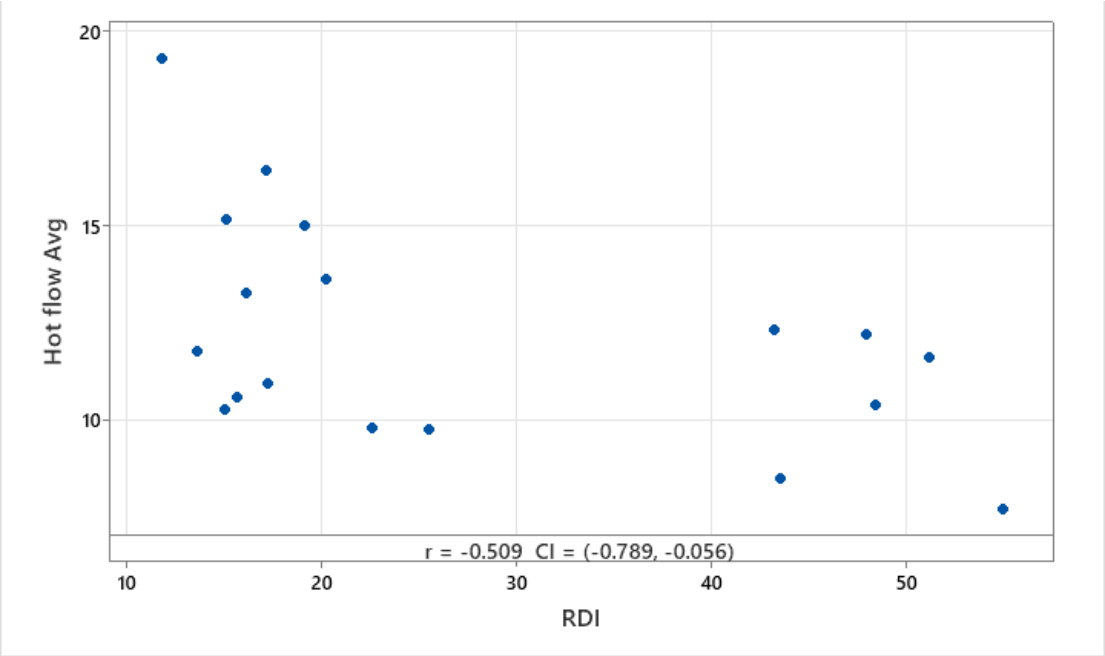

Figure 11.10 Pearson Correlation for RDI vs Hot Flow Average

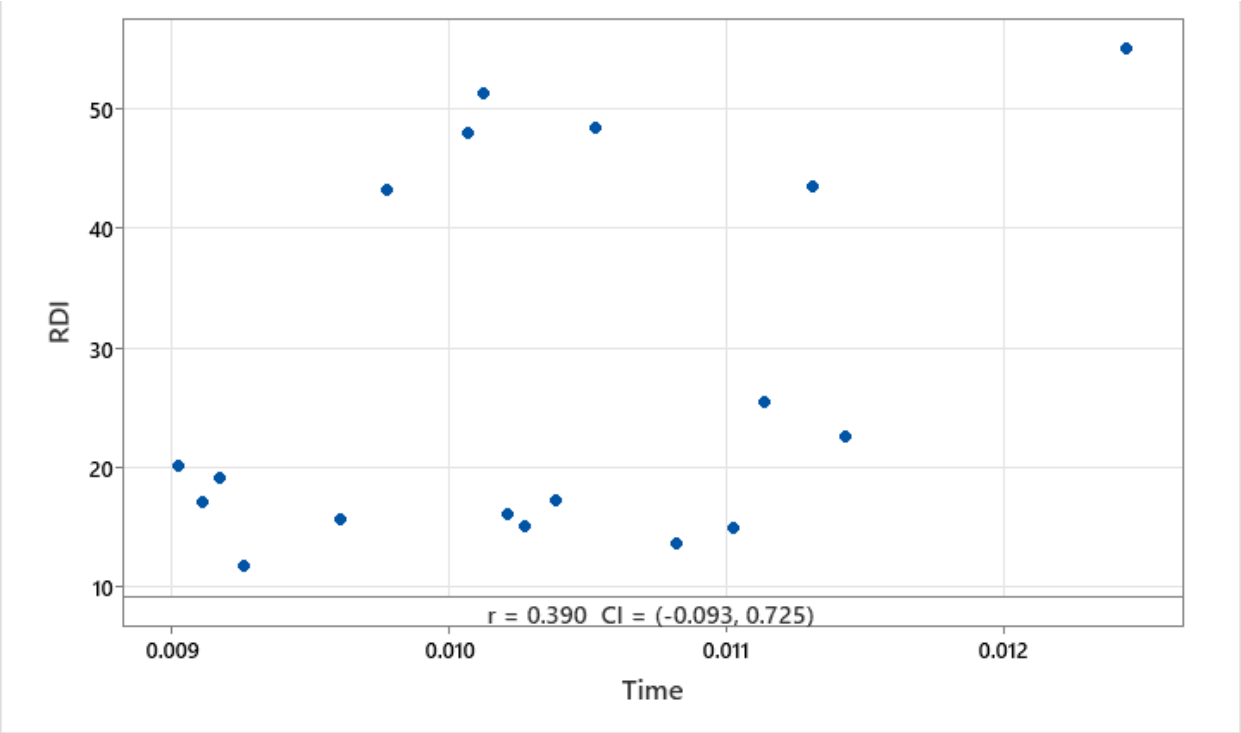

Figure 11.11 Pearson Correlation for Time vs RDI

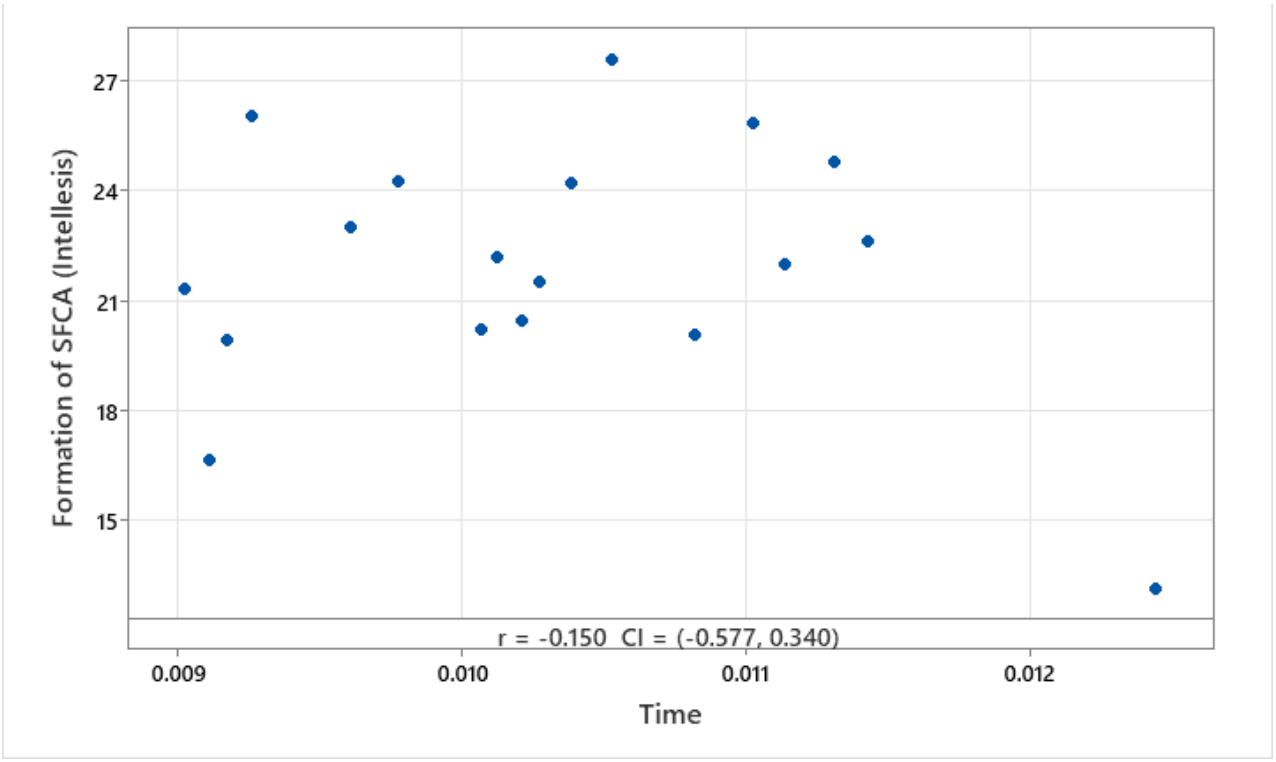

Figure 11.12 Pearson Correlation for Time vs Formation of SFCA (Intellesis)

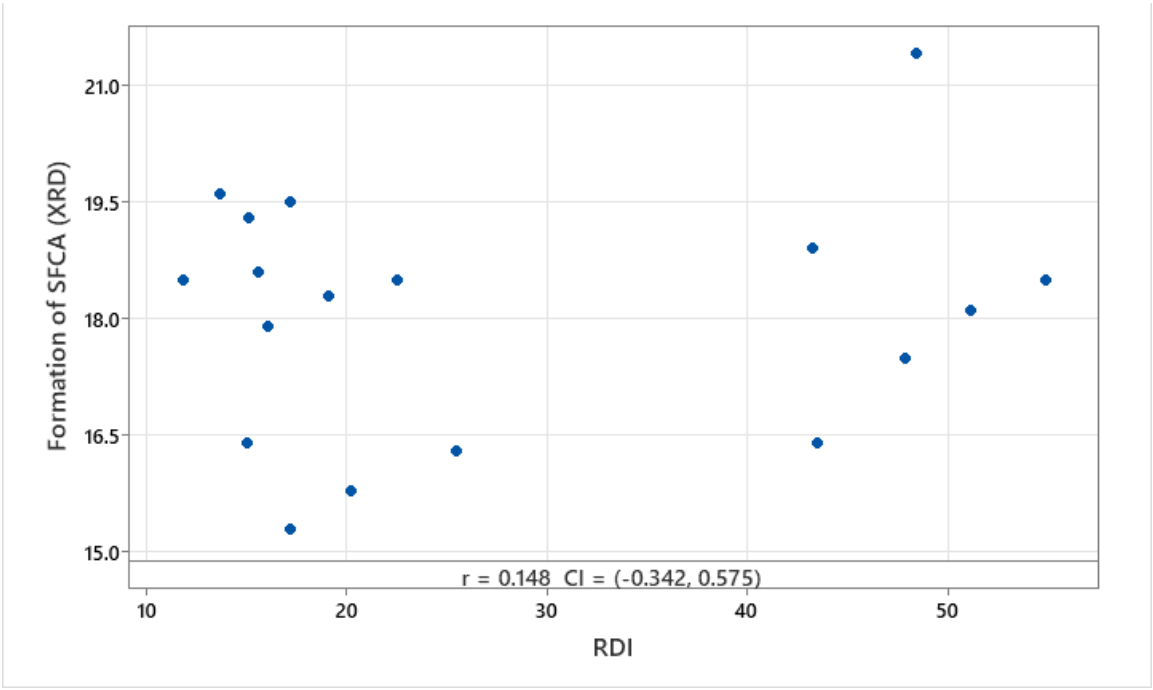

Figure 11.13 Pearson Correlation for RDI vs Formation of SFCA (XRD)

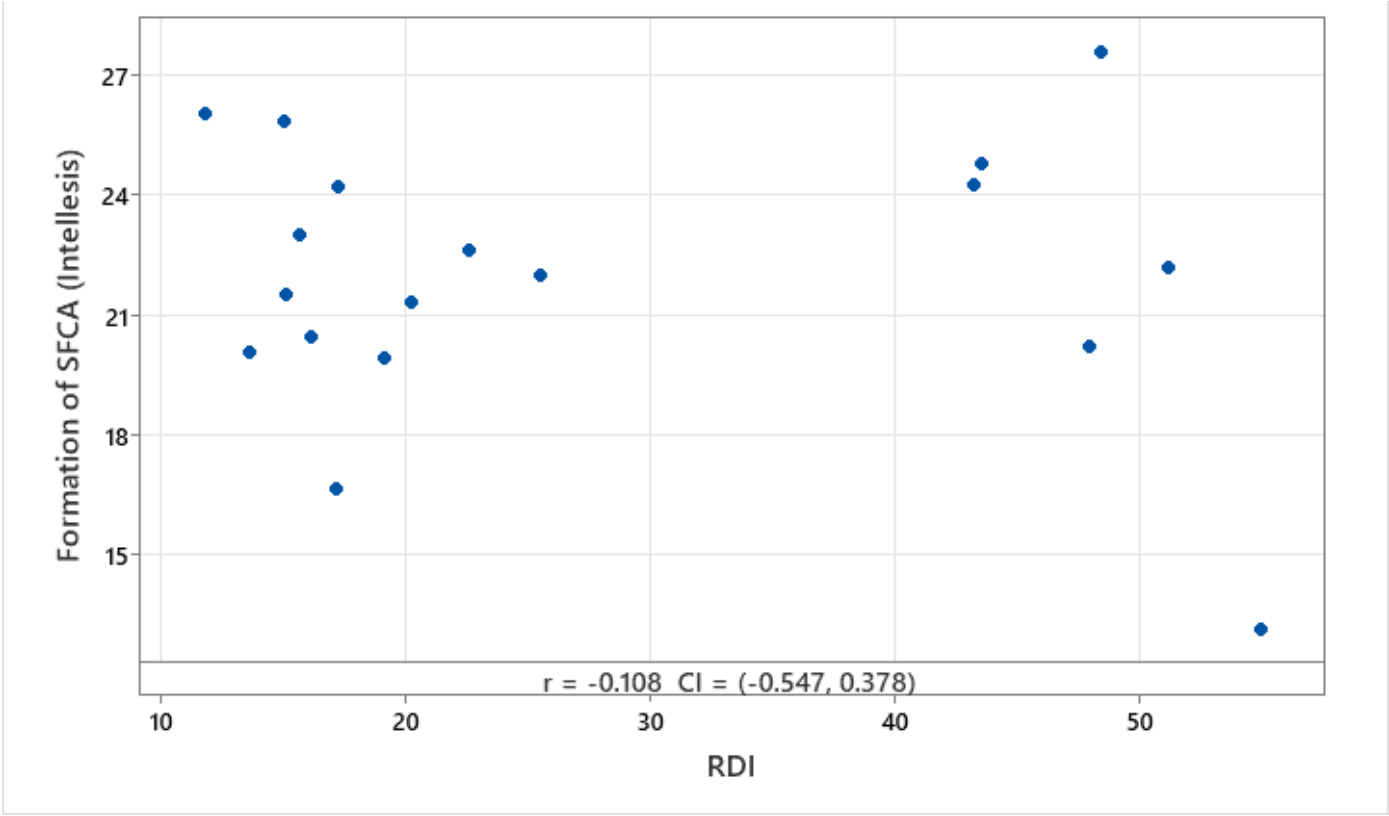

Figure 11.14 Pearson Correlation for RDI vs Formation of SFCA (Intellesis)

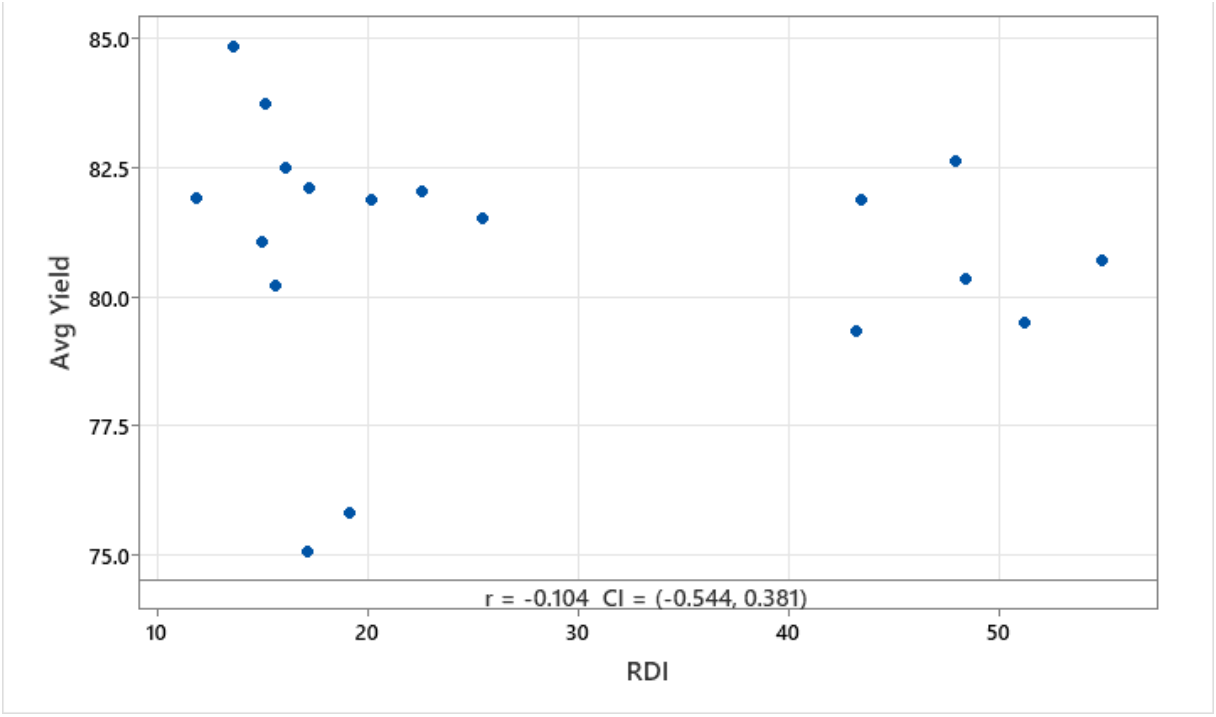

Figure 11.15 Pearson Correlation for RDI vs Average Yield

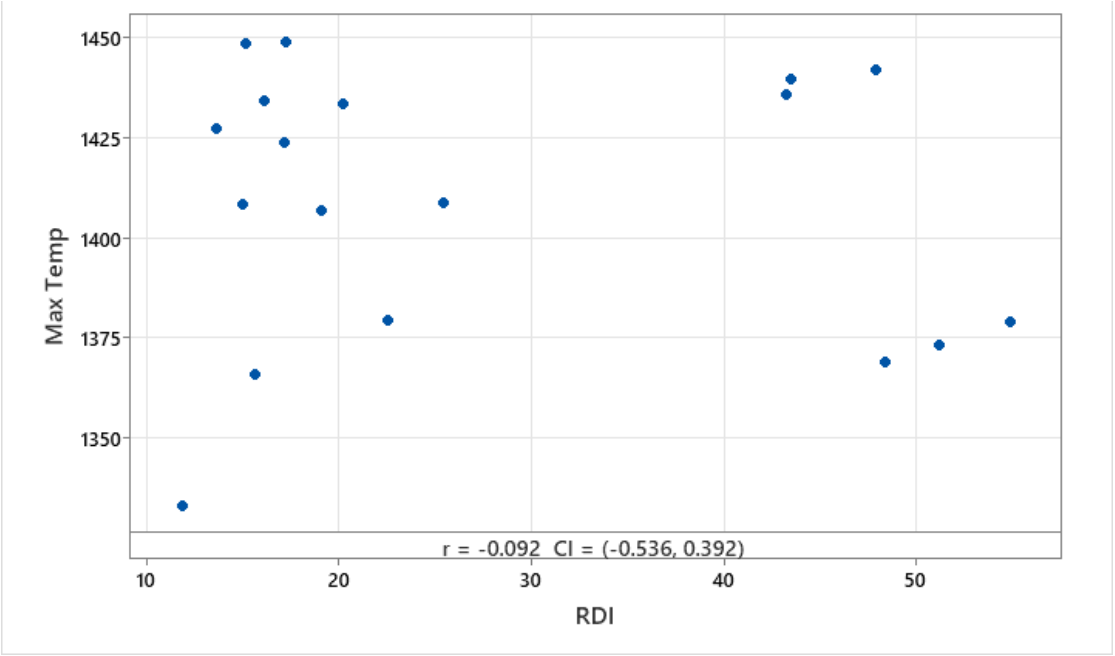

Figure 11.16 Pearson Correlation for RDI vs Max Temp

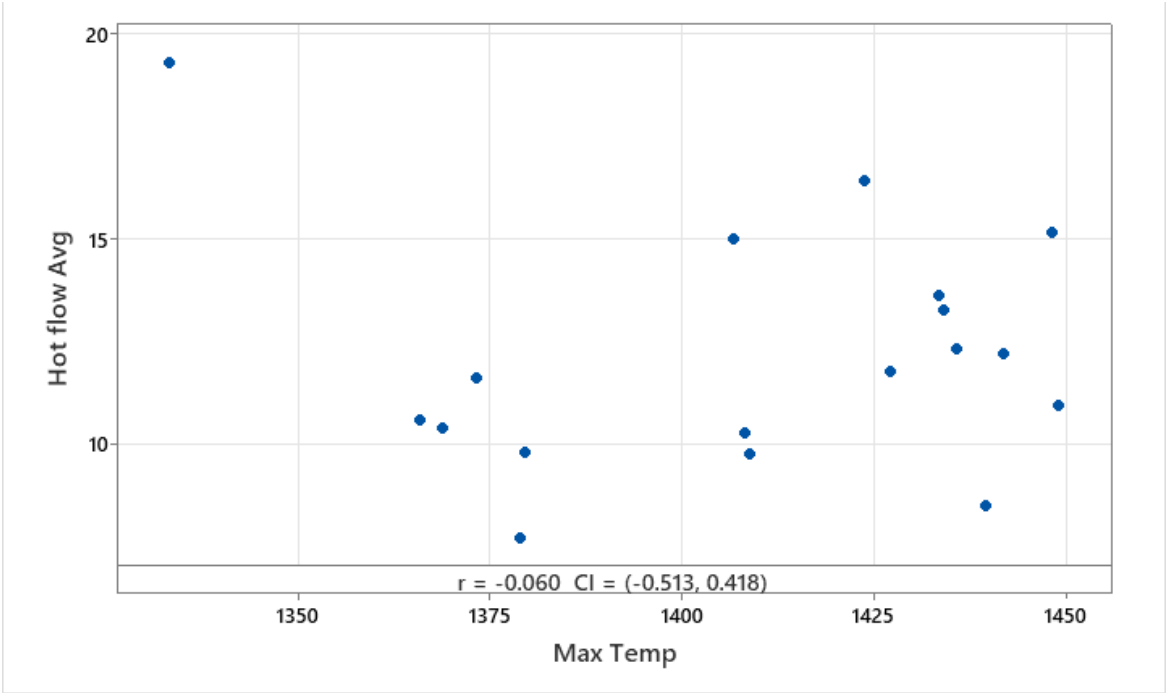

Figure 11.17 Pearson Correlation for Max Temp vs Hot Flow Average

11.3.2 Sintering parameters tables for the Taguchi Experiment

Blend	Factor Levels	SPM- system performance measurements								
		RDI	Average (t)	Average yield (kg)	rate kg/sec	Hot Flow avg	Total SFCA Intellesis	Total SFCA (XRD)	Max temp avg	16-40
1	5.5 SiO2, 2.0 MgO, B2=1.6	15	00:16:20	5.8	0.0059	8	27	16.70	1418	57
2	4.5 SiO2, 1.5 MgO, B2=1.5	14	00:15:35	6.6	0.0071	12	20	19.60	1427	30
3	4.5 SiO2, 2.0 MgO, B2=2.0	15	00:14:48	6.2	0.0069	15	22	19.30	1448	34
4	4.5 SiO2, 2.5 MgO, B2=2.5	17	00:13:07	6.4	0.0081	16	17	19.50	1424	29
5	5.0 SiO2, 1.5 MgO, B2=1.5	17	00:14:58	6.2	0.0068	11	24	15.30	1449	47
6	5.0 SiO2, 2.0 MgO, B2=2.0	16	00:14:43	6.3	0.0071	13	20	17.90	1434	43
7	5.0 SiO2, 2.5 MgO, B2=2.5	19	00:13:13	6.0	0.0076	15	20	18.30	1407	42
8	5.5 SiO2, 1.5 MgO, B2=2.0	26	00:16:02	6.5	0.0068	10	22	16.30	1409	49
9	5.5 SiO2, 2.0 MgO, B2=2.5	23	00:16:27	6.4	0.0065	10	23	18.50	1380	51
10	5.5 SiO2, 2.5 MgO, B2=2.5	15	00:15:53	6.6	0.0069	10	26	16.40	1408	48
11	6.0 SiO2, 1.5 MgO, B2=2.5	51	00:14:35	6.1	0.0070	12	22	18.10	1373	44
12	6.0 SiO2, 2.0 MgO, B2=1.5	48	00:14:30	5.8	0.0066	12	20	17.50	1442	42
13	6.0 SiO2, 2.5 MgO, B2=2.0	43	00:14:05	5.4	0.0063	12	24	18.90	1436	46
14	6.5 SiO2, 1.5 MgO, B2=2.0	55	00:17:55	5.7	0.0053	8	13	18.50	1379	53
15	6.5 SiO2, 2.0 MgO, B2=2.5	48	00:15:10	5.9	0.0064	10	28	21.40	1369	45
16	6.5 SiO2, 2.5 MgO, B2=1.5	44	00:16:17	5.9	0.0060	9	25	16.40	1440	49
17	7.0 SiO2, 1.5 MgO, B2=2.5	12	00:13:20	5.6	0.0070	19	26	18.50	1333	51
18	7.0 SiO2, 2.0 MgO, B2=1.5	20	00:13:00	5.8	0.0074	14	21	15.80	1433	48
19	7.0 SiO2, 2.5 MgO, B2=2.0	16	00:13:50	5.8	0.0069	11	23	18.60	1366	49

Figure 11.18 All factor levels and their results for their relative SPMs

Factor Levels	>40	25-40	16-25	10-16	5-10	<5
5.5 SiO2, 2.0 MgO, B2=1.6	14	25	18	14	12	17
4.5 SiO2, 1.5 MgO, B2=1.5	0	8	23	29	26	15
4.5 SiO2, 2.0 MgO, B2=2.0	2	15	18	26	24	16
4.5 SiO2, 2.5 MgO, B2=2.5	2	9	19	23	23	25
5.0 SiO2, 1.5 MgO, B2=1.5	4	20	23	19	16	18
5.0 SiO2, 2.0 MgO, B2=2.0	5	18	20	20	20	17
5.0 SiO2, 2.5 MgO, B2=2.5	9	16	17	14	20	24
5.5 SiO2, 1.5 MgO, B2=2.0	8	25	17	15	17	18
5.5 SiO2, 2.0 MgO, B2=2.5	4	27	20	17	14	18
5.5 SiO2, 2.5 MgO, B2=2.5	13	20	15	18	14	19
6.0 SiO2, 1.5 MgO, B2=2.5	4	23	17	20	16	20
6.0 SiO2, 2.0 MgO, B2=1.5	0	20	22	23	17	17
6.0 SiO2, 2.5 MgO, B2=2.0	2	22	21	14	20	21
6.5 SiO2, 1.5 MgO, B2=2.0	17	25	11	15	13	19
6.5 SiO2, 2.0 MgO, B2=2.5	9	15	21	21	15	20
6.5 SiO2, 2.5 MgO, B2=1.5	8	23	18	19	14	18
7.0 SiO2, 1.5 MgO, B2=2.5	8	24	20	19	12	18
7.0 SiO2, 2.0 MgO, B2=1.5	4	24	21	17	17	18
7.0 SiO2, 2.5 MgO, B2=2.0	8	22	20	16	15	20
Standard Deviation	5	5	3	4	4	2

Figure 11.19 PSD data with standard deviation.

12 References

1. Remus R, Roudier S, Aguado-Monsonet MA, Delgado Sancho L, Institute for Prospective Technological Studies. *Best Available Techniques (BAT) Reference Document for Iron and Steel Production : Industrial Emissions Directive 2010/75/EU: Integrated Pollution Prevention and Control.*; 2013. doi:10.2791/98516

2. Kumar D, Kumar D. *Latest Developments in the Iron and Steel Industry*. Vol 85.; 2016. doi:10.1016/b978-0-12-803160-5.00003-4

3. Yin X, Chen W. Trends and development of steel demand in China: A bottom-up analysis. *Resour Policy*. 2013;38(4):407-415. doi:10.1016/j.resourpol.2013.06.007

4. Bölükbaşi ÖS, Tufan B, Batar T, Altun A. The influence of raw material composition on the quality of sinter. *Life Sci J*. 2013;10(4):584-594. Accessed May 20, 2020. https://www.researchgate.net/publication/273011896_The_Influence_of_Raw_Material_Composition_on_the_Quality_of_Sinter

5. Mingming Z, Coe MS, Andrade MW. MINERALS Session Chairs : *Drying, Roasting, Calcining Miner*. Published online 2015.

6. Tsai JH, Lin KH, Chen CY, Ding JY, Choa CG, Chiang HL. Chemical constituents in particulate emissions from an integrated iron and steel facility. *J Hazard Mater*. 2007;147(1-2):111-119. doi:10.1016/j.jhazmat.2006.12.054

7. Tata Steel Limited. Integrated Report & Annual Accounts 15-16. Published online 2016. http://www.tatasteel.com/investors/annual-report-2015-16/Integrated-Report-&-Annual-Accounts-2015-16-(109th-Year).pdf

8. Ahindra Ghosh, Chatterjee A. *Ironmaking and Steelmaking: Theory and Practice.*; 2008.

9. Roberts WL. *Cold Rolling of Steel*. CRC Press; 2017.

10. Fernández-González D, Martín-Duarte R, Ruiz-Bustinza Í, Mochón J, González-Gasca C, Verdeja LF. Optimization of Sinter Plant Operating

Conditions Using Advanced Multivariate Statistics: Intelligent Data Processing. *Jom*. 2016;68(8):2089-2095. doi:10.1007/s11837-016-2002-2

11. Fernández-González D, Ruiz-Bustinza I, Mochón J, González-Gasca C, Verdeja LF. Iron Ore Sintering: Quality Indices. *Miner Process Extr Metall Rev*. 2017;38(4):254-264. doi:10.1080/08827508.2017.1323744

12. Lu L, Ishiyama O. *Iron Ore Sintering*.; 2015. doi:10.1016/B978-1-78242-156-6.00014-9

13. Debrincat D, Loo CE, Hutchens MF. Effect of iron ore particle assimilation on sinter structure. *ISIJ Int*. 2004;44(8):1308-1317. doi:10.2355/isijinternational.44.1308

14. Tomas da Rocha L, Cho S, Chung BJ, Jung SM. Effect of Replacing the Hearth Layer Used in the Sintering Process on the Reduction of NO and SO2. *Metall Mater Trans B Process Metall Mater Process Sci*. 2022;53(5):3071-3082. doi:10.1007/s11663-022-02587-2

15. Wilcox M. Environmental Optimisation of Iron Ore Sintering. Published online 2023.

16. Ooi TC, Campbell-Hardwick S, Zhu D, Pan J. Sintering performance of magnetite-hematite-goethite and hematite-goethite iron ore blends and microstructure of products of sintering. *Miner Process Extr Metall Rev*. 2014;35(4):266-281. doi:10.1080/08827508.2013.793681

17. Umadevi T, Naik DK, Sah R, Brahmacharyulu A, Marutiram K, Mahapatra PC. Studies on parameters affecting sinter strength and prediction through artificial neural network model. *Trans Institutions Min Metall Sect C Miner Process Extr Metall*. 2016;125(1):32-38. doi:10.1179/1743285515Y.0000000020

18. Umadevi T, Brahmacharyulu A, Roy AK, Mahapatra PC, Prabhu M, Ranjan M. Influence of iron ore fines feed size on microstructure, productivity and quality of iron ore sinter. *ISIJ Int*. 2011;51(6):922-929. doi:10.2355/isijinternational.51.922

19. Kubat C, Taşkin H, Artir R, Yilmaz A. Bofy-fuzzy logic control for the basic

oxygen furnace (BOF). Rob Auton Syst. 2004;49:193-205. doi:https://doi.org/10.1016/j.robot.2004.09.007

20. Wright RN. Relevant Aspects of Carbon and Low Alloy Steel Metallurgy. *Wire Technol*. Published online 2011:199-228. doi:10.1016/b978-0-12-382092-1.00014-2

21. Tupkary RH, Tupkary VR. *M Odern S Teel M Aking H Andbook*.

22. Fruehan RJ. The Making, Shaping and Treating of Steel: Steelmaking and Refining Volume. Published online 2012:761. https://www.mendeley.com/research/making-shaping-treating-steel/?utm_source=desktop&utm_medium=1.15&utm_campaign=open_catalog&userDocumentId=%7Baeb82e61-78da-43a6-bf4b-7e6a0cba8a86%7D

23. Legemza J, Findorák R, Fröhlichová M. Utilization of charcoal in the iron-ore sintering process. *Sci Iran*. 2016;23(3):990-997. doi:10.24200/sci.2016.3867

24. Fernández-González D, Ruiz-Bustinza I, Mochón J, González-Gasca C, Verdeja LF. Iron Ore Sintering: Process. *Miner Process Extr Metall Rev*. 2017;38(4):215-227. doi:10.1080/08827508.2017.1288115

25. Cores A, Verdeja LF, Ferreira S, Ruiz-Bustinza I, Mochón J. Iron ore sintering. Part 1. Theory and practice of the sintering process. *DYNA*. 2013;80(180):152-171.

26. Zhou H, Zhou M, Ma P, Cheng M. Experimental investigation on the flame front resistance of gas channel growth with melt formation in iron ore sinter beds. *Proc Combust Inst*. 2019;37(4):4607-4615. doi:10.1016/j.proci.2018.09.027

27. Chen C, Lu L, Jiao K. Thermodynamic modelling of iron ore sintering reactions. *Minerals*. 2019;9(6):361. doi:10.3390/min9060361

28. Arghya Majumder et al., AM et al. Study on Reduction Kinetics of Iron Ore Sinter Using Coke Dust. *Int J Metall Mater Sci Eng*. 2018;8(1):19-26. doi:10.24247/ijmmsefeb20183

29. Loo CE, Leung W. Factors influencing the bonding phase structure of iron ore

sinters. *ISIJ Int*. 2003;43(9):1393-1402. doi:10.2355/isijinternational.43.1393

30. Webster NAS, Pownceby MI, Madsen IC, Kimpton JA. Silico-ferrite of calcium and aluminum (SFCA) iron ore sinter bonding phases: New insights into their formation during heating and cooling. *Metall Mater Trans B Process Metall Mater Process Sci*. 2012;43(6):1344-1357. doi:10.1007/s11663-012-9740-5

31. Scarlett NVY, Pownceby MI, Madsen IC, Christensen AN. Reaction sequences in the formation of silico-ferrites of calcium and aluminum in iron ore sinter. *Metall Mater Trans B Process Metall Mater Process Sci*. 2004;35(5):929-936. doi:10.1007/s11663-004-0087-4

32. Pownceby MI, Clout JMF. Importance of fine ore chemical composition and high temperature phase relations: Applications to iron ore sintering and pelletising. *Trans Institutions Min Metall Sect C Miner Process Extr Metall*. 2003;112(APRIL). doi:10.1179/037195503225011402

33. Zhou M, Yu Z, Wang P, Xie H, Wen Y, Li J. Thermodynamic Analysis of Iron Ore Sintering Process Based on Biomass Carbon. *Energies*. 2020;13(22):5988. doi:10.3390/en13225988

34. Carson E, Watson J. Undergraduate students' understandings of entropy and Gibbs free energy. *Univ Chem Educ*. 2002;6(1):4-12.

35. Abu Tahari MN, Salleh F, Tengku Saharuddin TS, et al. Influence of hydrogen and various carbon monoxide concentrations on reduction behavior of iron oxide at low temperature. *Int J Hydrogen Energy*. 2019;44(37):20751-20759. doi:10.1016/j.ijhydene.2018.09.186

36. Zhao JP, Loo CE, Dukino RD. Modelling fuel combustion in iron ore sintering. *Combust Flame*. 2015;162(4):1019-1034. doi:10.1016/j.combustflame.2014.09.026

37. Lovel RR, Vining KR, Dell'Amico M. The influence of fuel reactivity on iron ore sintering. *ISIJ Int*. 2009;49(2):195-202. doi:10.2355/isijinternational.49.195

38. Umadevi T, Karthik P, Mahapatra PC, Prabhu M, Ranjan M. Optimisation of FeO in iron ore sinter at JSW Steel Limited. *Ironmak Steelmak*. 2012;39(3):180-189. doi:10.1179/1743281211Y.0000000080

39. Choudhary MK, Nandy B. No Title. *Tata Search*. Published online 2006:135.

40. Hosotani Y, Konno N, Yamaguchi K, Orimoto T, Inazumi T. Reduction properties of sinter with fine dispersed pores at high temperatures of 1 273 K and above. *ISIJ Int*. 1996;36(12):1439-1447. doi:10.2355/isijinternational.36.1439

41. Bhagat RP, Chattoraj US, Goswami MC, Singh DP, Sil SK. Effect of size parameters of mix ingredients on the porosity and reduction characteristics of sinter. *Steel Res Int*. 2007;78(6):451-454. doi:10.1002/srin.200706229

42. Wu SL, Liu XQ, Zhou Q, Xu J, Liu CS. Low temperature reduction degradation characteristics of sinter, pellet and lump ore. *J Iron Steel Res Int*. 2011;18(8):20-24. doi:10.1016/S1006-706X(11)60098-8

43. Loo CE, Wong DJ. Fundamental factors determining laboratory sintering results. *ISIJ Int*. 2005;45(4):449-458. doi:10.2355/isijinternational.45.449

44. Yamaoka H, Kawaguchi T. Development of a 3-D sinter process mathematical simulation model. *ISIJ Int*. 2005;45(4):522-531. doi:10.2355/isijinternational.45.522

45. Cheng Z, Yang J, Zhou L, Liu Y, Wang Q. Characteristics of charcoal combustion and its effects on iron-ore sintering performance. *Appl Energy*. 2016;161:364-374. doi:10.1016/j.apenergy.2015.09.095

46. Inazumi T. Iron ore sinter-Review of Steps Taken to Overcome the Challenges Posed Japan's Lack of Iron Ore Resources. *ISIJ Int*. Published online 2000:213.

47. Nicol S, Chen J, Qi W, Mao X, Jak E, Hayes PC. Measurement of process conditions present in pilot scale iron ore sintering. *Minerals*. 2019;9(6):374. doi:10.3390/min9060374

48. Zhou H, Liu Z, Cheng M, Zhou M, Liu R. Influence of coke combustion on NOx emission during iron ore sintering. *Energy and Fuels*. 2015;29(2):974-

984. doi:10.1021/ef502524y

49. German RM. Thermodynamic and Kinetic Treatments. In: *Sintering: From Empirical Observations to Scientific Principles*. Elsevier; 2014:183-226. doi:10.1016/b978-0-12-401682-8.00007-0

50. Webster NAS, Pownceby MI, Madsen IC, Kimpton JA. Effect of oxygen partial pressure on the formation mechanisms of complex Ca-rich ferrites. *ISIJ Int*. 2013;53(5):774-781. doi:10.2355/isijinternational.53.774

51. Webster NAS, Pownceby MI, Pattel R, Manuel JR, Kimpton JA. Fundamentals of silico-ferrite of calcium and aluminium (SFCA) iron ore sinter bonding phase formation: Effects of titanium on crystallisation during cooling. *ISIJ Int*. 2019;59(6):1007-1010. doi:10.2355/isijinternational.ISIJINT-2018-701

52. Litster JD, Waters AG. Kinetics of iron ore sinter feed granulation. *Powder Technol*. 1990;62(2):125-134. doi:10.1016/0032-5910(90)80075-A

53. Furui T, Sugawara K, Kagawa M, et al. No Title. *Nippon Steel Tech Rep*. 1977;10:36-46.

54. Litster JD, Waters AG. Influence of the material properties of iron ore sinter feed on granulation effectiveness. *Powder Technol*. 1988;55(2):141-151. doi:10.1016/0032-5910(88)80097-4

55. Mathur GP, Manya GVS, Narayanan PA. Sintering ofiron Ore Fines , and Raw Materials for Bhilai Steel Plant. *INDIAN Min J*. Published online 1957.

56. Dawson PR. Recent developments in iron ore sintering new development for sintering. *Ironmak Steelmak*. 1993;20(2):135-136.

57. Gupta SS, Venkataramana R. Mathematical model of air flow during iron ore sintering process. *Iron Steelmak*. 2000;27(12):35-41.

58. Oliveira D, Wu S li, Dai Y ming, Xu J, Chen H. Sintering Properties and Optimal Blending Schemes of Iron Ores. *J Iron Steel Res Int*. 2012;19(6):1-5. doi:10.1016/S1006-706X(12)60117-4

59. Bhagat RP, Pradhan SK, Nandi MCGB. Effect of Ores Granulometry and

related Parameters on the Sintering Indices. *Tata Search*. 2013;I:89-94.

60. Jaime O, Baena R, Federico C, Jiménez V, Oswaldo M, Rúa B. Influence of Ph in the Properties of Synthetic Goethite As a Pigment. *Año*. 2008;75:163-170.

61. Hapugoda S, Lu L, Donskoi E, Manuel J. Mineralogical quantification of iron ore sinter. *Trans Institutions Min Metall Sect C Miner Process Extr Metall*. 2016;125(3):156-164. doi:10.1080/03719553.2016.1164797

62. Chen X. Sinter Batcher. *Metall Ind Press*. Published online 2014:9-11.

63. Zhi JM, Li J, Wang JH, Jiang TY, Hua ZY. Effect of Basicity on the Microstructure of Sinter and Its Application Based on Deep Learning. *Comput Intell Neurosci*. 2021;2021. doi:10.1155/2021/1082834

64. Umadevi T, Sah R, Mahapatra PC. Influence of sinter basicity (CaO/SiO2) on low and high alumina iron ore sinter quality. *Trans Institutions Min Metall Sect C Miner Process Extr Metall*. 2014;123(2):75-85. doi:10.1179/1743285514Y.0000000052

65. Ostwald J. Mineralogy and micro-texture of Australian iron ore sinters. *BHP Tech Bull*. 1981;25:13.

66. Grebe K, Stricker KP. Improvement of blast furnace operation by new control techniques in the blast furnace and sinter plants. *Int Congr Sci Technol Ironmak 57 th Ironmak Conf*. 1998;2.

67. Gledhill PK, Carter GC, Ely CF. EFFECT OF MINERAL ADDITIONS AND MOISTURE CONTROL ON THE SINTERING OF SIERRA-LEONE CONCENTRATES. *J IRON STEEL Inst*. 1953;175(3):277-279.

68. Dongshim J, Ohaba A, Tanaka M. No Title. *Trans Nat Res Inst Met Jpn*. 1980;22:31.

69. Nyquist O. Agglomeration. *Interscience*. Published online 1962:809.

70. Honeyands T, Nguyen TBT, Pinson D, et al. Variation in Iron Ore Sinter Mineralogy with Changes in Basicity. *Minerals*. 2022;12(10). doi:10.3390/min12101249

71. Bagnall E. Influence of feed material properties on sinter for blast furnaces. *Agglomeration*. 1977;77:2.

72. Geerdes M. Modern blast furnace ironmaking : an introduction. Published online 2020.

73. Webster NAS, Pownceby MI, Madsen IC. In situ X-ray diffraction investigation of the formation mechanisms of silico-ferrite of calcium and aluminium-I-type (SFCA-I-type) complex calcium ferrites. *ISIJ Int*. 2013;53(8):1334-1340. doi:10.2355/isijinternational.53.1334

74. Umadevi T, Mahapatra PC, Prabhu M. Influence of MgO addition on microstructure and properties of low and high silica iron ore sinter. *Trans Institutions Min Metall Sect C Miner Process Extr Metall*. 2013;122(4):238-248. doi:10.1179/1743285513Y.0000000046

75. Umadevi T, Nelson K, Mahapatra PC, Prabhu M, Ranjan M. Influence of magnesia on iron ore sinter properties and productivity. *Ironmak Steelmak*. 2009;36(7):515-520. doi:10.1179/174328109X445741

76. Ji Z, Zhao Y, Gan M, Fan X, Chen X, Hu L. Microstructure and minerals evolution of iron ore sinter: Influence of SiO2 and Al2O3. *Minerals*. 2019;9(7). doi:10.3390/min9070449

77. Fedock MP, Kohl TG, Kusner RE. No Title. *ISS Ironmak Conf*. 1968;00:144-149.

78. Ponghis N, Poos A. No Title. *ISS Ironmak Conf*. 1977;36:91-99.

79. Yadav US, Pandey BD, Das BK, Jena DN. Influence of magnesia on sintering characteristics of iron ore. *Ironmak Steelmak*. 2002;29(2):91-95. doi:10.1179/030192302225002018

80. Liu J, Jiang W, Cheng D, et al. Effect of Silica Content on Iron Ore Sintering. Published online 2023:1-12.

81. Zhang M, Andrade MW. Effect of MgO and basicity on microstructure and metallurgical properties of iron ore sinter. *Charact Miner Met Mater 2016*. Published online 2016:167-174. doi:10.1007/978-3-319-48210-1_20

82. Long H, Wu X, Chun T, Di Z, Yu B. Assimilation Behavior of Calcium Ferrite and Calcium Diferrite with Sintered Al2O3 and MgO. *Metall Mater Trans B Process Metall Mater Process Sci*. 2016;47(5):2830-2836. doi:10.1007/s11663-016-0723-9

83. Zhang G liang, Wu S li, Su B, Que Z gang, Hou C gang, Jiang Y. Influencing factor of sinter body strength and its effects on iron ore sintering indexes. *Int J Miner Metall Mater*. 2015;22(6):553-561. doi:10.1007/s12613-015-1107-x

84. Guo XM, Xue MS. Effect of Al2O3 and SiO2 on formation and crystal structure of calcium ferrite containing Al2O3 and SiO2. *J Chin Rare Earth Soc*. 2008;26:205.

85. Panigrahy SC, Verstraeten P, Dilewijns J. Influence of MgO addition on mineralogy of iron ore sinter. *Metall Trans B*. 1984;15(1):23-32. doi:10.1007/BF02661059

86. Hino M, Nagasaka T, Katsumata A, Higuchi KI, Yamaguchi K, Kon-No N. Simulation of primary-slag melting behavior in the cohesive zone of a blast furnace, considering the effect of Al2O3, FetO, and basicity in the sinter ore. *Metall Mater Trans B Process Metall Mater Process Sci*. 1999;30(4):671-683. doi:10.1007/s11663-999-0028-3

87. Pimenta HP, Seshadri V, Cardose MB, Azevedo AT. No Title. *Proc 6th Int Symp Agglom*. Published online 1993:332.

88. Honeyands T, Manuel J, Matthews L, et al. Comparison of the mineralogy of iron ore sinters using a range of techniques. *Minerals*. 2019;9(6):1-17. doi:10.3390/min9060333

89. Shigaki I, Sawada M, Gennai N. No Title. *Trans Iron Steel Inst Jpn*. 1986;26:503.

90. J. Szekely, J. McKelliget, M. Choudhary. *Ironmaking Steelmaking*. Vol 10. 20th ed.; 1983.

91. Sugawara K, Shimizu R, Kawazu M. No Title. *Tetsu-To-Hagane/Journal Iron Steel Inst Japan*. 1971;57:S385.

92. Pimenta HP, Seshadri V. Characterisation of structure of iron ore sinter and its behaviour during reduction at low temperatures. *Ironmak Steelmak*. 2002;29(3):175.

93. Wang Z, Pinson D, Chew S, et al. Effects of sintering materials and gas conditions on formation of silico-ferrites of calcium and aluminium during iron ore sintering. *ISIJ Int*. 2016;56(7):1138-1147. doi:10.2355/isijinternational.ISIJINT-2015-598

94. Monazam ER, Breault RW, Siriwardane R. Reduction of hematite (Fe2O3) to wüstite (FeO) by carbon monoxide (CO) for chemical looping combustion. *Chem Eng J*. 2014;242:204-210. doi:10.1016/j.cej.2013.12.040

95. Nyembwe AM, Garbers-Craig AM. Study of iron ore sinter when fine ore is replaced with coarse ore, using infrared furnace and sinter pot tests. *Ironmak Steelmak*. 2014;41(3):173-181. doi:10.1179/1743281213Y.0000000115

96. Ferreira S, Cores A, Robla JI, et al. The influence of gangue and additives on the divalent iron content of magnetite pellets. *Steel Res Int*. 2014;85(2):261-272. doi:10.1002/srin.201300370

97. Harvey T, Pownceby MI, Chen J, et al. Effect of Temperature, Time, and Cooling Rate on the Mineralogy, Morphology, and Reducibility of Iron Ore Sinter Analogues. *Jom*. 2021;73(1):345-355. doi:10.1007/s11837-020-04452-6

98. Sarath H, Scientific TC, Donskoi E, Scientific TC, Pownceby MI, Scientific TC. Characterisation of SFCA phases in iron ore sinter by combined optical microscopy and electron probe microanalysis (EPMA) Characterisation of SFCA phases in iron ore sinter by combined optical microscopy and electron probe microanalysis (EPMA). 2021;(November).

99. Liang Z, Chen J, Huang Z, Huang B. Characteristics and Sintering Mechanisms of Iron Ores with a High Proportion of High-Al2O3 Limonite. *ACS Omega*. 2023;8(18):15951-15959. doi:10.1021/acsomega.2c07659

100. Standards B. Determination of tumbler strength of iron ores. Published online 1987.

101. Kalenga MK, Garbers-Craig AM. Investigation into how the magnesia, silica, and alumina contents of iron ore sinter influence its mineralogy and properties. *J South African Inst Min Metall*. 2010;110(8):447-456.

102. McAndrew J, Clout JMF. No Title. *Proc 4th China-Australia SympTechnol Feed Prep Ironmak*. Published online 1993:1-15.

103. Donskoi E, Hapugoda S, Manuel JR, et al. Automated optical image analysis of iron ore sinter. *Minerals*. 2021;11(6). doi:10.3390/min11060562

104. Brehm J, Buckner J, Profazi C, Hickman A. Incipient Melting in AA7075 Incipient Melting in AA7075. 2022;(June).

105. Umadevi T, Bandopadhyay UK, Mahapatra PC, Prabhu M, Ranjan M. Influence of limestone particle size on iron ore sinter properties and productivity. *Steel Res Int*. 2010;81(6):419-425. doi:10.1002/srin.201000020

106. Shigaki I, Sawada M, Yoshioka K, Takahashi T. Improvement of Productivity and Reduction Disintegration of Iron Ore Sinter By Increasing the Size of Limestone Particles. *Tetsu-To-Hagane/Journal Iron Steel Inst Japan*. 1985;71(16):1880-1887. doi:10.2355/tetsutohagane1955.71.16_1880

107. Bhagat RP. Effect of flux granulometry and other process variables on the sintering of iron ore at high basicity. *Natl Metall Lab*. Published online 1997:240-248.

108. Hannah J., Hass K. No Title. *Proc Ironmak Conf*. Published online 1960:287.

109. Yang YH, Standish N. Fundamental Mechanisms of Pore Formation in Iron Ore Sinter and Pellets. *ISIJ Int*. 1991;31(5):468-477. doi:10.2355/isijinternational.31.468

110. Umadevi T, Bandopadhyay UK, Mahapatra PC, Prabhu M, Ranjan M. Influence of limestone particle size on iron ore sinter properties and productivity. doi:10.1002/srin.201000020

111. Machemer SD. Characterization of Airborne and Bulk Particulate from Iron and Steel Manufacturing Facilities. *Environ Sci Technol*. 2004;38(2):381-389. doi:10.1021/es020897v

112. Aswath HS, Tudekar S., Ghosh P. *No Title*. Vol I-I. Bokor; 1979.

113. Bhagat R., Sil S., Chattoraj U., Goswami M., Singh D., Das B. *Tata Search*.; 2006.

114. Bhagat R., Gupta S., Roy H. *Proc. 48th Ironmaking Conference*.; 1989.

115. Shigaki I, Sawada M, Gennai N. Increase in Low-Temperature Reduction Degradation of Iron Ore Sinter Due To Hematite-Alumina Solid Solution and Columnar Calcium Ferrite. *Trans Iron Steel Inst Japan*. 1986;26(6):503-511. doi:10.2355/isijinternational1966.26.503

116. Bhagat RP, Chattoraj US, Sil SK. Porosity of sinter and its relation with the sintering indices. *ISIJ Int*. 2006;46(11):1728-1730. doi:10.2355/isijinternational.46.1728

117. Matsumura T, Maki T, Amano S, Sakamoto M, Iwasaki N. Effect of Moisture Absorption behaviour on Optimal Granulation Moisture Value of Sinter Raw Material. *ISIJ Int*. 2009;49:618-624.

118. Wang W, Chen X heng, Xu R sheng, Li J, Shen W jun, Wang S ping. Research progress on multiscale structural characteristics and characterization methods of iron ore sinter. *J Iron Steel Res Int*. 2020;27(4):367-379. doi:10.1007/s42243-020-00374-4

119. Adedeji FA, Complex DS. of Itakpe and Agbaja (N I G E R I a N) Iron Ores and. Published online 1984:843-856.

120. Kuila SK, Chatterjee R, Ghosh D. Kinetics of hydrogen reduction of magnetite ore fines. *Int J Hydrogen Energy*. 2016;41(22):9256-9266. doi:10.1016/j.ijhydene.2016.04.075

121. Hsieh LH. Effect of raw material composition on the sintering properties. *ISIJ Int*. 2005;45(4):551-559. doi:10.2355/isijinternational.45.551

122. Nagasaka T, Iguchi Y, Ban-ya S. No Title. *Tetsu-To-Hagane/Journal Iron Steel Inst Japan*. 1985;71:204.

123. Sato S, Ichidate M, Kato K, Kawaguchi T. No Title. *Tetsu-To-Hagane/Journal*

Iron Steel Inst Japan. 1983;69:S744.

124. Jeulin D, Latailleur A, Schneider M. No Title. *Agglomeration*. 1977;77:526.

125. Yang W, Choi S, Choi ES, Ri DW, Kim S. Combustion characteristics in an iron ore sintering bed-evaluation of fuel substitution. *Combust Flame*. 2006;145(3):447-463. doi:10.1016/j.combustflame.2006.01.005

126. Al-Haji T. Developments In Iron Ore Sintering Using A Laboratory Scaled Development Platform. 2022;(March). 10.23889/SUthesis.62668.oa

127. Mousa EA, Babich A, Senk D, Metallurgy F, Aachen R. Iron Ore Sintering Process with Biomass Utilization E . A . Mousa , A . Babich , D . Senk , Institute of Ferrous Metallurgy Iron Ore Sintering Process with Biomass Utilization. 2015;(September).

128. Mousa E, Wang C, Riesbeck J, Larsson M. Biomass applications in iron and steel industry: An overview of challenges and opportunities. *Renew Sustain Energy Rev*. 2016;65:1247-1266. doi:10.1016/j.rser.2016.07.061

129. Karabasov, Y. U S. Mechanism of the Influence of the Size of Coke Fines on the Sintering Process. *Steel USSR*. 1975;5(11):583-584.

130. Kornilova NK. Influence of the size of coke fines on the strength of sinter made from sintering ores. *Steel USSR*. 1973;3:1-2.

131. Murty CHVG., Chatterjee A, Rao V. Reduction of alumina in iron ore classifier fines and its influence on sinter. *Tata Search*. Published online 1994:7-13.

132. Kinnunen K, Laitinen P. Modeling of reduction degradation of iron ore sinter by feed-forward neural networks. *IFAC Proc Vol*. 2004;37(16):97-102. doi:10.1016/S1474-6670(17)30857-1

133. Thomas MH. Minimising Particulate Emissions From Sintering Operations. Published online 2022.

134. Mahanta CR, Sahoo PR, Mohanta MK, et al. Mineralogical Characteristics of Hematitic Iron Ore: A Geometallurgical Study on Ore from Eastern India. *Minerals*. 2023;13(9). doi:10.3390/min13091194

135. Endecotts. Precision Test Sieves | Sieve Shakers. *wwwENDECOTTSCOM*. Published online 2019.

136. ISO 113581. INTERNATIONAL STANDARD iTeh STANDARD iTeh STANDARD PREVIEW. *Int Organ Stand*. 2015;10406-1:20:3-6.

137. Malvern Panalytical. Malvern Panalytical. Published online 1997.

138. González MF, Saadatkhah N, Patience GS. Experimental methods in chemical engineering: X-ray fluorescence—XRF. *Can J Chem Eng*. 2024;102(6):2004-2018. doi:10.1002/cjce.25218

139. Bruker Corporation. Bruker. Published online 1960.

140. Note SAA. Semi-Quantitative Analysis by XRD. *Antimicrob Agents Chemother*. 2014;58(12):1-2.

141. Cuevas J, Cabrera MÁ, Fernández C, et al. Bentonite Powder XRD Quantitative Analysis Using Rietveld Refinement: Revisiting and Updating Bulk Semiquantitative Mineralogical Compositions. *Minerals*. 2022;12(6). doi:10.3390/min12060772

142. Zeiss C. Primotech Instruction Manual. *Microsc GmbH*. Published online 2014:63.

143. Thermfact/CRCT. FactSage 8.2. Published online 2020.

144. Waseda Y. *Phase Diagrams: Understanding the Basics*. Butterworth-Heinemann; 1999.

145. Zeiss C. Zeiss Intellesis. Published online 1846.

146. Rosa JL, Robin A, Silva MB, Baldan CA, Peres MP. Electrodeposition of copper on titanium wires: Taguchi experimental design approach. *J Mater Process Technol*. 2009;209(3):1181-1188. doi:10.1016/j.jmatprotec.2008.03.021

147. Semioshkina N, Voigt G. An overview on Taguchi Method. *J Radiat Res*. 2006;47 Suppl A(2):A95-A100. http://www.ncbi.nlm.nih.gov/pubmed/19879888

148. State College. Minitab Statistical Software. Published online 2010.

149. Pownceby MI, Clout JMF. Phase relations in the Fe-rich part of the system Fe2O3(-Fe3O4)-CaO-SiO2 at 1240-1300°C and oxygen partial pressure of 5 × 10-3 atm: Implications for iron ore sinter. *Trans Institutions Min Metall Sect C Miner Process Extr Metall*. 2000;109(JAN./APR.):36-48. doi:10.1179/mpm.2000.109.1.36

150. Wang Y, He J, Liu C, Chong WH, Chen H. Thermodynamics versus kinetics in Nanosynthesis. *Angew Chemie - Int Ed*. 2015;54(7):2022-2051. doi:10.1002/anie.201402986

151. Lu L, Holmes RJ, Manuel JR. Effects of alumina on sintering performance of hematite iron ores. *ISIJ Int*. 2007;47(3):349-358. doi:10.2355/isijinternational.47.349

152. Mochón J, Verdeja LF. IRON ORE SINTERING PART 2. QUALITY INDICES AND PRODUCTIVITY SINTERIZACIÓN DE MINERALES DE HIERRO PARTE 2. ÍNDICES DE CALIDAD Y PRODUCTIVIDAD ALEJANDRO CORES ÍÑIGO RUIZ-BUSTINZA JOSÉ IGNACIO ROBLA FERNANDO GARCIA-CARCEDO. 2014;81(183):168-177.

153. Rubin M. Do p values lose their meaning in exploratory analyses? It depends how you define the familywise error rate. *Rev Gen Psychol*. 2017;21(3):269-275. doi:10.1037/gpr0000123

154. Schober P, Schwarte LA. Correlation coefficients: Appropriate use and interpretation. *Anesth Analg*. 2018;126(5):1763-1768. doi:10.1213/ANE.0000000000002864

155. Dawson PR, Ostwald J, Hayes KM. The influence of the sintering temperature profile on the mineralogy and properties of iron ore sinters. *AIMM Bull Proc*. 1984;289(5):163-169.

156. Cai B, Watanabe T, Kamijo C, Susa M, Hayashi M. Comparison between reducibilities of columnar silico-ferrite of calcium and aluminum (SFCA) covered with slag and acicular SFCA with fine pores. *ISIJ Int*. 2018;58(4):642-

651. doi:10.2355/isijinternational.ISIJINT-2017-552

157. Maruoka D, Mataoka S, Murakami T, Kasai E. Influence of crystal structure and chemical composition of silico-ferrite of calcium and aluminum on its reducibility. *Proc 8th Int Congr Sci Technol Ironmak*. Published online 2018:25-28.

158. Li ZP, Fan XH, Yang GM, Wei JC, Sun Y, Wang M. Life Cycle Assessment of Iron Ore Sintering Process. *J Iron Steel Res Int*. 2015;22(6):473-477. doi:10.1016/S1006-706X(15)30029-7

159. Fernández-González D, Ruiz-Bustinza I, Mochón J, González-Gasca C, Verdeja LF. Iron Ore Sintering: Environment, Automatic, and Control Techniques. *Miner Process Extr Metall Rev*. 2017;38(4):238-249. doi:10.1080/08827508.2017.1288118